ZENTRALINSTITUT FÜR KERNFORSCHUNG
ROSSENDORF BEI DRESDEN



ZfK-491

# Proceedings

of the XII$^{th}$ International Symposium
on Nuclear Physics
– Heavy-Ion Collisions and Nuclear Fission –

November 22–26, 1982 in Gaussig (GDR)
Organized by the Technical University of Dresden

Edited by
R. Reif and J. Teichert

December 1982

ISSN 0138-2950

Postanschrift: Akademie der Wissenschaften der DDR
Zentralinstitut für Kernforschung Rossendorf
8051 Dresden
Postfach 19 Deutsche Demokratische Republik

Diese Publikation wurde in der Abteilung Literatur und Information des Zentralinstitutes für Kernforschung hergestellt

III-12-12 J 126—2 83

AKADEMIE DER WISSENSCHAFTEN DER DDR

ZENTRALINSTITUT FÜR KERNFORSCHUNG

ROSSENDORF BEI DRESDEN

ZfK - 491

# Proceedings

# of the XII$^{th}$ International Symposium on Nuclear Physics

## - Heavy-Ion Collisions and Nuclear Fission -

organized by

the Technical University of Dresden

November 22-23, 1982 in Gaussig (GDR)

edited by

R. Reif and J. Teichert

December 1982

**Organizing Committee**

R. Reif
R. Schmidt
D. Hermsdorf
H. Ludwig

Technical University Dresden, Section of Physics
Theoretical Physics Group Nuclear Physics Group

This report contains the contributions presented at the "XII$^{th}$ International Symposium on Nuclear Physics" organized by the Section of Physics of the Technical University Dresden.

The Symposium was devoted to current problems in experimental and theoretical investigations heavy-ion reactions and the dynamics of nuclear fission processes:

- emission of fast light particles in heavy-ion collisions, preequilibrium effects
- dynamics of deepinelastic heavy-ion reactions, TDHF
- selected topics in quasielastic heavy-ion collisions
- collective transport theory for fission, cross sections and neutron spectra of fission.

The scientific program covered also problems in neutron induced reactions and nuclear data evaluation.

We would like to thank all participants for their active work during the Symposium. Thanks are directed to the International Department of the Technical University Dresden for their support in organizing this Symposium. We are much indebted to the Central Institute for Nuclear Research Rossendorf for making possible the publication of this Proceedings as a ZfK-Report. The technical assistance of H. Ludwig in preparing the present volume is gratefully acknowledged.

R. Reif
J. Teichert

**CONTENTS**

LIST OF PARTICIPANTS

| | | |
|---|---|---|
| Arlt, R. | TU Dresden | GDR |
| Augustyniak, W. | INR Swierk | Poland |
| Betak, E. | SAS Bratislava | CSSR |
| Blochin, A.I. | PEI Obninsk | USSR |
| Bödy, Z.T. | Kossuth University, Debrecen | Hungary |
| Böhmer, B. | ZfK Rossendorf | GDR |
| Chevarier, N. | INP Lyon | France |
| Christov, Ch.V. | INR Sofia | Bulgaria |
| Dezsö, Z. | Kossuth University, Debrecen | Hungary |
| Dlouhy, Z. | CSAV Rez | CSSR |
| Dünnweber, W. | Universität München | FRG |
| Feldmeier, H. | MPI Heidelberg | FRG |
| Funke, L. | ZfK Rossendorf | GDR |
| Gersch, H.-U. | ZfK Rossendorf | GDR |
| Goel, B. | Kernforschungszentrum Karlsruhe | FRG |
| Gregoire, C. | CEA Saclay | France |
| Guzmen, F. | TU Dresden | GDR |
| Herbach, C. | TU Dresden | GDR |
| Hermsdorf, D. | TU Dresden | GDR |
| Hildenbrand, K.D. | GSI Darmstadt | FRG |
| Hofmann, H. | TU München | FRG |
| Ignatyuk, A. | PEI Obninsk | USSR |
| Janssen, D. | TU Dresden | GDR |
| Josch, M. | TU Dresden | GDR |
| Käubler, L. | ZfK Rossendorf | GDR |
| Kaun, K.H. | ZfK Rossendorf | GDR |
| Klein, H. | PTB Braunschweig | FRG |
| Kumpf, H. | ZfK Rossendorf | GDR |
| Kuminov, B.D. | PEI Obninsk | USSR |
| Lemmel, H.D. | IAEA Wien | Austria |
| Lovtschikova, G. | PEI Obninsk | USSR |
| Mädler, P. | JINR Dubna | USSR |
| Märten, H. | TU Dresden | GDR |
| Magner, A.G. | INR Kiev | USSR |
| Marcinkowski, A.M. | INR Swierk | Poland |
| May, F.R. | ZfK Rossendorf | GDR |
| Meister, A. | TU Dresden | GDR |
| Mihaly, K. | TU Budapest | Hungary |
| Mikheev, V.L. | JINR Dubna | USSR |
| Milek, B. | TU Dresden | GDR |
| Militzer, M. | TU Dresden | GDR |
| Mittag, S. | JINR Dubna | USSR |
| Münchow, L. | ZfK Rossendorf | GDR |
| Muzychka, Y.A. | JINR Dubna | USSR |
| Ortlepp, H.-G. | TU Dresden | GDR |

| | | |
|---|---|---|
| Pausch, G. | TU Dresden | GDR |
| Pfitzner, A. | ZfK Rossendorf | GDR |
| Pilz, W. | JINR Dubna | USSR |
| Prade, H. | ZfK Rossendorf | GDR |
| Reif, R. | TU Dresden | GDR |
| Rusek, K. | INR Swierk | Poland |
| Salnikov, O.A. | PEI Obninsk | USSR |
| Saupe, G. | JINR Dubna | USSR |
| Schmidt, D. | TU Dresden | GDR |
| Schmidt, R. | TU Dresden | GDR |
| Schulz, H. | ZfK Rossendorf | GDR |
| Seeliger, D. | TU Dresden | GDR |
| Seidel, K. | TU Dresden | GDR |
| Shigin, V.A. | Kurchatov Institute Moscow | USSR |
| Sodan, H. | ZfK Rossendorf | GDR |
| Stankiewicz, K. | INR Swierk | Poland |
| Starostov, B.I. | RIAP Dimitrovgrad | USSR |
| Streil, T. | TU Dresden | GDR |
| Teichert, J. | TU Dresden | GDR |
| Trufanov, A. | PEI Obninsk | USSR |
| Tschammer, R. | TU Dresden | GDR |
| Uhl, M. | IRK Wien | Austria |
| Unholzer, S. | TU Dresden | GDR |
| Wagner, V. | JINR Dubna | USSR |
| Zschau, H.E. | KMU Leipzig | GDR |

# THE FORMATION OF LIGHT CHARGED PARTICLES IN THE SYSTEM $^{nat}Ag+^{40}Ar$ (285MeV)

V.L.Mikheev, A.G.Artukh, G.F. Gridnev, M.Gruszecki, W.Karcz, A.N.Mezentsev, L.Pomorski and V.V. Volkov
Laboratory of Nuclear Reactions, Joint Institute for Nuclear Research, Dubna, USSR

Abstract:
The yield of light charged particles ranging from H to C can be divided into two parts: those having a symmetric relative to 90° c.m.angular distribution and particles with an angular distribution growing exponentially with decreasing emission angle in the forward hemisphere. It is assumed that particles with a symmetric angular distribution are formed partly as the initial dinuclear system ion + target nucleus evolves towards complete fusion in collisions with angular momentum $l \lesssim l_{crit}$. Particles having a forward peaked angular distribution are produced in massive transfer processes.

In recent years, in studies of heavy-ion reactions special attention is given to the emission of light charged particles which provide valuable information on the details of interactions between heavy ions and nuclei involved in the processes of both nucleon transfer and complete and almost complete fusion. The present paper deals with the results of studies of emission of light charged particles in the system $^{nat}Ag+^{40}Ar$

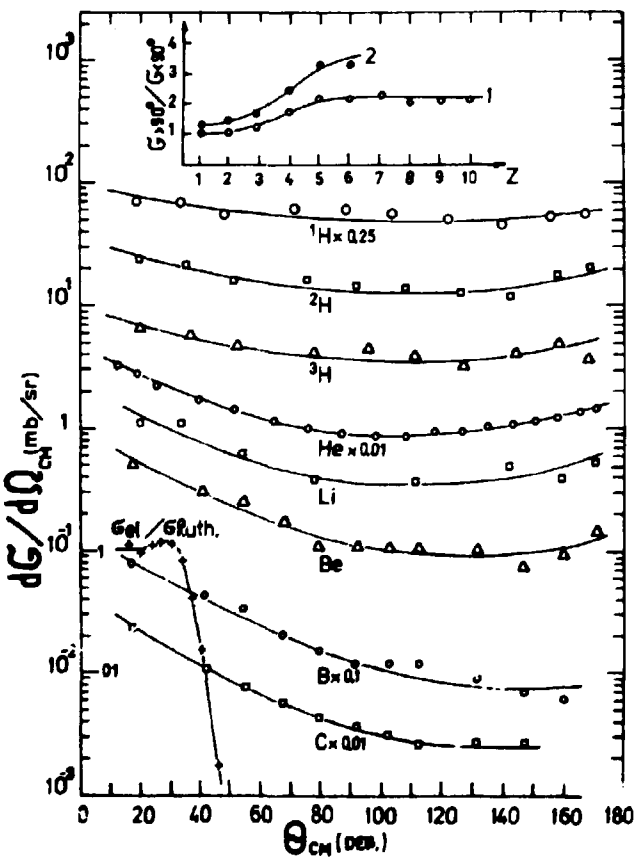


Fig.1. Angular distributions of reaction products from H to C. In the inset curves 1 and 2 give the ratios $\sigma(40°-90°)/\sigma(90°-140°)$ and $\sigma(10°-90°)/\sigma(90°-170°)$, respectively.

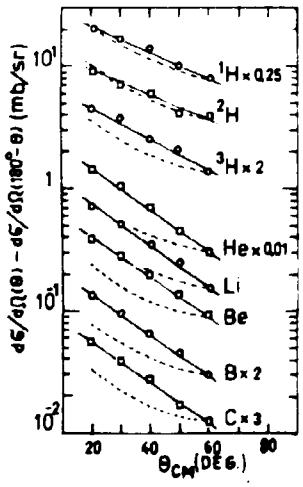


Fig.2. The asymmetric parts of the angular distributions of products from H to C. The dashed lines correspond to 1/sin θ.

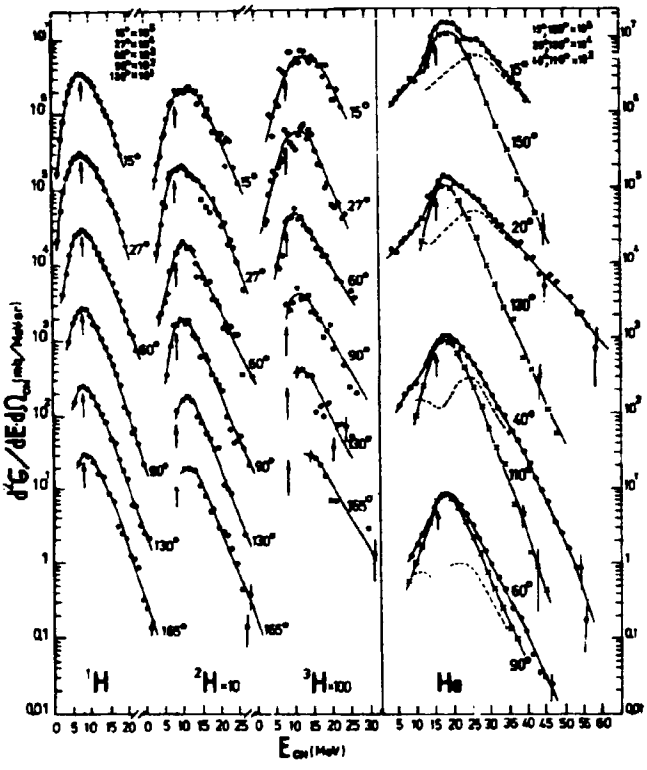


Fig. 3. The energy spectra of $^1$H, $^2$H, $^3$H and He.

(285MeV), carried out at the 310-cm heavy ion cyclotron of the JINR Laboratory of Nuclear Reactions [1,2]. In Fig. 1 are presented the angular distributions of products ranging from protons to carbon nuclei. They can be considered as a superposition of two distributions: one symmetric relative to 90°(c.m.s.) and the asymmetric one contributing to the total yield in the forward hemisphere. The asymmetric parts of the angular distributions are shown in Fig. 2. The energy spectra of $^1$H, $^2$H, $^3$H and $^4$He are given in Fig. 3. The difference between the α-particle spectra at forward and backward angles symmetric relative to 90°(c.m.s.) is showed by dashed lines. The dashed part of the spectra just forms the forward peaked part of the α-particle angular distribution shown in Fig. 2. The energy corresponding to the maxima of the dashed spectra exceeds substantially the value of the Coulomb barrier. The maxima are displaced with changes in the angle of observation. This is typical for a source moving in the system of the common centre of mass.

We also carried out measurements of the angular and energy correlations of two α-particles formed in one interaction. In Fig. 4 there are presented some data on cross sections for the formation of two α-particles in one plane including the beam axis as well as in mutually perpendicular planes. In these measurements one of the α-detector telescopes was placed at an angle of 90° to the beam, while the other was moved from 30° to 128° lab. s. The sign (+) for angles $\theta_2$ of the second telescope in one plane measurements corresponds to a configuration of telescopes on one side from the beam axis, and the sign (-) on both sides. The energy spectra of coincident α-particles, compared with inclusive ones, are presented in Fig. 5. The r.m.s. values of angular momenta obtained from the ratio of cross sections for α-particle coincidences in one plane and in mutually perpendicular planes by using expression (6) from paper [3] are listed in Table 1. Independent angular momentum estimates derived from the α-particle angular distribution in the backward hemisphere by using expression (5.38) from paper 4) give $I_{rms} = 52 \pm 7\hbar$. The critical angular momentum for the system Ag + $^{40}$Ar (285MeV) is equal to about 85ħ. The $I_{rms}$ we obtained for α-particle emitting nuclei are much smaller than $l_{crit}$. Hence it follows that deep inelastic nucleon transfer reactions proceeding at angular momenta close to

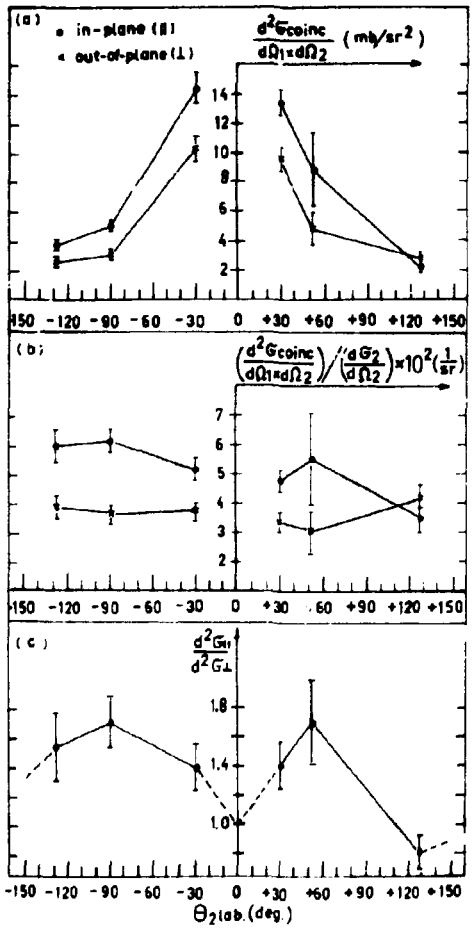


Fig.4. (a) Differential cross sections for the formation of two coincident α-particles with telescope 1 located at an angle of 90° to the beam and at different positions of telescope 2.
(b) the differential multiplicity of coincident α-particles.
(c) the ratio of differential cross sections for the formation of coincident α-particles emitted in one plane and in mutually perpendicular planes.

Table 1

Angular momentum estimates derived from the ratio between coincidences in one plane and in mutually perpendicular planes

| $\theta_2$, degrees | $d^2\sigma_{\parallel}/d^2\sigma_{\perp}$ | $I^{*}_{rms}$, ħ | $I^{**}_{rms}$, ħ |
|---|---|---|---|
| +30 | 1.41±0.16 | 36±7 | 53±10 |
| -30 | 1.40±0.16 | 36±7 | 53±10 |
| +52 | 1.72±0.32 | 46±10 | 47±10 |
| -90 | 1.70±0.18 | 46±5 | 46± 5 |
| +128 | 0.81±0.13 | - | - |
| -128 | 1.54±0.23 | 41± 9 | 64±15 |

* The reaction plane is set by the beam axis and telescope 2.

** The reaction plane is set by the beam axis and telescope 1.

$l_{crit}$ do not contribute substantially to the yield of coincident α-particles. It should be noted that coincident α-particles give about 90% of the yield of inclusive ones. From all the data obtained by us it follows that the heavy fragment similar to a compound nucleus formed in complete fusion is the main source of α-particles with a symmetric relative to 90° (c.m.s.) angular distribution. However the yield of α-particles with a symmetric angular distribution exceeds that expected on the basis of the statistical evaporation model. This can be caused by an increase in the α-particle transmission coefficients in taking into account the deformation of nuclei with high angular momenta [5]. This effect, however, depends sharply on the value of angular momentum and should be most pronounced only at $l \gtrsim l_{crit}$. Therefore we believe that an enhanced α-particle yield can be associated with the decay of the α-cluster configuration of the dinuclear system 1,6). Such a configuration can be formed in the process of nucleon transfer in the initial projectile + target system as it evolves in the direction of complete fusion at angular momenta $l < l_{crit}$. From this point of view a substanial part of α-particles with a symmetric relative to 90° c.m. angular distribution is emitted by the nucleus prior to the establishment of full statistical equilibrium. This agrees with some experimental results presented in 1), in particular, with the high nuclear temperature value determined from the slope of the α-particle energy spectra.

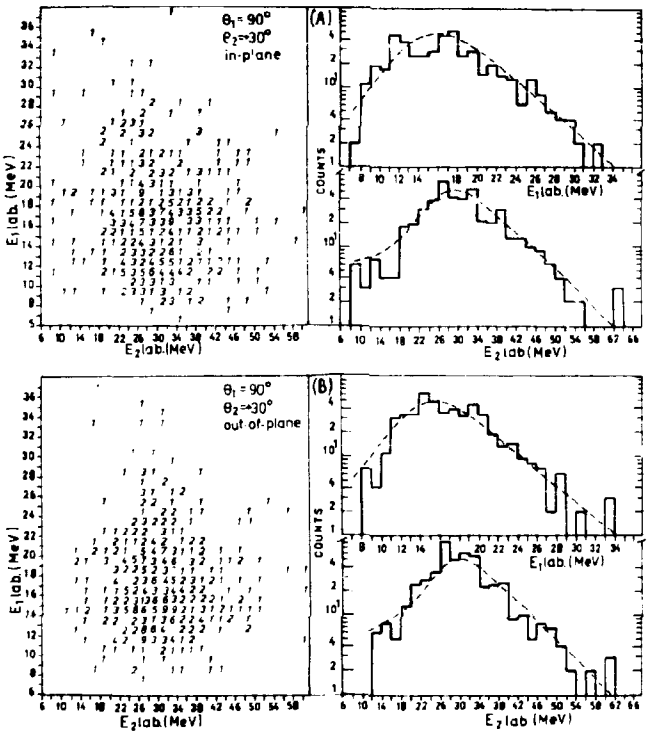


Fig.5. Energy spectra of coincident α-particles for $\theta_1=90^\circ$ and $\theta_2=+30^\circ$ with telescopes placed in one plane (A) and in mutually perpendicular planes (B). On the spectra projektions the histograms show data for coincident α-particles, the dashed lines stand for inclusive α-particles.

The low probability of coincidences of α-particles as they are emitted on one side of the beam at backward angles and in one plane (see Fig.4) can serve as additional evidence for the nonequilibrium emission of α-particles.

At an angle of 30° about 40% of α-particles are relatively energetic contributing to the forward peaked distribution. We have detected the coincidence of these α-particles with those emitted by the heavy reaction product. Thus evidence has been obtained for their formation in processes involving the capture of the main part of the ion in the target nucleus, termed as "massive transfers" 7).

The energy spectra and angular distributions of reaction products ranging from H to C are of the same kind qualitatively. Therefore it is possible to assume that the mechanisms of their formation are similar to those of forming α-particles in the case of both symmetric and forward peaked angular distributions.

## References


1. A.G. Artukh, G.F.Gridnev, M.Gruszecki, W.Karcz, A.N.Mezentsev, V.L.Mikheev, L.Pomorski, A.Popescu, D.G.Popescu, V.V.Volkov, Z. Phys., A 303 (1981) 41.
2. A.G. Artukh, V.V. Avdeichikov, G.F. Gridnev, M. Gruszecki, W.Karcz, A.N. Mezentsev, V.L. Mikheev, V.M.Morozov, L.Pomorski, A.Popescu, D.G.Popescu, V.V.Volkov, Preprint JINR P7-82-707, Dubna, 1982.
3. R.Babinet, B.Cauvin, J.Girard, J.M.Alexander, T.H.Chiang, J.Galin, B.Gatty, D. Guerreau, X. Tarrago, Z. Phys., A 295 (1980) 153.
4. T. Ericson, Advances in Physics, 9 (1960) 425.
5. M. Blann, Phys. Rev. C 21 (1980) 1770.
6. V.V. Volkov, Izv. Akad. Nauk USSR, ser. Fiz., 45 (1981) 1810.
7. D.R.Zolnowski, H. Yamada, S.E. Cala, A.C. Kahler, T.T.Sugihara, Phys. Rev. Lett., 41 (1978) 92.

# FAST PROCESSES IN HEAVY ION REACTIONS AT INCIDENT ENERGIES OF 15 MeV/u

K.D. Hildenbrand
GSI Darmstadt, Federal Republic of Germany

## 1. Introduction

Experiments which investigate reaction mechanisms in deep inelastic collisions between heavy nuclei were restricted in the past to incident energies up to a few MeV/u in excess of the Coulomb barrier. In this energy regime the relative velocity of the colliding nuclei stays well below the Fermi velocity of the nucleons. That is why the reactions proceed to a large extent adiabatically: Most of the internal degrees relax during the reaction time and the di-nuclear complex as a whole reacts on all the constraints imposed by e.g. available energy, driving forces or angular momenta. The dissipative character of practically all the involved processes is accounted for best by the expression 'dissipative collisions'[1].

It seems interesting to speculate how this picture will change if the bombarding energy is increased. The adiabaticity certainly will be reduced, but it is not yet clear in which experimental features this might result. If the energy is dissipated locally in space an enhanced emission of neutrons or light charged particles might show signatures different from those of sequential evaporation. At the same time the increased momentum of the coherent motion of the projectile nucleons might reduce the incoherent particle-hole excitation (which seems to dominate the energy-loss mechanism at lower energies[1] in favour of the excitation of collective modes which in turn could couple to different exit channels. The latter aspect certainly is the more important the more massive the colliding ions are. As conclusion one can say that the step to higher energies is connected with the expectation of finding signatures for any kind of preequilibrium or fast processes.

Three years ago we performed at 12 MeV/u (the highest energy available at that time) a first exploratory experiment; a $^{86}$Kr beam was used to bombard different targets like $^{89}$Y or $^{166}$Er. A surprisingly high probability for the projectiles to undergo a fragmentation into two massive products was found[2]. The availability of even higher energies has refocussed our interest onto this energy regime. After the upgrading program of the UNILAC in Darmstadt has been completed successfully[3], beam energies up to 17 MeV/u even for U-ions can be routinely handled; for medium-mass projectiles the maximum energy is even higher, 22 MeV/u seem to be possible for Ar ions[4].

In the next chapter I will briefly describe how our experimental set-up was improved in order to allow for kinematically complete experiments. The following chapters are devoted to results of our first experiments: In chapter 3 coincidence measurements between binary reaction products and α-particles in the reaction $^{98}$Mo + $^{154}$Sm at 12 MeV/u are described; chapter 4 discusses charge- and mass distributions at low energy losses, chapter 5 velocity and charge distributions of ternary fragments at high energy losses. There the main emphasis is laid on the results of the system $^{92}$Mo + $^{92}$Mo at 14.7 MeV/u.

## 2. Experimental set-up

At higher incident energies three- and even four-body processes are expected to become increasingly significant (the term two-, three- or four-body is used to specify the number of heavy fragments in the exit channel). For this reason our set-up, which originally was designed and optimized for the detection of two-body processes has been modified; some of the

components which are of relevance for the results to be discussed are briefly described in the following:

1) A large-area position-sensitive ionisation chamber (IC) with a parallel-plate timing counter in front is flanged to a spherical scattering chamber of 130 cm diameter; it can be moved around the target and determines the energy loss, the energy and the velocity a d thus the nuclear charge and the mass of the products.

2) Inside the scattering chamber 12 position sensitive parallel-plate counters with an active area of 20x30 $cm^2$ are mounted. They determine the velocity vectors of the products; the resolution is 4 mm both in x and y, the time resolution about 0.8 ns.

3) A series of solid state telescopes is used for the identification of light charged particles.

Fig.1 shows on the left a view along the beam axis into the scattering chamber. The extent to which the counter array covers the foreward hemisphere can be inferred from picture on the right: It shows a singles' measurement from a calibration run with Mo on Au at lower energies. The representation is chosen in a way to project the unity space vector of each event on a plane placed perpendicular to the beam direction. This corresponds to a photography along the beam axis taken from infinity. Depending on the position of the ionisation chamber one of the counters A, B, or E is moved downwards to open a slit by which the IC looks onto the target. On the photo counter A actually is in its lower position.

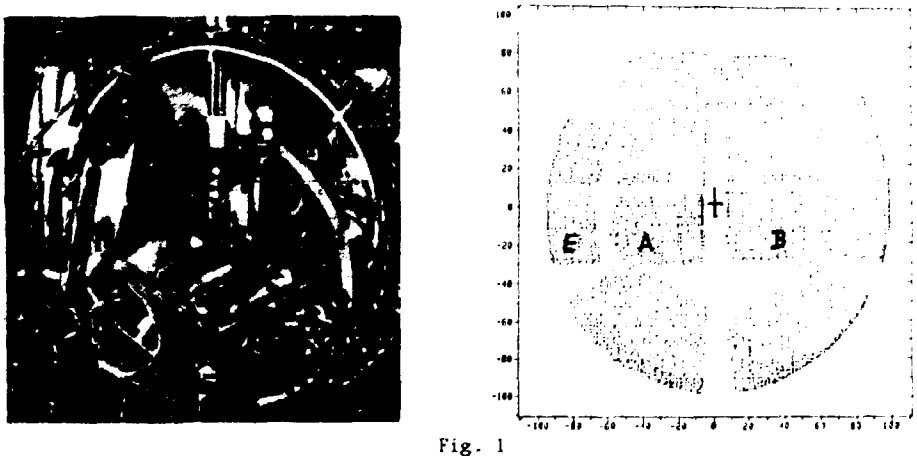


Fig. 1

Left: Photo of the array of position-sensitive parallel plate counters mounted inside the spherical scattering chamber. Right: Reconstruction of the fragments' position measured in an inclusive experiment (see text).

Although two-, three- and four body processes can be reconstructed from the measured velocity vectors alone, the described detection system is designed to measure also charge and mass of one of the outgoing products by means of the ionisation chamber. This offers the following advantages:

a) The full (N,Z)-distribution of the products can be determined what is of particular interest at small energy losses, and

b) the kinematic reconstruction can be improved in cases of ambiguities (e.g. when in a three-body reaction the C.M.-velocity vectors are aligned).

In addition, the ionisation chamber covers (in comparison to the parallel-plate counters) a broader dynamical range which will be important for the discussion of the fragment mass distribution in chapter 5.

Using the new set-up we performed two measurements: (i) The reactions $^{86}Kr$ on $^{166}Er$ and $^{98}Mo$ on $^{154}Sm$ were measured at 12.5 and 12 MeV/u, respectively, (ii) recently beams of $^{92}Mo$ and $^{98}Mo$ were used to bombard at 14.7 MeV/u targets of $^{92}Mo$, $^{98}Mo$, $^{147}Sm$, $^{154}Sm$ and $^{238}U$. As already pointed out I will restrict in the following to some selected results.

### 3. Preequilibrium light particle emission

At present direct evidences for preequilibrium light particle emission in collisions between heavy nuclei (A≥80) are very scarce. To our knowledge the best founded evidences for neutron emission prior to equilibration were obtained Tserruya et al.[5] in the $^{86}Kr$ + $^{166}Er$ reaction at 11.9 MeV/u. The left part of Fig. 2 shows the experimental set-up with an array of neutron detectors surrounding the target. Two of those which are placed behind the light and heavy fragment detector are used as reference counters to obtain the spectra of neutrons evaporated from the respective fragments. Using this information the yield and the spectra for all other counters can be calculated and compared to the measured ones. This comparison is shown on the right side of the figure: At forward angles close to the light fragment direction a component is left over which is not understood in the frame of the evaporation calculations; it is explained by a simple model which assumes a 10 % component of the neutrons being knocked out at an early stage of the reaction.

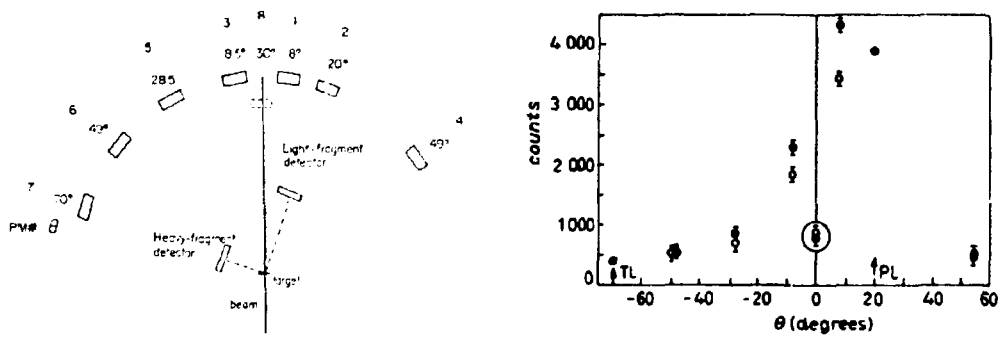


Fig. 2
Data of Tserruya et al. (Ref. 5): Using the set-up of particle detectors and neutron counters sketched on the left, the existence of a preequilibrium component is demonstrated in the reaction Kr+Er at 11.9 MeV/u by a comparison of measured (black points) and calculated (open points) neutron yields (see text).

The results on light charged particles are even more scarce than the ones on neutrons. Therefore in the run at 12 MeV/u we have performed a measurement[6] of the α-particles emitted in coincidence with the binary products in the reaction $^{98}Mo$ + $^{154}Sm$. The velocity vectors of the two heavy products were measured using the set-up of parallel-plate counters while the α-particles were identified by a solid state telescope placed at 20°. The binary events were selected by requiring coplanarity in the laboratory and collinearity in the CM-system (see Fig.3a). The kinematical reconstruction shows that the majority of the events is associated with TKE losses of several hundred MeV (Fig.3b). In the energy spectrum of the α-particles (Fig.3c) two components are seen, one peaked around 15 MeV, the other around 80 MeV. The gross structure of this spectrum can be understood in terms of evaporation of α-particles as can be inferred from Figs.3d and e. The measured yield is shown in contour plots as function of the α-particle velocity $v^{\alpha}$ and emission angle $\theta^{\alpha}$ for two different frames of reference: In Fig.3d the CM-system of α and projectile-like fragment and in Fig.3e the CM-system of α and target-like fragment. Projectile- and target-like products were defined according to their

laboratory velocities; the faster fragment was assumed to be projectile-like. The dashed bands within the plots mark the range of velocities calculated for α-particles evaporated from the respective reference particles. The absence of events beyond $\theta_{cm} \sim 100°$ is attributed to geometrical cuts. Altogether we do not find it possible to judge about the existence of other possible i.e. preequilibrium components in the α-spectra. This statement is still to be supported by Monte-Carlo simulations which are based on the experimental knowledge of angular and velocity distributions of the α-emitting heavy products, but it is already clear that the available energy is not yet sufficient to promote charged particles into the continuum with a significant probability. Within the present poor statistics a 10 % contribution as observed in the neutron measurements could hardly be detected.

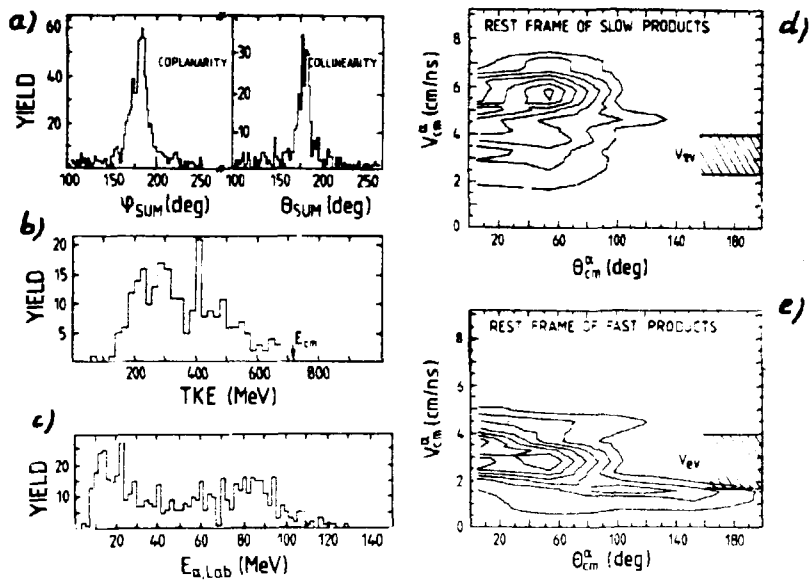


Fig. 3: Coincidences between α-particles (measured at 20°) and two heavy "binary" products measured in the parallel plate counters.

## 4. *Mass and charge distributions at low energy losses*

The search for neutrons or light charged particles which get lost in early stages of the reaction can be done in an alternative way, namely by looking onto the charge and mass distribution of the heavy reaction products at low energy losses. The choice of a system where target and projectile are identical offers the advantage that for binary processes the primary distributions have to stay symmetric with respect to the initial charge or mass regardless of the energy loss. That is why I will concentrate in the following on results of the $^{92}$Mo + $^{92}$Mo system which was measured at 14.7 MeV/u; these nuclides are rather neutron-poor so one might expect that -if present at all- the loss of charged particles might be enhanced e.g. in comparison to the system $^{98}$Mo + $^{98}$Mo which was studied as well.

In an inclusive experiment, where only secondary quantities are measured the data have to be corrected in order to arrive at the primary distributions. This has been done in the past by an event-by-event conversion which in a two-step iteration corrected for the neutron evaporation only. The appliance of his method to the inclusive results of the system under investigation lead for already moderate energy losses to Z-distributions with maxima definitely below the projectile charge, which were not compatible with evaporation calculations[7]. This made us tentatively postulate a non-understood drift at these high incident energies[8].

In the present case the reaction is overdetermined since velocities and angles of both binary partners have been measured as well. If the assumption holds that neither velocity nor angle of

a product changes on the average as a result of sequential particle emission, one can derive in different ways the primary distributions more directly. These, however, looked different from the inclusive results; it turned out that the two-step iterative procedure is no longer adequate at higher energies; an additional mistake is introduced by neglecting the charged particle evaporation.

We therefore performed a full multi-step iterative correction both for neutrons and protons, based on the predictions of the evaporation code CASCADE[7]. These calculations are believed to be reliable up to excitation energies of 100 MeV. The results are displayed in Fig. 4 as $d\sigma^2/dTKE.dZ$; this spectrum looks now the same regardless whether measured energies or velocities were used in the reconstruction of TKE. For the first 200 MeV of energy loss the distributions in Z stay symmetric and are centered around Z=42 of Mo. As a consequence one has to say that the formerly seen drift can be fully understood by sequential evaporation; no evidence for preequilibrium decay is to be seen in this range of energy losses.

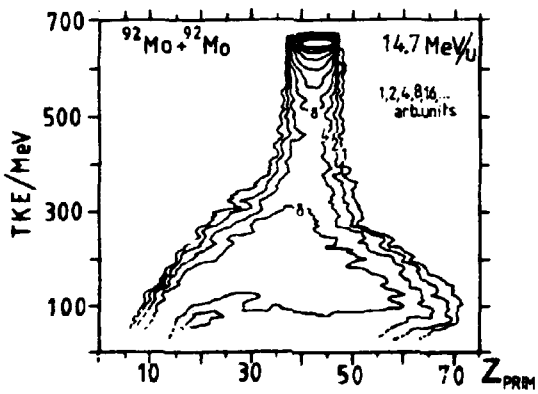


Fig. 4: $d^2\sigma/dTKE.dZ$, inclusive results, iteratively corrected for particle evaporation.

## 5. Splitting into more than two fragments

At higher energy losses the Z-distributions shown in Fig. 4 widen up and become apparently skewed which is caused by three- (and possibly four-) body events. As already observed in the first experiments at higher energies[2] these processes have an unexpectedly large probability which has given raise to the name 'splitting'. Glässel and v. Harrach et al.[9] have shown in the meantime by a complete reconstruction of three-body events in the Xe+Sn reaction that this formerly undetected process really must be regarded as being intermediate between three-body break-up and a sequential process.

In order to get rid of the bias of a reconstruction on the basis of two-body kinematics we prefer to use in the following the product velocity in the CM-system instead of TKE. Fig. 5a shows the inclusive distribution $d^2\sigma/dv_{cm}.dZ$; in Fig. 5b two-body events have been selected by requiring coplanarity, non-coplanar i.e. three-body events have been picked out by asking for coincidence with one of the parallel plate counters mounted out of plane (Fig.5c). The dashed line V represents the expected velocities of deformed binary fragments due to Coulomb repulsion (Viola energy). The two-body condition selects events extending mainly below the values for velocity and nuclear charge of the projectile and ranging down to the fully relaxed events along the V -line. The three-body events are mainly located below the V -line with broad velocity distributions especially for light elements: They correspond to products emitted forwards resp. backwards in the moving frames of the primary products.

A striking feature common to the three body and to the inclusive data is the long tail of the Z-distribution towards small Z-values as it can be seen best from the projected Z-spectra of Fig.5c resp. 5a. This component could only be observed after both the ionisation chamber and its parallel counter had been run in a way to detect light, fast particles down to at least carbon; the identification is done using the $\Delta E$ vs. $v_{lab}$ correlation of these fragments. In the light of these new results we have to assume that the mass (or charge) distribution of the

splitting fragments is much broader than expected from earlier measurements[2,9]. The question which role these light fragments play in the process can certainly not be answered before a complete reconstruction for the full spectrum of splitting products is achieved.

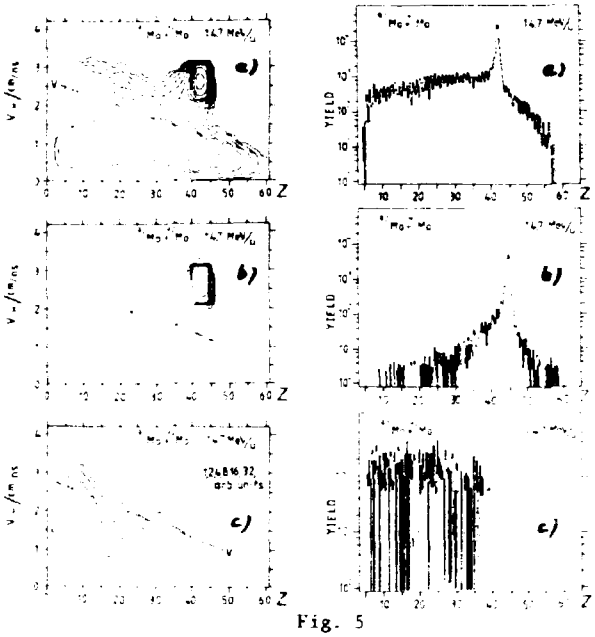


Fig. 5

Results of $^{92}Mo+^{92}Mo$ at 14.7 MeV/u. Left side: Contour plots $d^2\sigma/dZ\,dv^{cm}$; right side: Integrated element distributions. The spectra a) show inclusive data, spectra b) events with coplanarity condition ($\Delta\vartheta = \pm 2°$) and the spectra c) non-coplanar events.

## 5. Conclusions

The results of our experiments at energies up to 15 MeV/u did not show until now any conclusive evidence for fast processes as far as the emission of light charged particles is concerned. The 3-body break-up (called splitting) which is well established in the fully relaxed region probabely plays a role also at already lower energy losses. Recent results from the $^{58}Ni+^{58}Ni$ system at 15.1 MeV/u seem to support this assumption[10]. Nevertheless we need further experiments to really prove this process to be fast i.e. to be connected with the high incident velocity.

The experiments described in this talk were carried out at Darmstadt in a collaboration of R. Bock, M. Dakowski (Inst. of Nuclear Research, Swierk, Poland), A. Gobbi, G. Guarino (now at LBL Berkeley), S. Gralla, K.D. H., U. Lynen, W.F.J. Müller, A. Olmi, M. Petrovici (IPNE Bucharest, Romania), G. Rudolf (Univ. de Strasbourg, France), H. Sann, H. Stelzer, J. Töke (Univ. of Warsow, Poland) and H.J. Wollersheim.

## References

1. A. Gobbi and W. Nörenberg, in: Heavy Ion Collisions Vol.II, (ed. R. Bock), North Holland, Amsterdam
2. A. Olmi et al., Phys. Rev. Lett. 44 (1980) 383
3. D. Böhne, Annual Report, GSI 1981, p. 283
4. N. Angert, GSI-Nachrichten 10-82
5. I. Tserruya et al., Phys. Rev. Lett. 47 (1981) 16, and to be publ.
6. S. Gralla et al., Annual Report, GSI 1981, p. 25
7. F. Pühlhofer, Nucl. Phys. A280 (1977) 267
8. M. Petrovici, Nucl. Phys. A387 (1982) 313c
9. P. Glässel et al., Phys.Rev. Lett. 48 (1982) 1089
   D.v.Harrach et al., Phys.Rev. Lett. 48 (1982) 1093
10. F. Plasil, Contrib. Intern. Conf. on Nucleus-Nucleus Collisions, East Lansing, Michigan, Sept. 1982

# EMISSION OF HIGH-ENERGY CHARGED PARTICLES IN HEAVY-ION REACTIONS

Yu.A. Muzychka, B.I. Pustylnik, Yu.E. Penionzhkevich
Joint Institute for Nuclear Research, Dubna, USSR

In recent years a rapidly growing interest has been shown in the studies of the processes accompanied by the emission of non-equilibrium light charged particles. In particular, this interest is associated with the fact that light charged particles carry information on the time evolution of this process, beginning from the initial stage of the collision to the decay of the compound nucleus. Initially, $\alpha$-particles emitted with velocities not exceeding the projectile ion velocity were investigated, but the recent rapid development of experimental technique has made it possible to measure the spectra of light charged particles at the limiting energies determined by the process kinematics.

The use of a $\Delta E$-E telescope placed in the focal plane of a magnetic spectrometer located at an angle of $0^{\circ}$ to the beam allowed one for the first time to detect light charged particles ranging from hydrogen to beryllium isotopes with energies close to the kinematical limit for the corresponding two-body exit channel [1,2] (see Figs. 1 and 2). Measurements have been performed of the spectra of charged particles produced by bombarding Th, Au and Ta targets with Ne and Ar ions. Angular distribution measurements have shown that fast charged particles have the maximum yield at $0^{\circ}$ to the beam, rapidly decreasing with increasing observation angle.

At present there are fairly many theoretical models proposed to explain the emission of fast charged particles. However, the presently available experimental data are insufficient to give preference to any of them. Moreover, different mechanisms can contribute to various parts of the spectrum. All the models suggested can be divided roughly into two groups: direct reactions (stripping, knock-on, etc.) and pre-equilibrium processes. The first group of models considers peripheral collisions and the residue compound nucleus is expected to have an angular momentum near $\ell_{gr} - \ell_{\alpha}$, where $\ell_{gr}$ is the grazing angular momentum, and $\ell_{\alpha}$ is the average angular momentum carried off by the fast particle. In the second case where the central collisions are considered the angular momentum of the residual nucleus is considerably smaller.

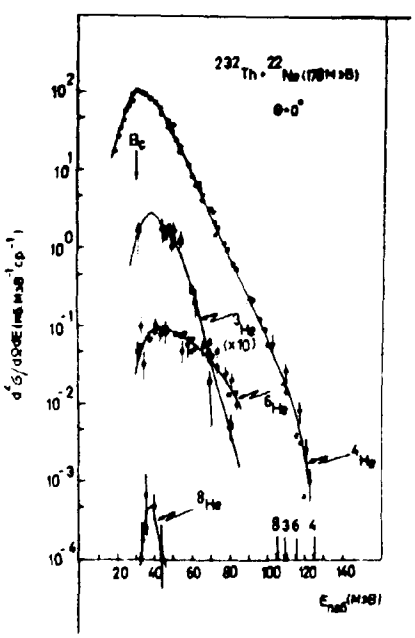


Fig.1. Energy spectra of the He isotopes measured in the $^{232}Th+^{22}Ne$ (178MeV) reaction.

The problem of the magnitude of the angular momentum of the nucleus remaining after fast particle emission is essential not only for the clarifica-

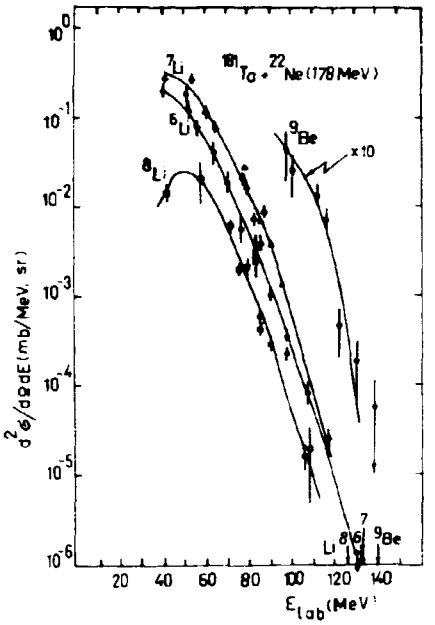


Fig.2. Energy spectra of the Li and Be isotopes measured in the $^{181}$Ta + $^{22}$Ne (178MeV) reaction.

tion of the reaction mechanism leading to the transfer of a large amount of energy to the light particle, but also in terms of the possible production of "cold" nuclei in reactions involving the emission of energetic $\alpha$-particles.

To obtain information on the angular momentum magnitude and clarify the mechanism of fast $\alpha$-particle formation it is necessary to investigate not only the characteristics of the $\alpha$-particles themselves (their energy spectra and angular distributions) but also the states in which the nucleus remains after the emission of a fast $\alpha$-particle. This can be achieved by measuring the excitation functions of $\alpha$ x n reactions at high bombarding energies, the yields and angular distributions of fission fragments in coincidence with fast $\alpha$-particles, and by studying the spectra and angular distributions of secondary $\alpha$-particles and protons. Finally, a very valuable information can be provided by measurements of the spectra and multiplicities of $\gamma$-rays in coincidence with fast charged particles and the simultaneous identification of the $\gamma$-ray emitting nuclei.

It, however, should be emphasized that the problem under consideration is a very complicated one, and each of the above-mentioned experiments has its own limitations and difficulties.

One of the possibilities indicated above was realized in measuring the excitation functions of the reaction $^{176}$Lu ($^{22}$Ne, $\alpha$ x n) in a wide Ne ion energy range, from 5 to 10MeV / nucleon, with the separation of the exit channels $\alpha 0$n, $\alpha$1n, ...$\alpha$4n by detecting the final products [3] (see Fig.3). By making the natural assumption that fast $\alpha$-particle emission leads to the formation of a compound nucleus with mass $(A_1 + A_2 - 4)$, charge $(Z_1 + Z_2 - 2)$, the set of initial excitation energies determined from the experimental spectrum of fast $\alpha$-particles and some initial angular momentum distribution determined by the distribution of momenta in the entrance channel and the average momentum carried away by an $\alpha$-particle and using the formulae of the statistical theory of nuclear reactions we have analysed the experimental excitation functions obtained. The maximum value of the residual nucleus angular momentum was the only free parameter. In order to fit the experimental excitation functions to the calculated ones it turned out necessary to assume that after the emission of a fast $\alpha$-particle the compound nucleus remains in a state with high angular momentum $\ell \sim 50 - 60$ at $^{22}$Ne ion energies between 180 and 210MeV, which corresponds to momentum values of $80 - 90\hbar$ in the entrance channel. And one can conclude that peripheral collisions occurring in the entrance channel play an essential role in the mechanism of fast $\alpha$-particle formation. It is natural

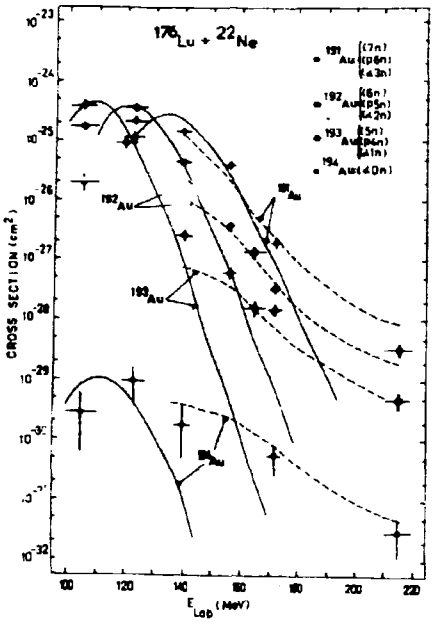


Fig.3. Excitation functions in the $^{22}$Ne + $^{176}$Lu reaction.

that this way of deriving information on the magnitude of angular momentum cannot be regarded as the only unambiguous and reliable method.

The $\gamma$-multiplicity studies also encounter certain difficulties. The $\gamma$-multiplicity measurements allow one to study the distribution of the residue angular momentum after the termination of the neutron cascade. The transition from these quantities to the parameters characterizing the range of orbital momenta in the entrance channel is neither simple nor straightforward, especially for nuclei that fission readily at high excitation energies and large angular momenta. We have calculated the distribution of the residual angular momentum after the neutron cascade which accompanied the emission of a fast $\alpha$-particle in the reaction $^{22}$Ne (165 MeV) + $^{181}$Ta. The average multiplicity of $\gamma$-rays in coincidence with fast $\alpha$-particles was measured in this reaction and the limiting value for the orbital momentum in the entrance channel, equal to 43 was obtained (ref.4). This value is considerably smaller than those corresponding to peripheral collisions. It should be noted that that experiment was carried out without separation of concrete channels of compound nucleus decay.

The calculations were performed in terms of the statistical theory of nuclear reactions. In the calculations neutron, proton and $\alpha$-particle evaporation and fission were taken into account. The calculations demonstrate that fission occuring at all stages of the evaporation cascade plays a crucial role in the formation of the momenta distribution preceding $\gamma$-ray emission. For $\ell > 50$ and excitation energies $E^* > 70$MeV (i.e. $E_\alpha < 65$MeV) fission constitutes the main channel of decay, thus "eating away" the residual momentum distribution at large values. As a result of the neutron cascade, the momentum distribution is transformed from the "triangular" (as it was in compound-nucleus formation) to a broad one with a plateau (see Fig.4).

The average value of the residue momentum $\ell_{res}$ depends on the $\alpha$-particle energy rather strongly since the latter determines the initial excitation energy of the excess nucleus and, consequently, the number of the neutrons evaporated. On the other hand $\ell_{res}$ depends weakly on the maximum momentum of the nucleus after $\alpha$-particle emission and this complicates substantially the establishment of the initial limiting momentum by measuring the average $\gamma$-ray multiplicity. In this context, the $\ell_{max}$ obtained in ref.[4] can be viewed upon as only a rough estimate for the lower limit of the $l_{max}$, the more so as the quite possible cases of the three-body exit channel will decrease substantially the average $\gamma$-ray multiplicity being measured.

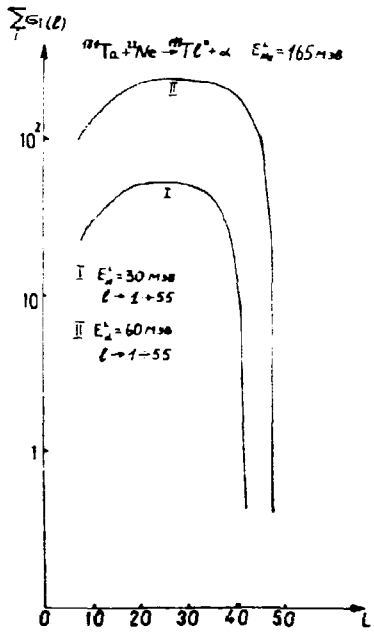


Fig.4. The distributions of the residual angular momentum at two α-particle energies.

It should be noted that more sensitive would be an experiment in which the γ-ray multiplicity would be determined for the separated products corresponding to the evaporation of a certain number of nucleons, rather than for all the compound-nucleus decay channels taken together.

Wide possibilities for solving this problem are offered by measurements of the fission cross sections and angular distributions of fragments in coincidence with a fast α-particle. The angular distributions carry some information on the distribution of momenta in the compound nucleus formed.

By measuring the fission cross section as a function of α-particle energy it is possible to give an answer to the extremely important question concerning the reaction mechanism, namely, what is the exit reaction channel - a two-body or three-body one. In the case of a two-body exit channel both the excitation energy and the $Z^2/A$ parameter of the heavy fragment will substantially exceed those for the three-body case. Consequently, the fragment yield per α-particle will also be considerably larger. Calculations demonstrate that combinations of lead and bismuth targets with $^{22}Ne$ and $^{18}O$ ions may prove to be most convenient for this purpose. In going to the lighter targets the fragment yield per α-particle becomes small for the two-body exit channel as well. For the heavier targets (Th or U) the fission fragments yield will be already large also in the case of the three-body exit channel, since the target nuclei themselves have a relatively low fission barrier. For the reaction $^{209}Bi + ^{22}Ne$, about 80% of the events of α-particle emission are expected to be accompanied by the fission of the heavy fragment in the case of the two-body exit channel.

References

1. C. Borcea et al. Nucl. Phys. A 351 (1981) 312.
2. C. Borcea et al. Nucl. Phys. A 391 (1982) 520.
3. H. Bruchertseifer et al. Jadernaja Fizika 33, 1453 (1981).
4. V.V. Kamanin et al. JINR Communication, Dubna, 7 - 726 (1981).

# PREEQUILIBRIUM EMISSION IN THE REACTION $^{14}N + ^{27}Al$ AT 100 MeV

R. Billerey, C. Cerruti, A. Chevarier, N. Chevarier, B. Cheynis, A. Demeyer, M. Stern and M.N. Namboodiri(*)

Institut de Physique Nucléaire (et IN2P3) -- Université Lyon-I
43, Bd du 11 Novembre 1918 - 69622 Villeurbanne Cedex (France)

Several studies of heavy ion reactions have been made recently where light particle-heavy fragment coincidence techniques have been employed to explore the existence of non-equilibrium phenomena. In this paper, we report the results obtained on the $^{14}N + ^{27}Al$ system at 100 MeV incident energy. The measurements have been performed at the isochronous cyclotron of the Institut des Sciences Nucléaires at Grenoble. We shall first give the schematic feature of what we mean by preequilibrium emission. The experimental data and their analysis will be split in three parts : reaction mechanisms observed in N + Al system, preequilibrium emission in fusion and deep inelastic process.

## I. Preequilibrium emission

Reactions induced by light projectiles have been interpreted quite successfully in terms of precompound models based on successive two body interactions. The schematic diagram is the following :

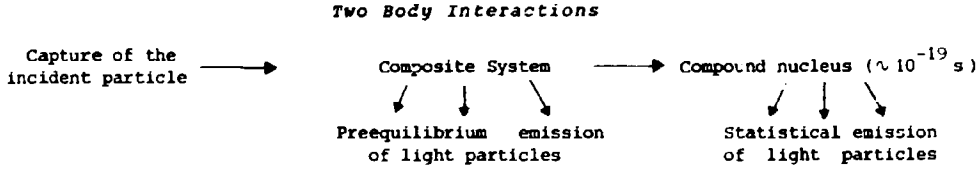


The experimental evidence of preequilibrium emission : high energy spectra component and forward peaked angular distribution was obtained by comparison of experimental data with statistical evaporation theory prediction. The N(100 MeV)+Al reaction is characterized by competition between fusion and deep inelastic collisions. When we expect to observ preequilibrium emission, we expect the diagram to be :

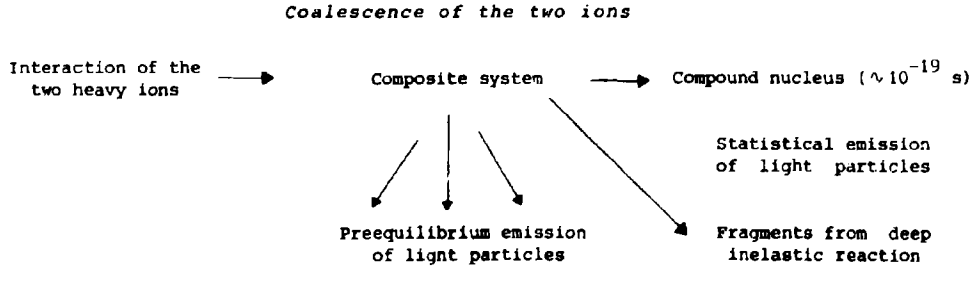

The time resolution of coincidence measurements being around 100 ps, we observ light particles in coincidence with either evaporation residues or deep inelastic fragments in their lower excitation states. The coincidence measurements have been performed using two telescopes. The heavy ion telescope (a ΔE gaz - ionization chamber followed by a 400 μm solid state detector) is placed at fixed laboratory angles either $\theta_{HI} = -10°$ or $\theta_{HI} = -30°$. The light particles telescope ( a 3solid state detectors system) is moveable in and out of the reaction plane for positive and negative angles. The charge identification obtained for heavy fragments is show in figure 1, the elements $Z \geq 10$ are considered to be mostly evaporation residues and $3 \leq Z \leq 10$ to be light fragments from inelastic reactions.

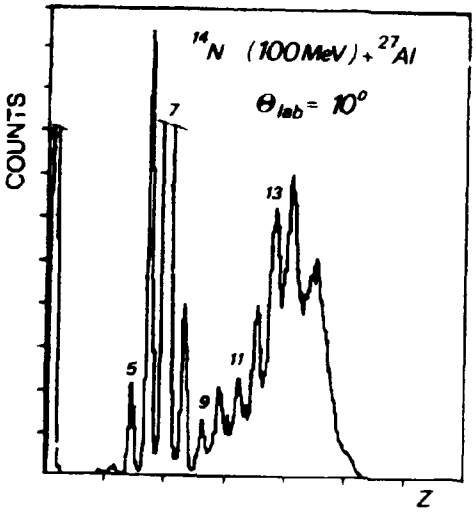


Figure 1

II. Reaction mechanism observed in N + Al system

The measured fusion cross section[1] $\sigma_{fusion} = 830 \pm 150$ mb leas to a $\ell_{crit} = 27 \pm 2\hbar$
The evaporation residues (E.R.) distribution is well reproduced by an evaporation code calculation with $\ell_{crit} = 27\ \hbar$.

From fragment-fragment correlation[2] we learn that most of the deep inelastic collisions are followed by light particle evaporation from the target like fragment. An example is given figure 2. The angular distribution for carbon ions in coincidence with heavy fragments observed at -30° is shown in the upper part. The charge distribution of fragments which are observed in coincidence with carbon are plotted in the lower part of the same figure. These fragment distributions are compared with predictions of statistical calculations. We determine the total excitation energy from two body kinematics and assume this excitation to be shared by the two initial DI fragments ($^{12}C$ and $^{29}Si$) according to their mass ratio. The calculated distribution are shown as solid curves. The agreement is good, the gross features of HI-HI angular correlation are well explained by evaporation from the relaxed target like DIC fragment. In such process their are no kinematical restriction for particle emission at backward angles. Consequently such emission cannot be discriminate from fusion evaporation in inclusive light particle measurements.

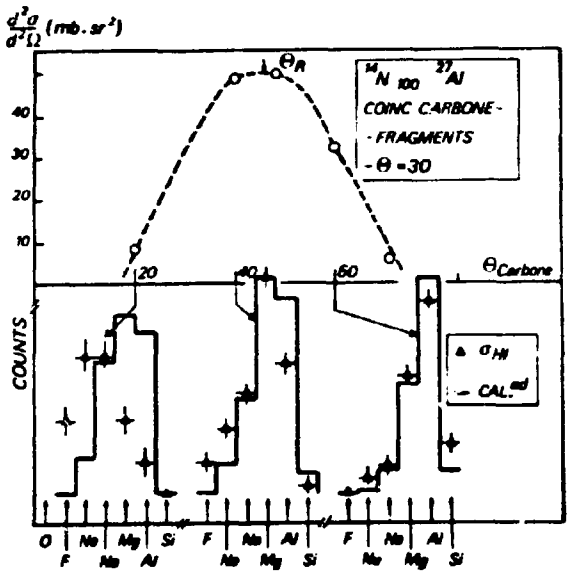


Figure 2

The inclusive measurements of light particles emission show a high energy component of α-spectra which cannot be explained by statistical emission. The inclusive center of mass angular distribution of H and He are fiven in figure 3. In the case of α-particle emission an extra cross section is observed in the forward direction. As seen in the inset such emission is concentrated in the grazing direction. In the H distribution no such forward peaking could be seen. The anisotropies in the H and He angular distribution in the backward hemisphere, as well as backward angle spectra are well described by the statistical model calculation with a critical angular momentum for fusion equal to 27 ħ (derived from ER cross section) and a radius parameter for the moment of inertia equal to 1.43 fm. The statistical and non statistical light particle emission cross section have been deduced from this experimental data and are compared to statistical model prediction in the next table.

| $\sigma_{mb}$ | Fusion E.R. | Light Particle Emission | | Non Statistical Emission | |
|---|---|---|---|---|---|
| | | Proton | Alpha | Alpha | Proton |
| Experimental | 830 ± 150 | 2000 ± 350 | 1850 ± 200 | 250 ± 80 | < 40 |
| Statistical Calculation | 830 | 1700 | 1250 | | |

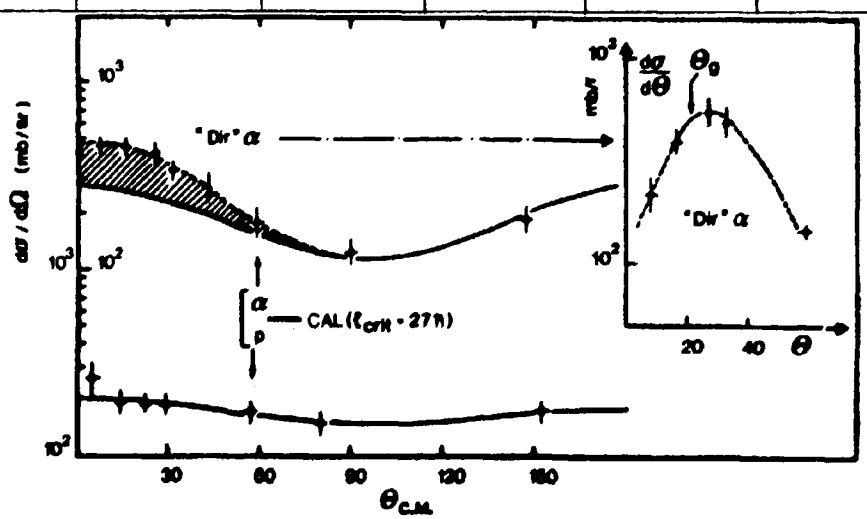


Figure 3 - Experimental and calculated (full lines) C.M. He and H angular distributions.

The experimental proton and alpha cross section is much larger than the statistical prediction. But such calculation don't take account of the evaporation from the target like DIC fragment.

## III. Particle - E.R. Correlation

The experimental results are going to be compared with statistical-model predictions. Such calculation are made with use of a multistep Monte-Carlo-Hauser-Feshbach code[3] which allowed the particle emission probabilities and kinematics to be followed over all the steps in a large evaporation cascades. The semi-classical formulation of Ericson and Strutinski was employed to calculate the angular momentum of the evaporation residues along the cascade. The only free parameters were the critical angular momentum for fusion which was set equal to 27 ħ to reproduce the E.R. cross-section and the radius parameter for the moment of inertia (1.43 fm) which has been chosen to fit the back angle light particle spectra Laboratory Angular and energy distributions of light particles and E.R. as well as angular correlation can be obtained for each evaporation stage.

The angular correlations give further insight into the mechanism of particle emission. For the plane He angular correlation with different E.R. elements we observe a flattening of the distribution as far as the E.R. is further from compound nucleus and more evaporated particles are concerned. This phenomena is well reproduced by the statistical model (figure 4). However, the experimental correlation measured for $\theta_\alpha = 15°$ is larger than the calculated one specially in phosphorius (P) and surfur (S) cases. Such extra cross section can be explained if one compare the energy distribution of the alpha observed at $\theta = 15°$ and $\theta = 60°$ in correlation with E.R. (figure 4) The 15° alpha energy distribution cannot be explained by statistical model. The high energy cross section enhancement correspond to the extra cross section we just observed in the angular correlation.

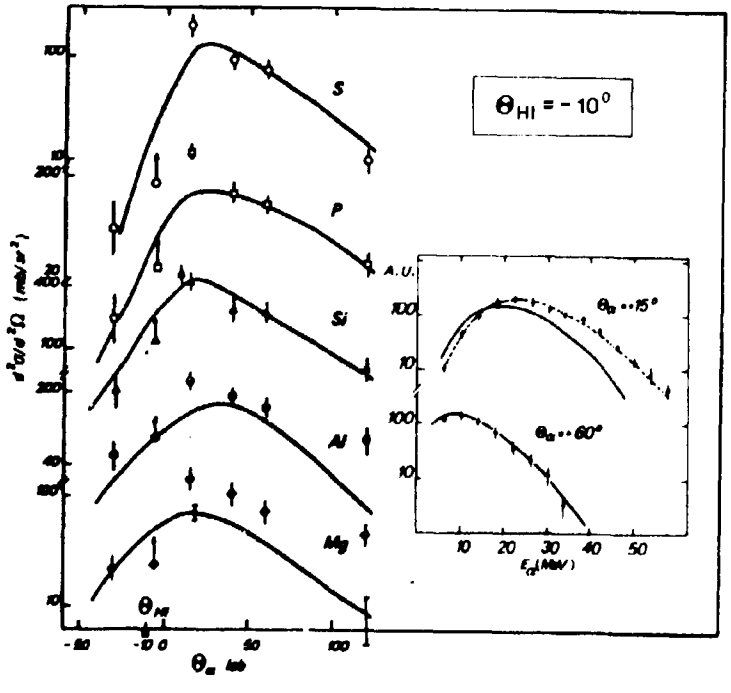


Figure 4

This non equilibrium alpha emission is also corroborate by observation of E.R. charge distributions in correlation with light particles. As far as the whole alpha energy spectra is concerned the E.R. charge distribution observed in the correlation $\theta_{HI} = -10°$ and $\theta = 15°$ is well reproduced by the statistical model. But a notable change appear if only α with $E_\alpha > 30$ MeV are involved (figure 5). The statistical model cannot reproduce the charge distribution observed and particularly the large P and S cross section. In order to reproduce such distribution we have to make the hypothesis that first an α is emitted with an energy around the energy beam (28 MeV) and then the compound nucleus $^{37}Ar[^{27}Al+^{10}B(72\ MeV)]$ is formed.

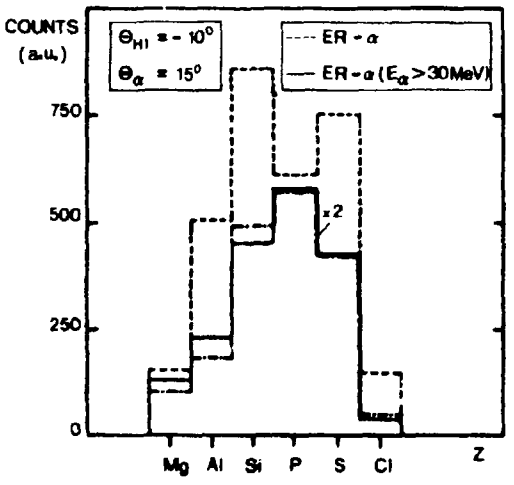


Figure 5

E.R. distribution $\theta_{HI} = -10°$ in coincidence with particles

-------- (E.R., α)
———— (E.R. - $E_\alpha$ > 30 MeV)
-·-·-·- Statistical calculation (B(72 MeV) + $^{27}Al$)

The out of plane correlation give information about the desalignment of the final E.R. nucleus from the initial direction. The experimental data concerning out of plane distribution are compared with the statistical model prediction (figure 6). There is a progressive desalignment along the evaporation cascade. The initial direction is essentially preserved in nuclear evaporation but as far as more than two α particles are emitted a substantial dealignment is obtained. Although there is an overall agreement between the experimental correlation and the statistical model the (α - S) and (α -P) experimental correlation show a larger anisotropy than the calculated one. This suggest a contribution from a process involving α emission in the forward direction which might preserve change of the alpha energy spectra as function of the out of plane angle. As shown on (figure 6) the high energy component observed at $\theta = 15°$ $\phi = 0$ completely disappear as far as the out of plane angle $\phi$ equal 30°.

Recently the analysis[4)] of velocity spectra of individual resolved residues masses in Ne (14 MeV/A) induced reaction showed clear evidence for fusion like residues with an incomplete momentum transfer. Although we did not get E.R. mass measurements we performed such analysis in the Si case assuming the average masse to be equal to 28. The centroïde $\bar{v}$ of the reduced velocity spectrom $N(v)/v^2$ was determined (figure 7) and compared to the velocity $V_c = V_{CM} \cos \theta$. $V_c$ is the most probable velocity provided there is a complete momentum transfer and symmetry about 90° CM in the decay of the compound nucleus. We find that $\bar{v}$ is smaller than $V_c$ which is indicative of the presence of preequilibrium emission or incomplete fusion process. If one tries to extract the evaporation residue

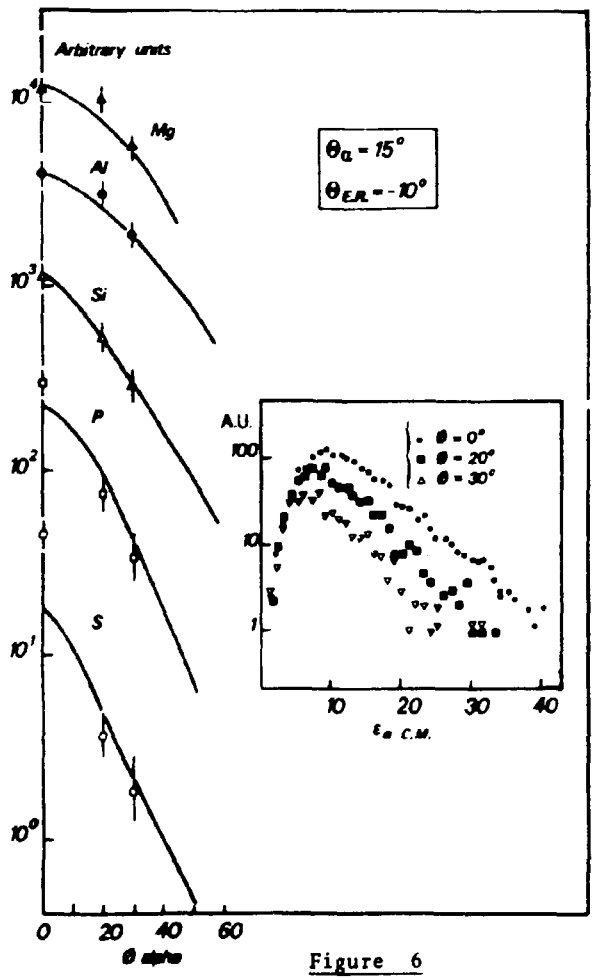


Figure 6

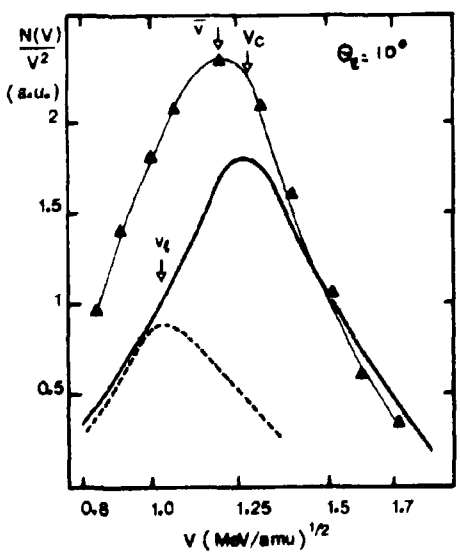


Figure 7

component by fitting the velocity spectra with a gaussian which has the maximum probability centered at $V_c$ and a variance calculated by a statistical evaporation code. One can deduce at lower velocity an other gaussian component centered at a velocity $\bar{v}$ which could be explained if one suppose an $\alpha$ is emitted in the first step of the reaction from the projectile with a velocity near to the projectile one while only the projectile like nucleus fuse with the target nucleus. $v_\ell$ is found to be equal to most probable velocity provided there is a complete momentum transfer in the fusion ($^{10}B$ + $^{27}Al$ 72 MeV). Such information given by the recoil velocity spectra of evaporation residue can be very significant when measured in coincidence with

light particle. We just give here an informative of what can be expected of such analysis.

To conclude with α-E.R. correlation the different observations lead to believe that a prompt α emission occur in the first state of the reaction followed by fusion of the remainding nuclei. In the proton E.R. case the in plane and out of plane correlations are well explained by statistical emission.

## IV. Particle - DIC fragments correlation

As we mentionned above fragment-fragment correlation show that in our system case the process is a two body interaction followed by evaporation from the relaxed target like nucleus. When we have three particle events it is worthwhile to check the observation in the three body kinematical frame. For the three body kinematical calculation[5] we use the following convention. The alpha particle is labelled by 2, the projectile like fragment by 1 and the target like fragment by 3. For example if boron and the α particle represent the two detected nuclei we may write the three reaction type as :

Process 1 2 $\quad {}^{14}N + {}^{27}Al \rightarrow {}^{27}Al + {}^{14}N^{*} \rightarrow ({}^{10}B + \alpha) + {}^{27}Al$

Process 2 3 $\quad {}^{14}N + {}^{27}Al \rightarrow {}^{10}B + {}^{31}P^{*} \rightarrow ({}^{27}Al + \alpha) + {}^{10}B$

Process 3 1 $\quad {}^{14}N + {}^{27}Al \rightarrow \alpha + {}^{37}Ar \rightarrow ({}^{27}Al + {}^{10}B) + \alpha$

For each couple of coincident angles we can observ whether the events are due to such sequential decay or not. We are going to study more accurately two case. In the first one the light inelastic fragment are detected at 30° laboratory angle which mean we are dealing with relaxed deep inelastic process. In the second one the light in elastic fragment are detected at 10° laboratory angle near the grazing angle.

### Alpha - DIC fragments correlation

In figure 8 is shown the diagram in case of carbon observed at 30° and α detected at 40° upper part or 15° lower part. The correlation (30° - 40°) is consistent with the picture of an α emission from the heavy recoil ($E_{23}$) which is calculate taking the most probable energy for α emission in the center of mass of the heavy recoil equal to 7 MeV. At 15° we observ an extra cross section for $E_{\alpha} > 25$ MeV. In that case the emission from the light fragment (line $E_{12}$) cannot account for the faster events. Let us consider the third process 31 : a prompt alpha particle is emitted followed by the rotation of the dinuclear system ${}^{37}Ar$ which may even turn a cross the beam axis before it disrupts into two fragments one of them being the carbon observed at -30°. The line $E_{31}$ represent the most probable energy for the carbon fragment ($E_{31}$ = 13 MeV correspond to the Coulomb repulsion C-Mg no selection on the α-energy being done). As seen on figure 8 the process 31 can be one explanation for the correlation observed.

On figure 9 is shown the diagram for α particles observed at 15° and boron observed at -10°. The most probable energy of the α emitted from the projectile like or the target like fragment is set equal to 1.5 the Coulomb barrier that is 4 MeV and 7 MeV. The corresponding $E_{23}$ and $E_{12}$ lines are drawn. As in the previous case a fraction of the cross section can be explained by emission from the heavy

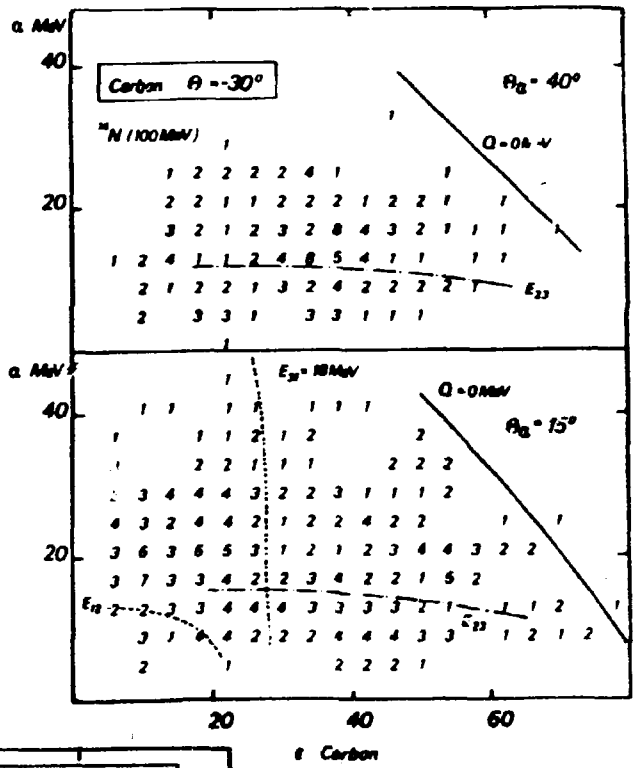


Figure 8

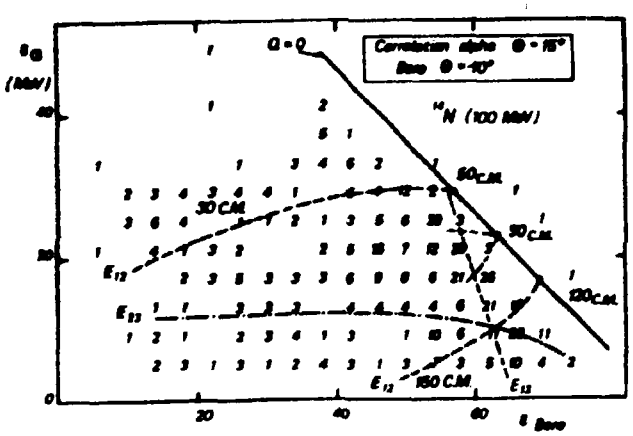


Figure 9

recoil. However a considerable number of event is observed for low $Q_3$ values $Q_3 = -6 \pm 2$ MeV. This maximum cannot be interpreted as a real projectile break-up ($Q_3 = 0$). An evaporation from the light fragment ($E_{12}$) cannot explain the data even if one consider the Coulomb barrier to be slightly different. The maximum of events in the correlation ($\alpha$-Li) and ($\alpha$-Be) correspond to more and more negative $Q_3$ values. Such behaviour can be reproduced by the process 31 if one suppose a prompt alpha is emitted followed by the disrupt of the $^{37}$Ar system in two fragments, the lighter one being observed at 10°.

The in plane angular correlation of prompt alpha and DI fragments are similar from lithium to oxygen, they a.e peaked in the beam direction. The out of plane correlations shows a large anisotropy. The integrated cross section corresponding to such non statistic alpha emission in correlation with DI fragment is $50 \pm 20$ mb.

Proton-DIC fragments correlation

The three body plots corresponding to the case of a light deep inelastic fragment detected at -30° are well explained by proton emission from the heavy fragment. In the case of correlation $\theta_c$ = -10° and $\theta_\alpha$ = 15° the proton emission from the light projectile is observed as seen figure 10. This emission is possible because of the low Coulomb barrier and binding energy (7.5 MeV) of proton in nitrogen. The smaller direct cross section (< 40 mb) deduced from inclusive measurements can be explained by this process.

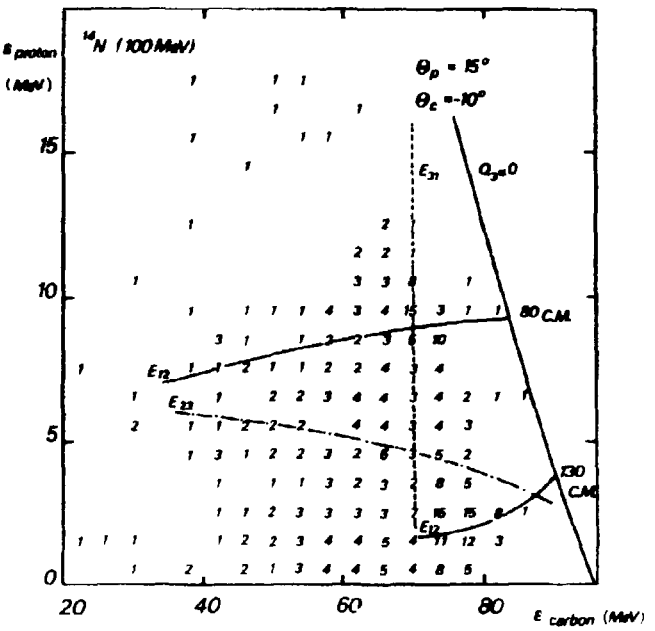


Figure 10

Conclusion

The similar behaviour observed from prompt alpha in correlation with E.R. or D.I. fragments argue in favour of alpha emission in the early reaction stage.

The preequilibrium model[6] is able to reproduced the different features observed which are the following :

- The alpha cross section are greater than the proton one and don't depend much on the projectile (N, C, O) or target (Al, V, Ti) involved in the reaction. The variation of prompt α cross section in function of energy per nucleon $\varepsilon_n$ in the entrance channel are given on figure 11. The values from the different experiments follow the same general trend. The non observed cross section for heavier projectile is due to a too low value of $\varepsilon_n$ in the entrance channel. Similar results have been obtained in preequilibrium emission observed in light particles induced reaction and are known to be well reproduced by the preequilibrium model.

- In the case of N + Al system the inclusive α spectra as well as the total direct alpha and proton cross section are well reproduced. Taking and initial configuration : 5 n, 5 p, 1 α in a agreement with the exciton number ($n_R$) deduced from the slope method $n_R = n_{initial} - 2 = 9 \pm 1$ (figure 12). A code is in progress which will take in account of preequilibrium emission together with the heavy ion reaction process leading either to fusion or deep-inelastic collisions. The first analysis will be done on the N + Al system at 100 and 150 MeV incident energy. We hope then get a global answer for all the observations we did and even more get information on the angular momentum range involved.

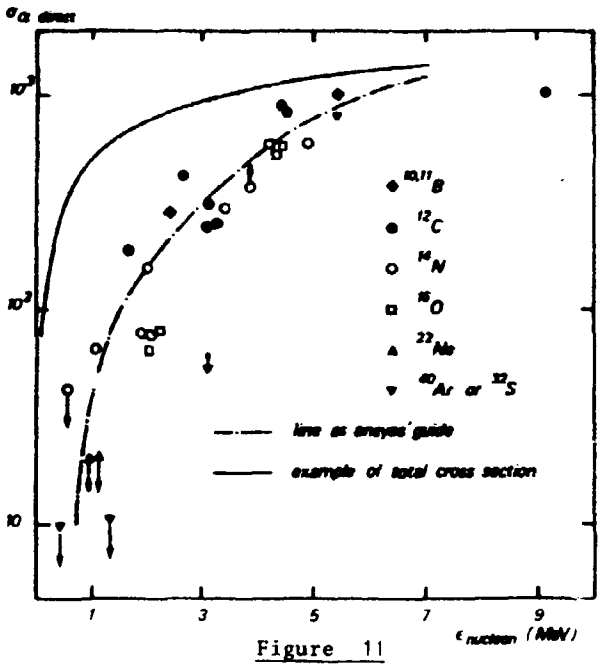


Figure 11

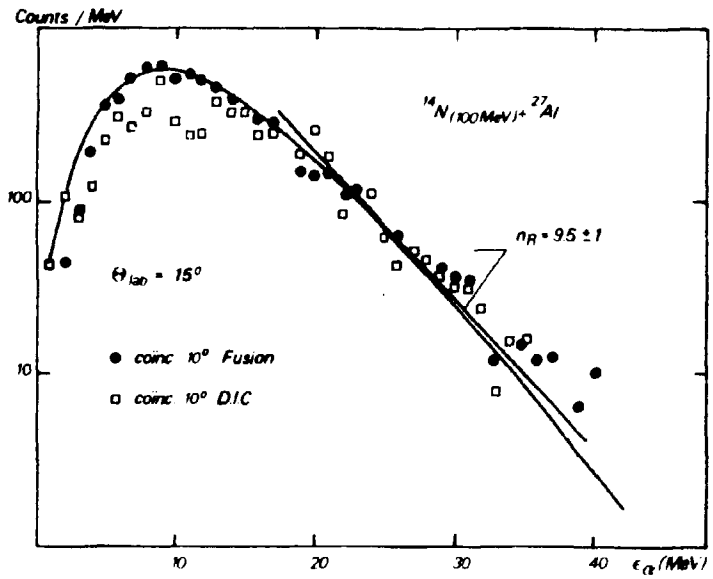


Figure 12


References

1) R. Billerey et al., Phys. Rev. Lett., 47, (1981), 639
2) R. Billerey et al., Zeit. für Phys., A-292, (1979), 293
3) J. Cole et al., Nucl. Phys., A-341, (1980), 284
4) H. Morgenstein et al., Phys. Lett., 113 B, (1982), 463
5) C.C. Ohlsen, Nucl. Instr. Meth., 37, (1965), 240
6) M. Blann, Phys. Rev., 23, (1981), 205


(*) On leave Texas A and M University, U.S.A.

# ANGULAR MOMENTUM RELAXATION AND THE ROLE OF BREAK-UP IN 270-MEV $^{20}Ne+^{168}ER$ COLLISIONS

W.Dünnweber, W.Hering, H.Puchta, R.Ritzka, W.Trautmann, W.Trombik
Sektion Physik, Universität München, D-8046 Garching

C.Egelhaaf, H.Homeyer
Hahn-Meitner-Institut, 1000 Berlin 39

The conception of a rigidly rotating double nucleus has been validated in many examples of deep-inelastic (DI) reactions at bombarding energies below 10 MeV/nucleon[1-4]. The fragment spins deduced from measurements of the γ-ray multiplicity, of the angular correlations in sequential particle decay and of the yrast population patterns are in good agreement with the classical sticking condition, corresponding to the minimum of the rotational energy of the system.

In asymmetric systems at higher bombarding energies the fragility of the light projectile introduces new degrees of freedom. Incomplete fusion and quasi-elastic break-up, both involving the dissociation of the projectile, become the principal reaction modes competing with fusion[5-8]. According to a sharp cut-off recipe, accounting well for fusion and incomplete-fusion cross sections[5,7] in asymmetric systems at $E \gtrsim 10$ MeV/nucleon, in the example of $^{20}Ne+^{168}Er$ the partial waves between $\ell_i = \ell_{crit}$(fusion) = 64 ħ and $\ell_i$ = 125 ħ are expected to lead to incomplete fusion, i.e. fusion of projectile subclusters with the target. Yet the DI reaction mechanism persists in such cases[6,9,10]. To track down the characteristics of angular momentum relaxation in this energy region we have studied the fragment spin in DI reactions of $^{20}Ne+^{168}Er$ at 13.5 MeV/nucleon. The concurrence of break-up is found to be essential for an interpretation of the presented data in terms of rigid rotation.

Isotopically enriched $^{168}Er$ targets of 2 to 4 mg/cm² thickness were bombarded with $^{20}Ne$ beams of intensities between 2 and 5 pnA delivered by the VICKSY facility, Berlin. Projectile-like reaction fragments were detected with telescopes consisting of axial-field ionization chambers and 2000-mm² Si detectors, subtending solid angles of 30 msr. Light-element contaminations of the target, determined by comparison to runs with Carbon and Oxide targets, require corrections of up to 10% of the heavy-ion singles yield at $\theta_{lab}$ = 35° and 55°. The yield of coincident γ-rays was measured with narrowly collimated (± 7°) NaI crystals (5"x6"). Contributions from neutrons were separated by time-of-flight. The multiplicity of γ-rays, $M_\gamma = N_{coinc}/(N_{singles} \times \text{efficiency})$, is obtained by integration over the γ-ray energy and by averaging over the almost isotropic out-of-plane distribution. The fragment spin is deduced from these data. In a second experiment the circular polarization $P_\gamma$ of the energy-integrated γ-radiation was measured with a doubly symmetric set-up of two heavy-ion telescopes at $\theta_{lab}$ = 35° and two polarimeters[11] in order to classify the trajectories by the sense of rotation.

A general view of the $^{20}Ne+^{168}Er$ reaction is obtained from a scatter plot of events in the ΔE-E representation (fig.1). One may recognize two components in these light-fragment inclusive data, a quasi-elastic component of $Z \leq Z_{projectile}$

nuclei with energies corresponding roughly to the beam velocity and a DI component with a broader element distribution and energies close to the mutual interaction barrier in the exit channels. The first one comprises incomplete fusion and break-up (probably of the sequential type[12]), i.e. processes in which the part broken off from the projectile is either transferred to the target or emitted into the continuum. In the Z=8 case, the yield of coincident transitions of the target-like fragments, measured in a γ-spectroscopic experiment[13], shows that α break-up with only little excitation of the target and α transfer contribute equally. The DI component is dominant at $\Theta_{lab}$ = 35° which is 15° behind the grazing angle (corresponding to $\ell_{graz}$ = 142 ħ). However, at smaller angles a strong preponderance of the beam-velocity component is observed while the total DI cross sections is comparatively small (about 200 mb).

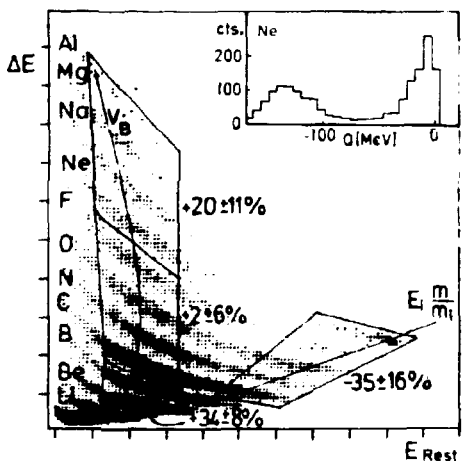


Fig.1: Gamma ray circular polarization along the scattering normal for three deep-inelastic groups and one beam-velocity group in a ΔE-E scatter plot of reaction products at $\Theta_{lab}$ = 35°. The insert shows a Z=10 particle singles spectrum.

The measured values of the γ-ray circular polarization $P_\gamma$ along the scattering normal $\underline{k}_i \times \underline{k}_f$ are given in fig.1 for three DI regions and one beam-velocity region. Since orbital angular momentum is lost, on the average, in the processes considered here, the average total fragment spin vector points into direction of the entrance-channel angular momentum $\underline{\ell}_i$. Hence a positive (negative) polarization signifies negative-(positive-) angle scattering. As expected, positive-angle scattering dominates in the beam-velocity component. In the DI component, the average over the three indicated regions, $P_\gamma^{DI}$ = (+ 14.6 ± 4.4)%, shows that the orbiting-conception is still applicable at 13.5 MeV/nucleon.

For a quantitative interpretation the effects of particle evaporation, of pre-yrast γ-radiation and of the misalignment in the primary reaction have to be taken into account . While the measured value of $P_\gamma$ in the case of a completely polarized initial state would amount to almost 100% in stretched γ-decay[11], a statistical-model calculation of the pre-yrast dealignment for the target-like fragments shows that in this case $|P_\gamma|$ = 70-90% is to be expected, depending on the relative contribution of non-stretched γ-decay to the total γ yield [see

ref.[14)]. The additional effect of the dealigned spin created in the primary reaction is estimated by fitting a Gaussian m-substate distribution to measured anisotropies of discrete transitions[13)]. As a result, $P_\gamma = (\pm)$ (40-60)% corresponds to pure negative-(positive-) angle scattering. For comparison, we note that both extremes are approximately reached in the cases of 100-MeV $^{16}O+^{58}Ni$ [ref.[14)]] and 620-MeV $^{86}Kr+^{197}Au$ [ref.[15)]] where the same reckoning results in a largest possible $P_\gamma$ of about $\pm$ 60%.

Contributions from either side of the interaction region to the differential cross section mutually cancel in the net polarization so that $P_\gamma^{DI}$ = + 15% corresponds to a negative-angle contribution of (60-70)%. However, a strong dependence of the relative contributions on the element number of the ejectile is apparent in fig.1. In the central DI group the polarization is consistent with zero, while it reaches approximately the value expected for pure negative-angle scattering in the group of lighter ejectiles and adopts an intermediate value in the group of heavier ejectiles where a transition into fusion-fission processes, to be associated with zero polarization, seems to take place[10)]. These polarizations impose severe restrictions on the interpretation of the currently much discussed fast-particle emission in DI reactions[16)].

The measured $\gamma$-ray multiplicities are shown in fig.2 as a function of the element number of the ejectile. Also given are the DI fragment spins deduced according to a calibration of $M_\gamma$ by fusion experiments in which the $\ell_i$ distribution of compound nuclei, in the region of the target-like nuclei of the present experiment, has been reconstructed[17)]. Between spins of 20 and 40 $\hbar$ and excitation energies of 80 and 140 MeV a set of data averaged over all xn channels is described well[17)] by $I = 2.06 \cdot M_\gamma - 5.2$. While contributions from fission are negligible in this region[18)], the spin removed by $\alpha$ evaporation would amount to about 5 $\hbar$ per heavy fragment if the $\alpha$ yield in ref. 17 were completely due to evaporation and not to incomplete fusion. Thus, $I = 2\ M_\gamma$ is adequate for the heavy DI fragments, overestimating I possibly by up to 5 $\hbar$. Contributions to $M_\gamma$ from the light fragments, identified as discrete lines in the NaI spectra, are small, e.g. less than 0.3 for $^{16}O(3^-)$ and $^{12}C(2^+)$. They are included in the presented values of $M_\gamma$ so that, with no significant change of the above calibration, the deduced spin is the mean value of the total fragment spin $I = I_1 + I_2$. A quantitative interpretation of the $M_\gamma$-values in the beam-velocity component is not attempted here, because these represent averages over the two fast reaction modes quoted above with strongly different spin transfers, as revealed by the $\gamma$ spectroscopic study[13)]. In an exclusive study of incomplete fusion in a similar system[7)] the spin transfer was found to be in good agreement with the prescription given in ref.5.

Application of the sticking-condition,

$$I/\ell_i = (\Theta_1 + \Theta_2)/(\Theta_1 + \Theta_2 + \mu D^2) \quad ,$$

with parameters ($D[fm] = 1.16\ (A_1^{1/3} + A_2^{1/3}) + 2.0$, rigid-sphere moments of inertia[19)], $\Theta_1$ and $\Theta_2$) working well in several cases of asymmetric systems[2-4)] at lower energies, e.g. 175-MeV $^{20}Ne$+Ag at 90° (ref.2), leads to a broad range of spins (hatched area in fig.2) the lower border of which corresponds to $\ell_i = \ell_{crit}$ = 64 $\hbar$. This value of $\ell_{crit}$ taken from the bin-model prescription[5)], describing fusion and incomplete fusion data of similar systems[5,7)] is considerably below

the predictions of fusion-models tailored for lower bombarding energies[20]. The calculated borderline in fig.2 is to be considered as a lower limit of the intrinsic fragment spin of a relaxed binary system with $\ell_i \geq \ell_{crit}$. It is satisfying that the experimental values are close to this line for $Z > 10$ where a continuous transition to the fusion-fission process is expected.

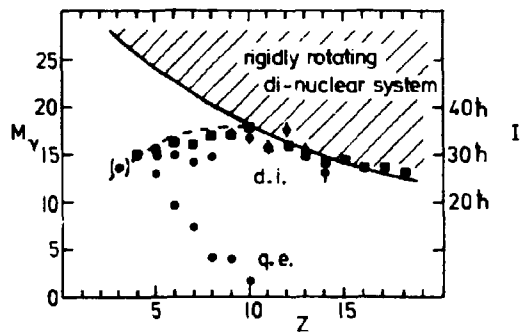


Fig.2: Gamma-ray multiplicity as a function of the light-fragment Z at $\Theta_{lab}$ = 35° (circles) and 55° (squares); deduced spin transfer I in the deep-inelastic reaction channels; calculated rigid-rotation values for binary reactions with $\ell_i \geq \ell_{crit}$ (hatched area) and for deep-inelastic processes in concurrence with break-up (dashed curve).

The salient feature of the data in fig.2 is the considerable spin deficit with respect to the borderline in those channels (Z=4-8) which are strongly dominant in the DI component. Also the Z-dependence is in contrast to the behaviour of asymmetric systems at lower bombarding energies[2-4]. The increase with increasing asymmetry, predicted for fixed $\ell_i$, may be flattened by an $\ell_i$-fractionation[2] which, however, would only give rise to different spin distributions within the hatched area of fig.2. A correction for possible light-particle evaporation from the primary light fragments would lead to $M_\gamma(Z_{primary})$-values with an almost identical behaviour as the $M_\gamma(Z)$ values for $Z_{primary} \lesssim 10$ (see fig.2).

Giving up the concept of rigid rotation may enable an explanation of the spin deficit, but the validity of this concept in the present case is suggested by several other observations. (i) The dominance of negative-angle scattering, in particular for those DI channels with the largest spin deficit (cf. figs. 1 and 2), (ii) the approximate independence on the angle, found for the spin transfer (fig.2) and the mean DI exit-channel energy and (iii) the large loss of the spin alignment between the beam-velocity and the DI component[13], all these are approved indicators of a relaxed system.

We now consider two modes of a DI reaction in concurrence with break-up (fig.3) which both lead to rigid rotation and propose a simple rule for the spin transfer, obeyed in both cases.

1) As a limiting case of incomplete fusion the DI exit-channel with light-fragment mass $m \lesssim 20$ will arise with largest probability from the partial-wave with $\ell_i = \ell_{crit}$ (Er,m) x 20/m. For smaller $\ell_i$ incomplete fusion (i.e. fusion of

$^{16}O+^{168}Er$ in the example chosen in fig. 3) will be favoured, for larger $\ell_i$ the balance of farces favours a different fragmentation in the early stage[5]. The remaining part of $\ell_i$ is carried away by beam-velocity particles with mass 20-m (solid line in fig.3). Thus, according to the phenomenological bin model[5] $\ell_i' = \ell_{crit}$ (Er,m) = 58 $\hbar$, 50 $\hbar$ and 33 $\hbar$ in the examples of the $^{16}O$, $^{12}C$ and $^{6}Li$ light fragments, respectively, are the actual critical angular momenta. However, this cannot be the only mode present in the DI component, since the number of coincident fast particles, distinguished from those emitted sequentially by either fragment, is found[20] to be less than one per light fragment and to increase not significantly with decreasing m.

2) For a partial wave with $\ell_i < \ell_{crit}$ the light fragment has a chance of escaping fusion if break-up occurs before the critical distance for fusion is reached. In contrast to case 1) the observed fragment is the outer remnant of the initial break-up and the part broken off is captured by the target. However, the same total angular momenta $\ell_i$ as the $\ell_i'$ of mode 1 are required for the balance of forces in the rigidly rotating system. (The critical values[5] obtained with $^{168}Er$ or with the heavy fragment after transfer are almost identical). Substantial contributions from partial waves with $\ell_i < \ell_{crit}$, flattening strongly the sharp cut-off distribution, have already been postulated on the basis of a study of exit channel energies in cases like 150-MeV $^{20}Ne+^{40}Ca$ deep-inelastic reactions[21].

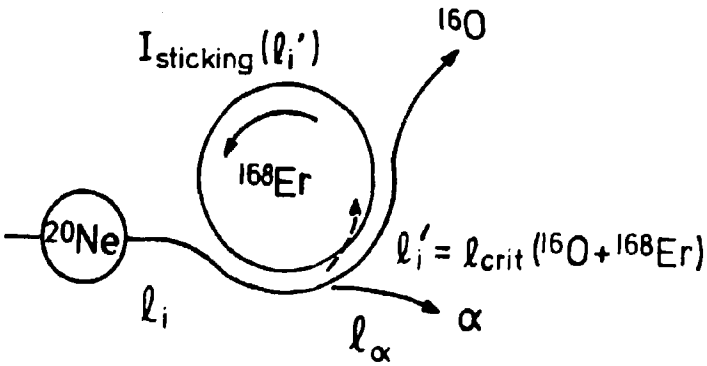


Fig.3: Schematic view of the angular momentum transfer in the two extreme modes of deep-inelastic reactions in concurrence with break-up, discussed in the text.

The relative probalities of the sketched reaction paths will be different for the different DI exit channels and intermediate paths are conceivable. These are probably associated with different polarizations. Since the entrance-channel partial-wave numbers $\ell_i$ are different for these modes, a broad $\ell_i$ range will contribute to the DI channels. Yet, a simple rule emerges from the consideration of the extreme cases 1 and 2: We apply the "sticking' condition to the critical total angular momentum $\ell_{crit}$ (Er,m) for the DI channel with ejectile mass m. With the phenomenological $\ell_{crit}$-values of ref.5 a reasonable reproduction of the data is obtained (dashed curve in fig.2). Mass diffusion in later stages of the interaction may modify this picture for which the early dissociation of the projectile was a basic requirement. It is of high interest to see how well the given recipe does in other systems at large bombarding energies.

References

1) M.Lefort and C.Ngo, Riv.Nuovo Cimento 2 (1979) part 12

2) L.G.Moretto and R.P.Schmitt, Rep.Prog.Phys. 44 (1981) 533 and references given there

3) M.N.Namboodiri, J.B.Natowitz, P.Kasiraj, R.Eggers, L.Adler, P.Gonthier, C.Cerruti and S.Simon, Phys.Rev. C20 (1979) 982

4) H.Puchta, W.Dünnweber, W.Hering, C.Lauterbach and W.Trautmann, Phys.Rev. Lett. 43 (1979) 623

5) K.Siwek-Wilczynska, E.H. du Marchie van Voorthuysen, J.van Popta, R.H.Siemssen and J.Wilczynski, Nucl.Phys. A330 (2079) 150

6) P.Gonthier, H.Ho, M.N.Namboodiri, L.Adler, J.B.Natowitz, S.Simon, K.Hagel, R.Terry and A.Khodai, Phys.Rev.Lett. 44 (1980) 1387

7) K.A.Geoffrey, D.G.Sarantites, M.L.Halbert, D.C.Hensley, R.A.Dayras and J.H.Barker, Phys.Rev.Lett. 43 (1979) 1303

8) H.Yamada, D.R.Zolnowski, S.E.Cala, A.C.Kahler, J.Pierce and T.T.Sugihara, Phys.Rev.Lett. 43 (1979) 603

9) Ch.Egelhaaf, H.Fuchs, A.Gamp and H.Homeyer, Phys.Rev. C24 (1981) 759

10) G.J.Mathews, J.B.Moulton, G.J.Wozniak, B.Cauvin, R.P.Schmitt, J.S.Swentek and L.G.Moretto, Phys.Rev. C25 (1982) 300

11) W.Trautmann C.Lauterbach, J.de Boer, W.Dünnweber, G.Graw, W.Hamann, W.Hering and H.Puchta, Nucl.Instr.Meth. 184 (1981) 449

12) H.Homeyer, M.Bürgel, M.Clover, Ch.Egelhaaf, H.Fuchs, A.Gamp, D.Kovar and W.Rauch, Phys.Rev. C26 (1982) 1335

13) W.Dünnweber, W.Hering, H.Puchta, R.Ritzka, W.Trautmann, W.Trombik, C.Egelhaaf and H.Homeyer, Proc.Int.Winter Meeting on Nuclear Physics (Bormio 1982) p.562

14) C.Lauterbach, W.Dünnweber, G.Graw, W.Hering, H.Puchta and W.Trautmann, Phys.Rev.Lett. 41 (1978) 1774

15) J.de Boer, C.Lauterbach, W.Dünnweber, G.Graw, W.Hering, H.Puchta, W.Trautmann and U.Lynen, Lecture Notes in Physics 92 (1978) 478

16) W.Dünnweber and K.M.Hartmann, Phys.Rev.Lett. 44 (1980) 729

17) D.G.Sarantites, L.Westerberg, M.C.Halbert, R.A.Dayras, D.C.Hensley and J.H.Barker, Phys.Rev. C18 (1978) 774

18) A.M.Zebelmann, L.Kowalski, J.Miller, K.Beg, Y.Eyal, G.Jaffe, A.Kandil and D.Logan, Phys.Rev. C10 (1974) 200

19) K.T.R.Davies and J.R.Nix, Phys.Rev. C20 (1976) 1977.
More realistic calculations for spheroidal shapes, taking also the non-aligned spin[13] into account, yield slightly larger values for $\langle I_1 \rangle + \langle I_2 \rangle$.

20) T.Fukuda, M.Ishihara, M.Tanaka, I.Miura, H.Ogata and H.Kamitsubo, Phys. Rev. C25 (1982) 2464

21) L. Adler, P.Gonthier, H.Ho, A.Khodai, M.N.Namboodiri, J.B.Natowitz and S.Simon, Phys.Rev.Lett. 45 (1980) 696

# LIGHT PARTICLE EMISSION FROM HEAVY ION REACTIONS AT MODEST ENERGIES

**E. Běták**
Institute of Physics E.P.R.C. S.A.S., 84228 Bratislava, Czechoslovakia + and
J.I.N.R. Dubna, 101000 Moscow, U.S.S.R.

and

V.D. Toneev
J.I.N.R. Dubna, 101000 Moscow, U.S.S.R.

A b s t r a c t : An attempt to estimate the relative role of processes contributing to the light particle (up to alpha) emission from heavy ion reactions is given. The overall agreement of the calculation and the data of $^{22}Ne + ^{197}Au$ reaction at 178 MeV is reasonable, though minor discrepancies indicate a presence of some another (nonequilibrium) mechanism and/or a need for modification of existing approaches.

## 1. Introduction

The studies of heavy-ion induced reactions attract much attention in the last years. One of their special questions, which receives a great deal of popularity, is the emission of light particles (nucleons to alphas) from reactions at modest incident energies ($\lesssim$ 20 MeV/A). The experimental data on the light particle double differential cross sections (see, e.g., refs. [1,2]) manifest a strong forward peaking, rather hard outgoing particle spectra reaching even the two-body kinematical limit, and - especially for alphas - remarkable integrated cross sections (up to $\frac{1}{2}\sigma_r$). The energy spectra and angular distributions have been analyzed in terms of direct reactions, deep-inelastic collisions, via the pre-equilibrium and/or equilibrium decay of the composite system. Apart of remarkable successes reached, the theoretical studies have usually been limited to one type of these processes only, what lowers their reliability in establishing the mechanism which is responsible for the light particle emission. We try to estimate namely the relative role of different processes. Our calculations are compared to the data of the $^{197}Au$ ($^{22}Ne$, $\alpha$) reaction at 178 MeV incident energy [3], where the available data seemed to be the most complete. To get a better image of this reaction, we have calculated the trajectories of interacting ions. This has been done by the use of TRAJEC code [4], which solves the Newton-type equations of motion including deformation, nucleon exchange, and friction. The latter was taken in the form of the so-called hard friction, which seems to be well justified now [5]. The interaction proceeds rather fast near the grazing angular momentum ($t_{int} \approx 2\times10^{-22}$s), increases with decreasing impact parameter ($\approx 10^{-21}$s for deep-inelastic collisions near $l_{cri}$), and a relatively long-living stable configuration is created for $l<l_{cri}$. The overlap of interacting nuclei is extremely small and can be estimated as more than few nucleons for such a long-living fusion-type configuration, and comparably less

+ permanent address

for deep-inelastic collisions. We shall list now possible mechanisms (in the order of increasing impact parameter and decreasing reaction time) and look, how much and into which energy and angle regions they are expected to contribute to the double differential cross section for the alpha-particle emission.

## 2. Compound nucleus and the pre-equilibrium decay

The compound nucleus (i.e. equilibrium) decay predicts soft emitted particle spectra, with angular distributions symmetric around $90^{\circ}$. The excitation energy is obtained from the energy balance, with the rotational energy subtracted. As seen from Fig. 1, the theoretical spectra are too far from the experimental data.

A natural generalization of the compound nucleus concept is the idea of pre-equilibrium decay, introduced into the heavy ion reactions by Blann [6] and used by many others thereafter. The energy spectra calculated within the exciton or the hybrid models depend strongly on the initial exciton number $n_0$. This parameter was put equal to the projectile mass number A in [6]. In the course of time the importance of the pre-equilibrium decay in heavy ion reactions, especially at modest energies, was questioned. For the pre-equilibrium calculations, the initial exciton number can be determined from the slope of the spectrum near its high-energy edge (for the nucleon emission $\frac{d\sigma}{d\varepsilon} \sim \varepsilon \sigma_{inv}(\varepsilon) U^{n_0-2}$). The values obtained in this way, as were reported by various authors, are depicted in Fig. 2. Though they are strongly author (or computer code?) dependent, a gross trend can be easily seen: $n_0 \ll A$ for low energies not far from the Coulomb barrier, whereas $n_0 \gtrsim A$ for higher energies. From the point of view of the trajectory calculations, resulting in small overlaps of nuclei, the low value of $n_0$ at energies $\lesssim 5$ MeV/A above the Coulomb barrier is not too surprising. We have got $n_0 \approx 8$ for our reaction (with the alpha emission treated in accord with Ribanský and Obložinský [12]). The angular distributions of complex particles were calculated as described in [13]. The resulting energy spectra at three different angles are presented in Fig. 1.

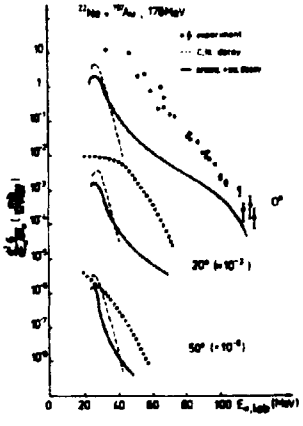

Fig. 1. The experimental [3] (points) and theoretical (curves) $\alpha$-particle spectra from $^{22}Ne+^{197}Au$ at 178 MeV, measured and calculated at three angles. The pure compound nucleus (=equilibrium) contribution is drawn as a dashed line, the combined pre-eq. plus equilibrium as a full line.

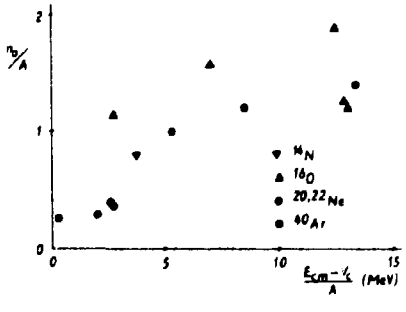


Fig. 2. Initial exciton number $n_0$ from analyses of n-, p-, and $\alpha$-emission from heavy ion reactions. The extracted values were taken from [7-11] and our results.

## 3. Deep-inelastic collisions

The deep-inelastic collisions (DIC) can contribute to the alpha-particle emission in two ways. The primary process (we'll refer to it as to the extreme DIC) consists of such a large mass transfer that the projectile-like fragment transforms into an alpha-particle, all the other nucleons being transferred to the target-like fragment [14]. Secondary, the alpha particles from DIC arise from decay of excited both the projectile-like and the target-like fragments.

### 3.1. Extreme DIC

If one attempts to get as extreme ejectiles, as the alphas, some modifications of standard procedure of calculating the DIC products are necessary. Usually, the mass and energy coordinates are supposed to be independent (see [15]). An estimate of the correlations of the two motions leads to substitution of $(p_r - p_r^c \frac{A_{eff}}{A_{eff}})$ instead of $(p_r - p_r^c)$ into the Fokker-Planck equation solution [16] (here, $p_r$ is the radial momentum). Together with this, we prefer the use of (reduced) realistic binding energies to the usual second-order polynomial approximation. Of course, this is difficult to be done within the Fokker-Planck equation approach, so that we calculate the element yields within the master equation, and then renormalize the Fokker-Planck double differential cross sections to the master equation calculated integrals [16]. As an example of goodness of our approach we present the element yields for "neighbourhood reaction" up to our knowledge, there are no such data for $^{22}Ne + ^{197}Au$ in Fig. 3, and the angular distributions, calculated by the Fokker-Planck equation (code of [4]) with the absolute value from the master-equation approach in Fig. 4. The agreement is more than reasonable in both the cases. We have calculated the alpha particle energy spectra at different angles in the same way, and present them in Fig. 5.

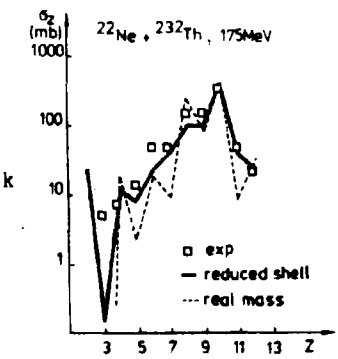


Fig. 3. Element yields for the $^{22}Ne + ^{232}Th$ reaction at 175 MeV. Points are the data of [17], curves are yields calculated by the master-eq. approach with real masses (dashed) and reduced masses (full line) of nuclei.

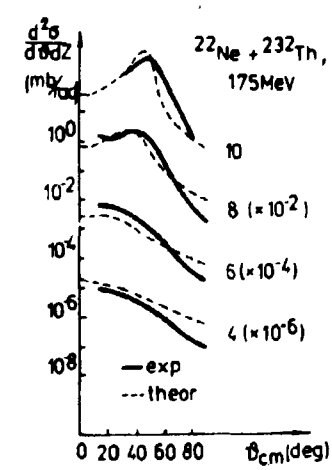


Fig. 4. The angular distributions from the reaction of $^{22}Ne$ on $^{232}Th$ at 175 MeV for four elements (their atomic number is indicated at corresponding curves). The full lines are the experimental data [17], the dashed lines our calculations.

### 3.2. Decay of DIC fragments

The nuclei resulting from DIC can bear sufficient energy as to undergo the Fermi breakup or the particle evaporation. We have supposed the Fermi breakup for light fragments (up to $^{16}O$), and the evaporation was calculated for all heavier nuclei. The results are depicted also in Fig. 5. As is easily seen, both the extreme DIC and the decay of DIC fragments contribute mainly to low energies and not too large angles of emitted alphas. If we compare the element yields from the primary DIC and the total "DIC-gated" channel (Fig. 6), we see that for Z>4 only a slight smoothing of the shell structure is observed. Some significant differences of primary and "total" yields can be seen for Z=4 (breakup of $^{8}Be$) and for Z≤2 (mainly due to the evaporation from the heavy fragment).

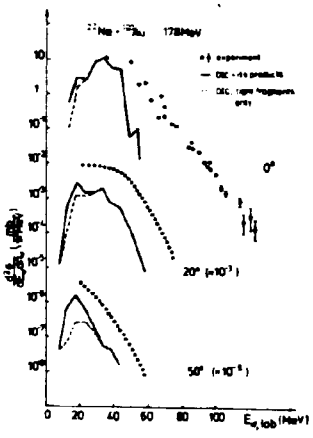

Fig. 5. DIC component of α-emission. Points are data of [3], dashed curves the extreme DIC with the breakup of light fragm. (in this scale this coincides with the extreme DIC only), full line with the evaporation from the heavy fragment added.

### 4. Direct reactions

Though many of nice analyses of direct reactions of heavy ions are reported [18-20] with remarkable success in describing the shapes of energy spectra and angular distributions, their importance is still questionable, because they cannot predict the absolute value. In order to estimate the direct reaction contribution, we have used the (oversimplified) plane-wave breakup description without any details of neither the nuclear structure nor the interacting potential [21]. Generally, two parameters enter these formulae: the width of the cluster impulse distribution in projectile and a normalization factor. The latter one was taken so as to describe the "missing part" of the spectrum (i.e. experiment minus all the other processes), while the former one from the shape fit. Of course, such a procedure might overestimate the importance of direct processes in our reaction. One further step was suggested to make the picture a little bit more realistical: we've included the Coulomb deflection of the projectile trajectory up to the (unknown) breaking point. We have denoted this angle as $\frac{1}{2}\vartheta_{gr}'$ and treated it as a parameter. The results, both for the direct part only and for the sum over all processes, are depicted in Fig.7. Probably the best fit is for $\vartheta_{gr}'=20^{\circ}$.

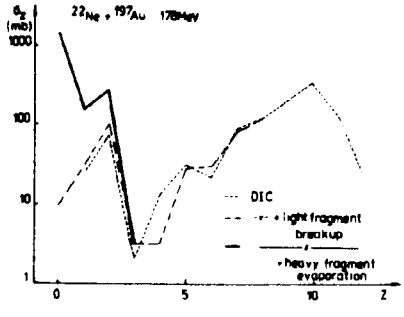


Fig. 6. Element yields arising from DIC as calculated from extreme DIC (dotted), with light fragment breakup included (dashed), and with both the light and the heavy fragment emission (full line).

## 5. Conclusions

As is seen from Fig. 7, we have arrived to a very reasonable agreement of the theory and the data. Cross sections of the alpha particle production were estimated to be following from various mechanisms: equilibrium emission 12 mb, pre-eq. emission 54 mb, extreme DIC 73 mb, DIC light fragment breakup 34 mb, DIC heavy fragm. evaporation 164 mb, direct reactions 80 mb (totally about 420 mb).

Nevertheless, even all the considered processes together are not able to reproduce all the data simultaneously. Some slight discrepancies which still remain indicate a presence of some nonequilibrium (or direct) mechanism of the alpha particle emission, characterized by its contribution to energies $\gtrsim$50 MeV at small angles. A better understanding would be achieved by further both experimental and theoretical work.

The authors are grateful to O.N. Karpov for supplying his Fermi breakup code.

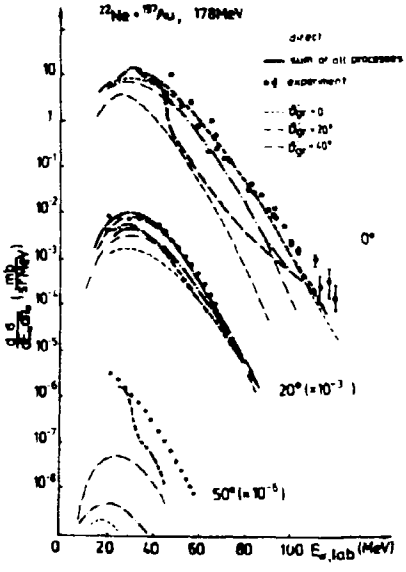


Fig. 7. Alpha particle spectra from $^{22}$Ne+$^{197}$Au from direct reactions (thin lines) and the sum of all processes considered (heavy lines) together with the experimental data [3]. The calculations for three values of $\vartheta_{gr}'$ are depicted: 0 (dotted), 20° (dashed-dotted), and 40° (dashed).

## References


1. E. Běták and V.D. Toneev, Particles and Nuclei 12 (1981) 1432
2. Yu.Ts. Oganessian, in Proc. Int. School on Nucl. Structure, Alushta 1980, p. 261
3. E. Gierlik et al., Z. Phys. A295 (1980) 295
4. R. Schmidt and J. Teichert, JINR reports E4-80-527 and E4-80-735
5. U. Brosa and D.H.E. Gross, Z. Phys. A298 (1980) 91
6. M. Blann, Nucl. Phys. A235 (1974) 211
7. T.J.M. Symons et al., Phys. Lett. B94 (1980) 131
8. M. Blann, Phys. Rev. C23 (1981) 205
9. R. Billerey et al., Phys. Rev. Lett. 47 (1981) 639
10. T.C. Awes et al., Phys. Rev. C25 (1982) 2361
11. E. Holub et al., in EI Topical Conf. Neutron Ind. Reacts, Smolenice 1982 (in press), also published as HMI preprint 82/11 R
12. I. Tibanský and F. Obložinský, Phys. Lett. B45 (1973) 318
13. K.K. Gudima et al., JINR reports P2-80-774 and P2-80-777
14. V.V. Volkov, Nuclear Reactions of Deep-Inelastic Collisions. Energoizdat, Moscow 1982 (in Russian)
15. C. Ngô, in Proc. Brasov Int. School Critical Phenomena in H.I. Reactions, Poiana-Brasov 1980, p. 395
16. E. Běták and V.D. Toneev, JINR report P7-82-630
17. A.G. Artukh et al., Nucl. Phys. A211 (1973) 299 and Yad. Fiz. 17 (1973) 1126
18. V.E. Bunakov et al., Izv. AN SSSR, ser. fiz. 44 (1980) 2831, ibid. 45 (1981) 1945
19. T. Udagawa and T. Tamura, Lecture at RCNP-Kikuchi Summer Sch., Osaka 1980; T. Tamura et al., Phys. Rev. C26 (1982) 379
20. L. Dehme and R. Reif, T.U. Inf. C5-12-82
21. V.K. Lukyanov and I.Z. Petkov, Nucl. Phys. 49 (1963) 529

# INCOMPLETE DEEPINELASTIC HEAVY-ION COLLISIONS

F. Guzman and R. Reif
Technische Universität Dresden, Sektion Physik, Dresden, DDR

In heavy-ion collisions with light projectiles and incident energies of 1o to 2o MeV/nucleon an appreciable amount of the total cross section is connected with processes producing fast light particles. The experimental data on such fast light particle emission during the course of heavy-ion induced reactions give strong evidence, that a non-equilibrium mode is involved, at least during the initial stage of the interaction. For example, in the reaction $^{2o}Ne$ (26o MeV) + $^{4o}Ca$ the inclusive kinetic energy spectra of the reaction product $^{16}O$ exhibit at forward angles a strong peak, located at an energy corresponding to the beam velocity (see fig. 2). The appearance of such a peak indicates, that in the field of the target a direct transition from a bound to a continuum state of the relative motion of the light and heavy fragment in the projectile occurs as the dominating non-equilibrium reaction.

In this reaction a further striking feature of the $^{16}O$ spectra is a well pronounced low-energy tail, which extends tens of MeV below the direct peak. Such an extra component is a clear indication of a more complex reaction mechanism governed by a final state interaction in the three-body channel, into which the system enters after the direct reaction. If one follows the change of the shape of the spectra with increasing reaction angle, one can establish, that the direct peak breaks down rapidly, while the low-energy component develops.

As pointed out by Udagawa and Tamura [1] this angular dependence of the spectral shape can be understood as a consequence of a breakup-fusion process, in which an elastic breakup of the projectile takes place first, but the $\alpha$-particle is fused into the target subsequently (see fig. 1). The compound nucleus formed than decays to another three-body final channel. Both amplitudes can be calculated approximately in DWBA. In a more pragmatic way, Hussein, McVoy and Saloner [2] decomposed the inclusive spectra, measured in similar reactions, in three parts: a primary direct fragmentation component in PWBA, a semi-direct component resulting from the inelastic scattering of the observed fragment and an empirical non-direct background. The second component has been determined by folding a direct-fragmentation-spectrum with an experimental inelastic scattering spectrum. The relative contributions of the first and second part has been used as a free parameter, adjusted to fit the data. Apart from the very low-energy end, the tail of the experimental spectra for $^{2o8}Pb(^{16}O,^{17}N)$ and $^{2o8}Pb(^{16}O,^{12}C)$ at 315 MeV have been well reproduced for one reaction angle.

In order to explain the low-energy component in the spectrum of the heavy projectile fragment, the present paper proposes a two-step reaction model, in which a direct projectile breakup is succeeded by a deepinelastic interaction of the heavy projectile fragment with the target, in which the fast heavy projectile fragment is strongly damped to the final low kinetic energy [3].

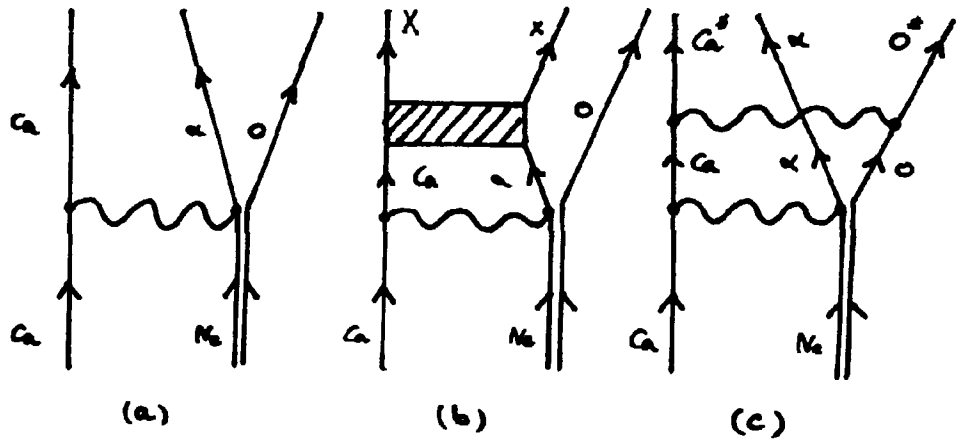


Fig. 1 Schematic diagrams for (a) elastic breakup, (b) breakup-fusion, and (c) incomplete DIC

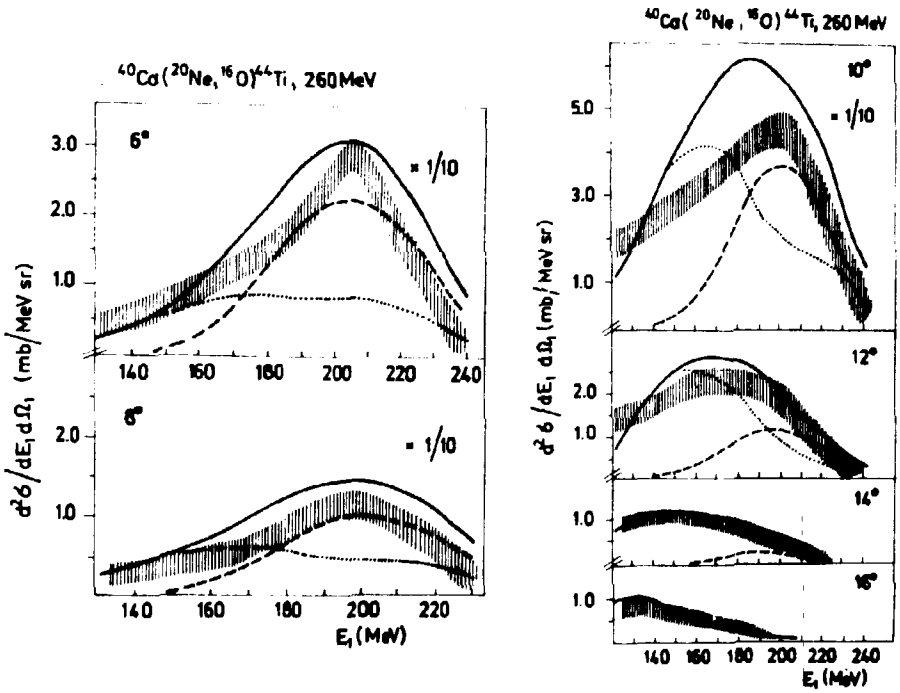


Fig. 2 Inclusive $^{16}O$ spectra in $^{20}Ne$ (260 MeV) + $^{40}Ca$.

Hatched area: experimental data. Elastic breakup: — — — . Incomplete DIC: ··· . Composed spectrum: ——— . Tamura and Udagawa[1]: —·—·

The qualitative picture of the course of the heavy-ion collision is the following. During the initial stage of the reaction, an elastic breakup of the projectile into an $\alpha$-particle and a heavy projectile fragment occurs, leading to a specific three-body channel. In order to simplify the situation it is assumed that this process is governed by the Alphaparticle-target interaction, leaving the heavy projectile fragment as a spectator. After the first stage of the interaction we are encountered with a composite system of three particles in contact with a certain distribution of energy and momentum for their relative motion. This system further develops in time. In order to have a two-body problem again, we assume, that the dominating force is the target-heavy projectile fragment (see fig. 1). Then, during the second stage of the reaction the target and the heavy projectile fragment are forming a double nuclear system, for the evolution of which the state after the first breakup acts as an initial state. Depending on the impact parameter in the ingoing channel and on the intermediate state after the breakup, this double nuclear system can fuse (incomplete fusion [4]) or undergo incomplete DIC. Within picture the entire double differential cross section for the emission of the heavy projectile fragment is constructed by superposition of a cross section $\sigma^{(1)}$ for the (first-order) breakup and a cross section $\sigma^{(2)}$ for a succeeding (higher-order) deeply inelastic interaction between the heavy projectile fragment and the target.

$$\sigma = \beta \left( \sigma^{(1)} + \alpha \, \sigma^{(2)} \right)$$

The coefficient $\alpha$, which regulates the relative contributions of both cross sections, is used to fit the <u>shape</u> of the experimental spectrum. The fit parameter $\beta$ gives the <u>magnitude</u> of the absolute cross section. The cross section $\sigma^{(1)}$ is estimated within a plane wave spectator model for $^{16}O$. It is expressed by the Fourier transform $\tilde{\phi}$ of the ground state wave function of the projectile, which is assumed to be a Gaussian with a width parameter $\sigma$.

$$\sigma^{(1)} \sim |\tilde{\phi}(\vec{k})|^2 \quad , \quad |\tilde{\phi}(\vec{k})|^2 \sim e^{-\frac{\hbar^2 \vec{k}^2}{2\sigma^2}}$$

The cross section $\sigma^{(2)}$ is calculated by folding a breakup cross section with the cross section for the deepinelastic collision $^{16}O$-target.

$$\sigma^{(2)} \sim \int dm \, \sigma^{(1)}(i \to m) \, \sigma_{DIC}(m \to f)$$

In order to simplify the integration over intermediate states it is assumed, that the breakup does not change the direction of the relative motion of $^{16}O$ and Ca ($\Omega^{(m)}_{O-Ca} = \Omega^{(i)}_{O-Ca}$). Differ nt from Hussein et al. the inelastic cross section is not taken from experiment, but calculated within a two-dimensional classical friction model for DIC, including statistical fluctuations of the collective variables.

Calculations have been performed for the reactions $^{20}Ne$ (149 MeV and 260 MeV) + $^{40}Ca$. Standard parameter values for the width $\sigma$ of the momentum distribution and the strength parameters $a_R$, $a_Q$ for the strength parameters of

the friction force:

$\sigma^2 = \sigma_0^2 A_1 A_2/(A_1+A_2-1)$ $\sigma = 90$ MeV/c or 83 MeV/c

$a_R = 12$ fm/cMeV $a_\Theta = 0.22$ fm/cMeV

The parameters $\alpha$ and $\beta$ have been fitted at one forward angle ($6^0$ lab.), and then the cross section has been predicted for five other angles without readjusting the parameters $\alpha$ and $\beta$. The results of the calculations are presented in fig. 2.

One can state, that the endpoint of the spectrum at lower energies is given correctly. This means, that the standard friction force produces the right magnitude of the energy loss during the final state interaction. For increasing reaction angle, as in the experimental data, the elastic breakup peak goes down rapidly, the spectrum becomes more broad, with a dominating contribution located at the low-energy end. Furthermore, it must be emphasized, that one has the same normalization factor $\beta$ for all reaction angles. So, the model reproduces simultaneously the shape of the spectrum and the angular distribution of the heavy projectile fragment, with similar results as DWBA-calculations for breakup-fusion (compare fig. 2). A more rigorous theory should treat the three-body nature of the interaction after the first reaction stage.

Some extensions of the model are demanded referring to angular correlations, mass distribution and angular momentum transfer in incomplete DIC.

## References


1. T. Udagawa and T. Tamura
   Lecture Notes of 1980 RCNP Kikuchi Summer School, Kobe, 1980, p. 171
2. M.S. Hussein, K.W. McVoy and D. Saloner
   Phys. Letters 98B (1981) 162
3. L. Oehme and R. Reif
   Phys. Letters (in press)
4. K. Siwek-Wilczynska et al.
   Nucl. Phys. A330 (1979) 150

# HIGH-ENERGY CHARGED PARTICLE EMISSION IN INCOMPLETE-FUSION REACTIONS

Chr.V.Christov, J.J.Delchev and I.J.Petkov
Institute of Nuclear Research and Nuclear Energy,Bulgarian Academy of Sciences, Sofia,Bulgaria

Recently,the light-particle emission in heavy-ion reactions has become a rather interesting but complicated problem. The emitted particles (mainly $\alpha$-particles) are peaked forward with an average velocity near to the beam velocity. Obviously, this process is conected with a transfer-reaction mechanism different from the evaporation. In order to determine the possible reaction mechanisms contributing to the $\alpha$-particle emission cross-section, the high-energy $\alpha$-particles have been detected in the region of their kinematic limits (the maximum possible energy for a given reaction channel evaluated by means of the conservation laws) [1-3]. The experimental data indicates that high-energy $\alpha$-particles are emitted with a significant probability near to the two-body kinematic reaction limit. The energy spectra fall approximately exponentially to this limit but there is a change of curve slope near to the limit. At lower incident energies the slope change almost coincides with the limit but it is removed with the increase of the energy. Tricoire et al. [4] have tried to explain the emission of the energetic $\alpha$-particles by the presence of light contaminants (such as $^{12}C$ and $^{16}O$) in the target. They have concluded that the $^{12}C$ contamination accounts for almost all high-energy $\alpha$-particles. It should be noted that their analysis is not very convincing since the $\alpha$-spectrum for a $^{12}C$-target in the c.m. system as represented [4] exceeds the two-body kinematic constraint. The analysis of the experimental data given in [2,3] does not agree with the above assumption as well.The comparison between the $\alpha$-particle cross-section in the case of 178 MeV $^{22}Ne$ projectile with different targets: $^{159}Tb$, $^{181}Ta$, $^{197}Au$, and $^{232}Th$ and the cross-section for the $^{12}C$-target shows, that in order to explain the $\alpha$-emission, the $^{12}C$ contamination in the first three targedts should be about of 30%, while the cross-section for the $^{232}Th$-target is larger than that for the $^{12}C$-target. The measurements of the high-energy part of $\alpha$-particle spectra allow one to distinguish the possible reaction mechanisms which contribute to it. The analyses [3] of the experimental results [2] with respect to the different reaction mechanisms suggest that it is only two-body processes which contribute to the emission of $\alpha$-particles with energies higher than 100 MeV. The $\alpha$-$\gamma$ coincidence experiments [5] confirm that the transfer reaction mechanism plays an important role in the $\alpha$-particle emission process.

In the present paper we consider the emission of high-energy $\alpha$-particles within the framework of a model [6] based on a simple quantum mechanical approach to the transfer process in which,however, the fusion process is included as an essential stage. We analyse reactions of the type

$$A + B \longrightarrow \alpha + (x + B),$$

where an $\alpha$-particle is emitted from the projectile $A$ and the fragment $x$ fuses into the target $B$ .The physical picture we accept supposes the formation of a

$X+B$ nuclear quasimolecule in accordance with a complete-fusion model [7] proposed earlier. The theoretical procedure is based on a modifucation of the PWBA in which along with the absorption (complete fusion) in the entrance channel kinematic Coulomb corrections are introduced. Then the total differential cross-section is given by

$$\frac{d\sigma}{dE_\alpha d\Omega} \sim \sum_{L=0}^{L_{max}} \frac{k_\alpha}{k_0} P^{NF}_{A+B}(L,k_0)\, T^{CF}_{X+B}(\ell,k_X)(2\ell+1)\tilde{R}^2_{\alpha-X}(|\bar{k}_\alpha - \frac{m_\alpha}{m_A}\bar{k}_0|) < R^\ell_{X-B}\bar{V}_{X,B}\, j_\ell >^2 . \qquad (1)$$

Here $L$ is the entrance-channel angular momentum related to the transferred momentum $\ell$ in terms of the classical conservation law

$$\ell \sim \frac{L}{k_0}|\bar{k}_0 - \bar{k}_\alpha| . \qquad (2)$$

The quantity $P^{NF}_{A+B}$ accounts for the absorption (quasimolecular formation) of the $L$-partial wave in the entrance channel and $T^{CF}_{X+B}$ is the formation probability of the $X+B$ quasimolecular $\ell$-state. Both quantities are evaluated in accordance with the model [7]. The function $\tilde{R}_{\alpha-X}$ is the Fourier transform of the function of $\alpha-X$ relative motion $\hat{R}_{\alpha-X}$ and it is taken in the form

$$\tilde{R}_{\alpha-X}(k) \sim \exp(-\frac{k^2}{4\sigma^2}) , \quad \sigma^2 = \frac{k_F^2}{5}\frac{m_\alpha m_X}{m_0 \cdot 1} . \qquad (3)$$

The matrix element is given by

$$< R^\ell_{X-B}\bar{V}_{X,B}\, j_\ell > = \int dr \left[R^\ell_{X-B}(r)\bar{V}_{X,B}(r)\, j_\ell(|\bar{k}_0 - \frac{m_B}{m_B+m_X}\bar{k}_\alpha|r)\, r^2\right], \qquad (4)$$

where $V_{X,B}$ is the "sudden" ion-ion potential of $X$ and $B$, and the function of the $X-B$ relative motion $R^\ell_{X-B}$ is the lowest quasibound solution of the Shrödinger equation with an ion-ion effective potential

$$W^\ell_{X,B} = \bar{V}_{X,B} + V^\ell_{rot} , \qquad (5)$$

where $V^\ell_{rot}$ is the centrifugal part.

Numerical calculations for the reactions of 178 MeV $^{22}$Ne-projectile with four different targets: $^{159}$Tb, $^{181}$Ta, $^{197}$Au and $^{232}$Th have been carried out. The numerical results have been normalized to the experimental data. A comparison between the calculated spectra and the experimental ones [2] is shown in Fig.1. As seen from Fig.1 the theoretical predictions are in a good agreement with the experiment [2]. There are some discrepancies to the experimental spectra at $\alpha$-particle energies smaller than 40 MeV. May be it is due to the presence of emitted $^8$Be-nuclei (practically two $\alpha$-particles) as well as to the presence of evaporated $\alpha$-particles both disregarded in our considerations. The contribution of $^8$Be-emission is essential at low $\alpha$-particle energies. At these energies a significant part of the entrance-channel $L$-window contributes to the $^8$Be-emission since its corresponding transferred angular momenta exceed the critical momentum for the $X+B$ system. The theoretical spectra reproduce well the experimental

ones at energies close to the $^{197}$Au and $^{232}$Th-targets. In

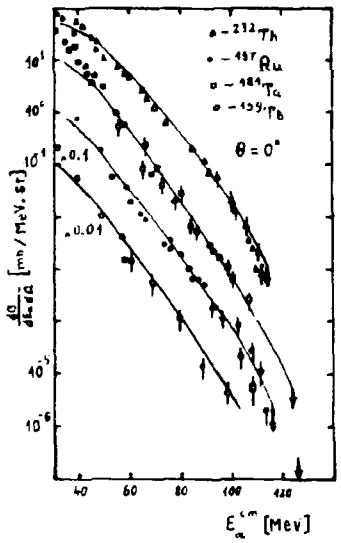


Fig.1
The theoretical spectra in a comparison with the experimental ones for 178 MeV $^{22}$Ne on different targets $^{159}$Tb, $^{181}$Ta, $^{197}$Au and $^{232}$Th at 0° [2]. The width $\sigma$ = 0.6 Fm$^{-1}$. The theory is represented by a solid line. The thick arrows indicate the two-body kinematic limits.

both cases the limits are comparetively lower and restrict the energy spectra. For the lighter targets the limits are higher and it seems that the change of the curve slope is not due to them. The slope change may be caused by the behaviour of the function of the relative motion $\tilde{R}_{\alpha-x}$ - taken rather schematically as a Gaussian in the numerical calculations. So, the model spectrum for $^{181}$Ta deviates from the experimental one at high $\alpha$-particle energies.

References


1. E.Gierlik et al. Z.Phys.A295(1980)295
2. C. Borcea et al. Nucl.Phys.A351(1981)312
3. C. Borcea et al. Nucl.Phys.(in press)
4. H. Tricoire et al. Z.Phys.A306(1982)127
5. T. Inamura et al. Phys.Lett.68 B(1977)51; D.R. Zolnowski et al. Phys.Rev.Lett 41(1978)92; T. Inamura et al. Phys.Lett.84 B(1979)71; K. Siwek-Wilczynska et al. Nucl.Phys.A330(1979)150
6. Chr.V. Christov et al. Preprint ICTR, IC/82/2,1982; Chr.V. Christov et al. Preprint ICTP(to be published)
7. J.J. Delchev et al. Preprint JINR,R4-8537, Dubna, 1975; J.J. Delchev et al. Z. Phys.A290(1979)273

# OBSERVATION OF DIRECT $^{12}C$-TRANSFER IN THE $^{12}C(^{14}N,d)^{24}Mg$-REACTION

K.P. Artemov, V.Z. Goldberg, M.S. Golovkov, I.P. Petrov, V.P. Rudakov, I.N. Serikov and V.A. Timofeev
Institute of Atomic Energy, Moscow, USSR

H.-U. Gersch, E. Hentschel, H. Schobbert, D. Wohlfarth and G. Lang
Zentralinstitut für Kernforschung, Rossendorf, DDR

The existence of $^{12}C$-clusters in $^{24}Mg$ is still an open problem. In particular the $^{12}C(^{16}O,\alpha)^{24}Mg$ reaction has been used to produce in a broad range excitations of $^{24}Mg$ and the hope was to find a correspondence between the $\alpha$-spectrum and the gross structure in $(^{12}C,^{12}C)$ elastic scattering. As reported recently by Stwertka et al. [1] there is, however, no evident demonstration of a $^{12}C$-clustering. Much of the structure in the $\alpha$-spectra comes from the sequential decay of the $^{16}O$ projectil and does not describe the nucleus $^{24}Mg$.
At excitation energies below 30 MeV many high spin levels of $^{24}Mg$ have been found from transfer reactions like $^{12}C(^{16}O,\alpha)^{24}Mg$, $^{12}C(^{14}N,d)^{24}Mg$ and $^{10}B(^{16}O,d)^{24}Mg$. The general behavior of the cross sections is in good accordance with the picture of complete compound nucleus formation and a following evaporation [2]. The cross sections alone, however, are not sensitive to the nuclear structure and calculations of the $^{24}Mg$ structure [3] seem to be correct only up to excitation energies of about 12 to 15 MeV.

The main idea of the present paper is to produce high spin states in the reaction $^{12}C(^{14}N,d)^{24}Mg$ and to select out those states which are formed at an early stage of the fusion process. If this is possible one can hope to find states with a structure different from that of the $^{24}Mg$ ground state band. May be there exist only few levels formed in a direct stripping process where the deuteron behaves like a spectator of the beginning $^{12}C$-$^{12}C$ fusion.
The experimental method to select out this mechanism has been developed by the Moscow group [4] to study $\alpha$-cluster states in light nuclei by means of the $(^{6}Li,d)$-reaction. Now we apply it to $^{12}C(^{14}N,d)^{24}Mg$. In both reactions the particles with spin 1 play an essential role. The idea is like the following.

We detect the deuteron from the $^{12}C(^{14}N,d)^{24}Mg$-reaction at $0^{o}$. If a CN formation takes place, the spin of the deuteron is in a random orientation relative to the orientation of the spin of the captured projectile $^{14}N$. Using the conservation of spin projections it is easy to show that the projection of the spin of an excited state in the final nucleus $^{24}Mg$ should have the values $0, \pm 1, \pm 2$. In the opposite case of direct transfer of a $^{12}C$ (ground state)-nucleus the orientation of the spin of $^{14}N$ is kept by the deuteron (of course we neglect spin orbital interaction). As a consequence the $^{24}Mg$ -nuclei are strongly aligned with the spin projection equal to zero. (The situation is much more complicated in the case of deuteron detection under other than $0^{o}$-angles. In this case it is necessary to make DWBA-calculations.)

Both discussed cases of $^{24}Mg$ -spin projection population can be easily distinguished by observation of the angular distribution of the $\alpha$-particle decay to the $^{20}Ne$ (ground state). In the case of CN formation the angular correlation function $W(\Theta)$ is:

$$W(\Theta) = \sum_{0}^{2} a_m^2 \, [P_J^m(\cos\Theta)]^2,$$

where $a_m$ is the amplitude of the population probability of the projection m of spin J in $^{24}Mg$. From the naive point of view different projections $a_m$ must be equally populated, but the calculations give ratios $a_0^2 \simeq a_1^2 \simeq 2 \cdot a_2^2$ with the normalization $\sum_0^2 a_m^2 = 1$ [5].

In the case of the direct mechanism we are dealing with only one projection m = 0 and the angular correlation function has the simple form

$$W(\Theta) = a_0^2 \, [P_J(\cos\Theta)]^2.$$

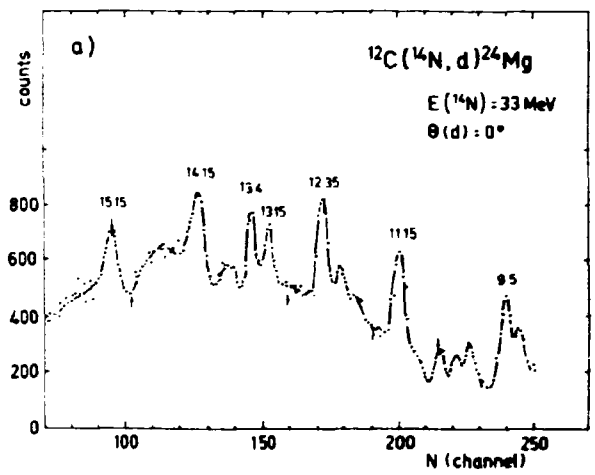


Fig. 1

Deuteron spectra of the reaction $^{12}C(^{14}N,d)^{24}Mg$ $\Theta_{lab} = 0^o$, $E_{lab}(^{14}N) = 33$ MeV, measured for angular correlations at the cyclotron of the Kurchatov institute

The measurement of the angular correlation was done at the Moscow cyclotron in two runs with bombarding energies 31 and 33 MeV. The corresponding excitation energy of $^{24}Mg$ covered the region 9.34 to 15 MeV. A typical deuteron spectrum at $0^o$ is shown in fig. 1. The energy values are preliminary ones. For all the levels in fig. 1 the correlation function has been measured. The most interesting result of the (d,α)-angular correlation measurement is shown in fig. 2. Only the one level labelled by the excitation energy 13.4 MeV in fig. 1 shows evidence for a predominant direct mechanism in the ($^{14}$N,d)-reaction. The full line which is in a nice agreement with the experimental points corresponds to the direct excitation of a $6^+$-level. The only one adjustable parameter is related to the branching ratio of the α-decay to the $^{20}Ne$ ground state. We obtained the branching ratio 27 ± 6 % which accords to the value 24 % given by Fifield et al. [6].

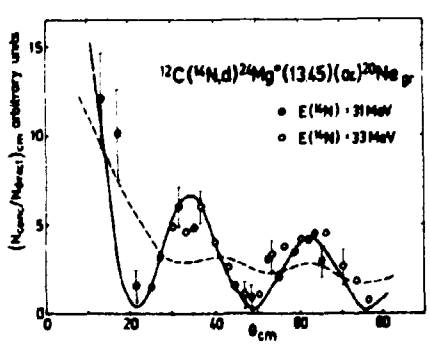


Fig. 2

d-α-particle angular correlation function for the state 13.45 MeV ($6^+$) in $^{24}Mg$. $\Theta_{CM}$ are angles in the rest system of $^{24}Mg$. Full line presents the function $[P_6(\cos\Theta)]^2$ (direct process) normalized to 27 % α-decay to the $^{20}Ne$ (ground state). The dotted line is the Hauser-Feshbach model prediction.

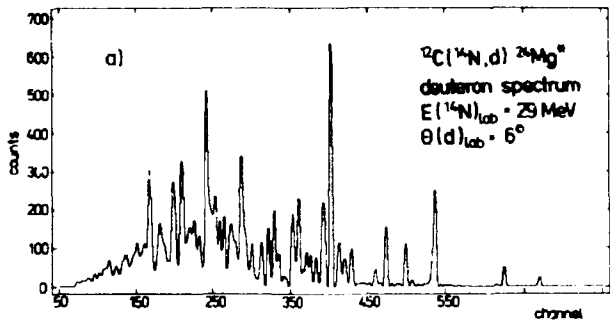


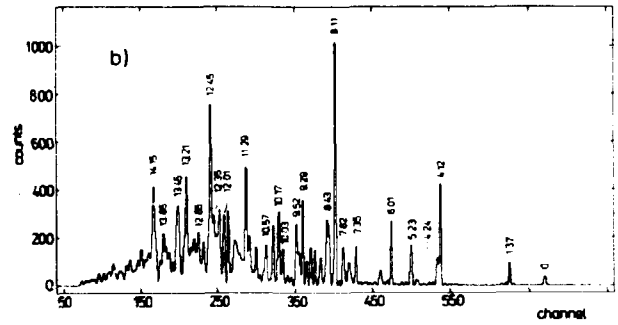


Fig. 3a

Deuteron spectrum (weakly smoothed) measured at 6° (LAB) by a conventional E/E telescope at the Rossendorf tandem van de Graaff. The bombarding energy was 29 MeV (LAB).

Fig. 3b

The spectrum shown in fig. 3a after applying a Wiener-Kolmogoroff-filter [7].

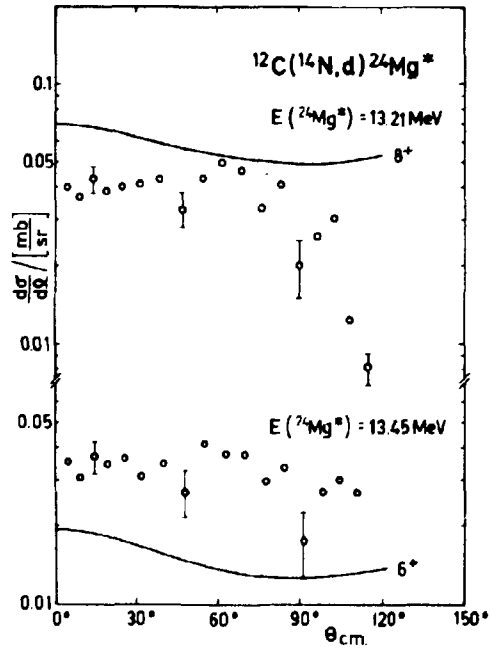


Fig. 4

Angular distributions of deuterons corresponding to $^{24}Mg$ -levels 13.21 MeV($8^+$) and 13.45 MeV($6^+$). The solid curves are the results of Hauser-Feshbach calculations.

Additional measurements of the deuteron angular distribution have been performed at the Rossendorf tandem van de Graaff. In fig. 3a a typical deuteron spectrum at 6°(lab) and the bombarding energy 29 MeV is shown. After application of a Wiener-Kolmogoroff-filter [7] we obtained an optimal resolution shown in fig. 3b. By careful energy determinations at several angles excitation energy values were obtained and are shown for some strong peaks. These values are accurate within ±15 keV. They are in good accordance with recent values by Szanto de Toledo et al. [2]. Our energy determination for the interesting $6^+$-level is 13.452 ± 0.015 MeV. Preliminary data of the angular distribution for the 13.45 MeV($6^+$) and the 13.21 MeV($8^+$)level are shown in fig. 4 together with the results of a Hauser-Feshbach (HF) calculation. The behavior is somewhat surprising. The experimental curve for the 13.45 MeV-level with a more direct excitation mechanism is closer to the HF result than in the case of the 13.21 MeV($8^+$)-level which is a member of the ground state band. Very preliminary data for the excitation function at 6°(LAB) measured between 27 and 30 MeV at the Rossendorf tandem show, however, for the 13.45 MeV-level a monotonic, weakly

increasing behavior while for other levels fluctuations occur like those published for the $^{12}C(^{14}N,\alpha)^{22}Na$ reaction by Cordell et al. [8].

Summarizing we state the existence of a level in $^{24}Mg$ which is excited in a direct transfer process in the $^{12}C(^{14}N,d)^{24}Mg$ reaction. From our arguments about the mechanism we can of course only say that the deuteron must be emitted early enough so that it's spin projection is not changed by the fusion process. Clearly this is not a proof for the existence of a highly deformed $^{12}C+^{12}C$ cluster structure. It is, however, a reasonable hope to expect at least some special nuclear structure for this level. Experiments are now in progress to look for the $\gamma$-decay and for neighbouring levels at higher energies with a similar behavior.

References

1. P.M. Stwertka et al.
Phys. Rev. Lett. 49 (1982) 640

2. A. Szanto de Toledo et al.
Nucl. Phys. A315 (1979) 500

3. I. Ragnarsson and T. Bengtsson,
Proceed. XIX Internat. Winter Meeting on Nuclear Physics, Bormio, Italy (1981), p. 48

4. K.P. Artemov et al.
Phys. Lett. 6 (1971) 378

5. V.Z. Goldberg,
Thesis, Moscow 1977

6. L.K. Fifield et al.
Phys. Rev. C8 (1973) 2217

7. E. Hentschel,
ZfK-324 (1976) 213

8. K.R. Cordell et al.
Nucl. Phys. A296 (1978) 278

# INFLUENCE OF THE TARGET EXCITATION ON THE SCATTERING OF POLARIZED $^{6}Li$ FROM $^{58}Ni$ AND $^{12}C$

K. Rusek
Institute of Nuclear Research, Warsaw, Poland, and
Max Planck Institut für Kernphysik, Heidelberg, Federal Republic of Germany

## 1. Introduction

Spin - orbit potentials found in recent Optical Model analysis of the elastic scattering of polarized $^{6}Li$ ions on $^{58}Ni$ and $^{12}C$ nuclei at 20 MeV and 19.24 MeV respectively [1], differ from those predicted by folding models [2,3]. The differences may be accounted for collective structure of the used target. In order to investigate the influence of the target excitation on the elastic scattering we have carried out detailed coupled channels /CC/ and DWBA calculations. For $^{12}C$ the existing inelastic scattering data were included in the analysis. The experimental data presented here have been obtained in the Max Planck Institut für Kernphysik in Heidelberg using the source for polarized lithium ions at the Heidelberg EN - Tandem [4].

## 2. Coupled channels and DWBA analysis

### 2.1 Inelastic scattering $^{12}C/^{6}Li$, $^{6}Li/^{12}C_{4.44\ MeV}$ at 19.24 MeV

Treating the first excited state of $^{12}C$ /4.44 MeV, $2^{+}$/ as a one phonon state, the DWBA calculations with complex coupling were performed. A process responsible for a transition between collective states is usually treated as spin independent therefore the spin transfer $\Delta s = 0$ was assumed in the calculations. The entrance channel Optical Model potential was the same as the one used recently [1]. The same central part of the potential was used in the exit channel. Several sets of the spin - orbit potentential parameters in the exit channel were tried to get a correct description of the measured vector /$iT_{11}$/ and tensor /$^{T}T_{20}$/ analyzing powers [5]. An example of the calculations is shown in Fig. 1 by dashed curves. The parametrization of the spin - orbit potential was the following: Thomas shape, $V_{ls} = 0.$ MeV, $r_o = 1.227$ fm, $a_o = 0.2$ fm. The calculated curves follow the common behaviour of the measured angular distributions but do not reproduce the absolute values of the analyzing powers.
The coupled channels calculations were performed using the code CHUCK [6]. In these calculations coupling between the first and the second /7.66 MeV, $0^{+}$/ excited states of the target nucleus was included. The results of the calculations of the differential cross sections and the vector analyzing powers are shown by solid curves in Fig. 1. For the vector analyzing powers the results do not differ from those obtained with the DWBA approach. The coupling constant $\beta_2 R = 1.64 - 2.09$ fm was extracted with the range of values depending on whether the real or imaginary radius is used. Previous values ranging from 1.1 to 1.94 fm have been reported [7,8,9].

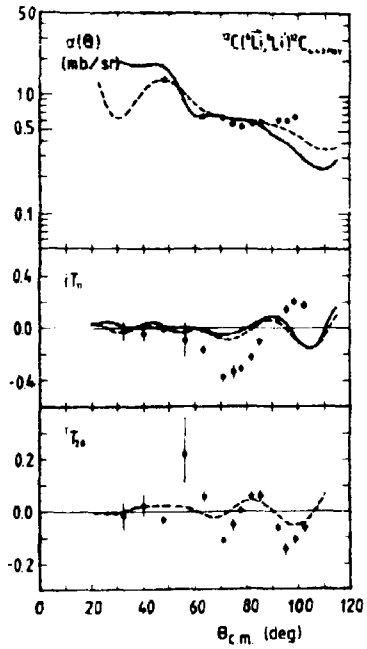


Fig. 1 Angular distributions of differential cross sections, vector /$iT_{11}$/ and tensor /$^{T}T_{20}$/ analyzing powers for inelastic scattering of polarized $^{6}$Li ions on $^{12}$C at 19.24 MeV. Solid and dashed curves show the results of CC and DWBA calculations, respectively.

## 2.2 Elastic scattering of polarized $^{6}$Li ions on $^{12}$C and $^{58}$Ni

In the recent Optical Model analysis of the elastic scattering of polarized $^{6}$Li ions on $^{12}$C and $^{58}$Ni nuclei at 19.24 and 20.0 MeV, respectively, the phenomenological spin - orbit potentials were found to give a good description of vector and tensor analyzing powers without any additional tensor terms in the OM potential [1]. However these potentials are larger in the region important for the scattering [3] than those predicted by folding models[2,3]. One of the possible explanation is the influence of target excitation which should reduce the strenght of the spin - orbit interaction due to the reduction of the imaginary part of the Optical Model potential.

The results of CC calculations for elastic scattering of $^{6}$Li on $^{12}$C at 19.44 MeV are shown by solid curves in Fig. 2. The imaginary part of the Optical Model potential was reduced from 10.3 MeV to 8.3 MeV in comparison with single channel calculations, to get correct description of the differential cross sections. The influence of the target excitation is explicity seen for the vector analyzing powers. In the angular region around 100 deg the CC calculations differ significantly from the signle channel ones and give better description of the experimental data. The strength of the spin - orbit interaction was reduced by about 15 precent in comparison with that found before [1] but it still differs from folding model prediction.

The CC calculations with complex collective formfactor were corried out also for elastic scattering of polarized $^{6}$Li on $^{58}$Ni at 20.0 MeV. Only the coupling between the ground and the first excited state of the target was involved. The value of the deformation parameter $\beta_2$ = 0.21 used in the calculations was taken from

the previous work [10]. In the calculations the imaginary part of the OM potential was reduced from 15.24 MeV to 9.5 MeV and spin - orbit interaction from 0.46 MeV to 0.30 MeV in comparison with OM analysis [1]. The results shown in Fig. 3 by solid curves describe well both presented angular distributions and do not differ too much from single channel predictions. The strength of the used spin - orbit interaction is still larger in the tail region than that found on the basis of the folding models [2,3]. The CC calculations with folding model spin - orbit potential [3] shown in Fig. 3 by dotted curve for comparison display oscillating structure and do not reproduce the data. In summary, this analysis of the elastic scattering data shows that the CC technique describes well the data and allows to reduce differences between phenomenological spin - orbit potentials and those predicted by folding models.

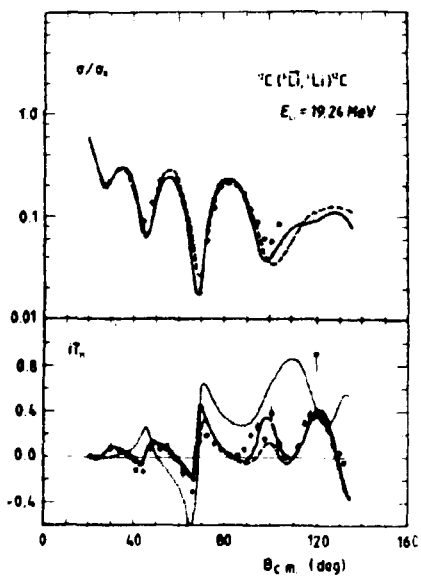


Fig. 2

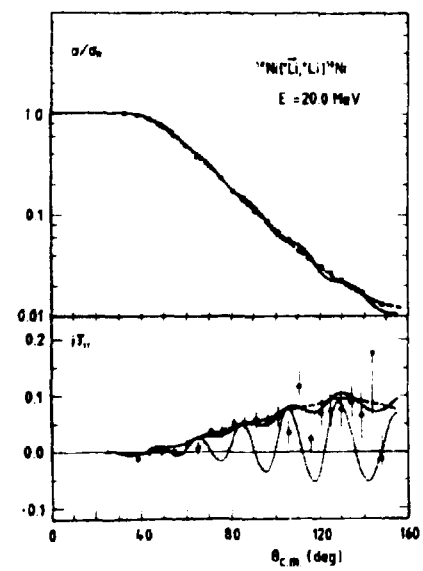


Fig. 3

Calculated results of the differential cross section /ratio to the Rutheford cross section/ and vector analyzing powers for elastic scattering of polarized $^6$Li on $^{12}$C and $^{58}$Ni. Dashed curves and solid curves are the results of the one channel and coupled channels calculations, respectively. Dotted curves are the results of the coupled channels calculations with spin - orbit potentials predicted by folding model[3].

## 3. Concluding remarks

Inelastic scattering of polarized $^6$Li ions on $^{12}$C leading to the first excited state of the target nucleus was analysed using the DWBA and CC methods. Each transition in the analysis was treated as a one phonon collective one. The re-

sults reproduce the shapes of the experimental data but do not reproduce their absolute values. The influence of the target excitation on the elastic scattering of polarized $^{6}Li$ on $^{12}C$ and $^{58}Ni$ was investigated. The influence was found to be important /especially for $^{12}C$/ but did not explain fully the descrepances between the spin - orbit potentiale found in the Optical Model analysis [1] and those predicted by folding models [2,3].

## References


1. K.Rusek et al, to be published
2. W.Weiss et al, Phys. Lett. 61B /1976/ 237
   H.Amakawa and K-I.Kubo, Nucl. Phys. A266 /1976/ 521
3. F.Petrovich et al, Phys. Rev. C17 /1978/ 1612
4. E.Steffens, Nucl. Instr. Meth. 184 /1981/ 173
5. M.Simonius, Lecture Notes in Physics vol 30, ed. D.Fick, Berlin - Springer 1974
6. P.D.Kunz, code CHUCK, unpublished
7. P.K.Bindal and K.Nagatani, Phys. Rev. C9 /1974/ 2154
8. P.Schumacher et al, Nucl. Phys. A212 /1973/ 573
9. H.G.Bingham et al, Phys. Rev. C11 /1975/ 1913
10. C.Williamson et al, Phys. Rev. C21 /1980/ 1344

# MONOPOLE EXCITATION IN ELASTIC AND INELASTIC NUCLEUS-NUCLEUS SCATTERING REACTIONS

G. Saupe
Vereinigtes Institut für Kernforschung Dubna, Dubna, UdSSR
Technische Universität Dresden, Sektion Physik, Dresden, DDR
K.V. Shitikova
Vereinigtes Institut für Kernforschung Dubna, Dubna, UdSSR

The aim of this work is the description of monopole excitations in elastic and inelastic scattering reactions of nuclei with A=16 in the framework of a microscopic model using various types of nucleus-nucleus interaction potentials (folding potential, energy-density formalism). The nuclear densities used for the calculation of the folding potential are obtained employing the method of hyperspherical functions with realistic nucleon-nucleon interaction [1].

In the method of hyperspherical functions the wave function of a nucleus A is given by $\Psi(1,2,\ldots,A) = \rho^{-\frac{1}{2}(3A-4)} \sum_{K\gamma} \chi_{K\gamma}(\rho)\, Y_{K\gamma}(\Omega_i)$

where $\rho$ denotes the hyperradius and the $Y_{K\gamma}(\Omega)$ are the K-harmonics polynominals. The Hamiltonian of this problem takes the form

$$H = -\frac{\hbar^2}{2m}\frac{1}{\rho^{3A-4}}\frac{\partial}{\partial\rho}\left(\rho^{3A-4}\frac{\partial}{\partial\rho}\right) - \frac{\hbar^2}{2m}\frac{1}{\rho^2}\Delta_\Omega + V(\rho),$$

from which one gets the Schrödinger equation for the radial functions $\chi_{K\gamma}(\rho)$

$$\left(\frac{d^2}{d\rho^2} - \frac{L_K(L_K+1)}{\rho^2} - \frac{2m}{\hbar^2}\left(E + W^{K\gamma}_{K\gamma}(\rho)\right)\right)\chi_{K\gamma}(\rho) = \frac{2m}{\hbar^2}\sum_{K\gamma \neq K'\gamma'} W^{K'\gamma'}_{K\gamma}(\rho)\,\chi_{K'\gamma'}(\rho)$$

with $L_K = K + \frac{3}{2}(A-2)$. In this equation $W_{K\gamma}(\rho)$ refers to the matrix element of the potential energy of the nucleon-nucleon interaction, which is described in a realistic way according to Brink and Boaker [2]. Then, the resulting eigenfunctions $\chi_{K\gamma}(\rho)$ determine the radial density distributions $n_{ij}(r)$ of the nucleus investigated for the ground state, the excited state, and the transition between them. For example, in the approach $K = K_{min}$ it is obtained [3]

$$n_{ij}(r) = \frac{16}{\sqrt{\pi}}\,\frac{\Gamma[\frac{1}{2}(5A-11)]}{\Gamma[\frac{1}{2}(5A-14)]}\int_r^\infty (\rho^2-r^2)^{(5A-16)/2}\,\rho^{-(5A-13)}\,\chi_i(\rho)\,\chi_j(\rho)$$
$$+\frac{8(A-4)}{3\sqrt{\pi}}\,\frac{\Gamma[\frac{1}{2}(5A-11)]}{\Gamma[\frac{1}{2}(5A-16)]}\int_r^\infty r^2(\rho^2-r^2)^{(5A-15)/2}\,\rho^{-(5A-13)}\,\chi_i(\rho)\,\chi_j(\rho)$$

In this picture it is also possible to compute the RMS-radius of the nuclear state. Furthermore, the radial density distributions can be used to construct the folding potentials describing the interaction of the two nuclei. The two-particle interaction $V_{12}(\vec{r}_2 - \vec{r}_1)$ is chosen as the Skyrms-interaction [4] with $\delta$-forces for various parameter sets and in the form of energy-dependend finite-range forces proposed by Satchler and Love[5], where the effect of the Pauli-principle is taken into account by an exchange term.

In order to investigate the influence of the repulsive core on the differential cross sections for the nucleus-nucleus scattering process the interaction potential was also calculated in the framework of the energy-density formalism [6] for symmetric systems.

These differential cross sections which can be compared with experimental data

are computed employing the coupled channels method, where the optical potential $V_{opt}(R)$ between the nuclei is chosen in the manner

$$V_{opt,ij}(R) = (\alpha + i\beta)\, U_{ij}(R).$$

Here, the parameters $\alpha$ and $\beta$ depend on the bombarding energy of the system and on the type of $U_{ij}(R)$ as it is described above.

This formalism was applied to the interpretation of experimental data of the reactions $^{12}C(^4He,^4He^{0+})^{12}C$, $E^*(^4He^{0+}) = 20.1$ MeV, $E_{Lab} = 65$ MeV [7], $^{12}C(^3He,^3He)^{12}C^{0+}$, $E^*(^{12}C^{0+}) = 20.3$ MeV, $E_{Lab} = 108.5$ MeV [8], $^{16}O(^4He,^4He)^{16}O^{0+}$, $E^*(^{16}O^{0+}) = 6.06$ MeV, $E_{Lab} = 40$ MeV [9], $^{16}O(^{16}O,^{16}O)^{16}O$, $E_{Lab} = 41, 49, 63$ MeV [10].

In order to describe the monopole excitation of $^{16}O$ at E = 6.06 MeV in the inelastic scattering reaction $^4He + ^{16}O$ the 4p - 4h configuration of $^{16}O$ has to be taken into account. Fig. 1 represents the result which was obtained with the parameters $\alpha = 1$ and $\beta = 0.3, 0.1$ for the elastic and inelastic channel, respectively. In this case one gets a better agreement with the experiment for the scattering in forward direction. The investigation of the elastic $^{16}O + ^{16}O$ scattering shows the improvement of the reproduction of the data if one uses finite-range forces instead of the Skyrme-interaction with $\delta$-forces.

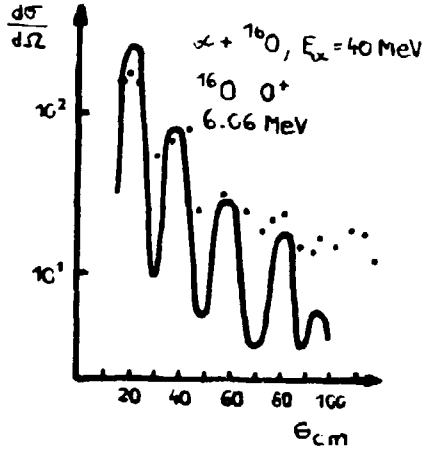


Fig. 1

## References


1. A.I. Baz, M.V. Shukov, UA3-1883 (1969)
2. M. Brink, E. Boeker, Nucl. Phys. A91 (1967) 1
3. M. Keschiev, K.V. Shitikova, Sov. J. Nucl. Phys. 30 (1979) 1479
4. N.v. Giai et al., Phys. Lett. 35B (1971) 135
5. G.L. Satchler, W.G. Love, Phys. Lett. 65B (1976) 415
6. H. Ngo, C. Ngo, Nucl. Phys. A348 (1980) 140
7. H.P. Morsch, P. Decowski, Phys. Lett. 82B (1979) 1
8. D. Lebrun et al., Phys. Lett. 97B (1980) 358
9. J.V. Maher et al., Phys. Rev. 188 (1969) 1665
10. A.I. Yavin, G.W. Farwell, Nucl. Phys. 12 (1959) 1

# DYNAMICS OF HEAVY ION COLLISIONS+

H. Feldmeier*
Max-Planck-Institut für Kernphysik, Heidelberg

H. Spangenberger
Institut für Kernphysik, Technische Hochschule Darmstadt

+ Work supported by Gesellschaft für Schwerionenforschung mbH, Darmstadt

* Heisenberg fellow

Like in any dissipative process the theoretical description of deeply inelastic heavy ion collisions has to begin with the separation of the dynamical variables into macroscopic and intrinsic, or slow and fast coordinates. Then the equations of motion for the macroscopic variables contain dissipative parts (friction) which have their origin in the interaction with the intrinsic degrees of freedom. This interaction is assumed to be of stochastic nature and is responsible not only for dissipation of macroscopic collective energy but also for the observed fluctuations of the macroscopic degrees of freedom.

The model which we apply to describe the dynamics of dissipative heavy ion collisions is based on this concept and allows to calculate trajectories as well as the diffusion in phase-space. The ingredients are

1) Macroscopic variables: Three macroscopic degrees of freedom determine uniquely a family of shapes. The shapes consist of two spheres smoothly joined by a hyperbolic neck.[1,2] The degrees of freedoms are denoted by: $s$ = distance between the two spheres, $\sigma$ = percentage of the volume in the neck, $\Delta$ = asymmetry. The total volume of the shapes with sharp surfaces is conserved and does not depend on $(s, \sigma, \Delta)$. Negative values of $\sigma$ mean a squeezing of shapes with $\sigma = 0$ such that we get oblate deformations for two separated objects. A complete family of shapes is shown in fig. 1. Furthermore we have three angles of rotation describing the relative and intrinsic rotations.

2) Kinetic energy: A Werner-Wheeler flow pattern $\vec{v}(\vec{r})$ inside the shapes which corresponds to a change in $(s, \sigma, \Delta)$ is assumed. The kinetic energy is thus given by

$$T = \frac{\rho_0}{2} \int_{\text{shape}} d^3r \, [\vec{v}(\vec{r})]^2 = \frac{1}{2} \sum_{ij} M_{ij} \dot{q}_i \dot{q}_j$$

where $(\dot{q}_1, \dot{q}_2, \dot{q}_3) = (\dot{s}, \dot{\sigma}, \dot{\Delta})$. The matrix element $M_{11}$ is illustrated in the center part of fig. 1. To compare this with the reduced mass $\mu$ the contour lines show the ratio $M_{11}/\mu$. In the region of binary shapes below the scission line (dash-dotted curve) it is close to one. For the three rotational degrees of freedom the rigid body moment of inertia is assumed.

3) Potential energy: Here we calculate for each shape a folding potential consisting of a Coulomb and a nuclear part:

$$V(s,\sigma,\Delta) = \frac{\rho_c}{2}\int_{shape} d^3r \int d^3r' \frac{1}{|\vec{r}-\vec{r}'|} + \frac{\gamma_s}{2}\int_{shape} d^3r \int d^3r' \left\{ \frac{1}{a} - \frac{2}{|\vec{r}-\vec{r}'|} \right\} e^{-\frac{|\vec{r}-\vec{r}'|}{a}}$$

The parameters a, $\gamma_s$ are taken from Krappe, Nix, Sierk.[3] The result is shown in the lower part of fig. 1 as a contour plot of the potential energy. The landscape exhibits the binary valley, the Coulomb barrier close to the touching point and a saddle point. To the left of the saddle the system gains energy in going to the compound sphere, to the right it gains energy by reseparating again.

4) Dissipation mechanism: We use the window-plus-wall dissipation. Utilizing the long mean-free-path of a nucleon in a nuclear medium at not too high an excitation energy we calculate friction and diffusion coefficients by considering the time evolution for small times of the one-body phase-space distribution close to the window between the nuclei or close to the wall.[2] The friction coefficients are the well known expressions for window and wall dissipation. The diffusion coefficients for the window dissipation are not related to the drift (friction) coefficients by an Einstein relation. Rather, the relative velocity of the two nuclei plays a similar role as the temperature in the region where the excitation of the two nuclei is still small. This is indicated in fig. 2, where the two occupied Fermi spheres in the single parparticle velocity space are shown at different times during a collision. In the beginning they are shifted by the initial relative velocity. Due to the Pauli Principle transitions which contribute to the dissipation are only possible in the dotted area. This in turn is proportional to the relative velocity $|\vec{u}_r|$. At a later stage of the reaction the nuclei are heated up and additional transitions are possible in the shell of partial occupied states. In a very late stage of the reaction where the relative velocity is negligible the available phase space for transitions is determined solely by the temperature $\tau$. Only in this limit we obtain the Einstein relation. This extreme limit, however, is not reached in reactions where the two nuclei reseparate again after less than one revolution.

Typical results for trajectory calculations (without diffusion) are shown in fig. 3. The experimentally observed large energy damping leading to values far below the Coulomb barrier is achieved by very stretched shapes of the system in the exit channel.

Another interesting feature of heavy ion reactions is the dynamical behaviour of two fusing nuclei. Studies in the direction[5] support Swiatecki's concept[4] of an "extra push".

Using the calculated diffusion coefficients in a moment expansion of the Fokker-Planck equation we obtain Wilczynski diagrams as shown in fig. 4. For these calculations we kept $\sigma$ and $\Delta$ fixed at their initial values which results in too low energy losses. However, the important point to note is that the peripheral collisions with small excitation energies already exhibit rather large fluctuations

in scattering angle and energy in agreement with the measured data. The reason is that for these reactions the diffusion is driven by the relative velocity (c.f. fig. 2) which is large and not by the temperature which is still small.

In summary we present a model which is based on known macroscopic properties of nuclei and nuclear matter in connection with a not too much simplified treatment of the geometry in coordinate as well as in velocity space. This leads without any adjustable parameters to an unexpected successful description of a large variety of phenomena in dissipative heavy ion collisions.

This contribution is a condensate of a lecture held at the International School of Physics "Enrico Fermi", Varenna, 26. July - 7. August 1982.[2)]

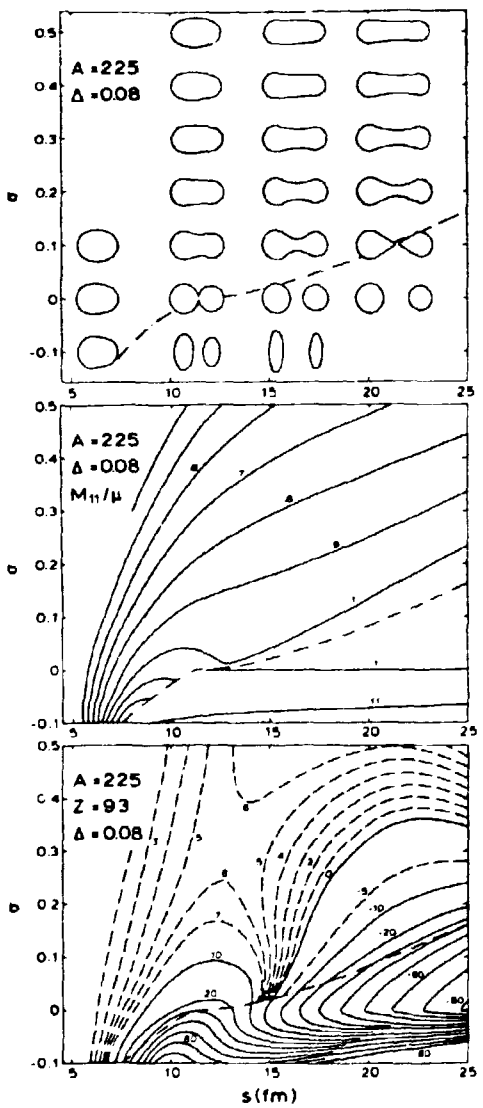


Figure 1:

Upper part: family of shapes for fixed asymmetry as a function of s and $\sigma$ . Center part: contour plot of the diagonal matrix element for the motion in the s-direction divided by the reduced mass in the Werner-Wheeler collective flow mass-tensor. Lower part: contour plot of the potential energy calculated with the folding-potential. Energies are in MeV and with respect to the compound sphere.

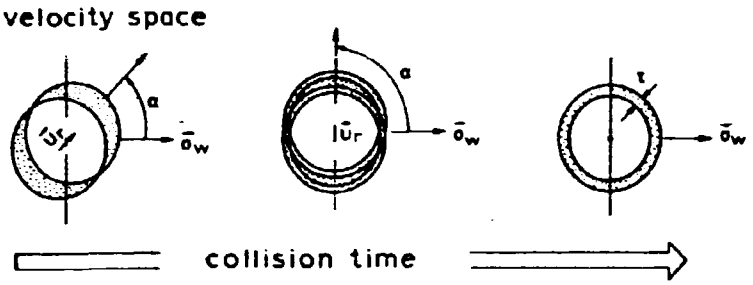


Figure 2 : Illustration of the contributing part of the velocity space (dotted areas). The left-hand part shows the case where $\tau = 0$ and the relative velocity part $|\vec{u}_r|\ D^u$ dominates, the center part is for an intermediate situation and the right hand part for the thermal limit with $|\vec{u}_r| = 0$.

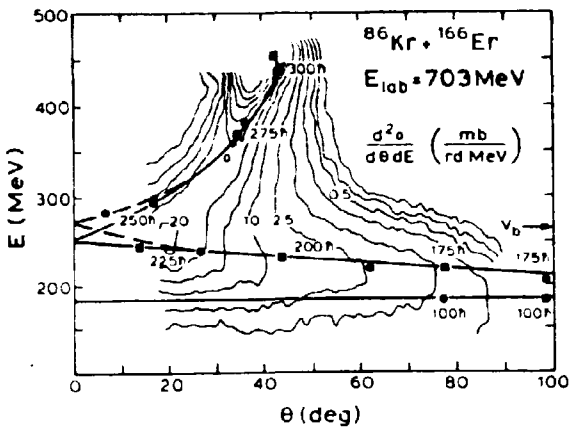


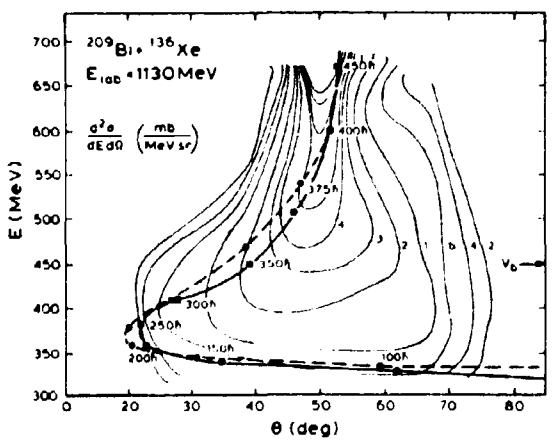


**Figure 3:**

Wilczynski diagram for $^{86}Kr$ + $^{166}Er$ at $E_{lab}$ = 703 MeV and $^{136}Xe$ + $^{209}Bi$ at $E_{lab}$ = 1130 MeV. Squares denote the result of trajectory calculations which include all degrees of freedom and the Werner-Wheeler flow for the mass. Circles denote the results of the reduced equations of motion with frozen asymmetry $\Delta$ and assuming a creeping motion in $\sigma$ .

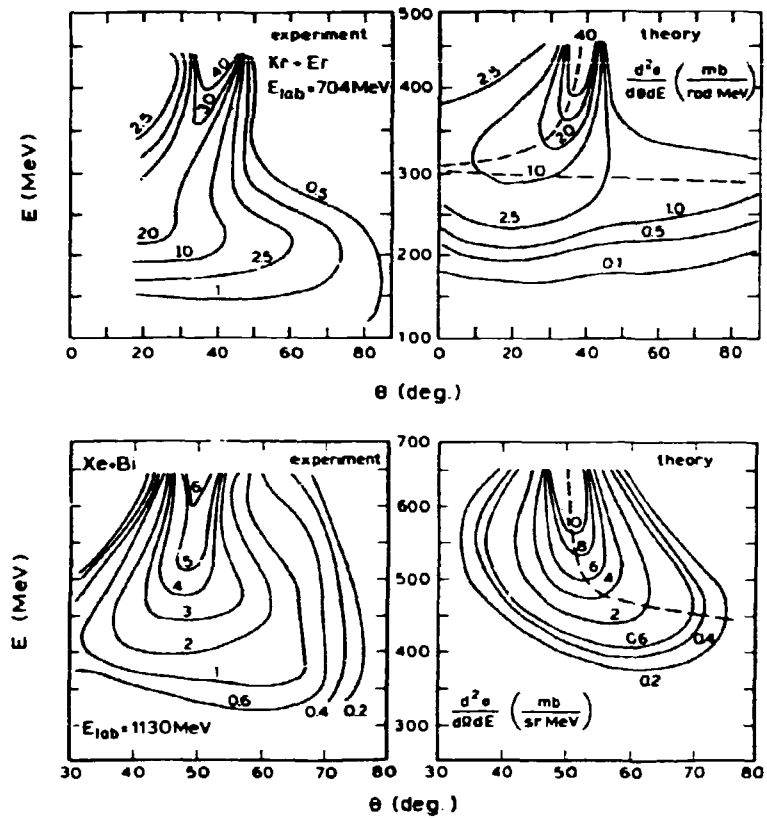


Figure 4:

Experimental and theoretical Wilczynski diagrams for $^{86}Kr + ^{166}Er$, $E_{lab}$ = 703 MeV and $^{136}Xe + ^{209}Bi$, $E_{lab}$ = 1130 MeV. The broad distributions close to the initial energy are due to the relative velocity part $|\vec{u}_r|\ D^u$ of the momentum diffusion. The dashed line denotes energy and scattering angle of the mean trajectories.

## References


1. J. Blocki, W.J. Swiatecki; preprint LBL-12811 (1981).
2. H. Feldmeier; Proceedings International School on Physics "Enrico Fermi", 26. July - 7. August 1982, to be published; IKDA 82/19 (1982).
3. H.J. Krappe, J.R. Nix, A.J. Sierk; Phys. Rev. C20, 992 (1979).
4. W.J. Swiatecki; Nucl. Phys. A376, 275 (1982).
5. H. Feldmeier; Proceedings International Workshop on Gross Properties of Nuclei and Nuclear Excitations X, Hirschegg 1982, p. 26, ISSN 0720-8715.

# CORRELATIONS BETWEEN COLLECTIVE AND INTRINSIC MOTION IN DIC

L. Münchow and A. Pfitzner
Zentralinstitut für Kernforschung, Rossendorf, DDR

## 1. Introduction

As we know from experiment the collision partners in a deep-inelastic collision of two heavy ions keep their identity in the average, inspite of the long interaction time of some $10^{-21}$ sec. This suggests to consider the relative distance r between the two ions as a physically relevant collective degree of freedom (d.f.), in addition to the intrinsic (nucleonic) d.f. $\{x\}$. Usually this additional d.f. is treated classically, i.e. the relative motion is described by trajectories. The argument for this is the small de Broglie wave length on account of the large reduced mass. This argument, however, becomes questionable near the turning point, where, in a head-on collision, the relative velocity is equal to zero. The question in how far a quantum-mechanical description of the relative motion would alter the dynamics of the collision process is still an open question. An interesting way to tackle this problem was proposed by Hasse[1] who described the relative motion by wave packets, simulating the coupling to the intrinsic d.f. by a frictional Schrödinger equation for the relative motion. We try to go beyond the trajectory concept in a more consistent way by introducing a total density matrix (d.m.) $D(\{x\}, \{x'\}, r, r', t)$, depending on both intrinsic and collective d.f.. The product ansatz $D(\{x\}, \{x'\}, r, r', t) \approx \varrho(\{x\}, \{x'\}, t) \cdot \sigma(r, r', t)$ leads to the mean-field approximation[2] and, in the classical limit, to the trajectory concept. Demanding this factorisation of D for all times would mean that we allow the collective and intrinsic d.f. to interact only via their mean fields, and that we exclude correlations in the strict sense. These correlations induce fluctuations of the mean fields, which in turn influence the dynamics of both collective and intrinsic motion. The influence on the collective dynamics was investigated by Gross[3] and by Takigawa[4]. These authors, however, retain the mean field approach for the intrinsic d.f. which are treated on the many-particle level. We focus, however, our attention to the influence of the correlations in D on the intrinsic motion. In passing to the one-particle level, we are able to make this influence transparent in the time-evolution of the single particle occupation numbers.

The description of the intrinsic motion on the one-particle level is, on the other hand, just the goal of TDHF. We therefore have to accentuate the differences of our approach with respect to TDHF. Simulating a low-energy heavy-ion collision by TDHF means to describe the time evolution of the one-particle d.m. in the time-dependent self-consistent field of the combined system, generated by all nucleons irrespective of their origin (target or projectile). The relative distance has not the meaning of a collective d.f., but is introduced by hand via classical initial conditions for the relative motion. Quantum fluctuations, therefore, are not accounted for. At later times, collective variables must be extracted indirectly by plausible prescriptions (see, e.g., ref.[5]).

In our model, we want to retain the collective variable as a genuine d.f.. The price we have to pay is the loss of selfconsistency for the combined system. We consider the mean field of the approaching projectile as an external perturbation with respect to the nucleons of the target, (and vice versa). The time-dependence of this perturbation originetes from the relative motion vis the dependence on the reduced d.m. $\sigma(r, r', t)$.

## 2. Intrinsic motion with external correlations

In what follows we focus our attention to the approach phase of the collision. The reason is that for not too heavy systems most of the collective energy is transferred into intrinsic excitation during a short time of order $10^{-22}$ sec at the beginning. If we assume that during this stage the overlap of the nuclei keeps small, it is reasonable to distinguish between nucleus A and nucleus B and to characterize their mutual interaction by $V^{AB}(r)$. The initial situation (t=0) is given by an internal d.m. $\varrho(0) = \varrho^A(0) \cdot \varrho^B(0)$. To postulate this factorization for t>0 is equivalent to approximate the average value $\langle V^{AB} \rangle_t$ by the sum of the mean fields of either nucleus acting on the other one: $\langle V^{AB}\rangle_t \approx \langle V^A\rangle_t + \langle V^B\rangle_t$ , with $V^A = tr_B\, \varrho^B(t)\, V^{AB}(r)$ and $\langle \cdots \rangle_t = tr_c\, \sigma(t) \ldots$ , the average over the collective d.f.. This means nothing else than neglection of two body collisions between nucleons from different nuclei, in accordance with the confirmed idea of "one-body dissipation" at low energies. To investigate the influence of external correlations on the intrinsic system it is then sufficient, within our model, to consider only one nucleus, say, nucleus A. We therefore drop any indication of the collision partners in the following.
To specify our model we introduce the total Hamiltonian

$$H = H_0 + V \qquad H_0 = H_{coll} + H_{in} \qquad V = \sum_{\nu\nu'} V_{\nu\nu'}(r)\, a_\nu^+ a_{\nu'} \tag{1 a}$$

The intrinsic Hamiltonian of the isolated nucleus reads

$$H_{in} = \sum_{\nu\nu'} t_{\nu'\nu}\, a_\nu^+ a_{\nu'} + \frac{1}{2} \sum_{\nu\nu'\mu\mu'} v_{\nu'\mu',\mu\nu}\, a_\nu^+ a_\mu^+ a_{\mu'} a_{\nu'} \tag{1 b}$$

The total d.m. follows the v. Neumann equation $i\dot{D} = [H, D]$ , with the initial condition $D(0) = \varrho(0) \cdot \sigma(0)$. To extract the uncorrelated part of D(t) for t>0 we use time-dependent projection techniques[6]. With the projection operators $P(t) = \sigma(t) tr_c$ and $Q(t) = 1-P(t)$, we find $P(t)D(t) = \varrho(t) \cdot \sigma(t)$ and $Q(t)D(t) = D^{cor}(t)$. If we apply P(t) on the v. Neumann equation we obtain

$$i\dot{\varrho} = [H_{in} + \langle V\rangle_t , \varrho] + tr_c [V, D^{cor}] \quad , \quad \varrho(0) = |0\rangle\langle 0| \ . \tag{2}$$

Dropping $D^{cor}$ yields the mean field approach (with respect to the external coupling) and, applying Ehrenfest's theorem to the external mean field, $\langle V \rangle_t \approx V(\langle r \rangle_t)$, provides the familiar semiclassical approximation. Because $D^{cor}(0)=0$, we find for the external correlator

$$D^{cor}(t) = \frac{1}{i} \int_0^t dt'\, \phi(t,t') \left\{ (-i\dot{\sigma}(t') + [H_{coll}, \sigma(t')])\, \varrho(t') + [\delta V(t'), \varrho(t')\sigma(t')] \right\} \tag{3}$$

Here we have introduced the traceless coupling $\delta V(t) = V - \langle V \rangle_t$ which describes the deviation of V from its mean value at time t, and the propagator in the

Q-subspace

$$\phi(t,t') = \underset{\leftarrow}{T} \exp\left\{-i\int_{t'}^{t} dt_1\, Q(t_1)[H,\cdot]\right\} \quad , \quad \phi(t,t) = 1 , \tag{4}$$

$\underset{\leftarrow}{T}$ being the time-ordering operator. By inspection of equ. (3) we find that the correlations introduce a memory into the equation for $\varrho$ . During the memory time we approximate the time-dependence of $\sigma(t')$ under the integral by that for the free relative motion. Then the first two terms within the curly brackets in equ. (3) cancel.

Taking $D^{cor}$ in first order perturbation theory with respect to $\delta V$ , we obtain the final equation for the many-body d.m. $\varrho$ ,

$$i\dot{\varrho} = [H_{in} + \langle V\rangle_t, \varrho] + \frac{1}{i}\int_0^t dt'\, tr_\tau\left[\delta V(t), G_0(t,t')[\delta V(t'), \varrho(t')\sigma(t')]G_0^\dagger(t,t')\right] . \tag{5}$$

Here we have introduced the propagator

$$G_0(t,t') = \exp[-iH_{coll}(t-t')]\cdot G_{in}(t,t') \quad , \quad G_{in}(t,t') = \underset{\leftarrow}{T}\exp\left\{-i\int_{t'}^{t} d\tau\,(H_{in} + \langle V\rangle_\tau)\right\} . \tag{6}$$

The correlation term in equ. (5) contains typical quantities like $\langle \delta\hat{V}(t-t')\, \delta V(t')\rangle_{t'}$, with $\hat{V}(t) = \exp[\,iH_{coll}t]\, V \exp[\,-iH_{coll}t]$ . These are correlation functions with maximum value at $t' = t$, which represents the fluctuation $\langle \delta V(t)^2 \rangle_t$ of the coupling $V$ around its mean value $\langle V \rangle_t$. We conclude that the correlation term reflects the effect of fluctuations of the external mean field on the intrinsic motion.

## 3. Evolution of the occupation numbers

To study the time-development of the intrinsic system we turn to the one-particle level. This is done by the method of quantum-kinetic equations[7]. The hierarchy of equations for the one-particle d.m. $\varrho^{(1)}_{nn'} = tr_{in}\,\varrho(t)\, a^\dagger_n a_{n'}$ , the two-particle d.m. $\varrho^{(2)}_{nmm'n'} = tr_{in}\,\varrho(t)\, a^\dagger_n a^\dagger_m a_{m'} a_{n'} = \varrho^{(1)}_{nn'}\varrho^{(1)}_{mm'} - \varrho^{(1)}_{nm'}\varrho^{(1)}_{mn'} + R^{(2)}_{nmm'n'}$ , and so on, is cut off putting the three-particle correlator $R^{(3)}$ equal to zero. Without the external mean field this procedure would lead to the self-consistent equation for the one-particle d.m. of the isolated nucleus, supplemented by a collision term arising from the internal two-body correlator $R^{(2)}$. In its structure this equation is identical with the TDHF-equation plus collision term. For heavy-ion collisions such an equation was derived, e.g., by Ayik[6] and Weidenmüller[9]. But, as already mentioned, the latter are equations for the single particle motion in the self-consistent field of the combined system and, therefore, represent a completely different tackling of the problem. Now, in our model, we specify single-particle states $|n\rangle$ for the nucleus under consideration, and ask for the time evolution of the one-particle d.m., in this basis, under the influence of the fluctuating external mean field. Using equ. (5), we arrive at

$$i\dot{\varrho}^{(1)}_{nn'} = -\langle n|\,[h(t), \varrho^{(1)}]\,|n'\rangle + \frac{1}{2}\langle n|[R^{(2)}, v^a]|n'\rangle + \frac{1}{i}\int_0^t dt'\, I^{(1)}_{nn'}(t,t') . \tag{7}$$

The one-body Hamiltonian h(t) consists of a self-consistent part $S(\varrho^{(1)}(t))$ arising from the two-body interaction introduced in equ. (1 b), and the external

mean field $\langle V \rangle_t$:

$$h(t) = S(\varrho^{(1)}(t)) + \langle V \rangle_t \quad , \quad S_{nm}(\varrho^{(1)}) = t_{nm} + \sum_{\mu\mu'} v^a_{n\mu',\mu m}\, \varrho^{(1)}_{\mu\mu'} . \tag{8}$$

Superscript "a" means the antisymmetrized matrix element of $v$. The integral term represents the influence of the external fluctuations. Although $\delta V^2$ is a two-particle operator, it turns out that $I^{(1)}(t, t')$ is a functional only of the one-particle d.m.. Replacing $G_{in}$ of equ. (6) by the mean field propagator

$$g(t,t') = \underset{\leftarrow}{T} \exp\{-i \int_{t'}^{t} d\tau\, h(\tau)\} , \tag{9}$$

we find

$$I^{(1)}(t,t') = \mathrm{tr}_c\, \hat{\sigma}(t')\left[g^{+}(t,t')\left(\varrho^{(1)}(t')\delta\hat{V}(t')\bar{\varrho}^{(1)}(t') - \bar{\varrho}^{(1)}(t')\delta\hat{V}(t')\varrho^{(1)}(t')\right)g(t,t'),\ \delta\hat{V}(t)\right] \tag{10}$$

Here we have introduced the notations $\hat{A}(t) = \exp[iH_{coll}t]\, A \exp[-iH_{coll}t]$ and $\bar{\varrho}^{(1)} = 1 - \varrho^{(1)}$.

To make equ. (7) a closed one we have to express the internal correlator $R^{(2)}$ by $\varrho^{(1)}$. By inspection of the equation for $R^{(2)}_{nmm'n'}$, which will be derived elsewhere, we find, in addition to the inhomogenous term representing incoherent two-body collisions, an integral term which is a functional of $\varrho^{(2)}$ and arises from the external correlations. If we neglect this influence of the external correlations on the internal correlator, and resign the inclusion of coherent effects via p-h- and p-p-correlations, as well as the damping of the single-particle states, we obtain approximately

$$R^{(2)}(t) \approx \frac{1}{i}\int_0^t dt'\, g^{+}(t,t')\left(\varrho^{(1)}(t')\varrho^{(1)}(t')\, v^a \bar{\varrho}^{(1)}(t')\bar{\varrho}^{(1)}(t') - \bar{\varrho}^{(1)}(t')\bar{\varrho}^{(1)}(t')\, v^a \varrho^{(1)}(t')\varrho^{(1)}(t')\right) g(t,t') , \tag{11}$$

Because we neglect ground-state correlations, we have $R^{(2)}(0) = 0$. Insertion of equ. (11) into equ. (7) provides the final equation for $\varrho^{(1)}$. The internal correlation term originating from $R^{(2)}$ has just the familiar structure of the collision term in extended TDHF. But, in contrast to the latter, our propagator $g(t, t')$ refers only to the states in one nucleus, but exhibits an explicite coupling to the relative motion via the external mean field $\langle V \rangle_t$, equ. (8). In order to make the role of the correlations in equ. (7) transparent, we choose the time-dependent single-particle basis, $|n\rangle_t$, generated by h(t). By inspection of the external correlations, equ. (10), we encounter products of matrix-elements $\delta V_{n,\nu}$ taken at different times. The same holds for products of matrix-elements $v^a_{n\mu,\mu'\nu'}$ appearing in the internal correlations, which are obtained if we insert solution (11) into equ. (7). Following the arguments given in[9] we make the approximation

$$\underbrace{v^a_{n\mu,\mu'\nu'}}_{t}\ \underbrace{v^a_{\nu'\mu',\mu n}}_{t'} \approx |v^a_{n\mu,\mu'\nu'}|^2 \exp[-(t-t')^2/2\tau^2_{corr}] , \tag{12}$$

and an analogous approximation for products of $\delta V(t)_{n\nu}$. The correlation time $\tau_{corr}$ introduced this way is a measure for the overlap, ${}_t\langle n|n\rangle_{t'}$, of the same

single-particle states at different times $t' \neq t$, in the sense that ${}_t\langle n|n\rangle_{t'} \simeq 0$ for $|t-t'| > \tau_{corr}$. During time intervals $|t-t'| \lesssim \tau_{corr}$ we assume that the states $|n\rangle_t$ develop diabatically[9], i.e. without any population of other states $n' \neq n$ :

$$g(t,t')|n\rangle_{t'} \approx |n\rangle_t \exp\left[-i\int_{t'}^{t} d\tau\, \varepsilon_n(\tau)\right] \quad , \qquad \varepsilon_n(\tau) = {}_\tau\langle n|h(\tau)|n\rangle_\tau \ . \tag{13}$$

This is plausible because the approach of the projectile is a rapid process which leaves, over small times, no time for the nucleons to redistribute into other states.

We are now ready to write down the final equation for the occupation numbers $\varrho_n^{(1)}(t) = {}_t\langle n|\varrho^{(1)}(t)|n\rangle_t$. On account of the correlations, also off-diagonal matrix elements of $\varrho^{(1)}$ come into play. As a first approximation, we neglect the off-diagonal elements, assuming that the time-dependent mean field is the dominant agent for the intrinsic motion[8]. If we disregard memory effects in the diagonal elements of $\varrho^{(1)}$, we may write the equation for $\varrho_n^{(1)}$ in the form of a master equation with gain and loss terms:

$$\frac{d}{dt}\varrho_n^{(1)} = \sum_\nu \left\{ (W+\mathcal{F})_{\nu\to n}\, \varrho_\nu^{(1)}(t)\, \bar{\varrho}_n^{(1)}(t) - (W+\mathcal{F})_{n\to\nu}\, \bar{\varrho}_\nu^{(1)}(t)\, \varrho_n^{(1)}(t) \right\}, \tag{14}$$

where

$$W_{n\to\nu} = \frac{1}{2} \sum_{\mu\mu'} |v^a_{n\mu,\mu'\nu}|^2\, \varrho_\mu^{(1)}(t)\, \bar{\varrho}_{\mu'}^{(1)}(t)\, \Delta^{coll}(t)_{n\mu,\mu'\nu} \tag{15}$$

and

$$\mathcal{F}_{n\to\nu} = \sum_{pq} \sigma(t)_{p+q/2,\,p+q/2}\, |\delta V_{n,\nu}(q)|^2\, \Delta^{fl}(t)_{n,\nu} \ . \tag{16}$$

Here, in performing $\mathrm{tr}_c\, \sigma(t)$ ... from equ. (10), we have used the momentum representation for $\sigma$ and neglected non-diagonal elements. The quantity q, then, just represents the transferred momentum from the relative motion, connected with the transition $n \to \nu$. The quantities $\Delta$ are, for the collision and the fluctuation term, respectively

$$\Delta^{coll}_{n\mu,\mu'\nu}(t) = \int_0^t dt'\, e^{-t'^2/2\tau_{corr}^2} \left( \exp\left[ i \int_{t-t'}^{t} d\tau\, \Delta\varepsilon(\tau)_{n\mu,\mu'\nu} \right] + c.c. \right) \tag{17}$$

and

$$\Delta^{fl}_{n,\nu}(t) = \int_0^t dt'\, e^{-t'^2/2\tau_{corr}^2} \left( \exp\left[ i \int_{t-t'}^{t} d\tau \left( \Delta\varepsilon(\tau)_{n,\nu} - pq/\mu \right) \right] + c.c. \right) , \tag{18}$$

with $\Delta\varepsilon(\tau)_{n\mu,\mu'\nu} = \varepsilon_n(\tau) + \varepsilon_\mu(\tau) - \varepsilon_{\mu'}(\tau) - \varepsilon_\nu(\tau)$ , $\Delta\varepsilon(\tau)_{n,\nu} = \varepsilon_n(\tau) - \varepsilon_\nu(\tau)$ and $pq/\mu$ the transferred kinetic energy from the relative motion.

Equ. (14) is the central result of our approach. The internal correlations W have the same structure as the collision term in extended TDHF and describe the thermalisation of the intrinsic excitations. The additional external correlations $\mathcal{F}$ exhibit the influence of the fluctuations on the development of the

occupation numbers. It is remarkable that they fit the gain minus loss structure and therefore preserve the form of a master equation for $\varrho_n^{(1)}(t)$.
It is instructive to discuss the relation to the quantal Boltzmann equation. To this end we pass over to an extended system. In our formulation this means to drop the time-dependence of $\Delta\mathcal{E}$ and to take the limit $\tau_{corr} \to \infty$. For times t larger than the memory time we may replace the upper limit in $\int_0^t dt'$ by $t = \infty$ and obtain, from equ. (17) and (18), respectively

$$\Delta^{coll}_{n\mu,\mu'\nu}(\infty) = 2\pi\,\delta(\varepsilon_n + \varepsilon_\mu - \varepsilon_{\mu'} - \varepsilon_\nu) \quad and \quad \Delta^{fl}_{n,\nu}(\infty) = 2\pi\,\delta(\varepsilon_n - \varepsilon_\nu - pq/\mu)\,. \qquad (19)$$

For an infinite system, of course, the conception of an external perturbation makes no sense, and we had to drop the fluctuation term. It remains the collision term with the energy-conserving $\delta$-function, as given by the Boltzmann equation. For a finite system, however, this $\delta$-function vanishes because the single-particle energies are discrete. The $\delta$-function in $\Delta^{fl}$, however, would not vanish because $pq/\mu$ is continuous. This means that the fluctuations remain operative, namely for "on-shell" transitions $\Delta\varepsilon_{n,\nu} = pq/\mu$. To make the collision term operative in a finite system, it is necessary to smooth the $\delta$-function. This is done, in our model, by the finite correlation time, $\tau_{corr}$, and the time-dependence of the single-particle energies, $\varepsilon_n(t)$. As argued in[9] the latter effect is the dominant one; an estimate given there provides a smoothing of the $\delta$-function over several MeV. In our model the time-dependence of the energies is mainly due to the external field $\langle V \rangle_t$ and thus, via $\sigma(t)$, to the time-development of the relative motion. The connection between the "opening of the collision window" by smoothing the $\delta$-function and the collective motion was already discussed qualitatively in[9]. In our approach this connection becomes more explicite.
We conclude with the following statements:

(i) A consistent treatment of collective and intrinsic motion allows to include external correlations beyond the mean field approach.
(ii) These correlations represent fluctuations of the external mean field.
(iii) These fluctuations change the occupation numbers of the single-particle states and must be considered together with the two-body collisions.
(iv) Equilibration and relative motion are intimately connected because the collision term becomes operative dominantly via the time-dependence of the external mean field.

References

1. R.W. Hasse and K. Hahn
Nukleonika 25 (1980) 133
2. S. Mukamel, U. Smilansky, D.H.E. Gross, K. Möhring and M.I. Sobel
preprint WIS-81/4/Jan-ph
3. D.H.E. Gross, K. Möhring, S. Mukamel, M. Smilansky and M.I. Sobel
preprint HMI-P81/17 Th
4. N. Takigawa, K. Nita, Y. Okuhara and S. Yoshida
Nucl. Phys. A 371 (1981) 130

5. S.E. Koonin
Progress in particle and nuclear physics 4 (1979) 283
6. C.R. Willis and R.H. Picard
Phys. Rev. A 9 (1974) 1343
7. B.A. Rumyantsev, S.A. Kheifets
Yad. Fiz. 21 (1975) 510
8. S. Ayik
Z. Physik A 298 (1980) 83
9. P. Grangé, H.A. Weidenmüller and G. Wolschin
Ann. Phys. 136 (1981) 190

# PARTICLE-HOLE DESCRIPTION OF HIC

R.V. Jolos
Joint Institute for Nuclear Research, Dubna, USSR
R. Schmidt and J. Teichert
Technische Universität Dresden, Sektion Physik, Dresden, DDR

The first stage of a HI-reaction at incident energies of about 10 MeV/N characterized by the conversion of relative kinetic energy into that of internal excitation should be described by nonstatistical theories. Today there does not exist a common understanding of this process. In principle there are three mechanisms which may contribute to the energy dissipation in the entrance channel, the excitation of collective states, the transfer of nucleons between projectile and target and the excitation of uncorrelated many particle-many hole states. Different models have been developed to describe the energy loss in terms of these mechanisms. The common basis of these models is the assumption that the excitation of the intrinsic system is expected to result from the rapid change of the mean field of the nucleons leading to their excitation. In this sense the TDHF-approximation should be a good candidate to describe the approach phase of a HIC. However, due to the lack of collective coordinates in the TDHF method, one can hardly derive from it a transparent physical picture of the relevant contributions to the energy loss. Therefore, simpler models which take into account collective degrees of freedom at the very beginning may contribute to a better surveyed understanding of the approach phase in HIC.

In the present paper we develop a microscopic model which is based on three assumptions: (i) The relative motion between the ions characterized by collective coordinates R, P is described classically. (ii) The rapid change of the mean field of the nucleons leads to the excitation of uncorrelated np-nh states within the nuclei. (iii) The many-body wave function of the internal system of the two ions is approximated by a product wave function $|\Psi\rangle = |\Psi_1\rangle \cdot |\Psi_2\rangle$ that means we neglect the mass transfer between the ions. A generalization of our model to include the nucleon transfer will be given elsewhere[1].

With the upper assumptions the hamiltonian of two interacting ions contains three parts

$$\hat{H} = H_{coll}(R,P) + \hat{H}_0(\hat{x}_i) + \hat{H}_{int}(\hat{x}_i, R) \qquad (1)$$

the collective energy $H_{coll}$ depending on the distance between the centres of the ions R and the conjugate momentum P, the internal hamiltonian of the separated ions $\hat{H}_0$ and the interaction between them $\hat{H}_{int}$.

From eq. (1) one obtains the equation of motion for the relative motion

$$\dot{R} = \nabla_P H_{coll} \qquad (2)$$

$$\dot{P} = -\nabla_R H_{coll} - \nabla_R \langle \Psi(t) | \hat{H}_{int} | \Psi(t) \rangle \qquad (3)$$

where the expection value of the interaction has to be calculated with the time-dependent many body wave function of the intrinsic system $|\Psi(t)\rangle$ . The interaction can be derived from the general expression

$$\hat{H}_{int} = \iint d\vec{r}_1\, d\vec{r}_2 \quad \Psi_1^+ \Psi_1 \quad V_{NN}(\vec{r}_1 - \vec{r}_2) \quad \Psi_2^+ \Psi_2 \tag{4}$$

with $V_{NN}$ the nucleon-nucleon interaction and $\Psi^+$ is the field operator expressed by the particle $\alpha_p^+$ and hole operators $\beta_h^+$

$$\Psi^+(\vec{r}) = \sum_{p=1}^{\infty} \varphi_p^*(\vec{r})\, \alpha_p^+ \quad + \sum_{h=1}^{A} \varphi_h^*(\vec{r})\, \beta_h \tag{5}$$

with the corresponding wave functions $\varphi_p$ and $\varphi_h$ . Inserting (5) into (4) and restricting only to mean-field-channels the interaction becomes

$$\hat{H}_{int} = U(R) + \sum_{ph}\left(V_{ph}(R)\ \alpha_p^+ \beta_h^+ + h.c.\right) + \sum_{pp'} V_{pp'}\, \alpha_p^+ \alpha_{p'} + \sum_{hh'} V_{hh'}\, \beta_h^+ \beta_{h'} \tag{6}$$

where U(R) is the ion-ion folding potential and $V_{ph}(R)$ the matrix element for the excitation of a ph-state due to the time-dependent mean field.
For the hamiltonian of the unperturbed internal system we use

$$\hat{H}_0 = \sum_p \epsilon_p\, \alpha_p^+ \alpha_p + \sum_h \epsilon_h\, \beta_h^+ \beta_h \tag{7}$$

that means, we neglect the residual interaction between excited particles and holes leading to the decay of the initial excited ph-states into more complex states and finally to thermalization. The inclusion of these effects [2] requires statistical assumption which are beyond the scope of this work. Note that within the traditional TDHF-description of HIC these two-body effects are neglected too. The influence of this type of residual interaction on the dynamics of HIC will be studied in detail within a separate work [2].

With (1), (6), (7) the many body wave function $|\Psi(t)\rangle$ can be expressed by the action of the time evolution operator U(t,0) on the HF-ground state $|HF\rangle$

$$|\Psi(t)\rangle = U(t,0)|HF\rangle = \sum_{n=0}^{\infty} \frac{(-i)^n}{n!} \int_0^t dt_1 \ldots \int_0^t dt_n \ T\left[\hat{H}_{int}(t_1) \ldots \hat{H}_{int}(t_n)\right]|HF\rangle \tag{8}$$

where T is the time ordering operator. The time ordered product in eq. (8) contains all possible processes which can be induced by the action of a time dependent mean field. In general these processes can be constructed by the combination of three basic graphs

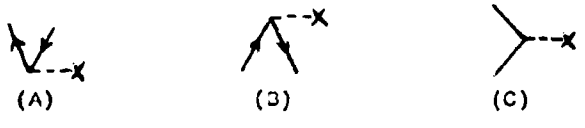

(A) (B) (C) (9)

the excitation (A) of a ph-pair, the annihilation (B) of a ph-pair and the rescattering (C) of a particle or hole state. Whereas a graph (A) represents a graph of first order the second order processes (B) and (C) appear only in combinations with (A). So, e.g. in second order three graphs can be constructed from (9)

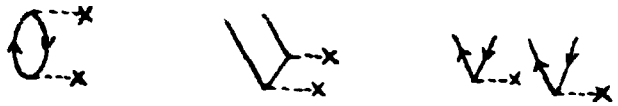

(D) (E) (F) (10)

where (D) contribute to the elastic channel, (E) gives the second order contribution to the 1p-1h states and (F) is the lowest order contribution for the excitation of 2p-2h-state. In general the wave function (8) can be written as

$$|\Psi(t)\rangle = e^{\sum_{ph} c_{ph}(t)\, \alpha_p^+ \beta_h^+} |HF\rangle \tag{11}$$

with $c_{ph}(t)$ the ph-amplitude.
The norm of this wave function reads

$$\langle\Psi|\Psi\rangle = 1 + \sum_{ph} |c_{ph}|^2 + \sum_{p_1>p_2}\sum_{h_1>h_2} c_{p_1h_1} c_{p_2h_2} \left\{ c^*_{p_1h_1} c^*_{p_2h_2} - c^*_{p_1h_2} c^*_{p_2h_1} \right\} + \ldots \tag{12}$$

where the mixed terms ($p_1h_2$, etc.) within the brackets $\{\ldots\}$ take into account the Pauli-principle. Neglecting these terms expection values of operators can be derived in a closed form. For the interaction energy $\hat{H}_{int}$ one obtains

$$\langle \hat{H}_{int} \rangle(t) = \frac{\langle \Psi(t) | \hat{H}_{int}(t) | \Psi(t) \rangle}{\langle \Psi(t) | \Psi(t) \rangle} = \sum_{ph} V_{ph}(t) \left\{ e^{i\epsilon_{ph}t} c^*_{ph} + e^{-i\epsilon_{ph}t} c_{ph} \right\} \tag{13}$$

and for the particle number operator giving the number of excited particles

$$\langle \mathcal{N} \rangle(t) = \sum_p \frac{\langle \Psi(t) | \alpha_p^+ \alpha_p | \Psi(t) \rangle}{\langle \Psi(t) | \Psi(t) \rangle} = \sum_{ph} |c_{ph}|^2 \tag{14}$$

The excitation probability $P_N$ of a Np-Nh state is given by

$$P_N(t) = \frac{\langle \mathcal{N} \rangle^N(t)}{N!}\, e^{-\langle \mathcal{N} \rangle(t)} \tag{15}$$

The results (13), (14), (15) are general (except the neglection of the Pauli-principle) and independent on the order in which the ph-amplitude $c_{ph}(t)$ is calculated. Approximated results are obtained by restricting to 1p-1h states in (11)

$$|\Psi^{(1)}\rangle = \left(1 + \sum_{ph} c_{ph}(t)\, \alpha_p^+ \beta_h^+\right) |HF\rangle \tag{16}$$

In this case the expection values (13), (14) read

$$\langle H^{(1)}_{int} \rangle = \sum_{ph} V_{ph}(t) \left\{ e^{i\epsilon_{ph}t} c^*_{ph} + e^{-i\epsilon_{ph}t} c_{ph} \right\} \Big/ \left[ 1 + \sum_{ph} |c_{ph}|^2 \right] \tag{17}$$

$$\langle \mathcal{N}^{(1)} \rangle = \sum_{ph} |c_{ph}|^2 \Big/ \left[ 1 + \sum_{ph} |c_{ph}|^2 \right] \tag{18}$$

and the excitation probabilities (15) are identical zero $P_N \equiv 0$ for $N \geq 2$. In contrast to (14) the ph-number (18) remains always smaller than one independent from the order in which $c_{ph}(t)$ is calculated. From (17) and (18) the results of a first order perturbation theory are obtained if in addition to the assumption (16) the ph-amplitude is calculated in first order

$$c_{ph}(t) = -i \int_0^t V_{ph}(t')\, e^{i\epsilon_{ph} t'}\, dt' \tag{19}$$

First order perturbation theory (16), (17), (18), (19) is applicable only as long as the excitation probability (18) is small compared to one, that means if

$$\sum_{ph} |c_{ph}|^2 \ll 1 \tag{20}$$

No such restriction is required for the use of expressions (13), (14), (15) even if $c_{ph}$ is calculated in first order, although the expressions for the interaction energy (13) and (17) are formally the same if (20) is fulfilled. This formal equivalence is a direct consequence of the neglection of the Pauli-principle in calculating expression (13). The main point is that the calculation of the ph-amplitude $c_{ph}(t)$ in first order does <u>not</u> mean that first order perturbation theory is applied for the many body problem. In a first application we use the first order ph-amplitude (19) and study the dynamics of a HIC under the influence of the induced force in eq. (3)

$$-\nabla_R \langle H_{int} \rangle = 2 \sum_{ph} \int_0^t dt'\, \nabla_R V_{ph}(t)\, V_{ph}(t') \sin \epsilon_{ph}(t-t') \tag{21}$$

obtained from (19) and (13). The sum over the ph-states in eq. (21) may be formally replaced by an integral over the ph-energies $\epsilon$

$$-\nabla_R \langle H_{int} \rangle = 2 \int_0^t dt' \int_0^\infty d\epsilon\, g(\epsilon)\, \nabla_R V_\epsilon(t)\, V_\epsilon(t') \sin \epsilon(t-t') \tag{22}$$

with $g(\epsilon) = \sum_{ph} \delta(\epsilon - \epsilon_{ph})$ the ip-ih density. Instead of making a complete microscopic calculation of the matrix elements and the density $g(\epsilon)$ we parametrize

$$g(\epsilon)\, V_\epsilon(t)\, V_\epsilon(t') \approx U_N(R(t))\, U_N(R(t'))\, V_0^2\, f(\epsilon) \tag{23}$$

For the radial formfactors $U_N(R)$ we use the proximity potential [3] and for the energy dependence the parametrization

$$f(\epsilon) = \frac{\epsilon}{\Delta^2}\, e^{-\epsilon/\Delta} \tag{24}$$

There are two model parameters within the ansatzes (23) and (24), the overall strength $V_0$ describing the effective N-N-interaction and $\Delta$ the effective range of s.p.-energies included. In fig. 1 we present the energy dependence $f(\epsilon)$ as function of the parameter $\Delta$ together with the corresponding Fourier-transforms of this functions appearing in the integral kernel of the induced force (22). It describes the "response" of the internal system originating

from the superposition of many ph-states with different energies and strengths $f(\epsilon)$.

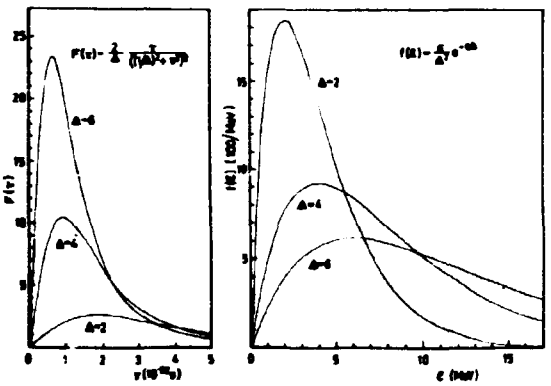

Fig. 1
Parametrized energy dependence of the matrix elements $f(\epsilon)$ for different ph-energy ranges $\Delta$ (right side) and the corresponding Fouriertransforms $F(\tau)$ (left side).

Solving the equations of motion (2), (3) we observe in dependence on the initial partial wave L three types of trajectories R(t) in our model. This is demonstrated in fig. 2 for the case $^{16}O + {}^{16}O$ at $E_{c.m.} = 62$ MeV.

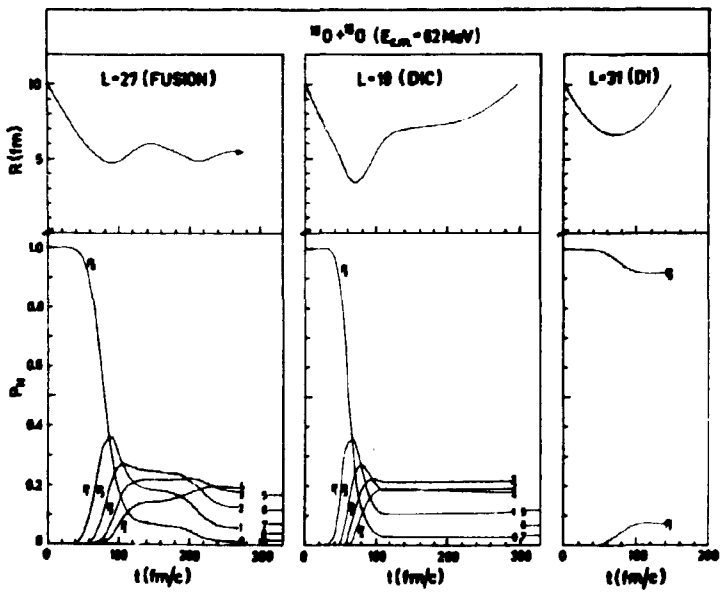


Fig. 2
The calculated distance between the centres of the ions R as function of time t for the $^{16}O + {}^{16}O$ ($E_{c.m.} = 62$ MeV) system for three orbital angular momenta L (upper part). Three types of trajectories are observed in our model calculation leading to different reaction channels, L=31 to quasielastic reactions, L=19 to deep inelastic scattering and L=27 to fusion.
The ground state probability of one of the $^{16}O$-nuclei $P_0$, the excitation probabilities for the 1p1h-states $P_1$, 2p2h-states $P_2$, etc. as function of time are plotted in the lower part of the fig.

For high partial waves (L=31) scattering occurs with no special structure within R(t). In this case the system remains nearly in its ground state $P_0$ and only 1p1h-excitations occur (lower part of fig. 2). Thus these quasielastic reactions can be described well in first order perturbation theory.
For L=19 the two ions stick within a certain time at a given distance R and after that they leave the interaction region. Many particle - many hole states are excited and the corresponding energy loss is comparable with the kinetic energy above the barrier in the entrance channel which represents the typical behaviour for deep inelastic events.
There exists a certain L-range where the ions do not leave the interaction region as seen for L=27 in fig. 2. The distance between their centres R(t) exhibits an oscillating behaviour with decreasing amplitudes. As in TDHF we interpret such types of trajectories as fusion.
The L-ranges in which the different processes appear depend on the model parameters $V_0$ and $\Delta$ . We fixed the parameters by a fit to the experimental fusion cross section for the $^{40}Ca + ^{40}Ca$ system at an energy of $E_{c.m.}$ = 150 MeV leading to $\Delta$ = 6 MeV and $V_0$ = 0.22. With the same parameters we calculate the fusion cross section as function of the incident energy and compare it with the experimental data (fig. 3). As seen from fig. 3 the experimental findings are well reproduced.

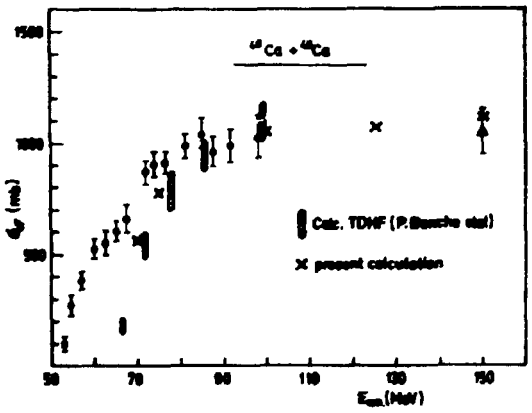


Fig. 3
Experimental [4], and calculated fusion cross sections $\sigma_{CF}$ for the $^{40}Ca + ^{40}Ca$ system as function of the incident energy $E_{c.m.}$. The 3dim.-TDHF results are from P. Bonche et al. [6].

As a further check of our model we compute the fusion cross section for $^{16}O + ^{16}O$ system as function of incident energy with exactly the same model parameters $V_0$, $\Delta$ as obtained in the case $^{40}Ca + ^{40}Ca$. An excellent agreement with the experimental fusion cross section is found (fig. 4).

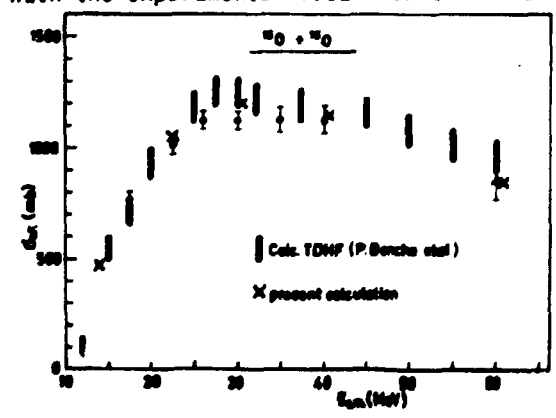


Fig. 4
The same as in fig. 3 for the $^{16}O + ^{16}O$ system. The experimental points are taken from [5]

One of the most striking feature of our calculations is the prediction of a fusion window within the L-space for high incident energies (compare the L-values for fusion and deep inelastic scattering in fig. 2). Such a L-window has been predicted first in 3dim. TDHF calculations for the same systems[6),7)]. Indeed our results are very close to that of these 3dim. TDHF calculations. This holds for the calculated fusion cross sections, the total kinetic energy loss, the deflection function and the time behaviour of the trajectories. In fig. 5 we compare the calculated trajectories in a two dimensional plot (R,$\Theta$) for two L-values which lead to fusion.

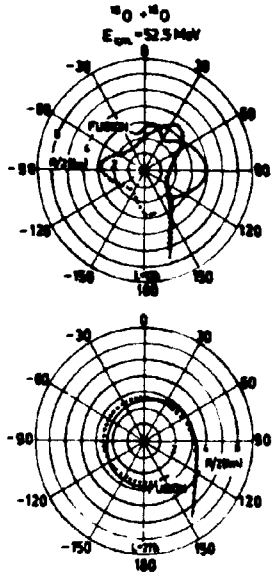

Fig. 5
Calculated two-dimensional trajectories (R,$\Theta$) for $^{16}O + ^{16}O$ at $E_{c.m.}$ = 52.5 MeV for L = 13 and L = 27, leading to fusion (dotted lines). The solid lines are the results of 3dim. TDHF calculation of Flocard et al. [7)].

The trajectory for L=27 exhibits only small oscillations with respect to R(t). Such a behaviour is typical for L-values at the upper end of the L-window for fusion. For partial waves in the vicinity of the lower L-cutoff for fusion (L=13) pronounced oscillations are observed in both models. The amplitudes increase with decreasing L leading to scattering for low partial waves. In our model these oscillations are the consequence of the interplay between the repulsive part of the conservative force in eq. (3) $\nabla_R U(R)$ and the attractive induced force (22).

## References


1. R. Schmidt, J. Teichert, these proceedings
2. R.V. Jolos, R. Schmidt
   II. Workshop on HIC, Dresden 1981, ZfK-467, p.16
   and to be published
3. J. Blocki et al., Ann. of Phys. 105 (1977) 427
4. H. Doubre et al., Phys. Lett. 73B (1978) 135 and
   J.C. Roynette et al., Phys. Lett. 67B (1977) 395
5. B. Fernandez et al., Nucl. Phys. A306 (1978) 259
6. P. Bouche et al., Phys. Rev. C17 (1978) 1700
7. H. Flocard et al., Phys. Rev. C17 (1978) 1682

# PARTICLE-HOLE FORMALISM FOR NUCLEON TRANSFER IN HEAVY-ION COLLISIONS

R. Schmidt and J. Teichert
Technische Universität Dresden, Sektion Physik, Dresden, DDR

In heavy-ion collisions dissipative phenomena may originate in the nucleon exchange between the collision partners [1, 2, 3]. However, typical experimental results are quite well reproduced in models where this effect is neglected or favoured (see also ref. [4]). The present paper considers uncorrelated single-particle excitations in one nucleus as well as the nucleon transfer from a common starting point within a non-statistical theory.

Using a classical description of the relative motion the centre of mass of the two nuclei move along the trajectories $\vec{S}_1(t)$ and $\vec{S}_2(t)$. For the consideration of the internal quantummechanical evolution of the ions and their interaction we use for the basis set at any time the eigenstates of the single-particle Hamiltonians of the two isolated nuclei $|\varphi_{k_1}\rangle$ and $|\varphi_{k_2}\rangle$. Thereby we restrict to bound states which are sufficient for the description of binary reactions. Due to the motion of the nuclei in the centre-of-mass system of reference these states are given by

$$|\psi_{k_1}\rangle = \hat{\mathcal{L}}_1(t)\,|\varphi_{k_1}\rangle\,, \qquad (1)$$
$$|\psi_{k_2}\rangle = \hat{\mathcal{L}}_2(t)\,|\varphi_{k_2}\rangle\,,$$

where the transformation operator (i=1, 2)

$$\hat{\mathcal{L}}_i(t) = e^{-\frac{i}{\hbar}\vec{S}_i(t)\hat{\vec{p}}}\, e^{\frac{i}{\hbar}m\dot{\vec{S}}_i(t)\hat{\vec{r}}}\, e^{\frac{i}{\hbar}\int_0^t dt'\,\frac{m}{2}(\dot{\vec{S}}_i(t))^2} \qquad (2)$$

performs the shift in the space coordinate $\hat{\vec{r}}$ and the change in the momentum $\hat{\vec{p}}$. Whereas the single-particle states which correspond to one nucleus are orthonormal there exists an overlap between states of different nuclei which can be expressed by the overlap matrix

$$\langle\psi_K|\psi_{K'}\rangle = M_{KK'}\,. \qquad (3)$$

Such a dual basis was first applied to heavy-ion collisions by Dietrich and Hara [5]. Adjoint states

$$|\tilde{\psi}_K\rangle = |\psi_K\rangle + \sum_{K'}\tilde{K}_{KK'}\,|\psi_{K'}\rangle \qquad (4)$$

are introduced which are derived from the overlap matrix: $M^{-1} = 1 + \tilde{K}$. Then, using these states particle and hole creation and annihilation operators can be defined which fulfil the usual anticommutation relations for fermions and are explicitly time-independent in the reference frame moving with the corresponding nucleus.

The Hamiltonian $\hat{H}(t)$ which govers the internal motion of the two nuclei can be written as

$$\hat{H}(t) = \hat{H}_{01} + \hat{H}_{02} + \hat{H}_{int}\,, \qquad (5)$$

where $\hat{H}_{o1}$ and $\hat{H}_{o2}$ are the isolated single-particle Hamiltonians of nucleus one and two

$$\hat{H}_{oi} = \sum_{p_i} \varepsilon_{p_i} \alpha^+_{p_i} \alpha_{p_i} - \sum_{h_i} \varepsilon_{h_i} \beta^+_{h_i} \beta_{h_i} \tag{6}$$

(i = 1, 2) and $\hat{H}_{int}$ represents the time-dependent interaction

$$\begin{aligned} \hat{H}_{int} = & \sum_{p_1h_1} v_{p_1h_1} \alpha^+_{p_1} \beta^+_{h_1} + v^*_{p_1h_1} \beta_{h_1} \alpha_{p_1} \\ & + \sum_{p_2h_2} v_{p_2h_2} \alpha^+_{p_2} \beta^+_{h_2} + v^*_{p_2h_2} \beta_{h_2} \alpha_{p_2} \\ & + \sum_{p_1h_2} v_{p_1h_2} \alpha^+_{p_1} \beta^+_{h_2} + v^*_{p_1h_2} \beta_{h_2} \alpha_{p_1} \\ & + \sum_{p_2h_1} v_{p_2h_1} \alpha^+_{p_2} \beta^+_{h_1} + v^*_{p_2h_1} \beta_{h_1} \alpha_{p_2} \end{aligned} \tag{7}$$

The first two terms on the r.h.s. describe the excitation in both nuclei, whereas the last two terms govern the nucleon exchange. The particle (hole) creation $\alpha^+_{p_i}(\beta^+_{h_i})$ and annihilation operators $\alpha_{p_i}(\beta_{h_i})$ are defined as proposed in ref. [5]. Then, the one-body matrix elements $v_{p_ih_j}$ in eq. (7) are given by

$$v_{p_ih_j}(t) = \langle \tilde{\varphi}_{p_i} | U_j^{ext} + U^{ov} + m \ddot{\vec{S}}_j (\hat{\vec{r}} - \vec{S}_j) | \varphi_j \rangle \tag{8}$$

(i, j = 1, 2), where $u_j^{ext}$ denotes the mean field of nucleus one acting on nucleus two and vice versa. The overlap between states of different nuclei yields to an additional potential part $u^{ov}$ and $m\ddot{S}_j(r-S_j)$ is a contribution which originates from the fact that the acceleration of the nuclei during the collision may also causes transfer or excitation.

The one-body interaction (7) allows to write the wave function of the system as

$$|\Phi(t)\rangle = e^{\sum_i \sum_{p_i} c_{p_ih_j}(t) \alpha^+_{p_i} \beta^+_{h_j}} |0\rangle \tag{9}$$

where $c_{p_ih_j}(t)$ is the ph-amplitude and $|0\rangle$ the ground state of the system. In order to calculate this wave function we apply a time-dependent pertubation expansion [4].

The change in the mass drift of the system can be expressed by the expectation value of the operator

$$\Delta\hat{A} = \sum_{p_1} \alpha^+_{p_1} \alpha_{p_1} - \sum_{h_1} \beta^+_{h_1} \beta_{h_1} \tag{10}$$

which is also needed for the determination of the mass dispersion

$$\sigma_A^2 = \langle \Delta\hat{A}^2 \rangle - \langle \Delta\hat{A} \rangle^2 \tag{11}$$

By restricting to second-order contributions in $v_{p_ih_j}$ and considering a symmetric initial fragmentation we get for the mass dispersion

$$\sigma_A^2 = \frac{2}{\hbar^2} \sum_{p_1h_2} \int_0^t dt_1 \int_0^t dt_2 \, v_{p_1h_2}(t_1) v^*_{p_1h_2}(t_2) e^{-\frac{i}{\hbar}(\varepsilon_{p_1} - \varepsilon_{h_2})(t_2 - t_1)} \tag{12}$$

As a first estimation of this quantity we make use of a simple model. First, we neglect the relative motion and assume that the interaction $H_{int}$ is switched on at t=0 and does not change its amplitude. Furthermore, we replace the sums over $p_1$ and $h_2$ in eq. (12) by an integration over the particle-hole energy $\varepsilon_{ph}$ and take a parametrization for the particle-hole density and the energy-dependence of the transfer matrix elements as proposed for their excitation in ref. [4]. The approximations made so far lead to

$$\sigma_A^2 = 2 g_0^2 \bar{V}^2 \hbar^{-2} \int_0^\infty d\varepsilon_{ph} \cdot \varepsilon_{ph} e^{-\varepsilon_{ph}/\Delta} \int_0^t dt_1 dt_2 \cos[\varepsilon_{ph}(t_2 - t_1)] \qquad (13)$$

where $g_0$ is the single-particle density. The quantity $\bar{V}$ represents an averaged interaction strength and $\Delta$ is the energy range parameter. The integrations in eq. (13) can be solved analytically and $\sigma_A^2$ becomes

$$\sigma_A^2 = 2 \bar{V}^2 g_0^2 \ln \left(1 + \frac{t^2 \Delta^2}{\hbar^2}\right) \qquad (14)$$

Expectation values for other quantities like the excitation energy $E^* = \hat{H}_{01} + \hat{H}_{02}$ etc. can be derived similarly. The time-behaviour of the quantity calculated is essentialy influenced by the responce of the system on the switching on of the interaction. In the model presented here this response is determined by the energy range of the excited states $\Delta$. In a more realistic treatment the time-dependent matrix elements give an additiol effect. They connect the time evolution of the internal system with the relative motion of the ions.

## References


1. J. Randrup
   Nucl. Phys. A307 (1978) 319 and A327 (1979) 490
2. F. Beck et al.
   Z. Phys. A269 (1978) 113
3. W.U. Schröder et al.
   Phys. Lett. 71B (1977) 283
4. R.V. Jolos, R. Schmidt, J. Teichert
   these proceedings
5. K. Dietrich and K. Hara
   Nucl. Phys. A211 (1973) 349

# DEEPINELASTIC PROCESSES IN TDHF-THEORY

D. Janssen, M. Militzer and R. Reif
Technische Universität Dresden, Sektion Physik, DDR

## 1. Representation of the TDHF-equation in terms of RPA-modes

It is well known, that the small amplitude limit of the TDHF-theory leads to the RPA-equation [1]. Nevertheless we would like to mention some special properties of the RPA-amplitudes in the p-p and h-h channel, which has been explicitly discussed in the group of S.T. Beliaev in Novosibirsk.
The TDHF-equation has the form

$$i\dot{\varrho} = [h(\varrho), \varrho] \quad , \quad h_{12}(\varrho) = t_{12} + S_{12}(\varrho) \quad , \quad S_{12}(\varrho) = \sum_{34} V_{1342}\, \varrho_{34} \tag{1}$$

$\varrho$ is the time dependent s.p. density matrix, t is the kinetic energy operator of a free particle and V describes the interaction between different particles. In the small amplitude limit $\varrho$ can be represented as follows:

$$\varrho(t) = \varrho_0 + \delta\varrho(t) \tag{2}$$

where $\varrho_0$ is the solution of the static Hartree-Fock equation $[h(\varrho_0), \varrho_0] = 0$. Using eq. (1) and neglecting quadratic terms in $\delta\varrho$ we obtain

$$i\delta\dot{\varrho}(t) = L(\varrho_0)\delta\varrho \quad , \quad L(\varrho_0)\delta\varrho \equiv [h(\varrho_0), \delta\varrho] + [s(\delta\varrho), \varrho_0] \tag{3}$$

The operator $L(\varrho_0)$ represents the (non hermitean) RPA-hamiltonian, which can be easily diagonalized

$$\begin{aligned} L(\varrho_0)\varphi_\alpha &= \omega_\alpha \varphi_\alpha \\ L^+(\varrho_0)\chi_\alpha &= \omega_\alpha \chi_\alpha \end{aligned} \tag{4}$$

The solution of the eigenvalue problem of eq. (4) can be characterized by the following properties:

1.) All frequencies $\omega_\alpha$ are real.
2.) For each solution $\omega_\alpha, \varphi_\alpha, \chi_\alpha$ with $\omega_\alpha \neq 0$ a second solution $\omega_{\bar\alpha}, \varphi_{\bar\alpha}, \chi_{\bar\alpha}$ exist with $\omega_{\bar\alpha} = -\omega_\alpha$, $\varphi_{\bar\alpha} = \varphi_\alpha^+$, $\chi_{\bar\alpha} = \chi_\alpha^+$.
3.) It is possible to divide the RPA-solution into two groups. The first group describes the excitation in the p-h channel and the amplitudes $\varphi_\alpha$ differ from zero only for matrixelements between particle and hole states.
The second group of solutions of eq. (4) are the solutions in the p-p(h-h) channel. Here the amplitudes $\chi_\alpha$ have the form

$$\chi_\alpha(1,2) = \delta_{\alpha_1 1}\, \delta_{\alpha_2 2}$$

4.) The whole set of solutions $\varphi_\alpha, \chi_\alpha$ normalized by the condition $Tr(\chi_\alpha^+ \varphi_\beta) = \delta_{\alpha\beta}$ is complete in the space of two particle states.

Using these properties we are able to expand the time dependent density matrix $\varrho(t)$ in terms of RPA-modes as follows

$$\varrho(t) = \varrho_0 + \Delta\varrho(t) \quad , \qquad \Delta\varrho(t) = \sum_\alpha a_\alpha(t)\, \varphi_\alpha \tag{5}$$

The time dependent expansion coefficients $a_\alpha(t)$ characterize the weight of the static RPA-mode $\alpha$ in the density matrix $\varrho(t)$.
Using this expansion and eq.(1) one can derive the following equation for the time evolution of a

$$\begin{aligned} i\dot{a}_\alpha &= \omega_\alpha a_\alpha + \sum_{\beta\gamma} W_{\alpha\beta\gamma}\, a_\beta a_\gamma \\ W_{\alpha\beta\gamma} &= \mathrm{Tr}\left( \chi_\alpha^+ \left[ s(\varphi_\beta), \varphi_\gamma \right] \right) \end{aligned} \tag{6}$$

This equation is completely equivalent to the standard TDHF-equation (1).

## 2. Calculation of energy and width of giant resonances in the framework of TDHF

By means of the transformation $a_\alpha(t) = e^{-i\omega_\alpha t}\, \bar{a}_\alpha(t)$, eq. (6) can be represented as follows

$$i\dot{\bar{a}}_\alpha = \sum_\beta V_{\alpha\beta}(t)\, \bar{a}_\beta(t) \quad , \quad V_{\alpha\beta}(t) \equiv \mathrm{Tr}\left( \chi_\alpha^+ \left[ s(\Delta\varrho(t)), \varphi_\beta \right] \right) e^{i(\omega_\alpha - \omega_\beta)t} \tag{7}$$

so for the time evolution operator $\hat{G}(t)$ defined by

$$\bar{a}(t) = \hat{G}(t)\, \bar{a}(0) \tag{8}$$

we obtain the formal solution:

$$\hat{G}(t) = T \exp\left( -i \int_0^t \hat{V}(t')\, dt' \right) \tag{9}$$

which can be expanded in a perturbation series with respect to V

$$G(t) = 1 + G^{(1)}(t) + G^{(2)}(t) + \ldots \tag{10}$$

$$\text{with} \qquad G_{\alpha\beta}^{(1)} = -i \int_0^t dt' \sum_\gamma \bar{a}_\gamma(t')\, W_{\alpha\gamma\beta}\, e^{i(\omega_\alpha - \omega_\beta - \omega_\gamma)t'} \tag{11}$$

$$G_{\alpha\beta}^{(2)} = -\int_0^t dt' \int_0^{t'} d\tau \sum_{\gamma\delta} W_{\alpha\gamma\delta}\, W_{\delta\gamma\beta}\, \bar{a}_\gamma(\tau+t')\, \bar{a}_\gamma(t')\, \exp\left\{ -i\tau(\omega_\gamma + \omega_\delta - \omega_\alpha) - it'(\omega_\gamma + \omega_\gamma - \omega_\alpha + \omega_\beta) \right\} \tag{12}$$

Now we will apply the following statistical assumption, which has been discussed in the paper of van Hove [2]

1. The diagonal matrix elements of V are relevant only.
2. The odd members of the perturbation series eq. (10) are neglegible.
3. For the "intrinsic" time integration a correlation time $\tau_{cor}$ exists, so that the subintegral function for $t > \tau_{cor}$ vanishes.

Then by the ansatz $\bar{a}_\alpha(t) = \bar{a}_\alpha(0) \exp(i\Delta_\alpha - \Gamma_\alpha)t$ the quantities $\Delta_\alpha$ and $\Gamma_\alpha$ are determined according to eq. (10) - (12) by

$$\Delta_\alpha = \sum_{\gamma\delta} \frac{W_{\alpha\gamma\delta}\, W_{\delta\gamma\alpha}\, (\omega_\alpha - \omega_\delta - \omega_\gamma + \Delta_\gamma)}{\Gamma_\gamma^2 + (\omega_\gamma - \Delta_\gamma + \omega_\delta - \omega_\alpha)^2} \quad , \quad \Gamma_\alpha = \sum_{\gamma\delta} \frac{\Gamma_\gamma\, W_{\alpha\gamma\delta}\, W_{\delta\gamma\alpha}}{\Gamma_\gamma^2 + (\omega_\gamma - \Delta_\gamma + \omega_\delta - \omega_\alpha)^2} \tag{13}$$

In this way in the framework of TDHF we have obtained the width $\Gamma_\alpha$ and the damping of oscillator-modes without introducting any collision term.

## 3. A microscopic version of the coherent surface excitation model in heavy ion reaction

In order to describe the collision of two nuclei we devide the 1.p. density matrix $\varrho_1(t)$ into two parts

$$\varrho = \varrho_a + \varrho_b$$

where the time evolution of $\varrho_a$ and $\varrho_b$ is given by

$$\begin{aligned} i\dot{\varrho}_a &= [h(\varrho_a+\varrho_b), \varrho_a] \\ i\dot{\varrho}_b &= [h(\varrho_a+\varrho_b), \varrho_b] \end{aligned} \tag{14}$$

Now we transform $\varrho_a$ and $\varrho_b$ into intrinsic systems, moving with the nuclei a and b by the following unitary transformations

$$\begin{aligned} \varrho_a &= e^{i\frac{p}{N_a}\hat{x}}\, e^{-q\frac{N_b}{N}\frac{\hat{d}}{dx}}\, r_a\, e^{q\frac{N_b}{N}\frac{\hat{d}}{dx}}\, e^{-i\frac{p}{N_a}\hat{x}} \\ \varrho_b &= e^{-i\frac{p}{N_b}\hat{x}}\, e^{q\frac{N_a}{N}\frac{\hat{d}}{dx}}\, r_b\, e^{-q\frac{N_a}{N}\frac{\hat{d}}{dx}}\, e^{i\frac{p}{N_a}\hat{x}} \end{aligned} \tag{15}$$

$N_a$, $N_b$ are the particle numbers of the nuclei a, b. q and p are time-function which will be specified later on. From (14) we get for the density matrices $r_a$ and $r_b$ in the intrinsic system of reference

$$\begin{aligned} i\dot{r}_a &= [h(r_a), r_a] + \frac{\dot{p}}{N_a}[x, r_a] + i\left(\frac{N_b}{N_a+N_b}\dot{q} - \frac{p}{N_a}\right)\left[\frac{d}{dx}, r_a\right] + [V_{qp}(r_b), r_a] \\ i\dot{r}_b &= [h(r_b), r_b] - \frac{\dot{p}}{N_b}[x, r_b] - i\left(\frac{N_a}{N_a+N_b}\dot{q} - \frac{p}{N_b}\right)\left[\frac{d}{dx}, r_b\right] + [V_{qp}(r_a), r_b] \end{aligned} \tag{16}$$

The first term on the right hand side of this equations is the usual "selfinteraction" of the nucleus, the second and third term arise from the coriolis interaction in the moving system and the third describes the interaction with the other nucleus.
Expanding now the matrices $r_a$ and $r_b$ in terms of RPA-modes of the nuclei a and b respectively

$$\begin{aligned} r_a &= r_a^0 + \sum_\alpha a_\alpha(t)\,\varphi_\alpha \\ r_b &= r_b^0 + \sum_\beta a_\beta(t)\,\varphi_\beta \end{aligned} \tag{17}$$

we obtain a system of coupled nonlinear equations for $a_\alpha$ and $a_\beta$.
Among these modes are the spurious modes with $\omega_{s_a} = \omega_{\beta_s} = 0$ in the p-h channel. The excitation of these modes corresponds to a translation of the hole nucleus in the coordinate and impuls space. So the amplitudes $a_{\alpha_s}$, $a_{\beta_s}$ of these

modes should be large. These modes can be eliminated by a proper choice of the time function q(t) and p(t). In this way it is possible to derive for q and p the following equations:

$$\dot{q} = \frac{N_a+N_b}{N_aN_b}\, p + i\, \frac{N_a+N_b}{N_aN_b}\, \mathrm{Tr}\,(x\,[V_{qp}(r_b^0), r_a^0])$$

$$\dot{p} = -\frac{d}{dq}\Big\{ \int dx\,dx'\, V(x-x'+q)\, r_a^0(x)\, r_b^0(x') + \sum_\alpha \mathrm{Tr}\,(V_{qp}(r_b^0)\,\varphi_\alpha)\, a_\alpha(t) + \sum_\beta \mathrm{Tr}\,(V_{qp}(r_a^0)\,\varphi_\beta)\, a_\beta(t) \Big\} \tag{18}$$

This are the well known classical equation describing the relative motion of two nuclei by a folding potential and the coupling to the intrinsic vibrational modes.

## References


1. G. Brown, Many Body Problems, North Holland Publishing Company, Amsterdam 1972
2. Van Hove, Physica XXI (1955) 517

# EXTENSION OF THE TDHF INITIAL VALUE PROBLEM INTRODUCING TIME-DEPENDENT JASTROW CORRELATIONS

P. Mädler
Joint Institute for Nuclear Research, Dubna, USSR

To look for possible dynamical realizations of short-range correlations in heavy ion reactions we propose an extension of the TDHF initial value problem which includes two-body correlations of short range in lowest order on a level of microscopic reversibility relating them to realistic nucleon-nucleon forces at short distances [1]. Higher order effects as well as the effect of long-range correlations are assumed to be effectively included in the readjusted mean field. The outlined extension is performed in the framework of the method of correlated basis functions (CBF) (see ref. [2] and refs. cited therein) choosing the wave function of the system as

$$\Psi(1\ldots A,t) = C \prod_{i<j} \sum_{\ell} f_\ell(r_{ij},t)\,\hat{P}_\ell\, \mathcal{A} \prod_i \phi_i(i,t) \tag{1}$$

with C being the normalization factor and, correspondingly, a local bare central symmetric nucleon-nucleon potential

$$V(ij) = \sum_\ell V_\ell(r_{ij})\,\hat{P}_\ell \ . \tag{2}$$

Our aim is to derive equations of motion for the correlation functions $f_l$ and the single particle orbitals $\phi_i$ invoking a least action principle

$$\delta \int_{t_1}^{t_2} dt \,\langle \Psi | i\hbar \frac{\partial}{\partial t} - H | \Psi \rangle = 0 \tag{3}$$

simultaneously varying with respect to both $f_l$, $\phi_i$.
The nuclear Hamiltonian is identically rewritten as

$$H = \sum_i t(i) + \sum_{i<j} V(ij) \equiv \sum_i H_1(i,t) + \sum_{i<j} V_{res}(ij,t) \tag{4}$$

with

$$H_1(i,t) = t(i) + U(i,t) \tag{5}$$

and

$$V_{res}(ij,t) = V(ij) - \frac{1}{(A-1)}\left[U(i,t) + U(j,t)\right] \quad , \tag{6}$$

U(i,t) being, in general, an arbitrary (redundant) one-body potential.
Assuming that the relative motion of the nucleons at large distances is sufficiently described by the mean field which is assumed to be known from a corresponding TDHF calculation (with a readjusted effective interaction) and choosen as U(i,t) we write

$$V_{res,\ell}(r,t) \equiv 0 \qquad \text{for} \qquad r \geq d_\ell(t) \tag{7}$$

where the time-dependent range parameters $d_l(t)$ are defined below.
We assume a spin-isospin symmetric system and decompose the Lagrangian in eq. (3) into a FAHT cluster expansion series [3] keeping only the lowest order. Then we separate c.m. and relative motion of the two-particle wave functions $|ij-ji\rangle$ appearing in this expansion only for $r < d_l(t)$, by truncating a Taylor expansion

of the orbitals $\phi_\nu$ in the position of their mass center at finite order.
Then eq.(3) yields for the real non-negative functions $f_l(r,t)$

$$-i\frac{\mathrm{Im}\,\gamma_l(t)}{\beta_l(t)} f_l(r,t) = \left\{-\frac{\hbar^2}{m}\left[\vec{\nabla}^2 + \frac{Q_l}{r}\frac{\partial}{\partial r} + \frac{\delta_l(t)}{4\beta_l(t)}\right] + V_l(r) + \frac{2(A-2)}{(A-1)}\frac{\eta_l(t)}{\beta_l(t)}\right\} f_l(r,t) \quad (8)$$

where, for the relative s-wave

$$\begin{pmatrix} \beta_0(t) \\ \gamma_0(t) \\ \delta_0(t) \\ \eta_0(t) \end{pmatrix} = \frac{1}{2}\sum_{\mu,\nu=1}^{\frac{1}{2}A} \int d\vec{R}\, \phi_\mu^*(\vec{R},t)\phi_\nu^*(\vec{R},t) \begin{pmatrix} 1 \\ \frac{\partial}{\partial t} \\ \vec{\nabla}^2 \\ U(\vec{R},t) \end{pmatrix} \phi_\mu(\vec{R},t)\phi_\nu(\vec{R},t) \quad (9)$$

For higher partial waves instead of $\phi_\mu\phi_\nu$ eq.(9) enter more complicate combinations of the orbitals $\phi_\nu$ and their spatial derivatives.
Variation with respect to $\phi_\nu^*$ gives

$$\left[i\hbar\frac{\partial}{\partial t} + \frac{\hbar^2}{2m}\vec{\nabla}^2 - U(\vec{r},t)\right]\phi_\nu(\vec{r},t) = \sum_{\mu,l} I^l_{\nu\mu}(\vec{r},t) \quad (10)$$

with $I^l_{\nu\mu}$ being composed of the single-particle orbitals $\phi_\mu$ and correlation functions $f_l$, their temporal and spatial derivatives, the mean field as well as the potentials $V_l(r)$ [1].
The boundary conditions

$$f_l(r=d_l(t),t) = 1 \quad , \quad f_l'(r=d_l(t),t) = 0 \quad (11)$$

and the constraint

$$0 \leq f_l(r,t) \leq 1 \quad (12)$$

complete eqs.(8) and define the quantities $d_l(t)$ .
Eq.(8) formally resembles a Schrödinger equation with a kinetic energy term describing the uncorrelated motion of the pair, a correlational kinetic energy term, a cross term (which crucially depends on the truncation, e.g. $Q_l=0$ if only the s-wave is considered) and a time-dependent potential which is composed of the bare potential and a term which describes the influence of the mean field on the relative motion of the pair. This influence dis appears if the system consists of only 2 particles. We emphasize that eq.(10) leads to usual TDHF in the limit $d_l(t) \to 0$ (i.e. $f_l \equiv 1, \forall r$) since in this limit the r.h.s. vanishes [1].
Appropriate initial conditions for a heavy ion reaction are formulated showing that a uniformly translated stationary solution of the correlated problem obeys the time-dependent eqs.(8),(10). The one-body density matrix is evaluated in the same approximations as described above. The s.p. overlap matrix, total energy and particle number are conserved exactly by derivation [1].

## References


1. P. Mädler, JINR Communication E4-82-693, Dubna, 1982; submitted to Nucl.Phys.
2. J. W. Clark, in The many-body problem, Jastrow correlations versus Brueckner theory, Lecture Notes in Physics, eds. R. Guardiola, R. Ros, vol.138 (Springer, Berlin, 1981) 184
3. J. W. Clark and P. Westhaus, J. Math. Phys. 9 (1968) 131, 149

# ENERGETIC HEAVY ION COLLISIONS AND THE PROPERTIES OF HOT NUCLEAR MATTER+)

H. Schulz and L. Münchow
Central Institute for Nuclear Research, Rossendorf (GDR)

G. Röpke and M. Schmidt
Wilhelm - Pieck - University, Rostock (GDR)

## 1. Introduction

The energetic heavy ion reactions represent a comparetively new domain of nuclear physics. In describing the basic physics involved simple thermodynamic models have successfully been applied (cf. refs.[1]). These models treat the exploding nuclear system as a non-interacting gas of different clusters like deuterons, $^3H$, $^3He$, $\alpha$-particles ... However, the gas approximation is justified for dilute systems only. To comprehend the main properties of an interacting nuclear system at finite temperature one has to start with a quantum statistical (QS) theory which describes the formation of clusters. In this way one finds an answer to the question why, f.i., the deuteron abundances in hot nuclear matter are rather large, although, as we know, deuterons do not exist at normal nuclear matter density $\rho_0 = 0.17\ fm^{-3}$ at zero temperature. Concerning the cluster formation one has to solve a Bethe-Goldstone type equation allowing for a systematic study of the clusters embedded in a nuclear medium. A consequence of this correct QS treatment is the appearance of a Mott mechanism[2,3] preventing the formation of clusters at sufficiently high densities. The quenching results mainly due to the account of the Pauli principle.
In the present paper we will give a summary of the main results obtained on the basis of a QS treatment of hot nuclear matter. Especially, we will discuss the cluster composition at given temperature and density, the phase stability of hot matter, the entropy problem, the phase transition below T = 20 MeV and the Bose condensation of $\alpha$-particles. The results base on previous publications (refs.[2-9]).

## 2. The equation of state

The equation of state is defined via the imaginary part of the thermodynamic Green function G(1, Z) (for notations see ref.[2])

$$\rho(\beta=\frac{1}{T}, \mu)=\frac{1}{\Omega}\sum_{\lambda}\int\frac{d\varepsilon}{\pi}\,\mathrm{Im}\,G(1,\varepsilon-i0^+)\,f(\varepsilon), \tag{1}$$

+) Talk given by H. Schulz at XII International Symposium on Nuclear Physics, Gaußig 1982

where $\mu$ is the chemical potential, $\Omega_0$ denotes the normalization volume and $f(\varepsilon) = [\exp\beta(\varepsilon-\mu)+1]^{-1}$ is the Fermi distribution function. The thermodynamic Green function obeys the Dyson equation ( $E(1) = P_1^2/2m$ ):

$$G^{-1}(1,z) = z - E(1) - \Sigma(1,z) \quad . \tag{2}$$

For the self-energy $\Sigma$ (1, Z) different approximations are possible leading to different approximations for the equation of state[4]:

(i) Hartree-Fock approximation (HF)

$\Sigma^{HF} =$  $= \Delta^{HF}(1)$ (3)

The equation of state reads

$$\rho^{HF}(\beta,\mu) = \frac{4}{(2\pi)^3}\int d^3p\, f\left(E(p) + \Delta^{HF}(p)\right) \tag{4}$$

No bound states (clusters) occur in this approximation. Since $\Delta^{HF}$ depends on the density the equation of state (4) permits one to define a region of phase instability and to study the coexistence of two different phases. This can be shown by using a Skyrme type interaction (see also refs.[11-13]).

(ii) Ladder-bound state approximation

$\Sigma^{LB}(1,z) =$ 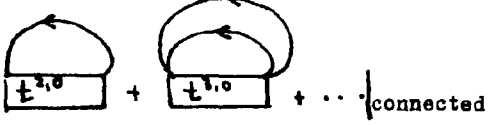 (5)

The ordinary chemical picture (detailed balance or law of mass action (LMA)) is obtained in this approximation. The equation of state reads

$$\rho^{LB}(\beta,\mu) = \frac{4}{(2\pi)^3}\int d^3p\, f(E(p)) + \frac{6}{(2\pi)^3}\int d^3p\, g_2\left(E_d^0 + p^2/4m\right) + \cdots \tag{6}$$
$$= \rho_{free} + 2\rho_{deut} + \cdots$$

where the second term gives the deuteron contribution (binding energy of the deuteron $E_d^0$) and $g_2(\varepsilon) = [\exp\beta(\varepsilon-2\mu)-1]^{-1}$ is the respective Bose distribution function. The ordinary LMA is obtained from ( 6 ) in the low density limit where the Boltzmann distribution function can be applied. In this case one has

$$\rho(\beta,\mu) = \rho_{free} + 2\rho_{deut} + \cdots, \tag{7}$$

where $\rho_{free} = \frac{4}{\Lambda^3}\exp\beta\mu$ is the free nucleon density and $\rho_{deut} = \Lambda^3\frac{3}{4\sqrt{2}} \cdot \exp(-E_d^0/T)\rho_{free}^2$ is deuteron density $\left(\Lambda^3 = \left(\frac{2\pi\hbar^2}{mT}\right)^{3/2}\right)$.

(iii) Ladder-HF approximation

$\Sigma^{LHF} =$ 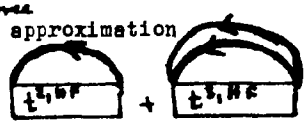 (8)

In this approximation the one-particle Green functions are calculated in HF approximation which accounts for in-medium corrections. The t-matrices in (5) and (8) are determined by Bethe-Goldstone equations. The ladder HF approximation takes into account the HF shifts of the free nucleons and the bound states. The continuum correlations are calculated in HF approximation.
Considering symmetric nuclear matter, taking into account the light clusters (deuteron, tritons, $^3$He and $\alpha$-particles) explicitly and neglecting the binding energy difference between $^3$H and $^3$He the equation of state can be written [6,7]

$$\rho(\beta,\mu) = \frac{1}{\Omega_0}\sum_{n_A}\sum_{P_A}\sum_{A=1}^{4} A f_A(E^A_{P,n_A}) = \rho_{free} + 2\rho_{deut} + 3\rho_t + 4\rho_\alpha, \quad (9)$$

where the quantum number $n_A$ specifies the intrinsic cluster state. The distribution function

$$f_A(E^A_{P,n_A}) = \left[\exp\beta(E^A_{P,n_A} - A\mu) - (-1)^A\right]^{-1} \quad (10)$$

reflects the Fermi or Bose character of the cluster. For a Skyrme type interaction the explicit form of the relevant energy shifts of the clusters and the expressions for the partial densities $\rho_{free}$, $\rho_{deut}$,... are given in ref.[6,7]. The subsequent discussions base on the equation of state (9). Improvements of the equation of state (9) are discussed in ref.[7].

3. The deuteron to proton ratio $R_{dp}$ and the Pauli quenching

One of the striking experimental results of energetic heavy ion reactions is the large ratio of deuterons to protons observed in the disintegration process [1]. In fig. 1 we show theoretically calculated $R_{dp} = \rho_{deut}/\rho_{proton}$ values as a function of temperature for different densities. The deviations between the ordinary LMA and the QS treatment are rather pronounced at increasing densities or low temperatures. The QS calculations shows the strong influence of the Pauli quenching. Since $R_{dp}$ shows a saturation as function of the temperature or density, actually a whole range of freeze-out densities can cope with the data. Therefore a more rigorous test of the importance of the Pauli quenching is obtained by considering the rate equation for the deuteron production

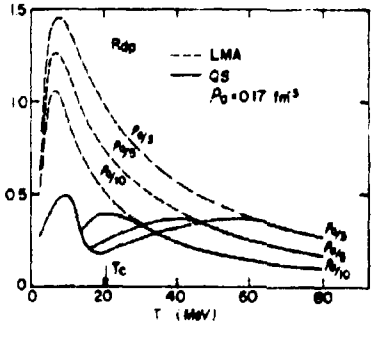


Fig. 1. The deuteron to proton ratio $R_{dp} = 2\rho_{deut}/\rho_{free}$ as a function of the temperature at given density
Full lines: QS approach, below $T < T_c$ the results are due to eq. (14)
Thin lines: Ordinary law of mass action

$$\dot{\varrho}_N = \langle \sigma_{break} v_{dN} \rangle \left[ -\varrho_d \varrho_N + \varrho_N^3 \left( \varrho_d / \varrho_N^2 \right)_{eq.} \right], \qquad (11)$$

where $\varrho_N$ and $\varrho_d$ are the respective particle number densities for nucleons and deuterons and $\sigma_{break}$ denotes the deuteron break-up cross section. The velocity between the nucleon and the deuteron is given by $v_{dN}$ and the brackets mean the average over the momentum distribution of the particles in the expanding fireball. The hadrochemical model uses this rate equation in connection with the gas dynamical description of the expansion of the gas cloud, where pionic excitations of the nuclear matter are taken into account. For details we refer to refs.[9,10]. Our results for the ratio $R_{dp}$ of deuterons to protons are given in figs. 2 and 3. The fig. 2 shows the time evolution of $R_{dp}$ while the comparison of their post break-up values to experimental data is made in fig. 3. In addition we show the results calculated on the basis of non-interacting gases (LMA). Especially, in this case the time evolution of $R_{dp}$ shows a rather steep increase at densities around $\varrho_0$. This behaviour is connected with the fact that the LMA disregards any kind of correlations effects and overestimates the cluster formation at increasing densities. As can be seen from fig. 3 the QS-calculations are in line with experimental findings and reflect the relevance of the account of the Pauli quenching at the early stage of the fireball expansion where the gas cloud is still rather dense and hot.

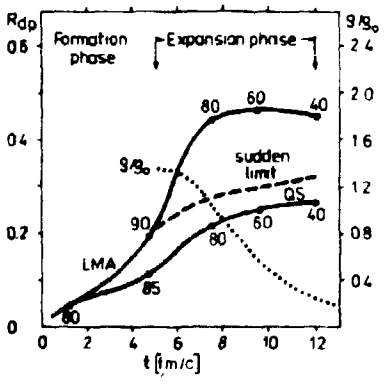


Fig. 2. The time evolution of the deuteron to proton ratio for the reaction Ne+NaF at 800 MeV/N. The numbers on the curves give the temperature of the fireball. The dashed line gives the result of the sudden limit where the deuterons are formed instantaneously according to their equilibrium value. The dotted line shows the baryon number density.

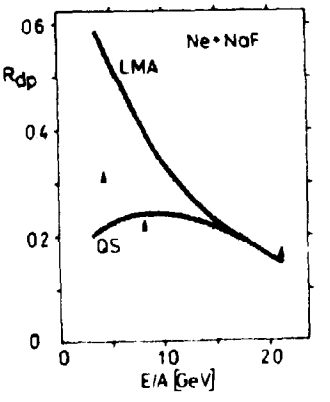


Fig. 3. The observed $R_{dp}$ values ref.[1] compared to the theoretical predictions which are corrected due to the subsequent decay of the $\Delta$ - resonances.

## 4. The entropy problem

In ref.[14] has been suggested a calibration of the entropy attained during the

hot phase of a relativistic heavy ion collision by means of the observed deuteron abundances. The entropy per nucleon S is calculated by the free fermion gas law

$$S = 5/2 - \ln\left(\rho \frac{\Lambda^3}{4}\right) . \tag{12}$$

In terms of the LMA (sec. 2 (ii)) one could write

$$S = 3.945 - \ln R_{dp} \tag{13}$$

connecting the entropy with the experimentally observed $R_{dp}$ values. From these assumptions values of 5.0 to 6.0 units in entropy per baryon are deduced. It has been shown in ref.[5] that the free fermion gas assumption (12) is still justified but the use of the LMA in deriving (13) may meet serious difficulties. In fact, only in the low density limit one has $R_{dp} \approx 3\sqrt{2}\,\Lambda^3 \rho$ (sec. 2 (ii)) but as soon as the Pauli quenching becomes operative the $R_{dp}$ value is not any more proportional to $\rho$ as given by the simple LMA form. In calculating the entropy expression (13) has to be used on place of (12). This reduces the entropy per baryon by about two units and becomes in agreement with conventional expections (see ref. [5]). A consideration of new degrees of freedom during the reaction (e.g. quarks) as proposend in ref.[14] seems therefore not necessary.

## 5. The ( $\rho$ - T) phase diagram

The equation of state (9) (see fig. 4) shows a behaviour similar to that of a non-ideal gas with the characteristic van-der-Waals instabilities[4,7,8].

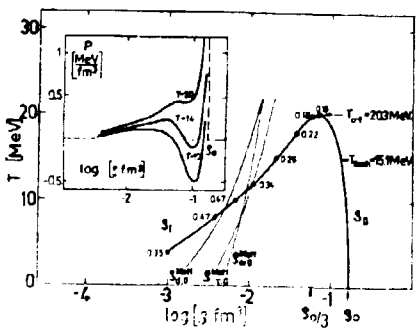


Fig. 4. The pressure as a function of density at a given temperature and the borderline of the two-phase liquid-vapor equilibrium. $R_{dp}$ gives the ratio of deuterons to free protons. The respective Mott curves $\rho^{Mott}$ indicate the borderline beyond which the clusters with total momentum P = 0 do not exist.

The possible experimental signature of a first order phase transition in hot nuclear matter has been firstly discussed in ref.[4]. A comparison with experimental data has been given in ref.[8]. For $T < T_c$ we are mainly interested in the number of composites ($N_A^I$) which are in the vapor phase. Their ratio to the total particle number (N) is defined by

$$N_A^I/N = A\,\rho_A^I / \rho_{break\text{-}up} \cdot \left(\frac{\rho_{II} - \rho_{break\text{-}up}}{\rho_{II} - \rho_I}\right) , \tag{14}$$

where $\rho_I$ and $\rho_{II}$ are defined by the borderlines of the phase instability region (see fig. 4). From (14) it follows for $R_{dp} = N_2^I/N_1^I$ and although the ratio of protons $N_2^I$ in the vapor phase is decreasing for $T \to 0$ their ratio is not

monotonic and exhibits around T ≈10 MeV a maximum (see fig. 4). Similar results are obtained for larger clusters. Fig. 5 shows some recent experimental data[15].

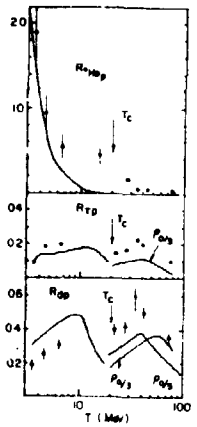


Fig. 5. The yields of different clusters as a function of the temperature. The experimental data are from ref.[15].

It turned out that at high incident energies (high temperatures) the yield drops monotonically as a function of the emitted particle mass. But for T ≈ 20 MeV one observes a characteristic change in the pattern. Now $\alpha$-particle yield becomes more dominant and for still smaller temperatures it exceeds that of lighter clusters. This behaviour has been discussed in ref.[8] in terms of an onset of a "liquid-vapor" phase transition (see also ref.[16]). Our results are shown in fig. 5. The overall agreement between theory and experiment seems to be satisfactory if one considers that any dynamical aspects (sec. 3) are disregarded and no effort has been made to reproduce the data better by changing temperature and break-up densities. The interesting conclusion that seems to be drawn is that the experimental data represented in fig. 5 and the corresponding theoretical calculations support the assumption that a first order phase transition around T ≈ 20 MeV might be observed. To support the scenario described more detailed calculations including dynamical aspects as discussed in sec. 3 have to be performed.

## 6. Bose condensation of $\alpha$-particles

An interesting effect which follows from the equation of state (9) in the low temperature region is the Bose condensation of $\alpha$-particles[6]. We will give here only a preliminary discussion concerning the Bose condensation in connection with the Mott mechanism. Considering an ideal Bose gas of $\alpha$-particles, Bose condensation appears if the density $\rho(T, k)$ approaches the critical density $\rho_{BC}^{(0)}$ defined by

$$\rho_{BC}^{(0)} = 2.61 \cdot 4 \left(\frac{4MT}{2\pi\hbar^2}\right)^{3/2} \tag{15}$$

This expression indicates that Bose condensation of $\alpha$-particles should be possible up to rather high temperatures (see fig. 6 and continue the broken curve). A similar result has recently been discussed in ref.[17] considering density effects only via the eigenvolume of the composites. This approach leads to the artifact that a Bose condensate still exists at densities beyond $\rho_0$ and high temperatures. Our equation of state (9) predicts a borderline $\rho_{BC}$ (fig. 6) which is rather constricted in the ($\rho$, T) plane, because due to the Mott mechanism bound states with total momentum P = 0 disappear beyond $\rho^{Mott}$.

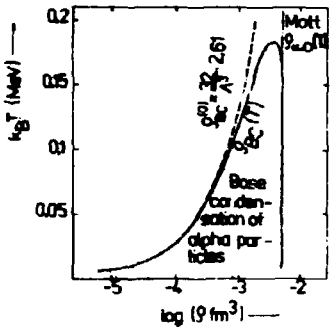


Fig. 6. The Bose condensation of $\alpha$ - particles (hatched region) within the phase diagram of nuclear matter

7. Concluding remarks

Relying on a model calculation, which bases mainly on a simple nucleon-nucleon interaction of the Skyrme type and on a perturbation treatment of the motion of composites in a hot nuclear medium, some of the interesting properties of hot nuclear matter as produced in course of an energetic heavy ion collision have been discussed. The results are consistent with recent investigations of hot nuclear matter (see refs.[11-13]) performed in connection with stellar problems where only bulk properties (e.g. critical temperature, phase instability region) are of great interest. The comparison with data obtained from energetic heavy ion collision permits one to test the equation of state in a new domain.

References

1. S. Nagamiya, M.C. Lemaire, E. Möller, S. Schnetzer, H. Schapiro, H. Steiner, and I. Tanihata; Phys. Rev. C24(1981)917
2. G. Röpke, L. Münchow, and H. Schulz; NBI-preprint 81-21(1981); Nucl. Phys. A379(1982)536
3. G. Röpke, D. Kremp, M. Schlanges, L. Münchow, and H. Schulz; Dubna-preprint P4-81-596, Yad. Fiz. Vol. 36(607)1982
4. G. Röpke, L. Münchow, and H. Schulz; Phys. Lett. B110(1982)21
5. J. Knoll, G. Röpke, L. Münchow, and H. Schulz; Phys. Lett. B112(1982)13
6. L. Münchow, H. Schulz, G. Röpke, M. Schlanges, and M. Schmidt; J. Phys. G (Lett) 8(1982)L135
7. G. Röpke, M. Schmidt, L. Münchow, and H. Schulz; NBI-preprint 82-23(1982), Nucl. Phys. in press
8. H. Schulz, L. Münchow, G. Röpke, and M. Schmidt; NBI-preprint 82-10(1982), Phys. Lett. in press
9. H.W. Barz, H. Schulz, H. Iwe, L. Münchow, G. Röpke, M. Schmidt, T. Biro, and J. Zimanyi; Z. Phys. 308 (1982) 187
10. T.S. Biro, H.W. Barz, B. Lukács and J. Zimanyi; KFKI report, KFKI-1981-90, Phys. Rev. to be published

11. D.Q. Lamb, J.M. Lattimer, C. Pethick, and D.G. Ravenhall; Phys. Rev. Lett. 41(1978)1623, Nucl. Phys. A360(1981)459
12. M. Barranco and J.R. Buchler; Phys. Rev. C22(1980)1729
13. B. Friedman and V.R. Pandharipande; Nucl. Phys. A361(1981)502
14. P.J. Siemens and J.I. Kapusta; Phys. Rev. Lett. 43(1979)1486
15. G.D. Westfall et al.; Michigan State University preprint № MSUCL-365(1982)
16. M.W. Curtin, H. Toki, and D.K. Scott; to be published
17. P.R. Subramanian, L.P. Csernai, H. Stöcker, J.A. Maruhn, W. Greiner, and H. Kruse; J. Phys. G 7(1981)L241

# ON THE DYNAMICS OF FISSION AT FINITE TEMPERATURE

H. Hofmann
Physik-Department, TU München, BRD

A.S. Jensen
Physics Institute, University of Aarhus, Aarhus, Denmark

F.J. Scheuter
C.E.N. Saclay - D.A.P.N./M.F., Gif-sur-Yvette, France

## 1. Introduction

We want to describe the decay of a compound nucleus through fission. The nucleus is assumed to be excited by some mechanism, which we will not study, and is supposed to have an excitation corresponding to a temperature T of the order of one to three MeV ($\hbar$=1). A description of the fission dynamics is possible only in terms of collective variables: the system will go through a sequence of shapes and then split into two fragments. This dynamics will be largely influenced by the conservative force and the effective inertia. At finite temperature, however, we can expect that dissipative forces will be present and thus fluctuating forces as well. What will be the equation of motion in this case? H.A. Kramers[1] gave an answer to that question as early as 1940: We have to follow the distribution in the phase space of the collective variables and their conjugate momenta. For one collective degree of freedom this equation reads:

$$\frac{\partial f(Q,P,t)}{\partial t} = -\frac{P}{m}\frac{\partial f}{\partial Q} - K(Q)\frac{\partial f}{\partial P} + \gamma\frac{\partial}{\partial P}\left(\frac{P}{m} + T\frac{\partial}{\partial P}\right)f \qquad (1)$$

Here and in the following we will assume that quantum effects can be neglected completely. This should be a very good approximation in the temperature region considered. Look for instance at the decay rate: Quantum mechanically it will be proportional to $\exp(-B2\pi/\hbar\Omega)$, with B being the height and $\Omega$ the effective frequency of the barrier. The decay due to thermal processes, on the other hand, can be estimated by means of the transition state method. This leads to a decay rate proportional to exp(-B/T) (modifications will be discussed below). As $\hbar\Omega$ is of the order of typically 1 MeV the number $\hbar\Omega/2\pi$ is considerably smaller than T.

## 2. Discussion of the Markoff-Limit

Modern derivations of this equation may lead to modifications of some terms and reinterpretations of the transportcoefficients, as for instance of the Einsteinrelation $D=\gamma T$ where D is the coefficient in front of $\partial^2/\partial P^2 f$. Let us not bother about such details here but rather concentrate on the essential question whether or not the Markoff-limit is appropriate. Clearly such an approximation is involved in the derivation of eq.(1). Otherwise the distribution would depend on the history of the motion. The Markoff-approximation is valid if the two relevant time scales for intrinsic and collective motion are separated:

$$\tau \ll \tau_{coll} \qquad (2)$$

Within the linear response approach of refs.[1)2)3)] the microscopic time $\tau$ is defined as the decay time of response functions $\tilde{\chi}_{F_\mu F_\nu}(t)$. Here, the $F_\mu$ are determined as the single particle fields which couple the collective motion to the nucleonic degrees of freedom: $F_\mu(X_i, Q_\nu) = \partial V / \partial Q_\mu$, with $V(X_i, Q_\nu)$ being the single particle potential. The $\tilde{\chi}_{F_\mu F_\nu}(t)$ determine the response of the nucleonic degrees of freedom to external changes. Suppose the mode $\langle F_\mu \rangle$ of the intrinsic system would be excited instantaneously (by a sharp knock). In this case the disturbance of $\langle F_\mu \rangle$ would be proportional to $\tilde{\chi}_{F_\mu F_\mu}(t)$ for $t > 0$:

$$\delta \langle F_\mu \rangle_t = \langle F_\mu \rangle_t - \langle F_\mu \rangle_{eq} \sim \tilde{\chi}_{F_\mu F_\mu}(t) \tag{3}$$

Now suppose $\tilde{\chi}_{F_\mu F_\mu}$ tends to zero within a time of the order of $\tau$. In this case the excitation $\langle F_\mu \rangle_t$ tends to its equilibrium value $\langle F_\mu \rangle_{eq}$ within the same time $\tau$.

Let us now look at a microscopic computation of such a response function (see ref.[3)]). We pick the case of an $^{238}U$ nucleus which is supposed to be excited to a temperature of T=1 MeV and to be deformed to a shape corresponding to the second asymmetric saddle. Then the nucleus is assumed to be disturbed in a direction along its elongation, the c-direction in the parametrization of ref.[4)]. The response is calculated on the basis of the shell model with a deformed Woods-Saxon potential (cf.ref.[4)]) including pairing correlations. The result is shown in fig.1. For the fully drawn curve a coupling to more complicated states was taken into account as well. It was parametrized via an introduction of complex selfenergies of the particles and holes. These selfenergies can be related to the optical model for the motion of nucleons inside a nuclear medium. In the case of no pairing and for typical p-h excitations being close to the fermi energy $\lambda$ one obtains the following simple expression:

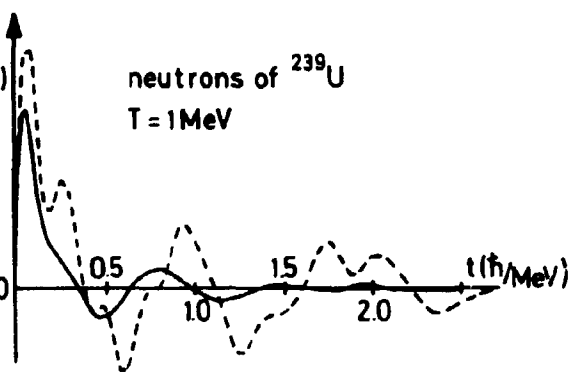


$$\mathrm{Im}\,\Sigma(\omega) \cong \frac{1}{\Gamma_0}\left\{(\omega-\lambda)^2 + \pi^2 T^2\right\} \tag{7}$$

The value for $\Gamma_0$ chosen in the figure is 33.3 MeV. For more details as well as for the extension of formula (7) to pairing we refer to ref.[6)].

The dashed curve was calculated for $\Gamma_0^{-1} = 0$, i.e. for the case of no coupling to more complicated states. The typical feature of both curves is a sharp rise at very short times and a decay to oscillations with smaller amplitudes within a time of the order of

$$\tau \lesssim 0.3\ \hbar/\mathrm{MeV} \tag{8}$$

For $\Gamma_0^{-1} \to 0$ these oscillations are damped out, essentially after a time of the order of

$$\tau^* \cong 1\ \hbar/\mathrm{MeV} \tag{9}$$

The latter time we called $\tau^{\downarrow}$ in accordance with the fact that its physical origin is related to the average width $\Gamma^{\downarrow} = \mathrm{Im}\,\Sigma = \hbar(\tau^{\downarrow})^{-1}$ of the decay of the 1p-1h states into more complicated states. This time should not be confused with the equilibration time of those excitations of the intrinsic system which come about due to the collective motion. We have argued before (see eq.(3) and the text below) that this equilibration time will be related to the decay time $\tau$ of the response function. According to the estimate (8) $\tau$ is appreciably shorter+ than $\tau^{\downarrow}$. On the other hand, the figure clearly also shows that the decay mechanism with $\Gamma^{\downarrow} \neq 0$ cannot be neglected. This sheds some doubts on TDHF calculations which neglect collision terms, as well as on theories which base on the Landau-Zener effect (for a discussion of this latter point see ref.[8]). In order to see to which extend the condition (2) is fulfilled we need an estimate of $\tau_{coll}$. A fair estimate is $\tau_{coll}^{-1} = |\omega_{coll}|$ with $\omega_{coll}$ being the local frequency. Any reasonable estimate which includes dissipative effects can make $\tau_{coll}$ only larger. As $|\hbar\,\omega_{coll}|$ is typically of the order of 1 MeV, we see that $\tau_{coll}$ is at least about three times larger than $\tau$. Within such a margin the Markoff-limit is justified.

## 3. Motion Across the Saddle

For the motion inside the fission well and around the top of the barrier the distribution f will be too broad to allow for a Gaussian approximation. Then the usual simple tricks to solve eq.(1) break down. On the other hand, a Gaussian is easy to compute and to handle. To benefit from this feature one may use propagators as a vehicle. Suppose f is known at some time $t_n$. We may then construct the function at a later time as:

$$f(Q,P,t) = \int dQ_n dP_n \; K(Q,P,t;Q_n,P_n,t_n)\, f(Q_n,P_n,t_n) \tag{10}$$

At $t=t_n$ the propagator must fulfill the initial condition:

$$\lim_{t\to t_n} K(Q,P,t;Q_n,P_n,t_n) = \delta(Q-Q_n)\,\delta(P-P_n) \tag{11}$$

For t close to $t_n$ the propagator itself can be expected, therefore, to have narrow widths and thus may be approximated by a Gaussian. This may be valid for all times smaller than some value, say $t_{n+1}$. To describe the dynamics for times larger than $t_{n+1}$ we have to repeat the folding procedure.

In ref.[9] this technique is applied to fission by assuming a schematic potential with one hump and constant inertia m, friction and temperature. As we will not have space enough to explain more details we refer to the original paper and concentrate here to describe the main results:

a) Dependence on Temperature. It is found that both the mean energy $\bar{E}$ and its variance $\sigma_E^2$ vary almost linear with T. This will be explained below.
b) Dependence on the Initial Distribution. It is found that the final distribution

+In a previous publication[7] response functions have been calculated for the typical situation of the entrance channel of a heavy ion collision. There for $\tau$ a very similar value was estimated.

around the scission is rather insensitive to the initial distribution, provided friction is reasonably large (more precisely for $q \gtrsim 0.1$, see below). It is confirmed that for obtaining sensible values for the mean energy $\bar{E}$ and its variance $\sigma_E^2$ one may start on top of the barrier, if only the average mean initial moment $P_o$ is chosen within reasonable limits.

c) Dependence of the Decay Rate, the Mean Energy and its Variance on the Transport Coefficients. In a locally harmonic approximation it is convenient to parametrize the dynamics in terms of the dimensionless quantity

$$q = \frac{\gamma}{2m|\Omega|} \tag{12}$$

with $\Omega$ being the effective local frequency. In the model considered in ref.[9] both m and $\gamma$ are constant (up to scission). The results are parametrized in terms of a q where $\Omega$ is the frequency of the inverted oscillator representing the barrier. For the decay rate r one finds that r is well represented by Kramers' socalled "high viscosity limit"

$$r = \frac{\omega}{2\pi}\left(\sqrt{1+q^2}-q\right) \exp\left(-\frac{B}{T}\right) \tag{13}$$

for all q larger than the very small value of 0.1. (In (13) $\omega$ represents the frequency of the oscillation around the potential minimum). The mean energy $\bar{E}$ decreases with q. The precise behaviour will be described below. The dependence of the variance $\sigma_E^2$ on q is shown in fig. 2. We will come back to this curve lateron.

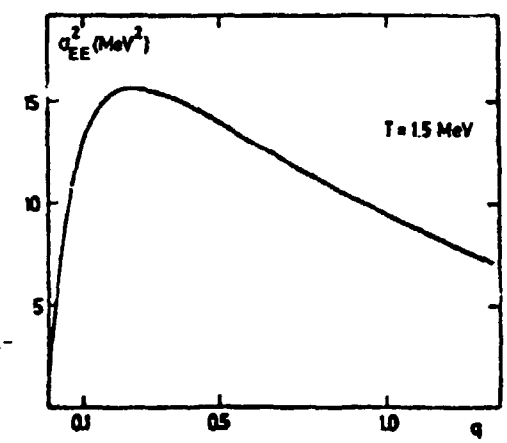

Fig. 2

## 4. Simplified Model

We are now going to discuss the possibility of estimating $\bar{E}$ and $\sigma_E^2$ in a simpler, eventually even analytical way. The insensitivity of these quantities to the initial distribution and, hence, to the motion inside the well suggest that one might try to represent the fission potential by an inverted oscillator. In the scission region, of course, there might and will be appreciable deviations from that simple form. Their influence cannot be completely neglected. We will come back to this point later. For the inverted oscillator there exist analytical solutions not only for the time dependent case[10], but for the stationary situation as well. The latter solution was found by Kramers in his early paper[1]. It reads:

$$f_K(Q,P) = N \exp\left(-\frac{P^2}{2mT} + \frac{m\Omega^2 Q^2}{2T}\right)\left(1 + \mathrm{erf}\left\{\left[\left(\sqrt{1+q^2}-q\right)P - m\Omega Q\right]/4mqT\right\}\right) \tag{14}$$

If one applies the time dependent solution to fission, one has to perform an integration over time[11] to sum up all events which move across the scission point, like

$$f_I(Q,P) = \int_0^\infty \frac{dt}{I}\, f(Q,P,t) \tag{15}$$

(I is a normalization constant) for $Q=Q_{sc}$. For suitable initial conditions, $f(Q,P,t)$ is a Gaussian with all mean values and second moments being analytical functions of time. But the integral is complicated and can be done numerically only, at least so far. If, on the other hand, Kramers' stationary solution is used all relevant moments in P can be calculated analytically. This enables one to derive[12] the following formulas for the prescission kinetic energy $\overline{E}_{kin}$ and its variance $\sigma^2_{kin}$: (with $\Delta U = U(Q_{Barrier}) - U(Q_{scission})$)

$$\overline{E}_{kin} = T\left\{1 + q\left(\sqrt{1+q^2}-q\right) + \frac{\Delta U}{T}\left(\sqrt{1+q^2}-q\right)^2\right\} \tag{16}$$

$$\sigma^2_{kin} = T^2\left\{1 + 2q^2\left(\sqrt{1+q^2}-q\right)^2 + 4\frac{\Delta U}{T}\, q\left(\sqrt{1+q^2}-q\right)^3\right\} \tag{17}$$

There are two reasons why the stationary solution can be used. First of all, the whole decay process of fission is to a large extend stationary. In almost all cases the decay time $\tau_{fis}$ will be much larger than the typical collective time $\tau_{coll}$. The latter was introduced before as the time it needs for typical parts of the distribution to move across the potential. Under these conditions the motion can be said to be stationary. But there is a second, and to some extend peculiar, reason for the stationary solution to apply. It is easy to see (cf.ref.[9]) that the time integrated solution (15) satisfies the the stationary Fokker-Planck equation in those parts of the phase space where $f(Q,P,t)$ is zero at t=o and $t=\infty$. But it is more difficult to understand that for the inverted oscillator $f_I(Q,P)$ tends to $f_K(Q,P)$ for increasing Q. This is demonstrated in fig.3 for the ratio of the fifth moments in P; as a function of Q:

$$R^5(Q) = \frac{\int_{-\infty}^{+\infty} dP\; f_I(Q,P)\, P^5}{\int_{-\infty}^{+\infty} dP\; f_K(Q,P)\, P^5} \tag{18}$$

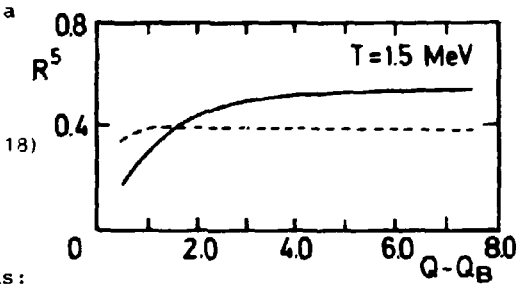


Fig. 3

For $f(Q,P,t)$ the initial distribution was:
$f(Q,P,t=o) = \delta(Q-Q_B)\,\delta(P-P_o)$, with $P_o = 1\hbar$/fm which may be considered as typical for the fission process[9]. The figure shows two curves, the full one for q=o.3 and the dashed one for q=1.8. We observe that $R^5(Q)$ reaches a constant value for Q much smaller than five which about corresponds to the scission region. ($R^5(Q)$ does not become one because $f_I$ and $f_K$ were not normalized to the same current.) This behaviour is typical and was found for other parameters and for other ratios as well. It explains why the analytical results of ref.[12], i.e. the formulas (16) and (17), are completely identical to the ones of ref.[11]. A comparison with the results of ref.[9] shows that (17) overestimates the variance to a not completely neglibible extend. This can be understood as the potential used in ref.[9] has a tail with a positive curvature after the scission point. The result for $\overline{E}$ of ref.[9] is adequately described by (16), however.

## 5. Conclusions

We have briefly described a microscopic picture which may serve as a basis to derive a collective transport equation. We have argued that the Markoff-approximation most likely is valid and that, therefore, this equation can be reduced to Kramers' form. Solutions of Kramers' equation were studied, for the case of one collective variable, both for a realistic potential as well as for the inverted oscillator. In the latter case analytical expressions can be derived not only for the decay rate, as was done by Kramers already, but for the mean energy and its variance as well (an analytical expression for the mean time from saddle to scission was not described here, see ref.[12]). All these quantitites depend on T and the dimensionless quantitis q. What do microscopic estimates tell about q? If we calculate the friction coefficient $\gamma$ within the picture described before, estimate an average value for the inertia from ref.[5] and use for $\hbar\Omega$ the typical value of 1 MeV, we obtain $q \cong 0.5$. An estimate of $\gamma$ by the wall formula would lead to a slightly higher value. A thorough discussion of these computations will be given in ref.[4]

The studies described here should be extended, of course, to more than one collective variable. First attempts have been made in ref.[13]. For instance, the inclusion of additional shape degrees may bridge the gap between the theoretical and experimental values for $\sigma_E^2$ (cf.ref.[14]). Furthermore, all the transport coefficients should be calculated microscopically (cf.ref.[4]), and a realistic approach should try to give information on the extend to which the nucleons are paired when the system approaches scission. In ref.[4] it will be suggested to treat the pairing gap as one of the several dynamical variables.


1. H.A.Kramers,Physica 7(1940)284
2. H.Hofmann and P.J.Siemens,Nucl.Phys.A257(1976)165 and A275(1977)464
3. H.Hofmann,A.S.Jensen,C.Ngô and P.J.Siemens,Proc.Conf.on Large Amplitude Collective Nuclear Motions, Keszthely, Hungary, June 1979
4. H.Hofmann,A.S.Jensen,C.Ngô and P.J.Siemens, to be published
5. M.Brack,Jens Damgaard,A.S.Jensen,H.C.Pauli,V.M.Strutinsky and C.Y.Wong Rev.Mod.Phys.44(1972)320
6. A.S.Jensen,H.Hofmann and P.J.Siemens, to appear in Phys.Lett.B
7. P.J.Johansen,P.J.Siemens,A.S.Jensen, and H.Hofmann,Nucl.Phys.A288(1977)152;
8. P.J.Siemens,Nucl.Phys.A387(1982)247c.
9. F.Scheuter and H.Hofmann,Nucl.Phys. in print
10. H.Hofmann and P.J.Siemens,Phys.Lett.58B(1975)417
11. P.Grangé,H.C.Pauli and H.A.Weidenmüller,Phys.Lett.88B(1979)9
12. H.Hofmann and J.R.Nix, submitted to Phys.Lett.
13. C.Grégoire and F.Scheuter,Z.f.Physik A303(1981)331 and C.Grégoire,these proceedings.
14. J.R.Nix in: Proc.Third Conf. on Reactions between complex nuclei (Asilomar, Pacific Grove,California,1963), see also ref.12.

# USE OF A TRANSPORT EQUATION FOR THE DYNAMICAL BEHAVIOUR OF THE NUCLEAR FISSION

F. Scheuter and C. Grégoire
DPh-N/MF, CEN Saclay 91191 Gif-sur-Yvette, Cedex, France

Abstract

A Fokker Planck equation is used for the problem of nuclear fission. The decay rate is computed within a three dimensional calculation and the influence of coupling terms in the transport coefficient tensors is considered. Initial conditions at the saddle point for the collective degrees of freedom are dynamically obtained in the stationary situation. Finally, dynamics of fluctuations from saddle to scission is treated under the same assumptions on the propagation.

## 1. Introduction

Dynamical aspects of the nuclear fission could be considered in two steps, namely the path through the fission barrier and the descent from the saddle point to the scission region. On the other hand, it turns out that the coupling between the intrinsic (i.e. nucleonic) degrees of freedom and the relevant collective coordinates (i.e., in the fission problem, the elongation, the mass asymmetry and the striction) leads to a dynamical equation[1] for the density d relative to the collective space. This equation is a Fokker-Planck equation (FPE). It is a transport equation and can be applied to the two steps of the fission process. As a matter of fact, the transport equation provides some flux at the top of the fission barrier by coupling of states inside the first well. We can get a determination of the escape rate through the barrier, as far as excited nuclei are concerned. Furthermore initial conditions at the saddle point can be evaluated, starting from a statistical equilibrium in the first well. It is finally straightforward to extend the treatment from saddle to scission in order to compute macroscopic observables and the fluctuations around the mean values.

As it was already shown by F. Scheuter and H. Hofmann[2] the main difficulty for applying the FPE to the problem of the nuclear fission is due to the breakdown of the local harmonic approximation for the density d. (We will avoid here the questionable validity of the Markov approximation in the fission problem). Nevertheless use of propagators in time[2] seems to offer a way in order to solve the FPE and to treat the two steps of the nuclear fission on an equal footing. For realistic cases, conditions on the propagation make the computation tractable by introduction of propagators on gaussian bundles[3].

In this contribution, we would like to report some recent calculations obtained in a three dimensional framework. In a first part, we will give the main ideas of our dynamical calculations. In a second one, we will discuss the question of the escape rate for the multidimensional situations. In a third part, fluctuations will be considered and comparisons with some experimental results will be given.

## 2. Propagation on gaussian bundles

Let us write the FPE in the one-dimensional case[1], where Q is the coordinate and P the associated momentum

$$\frac{\partial\, d(Q,P,t)}{\partial t} = -\{d(Q,P,t),\mathcal{H}_{coll}\} + \frac{\gamma}{B}\frac{\partial}{\partial P}\left(P\, d(Q,P,t)\right) + D\,\frac{\partial^2}{\partial P^2}\, d(Q,P,t) \qquad (1)$$

$\mathcal{H}_{coll}$ is the collective hamiltonian

$\gamma$, B, D are the friction, the inertia and the diffusion coefficients and could be evaluated by li-

near response theory[4]. The resolution of this FPE proposed in ref.[2] is based on the evaluation of the propagator $K(Q,P,Q_o,P_o,t)$ defined as :

$$d(Q,P,t) = \int dQ_o\, dP_o\, K(Q,P,Q_o,P_o,t)\, d(Q_o,P_o,\, t=0) \tag{2}$$

It fulfills the relation

$$\lim_{t\to o} K(Q,P,Q_o,P_o,t) = \delta(Q-Q_o)\, \delta(P-P_o). \tag{3}$$

One can check that K satisfies the same FPE as d itself.

The initial condition (3) allows to make to local harmonic approximation for the propagator during a time interval $\Delta\tau$. According to (2), the distribution d can be reconstructed after $\Delta\tau$ and a new propagator $K^{(1)}$ can be defined as :

$$d(Q,P,\Delta\tau+t) = \int dQ_1\, dP_1\, K^{(1)}(Q,P,Q_1,P_1,\Delta\tau+t)\, d(Q_1,P_1,t). \tag{4}$$

By iteration on time, one finally gets the solution of the FPE :

$$d(Q,P,t) = \int \prod_{j=0}^{n-1} dQ_j\, dP_j\, K^{(j)}(Q_{j+1},P_{j+1},Q_j,P_j,j\Delta\tau)\, d(Q_o,P_o,t=0) \tag{5}$$

with

$$t = n\Delta\tau \text{ and } \lim_{\Delta\tau\to 0} K^{(j)}(Q_{j+1},P_{j+1},Q_j,P_j,\Delta\tau) = \delta(Q_{j+1} - Q_j)\, \delta(P_{j+1} - P_j). \tag{6}$$

Let us now add some condition on propagation[3]. As long as the potential energy and the transport coefficients are momentum independent, the collective hamiltonian can be seen as a quadratic one in momentum. Consequently, deviations from the quadratic behaviour are essentially expected in the coordinate direction. Therefore, we have assumed a gaussian momentum distribution for each given value $Q_o$ of the coordinate. The phase space is considered as a bundle $\{Q_o, \mathcal{F}_{Q_o}\}$ where the density along each bundle is a gaussian.

This decomposition is schematically drawn in fig. 1 and can be expressed by :

$$d(Q,P,t) = \int dQ_o\, d_{red}(Q_o)\, \frac{1}{\sqrt{4\pi\omega_o}} \exp - \frac{(P-\langle P_o\rangle)^2}{4\omega_o}\, \delta(Q-Q_o) \tag{7}$$

where $P_o$ is the local momentum for a fixed $Q_o$ value

$$\omega_o \equiv \frac{1}{2} \int dP (P-\langle P\rangle)^2\, d(Q_o,P,t) \quad \text{the local variance}$$

$$d_{red}(Q_o) = \int dP_o\, d(Q_o,P_o,t) \quad \text{the reduced density.}$$

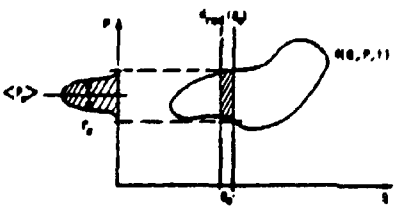

Fig. 1 : Definition of the bundled space $\{Q_o, \mathcal{F}_{Q_o}\}$. The $\mathcal{F}_{Q_o}$ is here along the momentum P and is assumed to be a gaussian.

The propagation in time is obtained in its simplified version by means of propagators on gaussian bundles $K_{bundled}$ :

$$d(Q,P,t) = \int dQ_o\, K_{bundled}(Q,P,Q_o,t)\, d_{red}(Q_o) \tag{8}$$

with

$$\lim_{t\to o} K_{bundled}(Q,P,Q_o,t) = \delta(Q-Q_o)\, \frac{1}{\sqrt{4\pi\omega_o}} \exp - \frac{(P-\langle P_o\rangle)^2}{4\omega_o}. \tag{9}$$

The assumption of gaussian bundles tremendously reduces the computation of the propagation and can be extended for multidimensional purposes. As far as the fission process is concerned, the consideration of two potential regions (on one hand, the first well and the saddle point region and on the other hand, the descent from saddle to scission) permits to estimate the escape rate, the initial conditions at the saddle point and the fluctuations in the scission region.
Here, the collective coordinates[6] are the elongation c, the mass asymmetry $\alpha$ and a neck degree of freedom h. We assumed non diagonal inertia and friction tensors[4,5] :

$$[B] = \begin{bmatrix} B_c & B_{ch} & 0 \\ B_{hc} & B_h & 0 \\ 0 & 0 & B_\alpha \end{bmatrix} \quad \text{and} \quad [\gamma] \begin{bmatrix} \gamma_c & \gamma_{ch} & 0 \\ \gamma_{hc} & \gamma_h & 0 \\ 0 & 0 & \gamma_\alpha \end{bmatrix}$$

with

$$B_c = B_\alpha = m_o = \frac{1}{160} A^{5/3} \left[\frac{\hbar^2}{\text{MeV}}\right] , \; B_h = \frac{m_o}{1.2}$$

which are similar values as in ref.[7]
and $\gamma_c = \gamma_\alpha = f\,\gamma_o$, $\gamma_h = f\,\gamma_o/1.2$ where $\gamma_o = \frac{m_o}{\hbar}$ .

The coupling terms are equal to $m_o$ (resp. $f\,\gamma_o$) multiplied by a reduction factor.
For a given elongation value $c_o$, the bundle is defined like the $\{P_c, h, P_h, \alpha, P_\alpha\}$ space, where $p_c$ (resp. $P_h, P_\alpha$) is the associated momentum to c(resp. $h, \alpha$).
The stationary solution of the FPE (1) provides[8] the escape rate r (or decay rate for the fissioning nucleus) according to :

$$r = \int d\Gamma_{red} ([B]^{-1}\,[P]\,d_{st})_{c_{saddle}} \tag{10}$$

where $[P] = (P_c, P_h, P_\alpha)$

$d_{st}$ the stationary solution of (1)
$c_{saddle}$ the elongation at the saddle point
$d\Gamma_{red} = dP_c\,dh\,dP_h\,d\alpha\,dP_\alpha$.

The full distribution at the left hand side of the saddle point is assumed to be normalized to unity at each time. The half life time $\tau$ for a nucleus decaying by fission can be estimated in such a case by $\tau = 1/r$.
Since $d_{st}$ $(c_{saddle})$ defines the initial conditions in the associated bundle $\mathcal{F}_{c_{saddle}}$, we are able to follow the subsequent dynamical behaviour from saddle to scission. For instance, the fluctuation $\chi^{\alpha\alpha}$ around the mean value for the mass asymmetry coordinate $\alpha$ gives the fluctuation for the mass ratio of the fission fragments at the scission point. Using the relationship[5] :

$$\frac{A_1}{A_2} = \frac{1 + \frac{3}{8}\alpha c^3}{1 - \frac{3}{8}\alpha c^3} \tag{11}$$

we obtain directly :

$$\frac{\sigma_{AA}^{\;2}}{2} = \left(\frac{3}{16} A\, c^3\right)^2 \chi^{\alpha\alpha} \tag{12}$$

if $\chi^{\alpha\alpha} = \frac{1}{2} \int d\Gamma_{red}\,(\alpha - \langle\alpha\rangle)^2 d_{red}$ at the scission point.

## 3. The escape rate through the fission barrier

First of all, in order to test our procedure, we studied a simple model case. We defined the po-

tential $U(c,h,\alpha)$ to be

$$U(c,h,\alpha) = \begin{cases} (37.46\ (c-1)^2 + 500\ h^2 + 200\ \alpha^2)[\mathrm{MeV}] & \text{for } 0 < c < 1.27 \\ (8.- 18.73\ (c-1.8)^2 + 500\ h^2 + 200\alpha^2)[\mathrm{MeV}] & \text{for } 1.27 < c < \infty \end{cases}$$

The coupling between c and h in the inertia and in the friction tensor is neglected in this model case ($B_{ch} = \gamma_{ch} = 0$). The nucleus under consideration is $^{205}$At.

This model is for the elongation degree of freedom c essentially identical to the one dimensional model used before for the calculation of the decay rate by Kramers[8], Visscher[4] and Scheuter and Hofmann[2]. For the $(h,\alpha)$ degrees of freedom, we added the potentials of two harmonic oscillators with constant stiffness along c. As far as the computation of the decay rate is concerned this choice of the potential and the transport coefficients reduces the problem to the one-dimensional one studied before. The numerical results of[2,9] show that Kramers formulae[8] are virtually exact except for a very small $\gamma$-interval in the transition from the small friction (L) to the high friction regime (H). These formulae can be written in the following way :

$$r = \frac{\gamma_c}{B_c}\left(\frac{T}{U_B}\right)^{\alpha} \exp\left(-\frac{U_B}{T}\right) \qquad \text{for} \quad \frac{\gamma_c}{B_c} \lesssim \frac{\Omega_o T}{U_B} \tag{L}$$

$$r = \frac{\Omega_o}{2\pi\,\Omega_B}\left(\sqrt{\Omega_B^2 + \left(\frac{\gamma_c}{2B_c}\right)^2} - \frac{\gamma_c}{2B_c}\right) \exp\left(-\frac{U_B}{T}\right) \quad \text{for} \quad \frac{\gamma_c}{B_c} \gtrsim \frac{\Omega_o T}{U_B} \tag{H}$$

where $\Omega_o = \left(\sqrt{\frac{\partial^2 U}{\partial c^2}} / B_c\right)_{\text{minimum}}$ and $\Omega_B = \left(\sqrt{\left|\frac{\partial^2 U}{\partial c^2}\right|} / B_c\right)_{\text{saddle}}$ are the local frequencies in the minimum c=1 and at the saddle point c=1.8 and $U_B$, T are the barrier height and the temperature respectively.

For the practical calculation, we assumed an excitation energy of $E^* = 80$ MeV and the relations :

$$E^* = a\,T^2 \ , \quad a = \frac{A}{10}$$

between the excitation energy and the temperature T. We assumed this temperature to be a constant along the path in order to make the comparison with Kramers results meaningful. To achieve the stationary solution as fast as possible, we decided to choose locally the following initial conditions (t=o) :

$$d_{red}(c) = \begin{cases} N \exp\left(-\frac{U(c,h_m = 0,\alpha_m = 0)}{T}\right) d^{eq}_{red}(c) & \text{for } c < c_{saddle} = 1.8 \\ d_{red}(c_{saddle}) & \text{for } c > c_{saddle} \end{cases}$$

This means that we start locally with an equilibrium distribution $d^{eq}_{red}(c)$ weighted properly by the factor $\exp(-U/T)$. N is a normalisation factor.

In figure 2 we plotted the flux at the barrier as a function of time for a typical friction $f = \frac{\gamma}{\gamma_o} = 1$. It shows how the stationary solution is obtained. After a small oscillation the flux converges quite rapidly to its stationary value, which is almost identical to Kramers estimation.

In fig. 3 we show the decay rate (full line) in comparison with Kramers result (dashed line) as a function of $f = \gamma/\gamma_0$. The agreement between the two calculations is excellent if we consider the need to discretise the bundled propagation problem. The used discretisation induces some numerical uncertainties and could be ameliorated in further calculations. Nevertheless the most striking feature is the obtention of a nice bending over of our curve in the transitional friction regime.

Let us now treat the realistic case of the fission of $^{205}$At at the rather high excitation energy of 80 MeV, which allows us to neglect shell effects and pairing. We use the shape parametrization

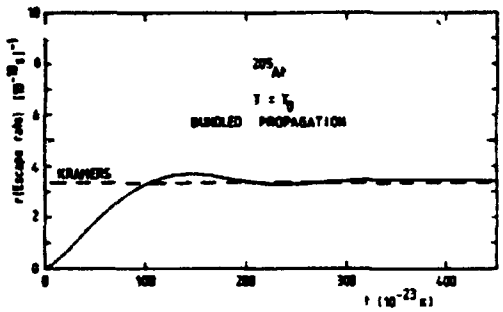


Fig. 2 : Flux at the top of the fission barrier as a-function of time. The escape rate r computed in the stationary situation with a propagation on gaussian bundles (full line) is compared to the Kramers calculation for a model case $\gamma = \gamma_o$ and A = 205.

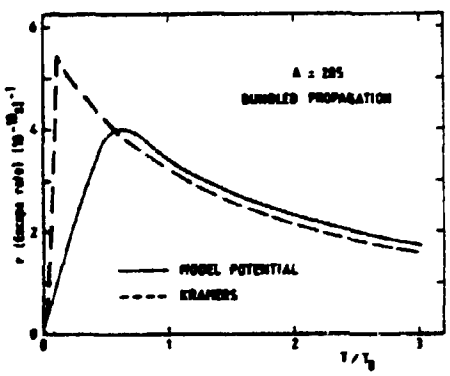


Fig. 3 : Comparison of the calculations for the escape rate with a bundled propagation and with the Kramers expressions. The escape rate r is shown as a function of the friction strength $\gamma/\gamma_o$, where $\gamma_o$ is a reference value.

$\{c,h,\alpha\}$ of (6) with the modification of (5) for $B \equiv 2h + \frac{1}{2}(c-1) \leq 0$. The potential landscape in this functional space is shown in (6). It turns out that the path of steepest descent is not a straight line in the $\{c-h\}$ plane as in our simple model case. In the practical calculation we adjust now the temperature T along the path. We assume that the total energy is conserved in the mean, viz:

$$(E^*)_c + \langle E_{coll}\rangle_c = 80 \text{ MeV}$$

where the mean collective energy $\langle E_{coll}\rangle$ is the sum of the collective kinetic and potential energy. We calculate the coordinate dependent temperature $(T)_c$ by means of :

$$(E^*)_c = \frac{A}{10}(T)_c^2 .$$

As a further modification with respect to our previous model calculation, we introduce now the generalized Einstein relation between the friction and diffusion coefficients, which, in a one dimensional case, reads :

$$D(\langle Q\rangle,T) = \gamma(\langle Q\rangle).\ T^*(\langle Q\rangle,T).$$

This relation was proven within the framework of linear response theory[10]. $T^*$ can be interpreted as an effective temperature and is given by the formula :

$$T^* = \frac{\hbar\Omega}{2}\ \text{cotgh}\ \left(\frac{\hbar\Omega}{2T}\right)$$

where the local frequency $\Omega(Q)$ is defined as :

$$\left[\Omega(Q)\right]^2 = \left.\frac{\partial^2 U}{\partial Q^2}\right|_{<Q>} / B(<Q>).$$

In the multidimensional case, the effective temperatures can be properly defined locally in the system of normal coordinates . For details we refer the reader to ref.[11].

Since the mean path out of the minimum over the barrier towards scission is of a particular interest, we show in fig. 4 how this path is affected by the coupling $B_{ch}$ for the typical friction $f = \gamma/\gamma_0 = 1$. For $B_{ch} = 0$ the system remains close to the line of steepest descent as it could be expected from purely static considerations. But after the switching on of the coupling $B_{ch} = B_c/3$ one observes a dramatic change of the mean trajectory in the region of the potential minimum. In spite of this strong deviation it comes again rather close to the line of steepest descent between saddle and scission. On the other hand the escape rate is practically independent of the coupling. For $B_{ch} = 0$ we find $r = 6.7 \times 10^{17}$s compared to $r = 6.3 \times 10^{17}$s in the case $B_{ch} = B_c/3$. One can get a remarkable decrease of the escape rate only for very strong coupling $B_{ch}$.

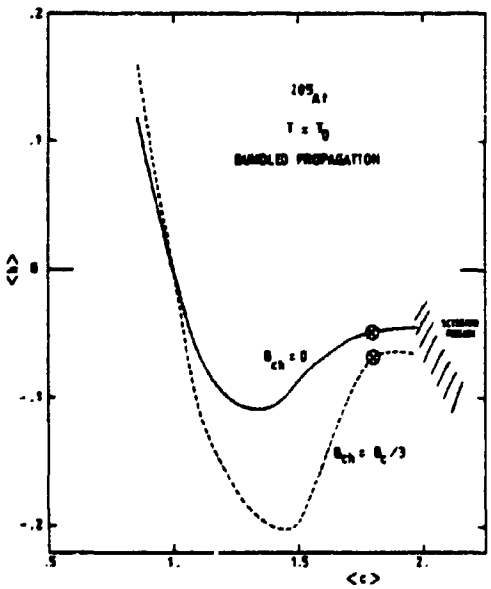


Fig. 4 : Dynamical paths for the fission of $^{205}$At in the {<c>,<h>} plane. The saddle points are represented by the symbol ⊗ for two paths obtained with coupling and without coupling terms in the transport coefficient tensors.

## 4. Fluctuations of the collective coordinates

The initial conditions at the saddle point have been calculated in the corresponding bundle for the precedent cases (with and without coupling). Especially for the fluctuation in mass asymmetry $\chi^{\alpha\alpha}$, in the neck coordinate $\chi^{hh}$ and in momentum along the elongation $\omega_{cc}$, it is interesting to compare the dynamical values in the stationary situation with the bare static values obtained for a statistical equilibrium at the saddle point. As reported in Table 1, the dynamical values are slightly larger for $\chi^{\alpha\alpha}$ and $\chi^{hh}$ than expected from a statistical equilibrium assumption. This fact seems to indicate that this equilibrium is not completely reached even in the stationary situation. Nevertheless, as far as the absolute values are concerned, some coordinate dependence of the transport coefficients could somewhat modify the presented results. On the other hand some smaller values of $\omega_{cc}$ are obtained in our calculation than in the equilibrium estimation. This particular result is

identical to the one obtained in the one dimensional model of ref.[2)]

Table 1

Initial conditions at the saddle point for $\chi^{\alpha\alpha} = \frac{1}{2}\int d\Gamma_{red}\,(\alpha-\langle\alpha\rangle)^2 d$, $\chi^{hh} = \frac{1}{2}\int d\Gamma_{red}\,(h-\langle h\rangle)^2 d$, $\omega_{cc} = \frac{1}{2}\int d\Gamma_{red}\,(P_c = \langle P_c\rangle)^2 d$ where $d\Gamma_{red} = dP_c\, d\alpha\, dP_\alpha\, dh\, dP_h$. These values are obtained by considering for the density d ; i) a statistical distribution, ii) the stationary value dynamically computed for two different assumptions on the coupling between c and h. $B_c$ is the inertia parameter along the c coordinate and $B_{ch}$ the cross term between c and h in the inertia tensor.

| | $\chi^{\alpha\alpha}$ | $\chi^{hh}$ | $\omega_{cc}$ [GeV $10^{-23}$s]$^2$ |
|---|---|---|---|
| Statistical equilibrium with $B_{ch} = 0$ | $1.75 \times 10^{-3}$ | $3.02 \times 10^{-3}$ | $1.67 \times 10^{-1}$ |
| Dynamical calculation with $B_{ch} = 0$ | $2.50 \times 10^{-3}$ | $3.61 \times 10^{-3}$ | $1.19 \times 10^{-1}$ |
| Statistical equilibrium with $B_{ch} = B_c/3$ | $1.75 \times 10^{-3}$ | $3.10 \times 10^{-3}$ | $1.84 \times 10^{-1}$ |
| Dynamical calculation with $B_{ch} = B_c/3$ | $2.92 \times 10^{-3}$ | $5.74 \times 10^{-3}$ | $1.30 \times 10^{-1}$ |

Finally, the statistical equilibrium values are reasonable for starting a dynamical path from saddle to the scission region.

According to eq. (12) the variance in mass asymmetry was computed as a function of $f = \gamma/\gamma_0$. The width $\Gamma$ of the mass distribution is merely :

$$\Gamma = \sigma_{AA}\sqrt{8\mathrm{Ln}2}$$

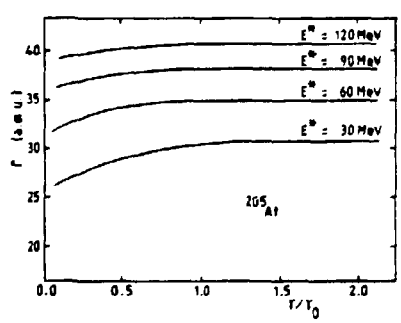


Fig. 5 : Calculated widths $\Gamma$ of the mass distribution for the fission of $^{205}$At. The widths are obtained for various strengths of the friction $\gamma$ and for different excitation energies.

In figure 5, different curves were calculated for four excitation energies with initial conditions at the saddle chosen in a statistical equilibrium. It turns out that the final result is independent on the friction strength as far as $\gamma$ exceeds roughly $\gamma_0/2$. For a comparison with the experimental

values, it must be quoted that our calculation gives $\Gamma = 35.2$ a.m.u. at an excitation energy $E^* = 60$ MeV and that the experimental result of ref.[12] is $\Gamma_{exp} = 33 \pm 3$ a.m.u. This agreement is stimulating for further computation of macroscopic quantities by use of the transport equation (1, with a bundled propagation.

## Conclusion

It was shown that the use of propagators permits to obtain a time dependent solution of the Fokker-Planck equation[2]. We have shown that the method of a bundled propagation with gaissian bundles is an excellent approximation in model cases, especially in the crucial estimation of the decay rate through a barrier. Furthermore the bundled propagation makes the solution of multidimensional Fokker Planck equationsnumerically tractable. Its application to a three-dimensional treatment of the fission process gives us a lot of information on the various steps of the dynamics. First of all the decay rate can be obtained by looking on the flux at the saddle point. Surprisingly, it appears rather insensitive to the non diagonal terms in the transport coefficient tensors. Secondly, the dynamical calculation of the initial conditions at the saddle point, starting with an equilibrium distribution in the first well, shows that the current assumption of a statistical equilibrium is reasonable in view of the small deviations that appear. Finally, first calculations concerning the width of the mass distribution for fission fragments are in remarkable agreement with the experiments. Further calculations will now be possible for estimating a lot of macroscopic quantities of interest in nuclear fission. In this spirit, microscopic transport coefficients would be required[13]

The authors would like to thank their colleagues for fruitful discussions, especially H. Hofmann and K. Dietrich. F.S (resp C.G) thank for the hospitality of the CEN Saclay (resp. TU München) during their stay there.

## References

1. H. Hofmann and P.J. Siemens, Nucl. Phys. A275 (1977) 464.
2. F. Scheuter and H. Hofmann, Preprint 1982, to be published in Nucl. Phys. A
3. C. Grégoire and F. Scheuter, Z. Phys. A303 (1981) 337
   and International Workshop on Gross Properties of Nuclei
   and Nuclear Excitation X, Hirschegg (1982).
4. A.S. Jensen, K. Reese, H. Hofmann, P.J. Siemens, Physics and Chemistry of Fission, Jülich 1979, IAEA-SM/241-114.
5. T. Ledergerber and H.C. Pauli, Nucl. Phys. A207 (1973) 1.
6. M. Brack et al., Rev. Mod. Phys. 44 (1972) 320.
7. A. Sobiczewski, Sov. J. Part. Nucl. 10 (1979) 466.
8. H.A. Kramers, Physica 7 (1940) 284.
9. P.B. Visscher, Phys. Rev. B14 (1976) 347.
10. H. Hofmann, A.S. Jensen, C. Ngô, P.J. Siemens, to be submitted to Reviews of Modern Physics ; see also Proc. IV th Balaton Conference on Nuclear Physics, Keszthely, Hungary, June 1979.
11. F. Scheuter and C. Grégoire, to be published
12. B. Borderie, M. Berlanger, D. Gardes, F. Hanappe, L. Nowicki, J. Peter, B. Tamain, S. Agarwal, J. Girard, C. Grégoire, J. Matuszeck, C. Ngô, Z. Phys. A299 (1981) 263.
13. H. Hofmann, A.S. Jensen, F. Scheuter, this conference.

# ОБЩАЯ ТЕОРИЯ НУКЛОННЫХ ОБОЛОЧЕК И БАРЬЕРЫ ДЕЛЕНИЯ

А.Г.Магнер
Институт ядерных исследований АН УССР, г.Киев, СССР

Сравнительно недавно в связи с исследованием оболочечной структуры ядер были достигнуты значительные успехи в развитии представлений о процессе деления ядер. В работах Струтинского было сформулировано положение об общем явлении больших оболочек в ядрах как значительной неоднородности одночастичного спектра, аналогичной зонной структуре электронных спектров в кристаллах. Многочисленные расчеты оболочечных эффектов в массах и энергиях деформации ядер при помощи метода оболочечных поправок Струтинского показали, что плотность одночастичных уровней $g(e,\eta)$ как функция энергии e в среднем поле ядра при любой форме ядра $\eta$ и для любого одночастичного ядерного потенциала содержит гладкую $\tilde{g}(e,\eta)$ и осциллирующую $g_{osc}(e,\eta)$ компоненты. Осциллирующая часть $g_{osc}(e,\eta)$ плотности уровней определяет оболочечную поправку $\delta E$ к некоторой гладкой энергии ядра, соответствующей капельной модели. Большими оболочками (зонной структурой уровней в ядрах) объясняются многие свойства не только сферических, но и деформированных ядер. Они являются причиной таких фундаментальных явлений, как несферичность формы редкоземельных элементов и актиноидов (первая яма на двугорбой кривой энергии деформации), существование квазистационарных промежуточных состояний в делении, известных как изомеры формы (вторая яма). Для качественного понимания происхождения такого двугорбого барьера деления полезно найти общие законы зонных распределений собственных значений энергии в трехмерной потенциальной яме, которые определяют $g_{osc}(e,\eta)$.

Для этого была развита общая теория больших нуклонных оболочек[1)-3)], которая дает схему расчета осциллирующей компоненты $g_{osc}(e,\eta)$ плотности уровней в любой потенциальной яме при произвольной ее форме. Задача была решена в квазиклассическом приближении с помощью фейнмановского представления интеграла по траекториям для пропагатора. Величина $g_{osc}(e,\eta)$ получена в виде суммы по классическим периодическим траекториям $\beta$,

$$g_{osc}(e,\eta)=\sum_{\beta} g_{osc}^{(\beta)}(e,\eta) = \sum_{\beta} A_{\beta}(e,\eta)\sin\left[\frac{1}{\hbar}S_{\beta}(e,\eta)+\gamma_{\beta}\right], \quad (1)$$

где $S_{\beta}(e,\eta)$ - интеграл действия для орбиты $\beta$, $A_{\beta}$ - амплитуда, а $\gamma_{\beta}$ - фазы. Особое значение имеют решения для гамильтонианов с симметрией, когда возникают семейства вырожденных периодических орбит, непрерывно переходящих друг в друга, а интеграл действия $S_{\beta}(e,\eta)$ стационарен в конечных областях фазового пространства. Тогда сумма берется по орбитам $\beta$, принадлежащим различным семействам орбит.

Анализ решений для осциллирующей компоненты $g_{osc}(e,\eta)$ плотности уровней позволил найти основные величины, характеризующие зонную структуру одночастичного спектра, - период $\hbar\Omega$ (расстояние между большими оболочками или зонами уровней) и амплитуду $A$ осцилляций величины $g_{osc}(e,\eta)$ в зависимости от энергии e. Величина $\hbar\Omega$ определяется обобщенным правилом квантования, внешне сходным с известным правилом Бора-Зоммерфельда для квантования одномерного периодического движения,

$$\hbar\Omega_{\beta} = 2\pi\hbar/[\partial S_{\beta}(e,\eta)/\partial\eta] = 2\pi\hbar/T_{\beta} \quad , \quad (2)$$

где $T_\beta$ - классический период обращения вдоль орбиты $\beta$,

$$T_\beta = \partial S_\beta(e,\eta)/\partial e \quad . \tag{3}$$

Однако, в отличие от правила Бора-Зоммерфельда условия квантования в многомерном движении дают не положение отдельных уровней, а распределение зон уровней. Амплитуда осцилляций плотности уровней $A$ определяется такими классическими величинами, как степень вырождения К непрерывного семейства орбит типа $\beta$ с одним и тем же значением интеграла действия $S_\beta(e,\eta)$, показателем устойчивости орбит и объемом фазового пространства, заполненного семейством орбит данного типа. Оболочечная поправка к энергии деформации $\delta E$ также выражается через классические величины,

$$\delta E = \sum_\beta \left(\frac{\hbar}{T_\beta}\right)^2 g_{osc}^{(\beta)}(\lambda,\eta) = \sum_\beta \left(\frac{\hbar}{T_\beta}\right)^2 A_\beta \sin\left[\frac{1}{\hbar} S_\beta(\lambda,\eta) + \nu_\beta\right] , \tag{4}$$

где $\lambda$ - энергия Ферми. Ее амплитуда возрастает при увеличении степени вырождения К и резко убывает с увеличением периода обращения $T_\beta$ (или длины орбиты). Поэтому для анализа больших оболочек в ядрах нужно учитывать только кратчайшие орбиты.

Квазиклассическая теория нуклонных оболочек позволила дать интерпретацию двугорбой кривой энергии деформации ядер при помощи классических величин[4]. Мы сравнили результаты расчетов оболочечной поправки к энергиям деформации $\delta E$ в случаях бесконечно глубокой эллипсоидальной ямы и деформированного гармонического осциллятора с результатами численных расчетов по методу оболочечной поправки для реалистического потенциала Вудса-Саксона и осцилляторного потенциала. Сравнение этих расчетов показало, что основной вклад в оболочечные энергии деформации ядер при небольших деформациях $1 \lesssim \eta \lesssim 1{,}5$ дают кратчайшие плоские орбиты с достаточно высокой степенью вырождения К=2 (ромбоиды в плоскости, проходящей через ось симметрии в эллипсоидальной яме и фигуры Лиссажу в перпендикулярной плоскости в случае осциллятора). Наклоны долин минимумов оболочечной энергии деформации (4) можно получить из условия

$$S_\beta(N,\bar\eta) = const \quad , \tag{5}$$

которое связывает равновесные деформации ядер $\bar\eta$ и число частиц $N$,

$$d\bar\eta(N)/dN = -\left[T_\beta / g(\lambda,\bar\eta)\right] \times \left[\partial S_\beta(N,\bar\eta)/\partial\eta\right]^{-1} . \tag{6}$$

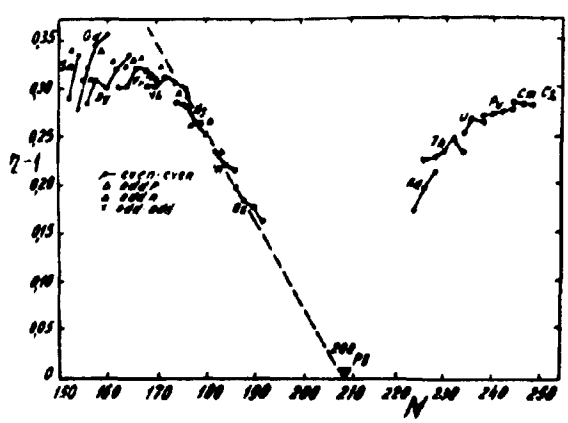


Рис.I. Квадрупольные деформации ядер сравниваются с квазиклассическим расчетом для орбит-ромбоидов в плоскости оси симметрии.

Эти наклоны для вклада ромбоидов в оболочечную поправку (4) хорошо согласуются с численными расчетами для реалистического потенциала Вудса-Саксона и с экспериментальными значениями рав-

новесных деформаций ядер редкоземельной области, см. рис.I. Большие оболочки, связанные с указанными плоскими орбитами приводят к формированию первого минимума в энергии деформации. Появление простейших трехмерных орбит при большой деформации $\eta$ дает локальное усиление оболочечной структуры, связанной с плоскими орбитами. В эллипсоидальной яме трехмерные орбиты со степенью вырождения K=2 появляются при деформации $\eta \gtrsim 1,6$, а в осцилляторном потенциале орбиты с K=4 возникают при деформации $\eta = 2$, что соответствует отношению парциальных частот 2:I. В результате образуется второй минимум в энергии деформации. Такая интерпретация двугорбого барьера деления не опирается на специфические свойства гармонического осциллятора и является гораздо более общей.

Теория предсказывает также температуру $t_{кр}$, при которой исчезает влияние больших оболочек на деление и происходит переход к капельной модели деления,

$$t_{крит} = \frac{1}{\pi}\hbar\Omega = 2,0 \div 2,5 \text{ Мэв.} \qquad (7)$$

Такая температура соответствует энергии возбуждения 50-80 МэВ. Этот вывод подтверждается многочисленными расчетами при помощи термодинамического варианта метода оболочечной поправки, а также экспериментальными данными.

Литература

I. V.M.Strutinsky, Nucleonika, 20, (1975) 679
2. В.М.Струтинский, А.Г.Магнер, ЭЧАЯ, 7, (1976) 356
3. А.Г.Магнер, ЯФ, 28, (1978) 1479
4. V.M.Strutinsky, A.G.Magner, S.R.Ofengenden, T.Dössing, Z. Phys., A283, (1977) 269.

# THE NEUTRON ENERGY SPECTRUM FROM THE SPONTANEOUS FISSION OF $^{252}$CF

H. Klein

Physikalisch-Technische Bundesanstalt (PTB)
Bundesallee 100, D-3300 Braunschweig, Fed. Rep. of Germany

## 1. Introduction

Up to now the NBS evaluation [1], which is the Maxwellian distribution with an energy parameter $E_o$ = 1.42 MeV, slightly modified in 6 segments by polynomial correction functions, has been recommended for describing the neutron energy spectrum from the spontaneous fission of $^{252}$Cf. In his comprehensive review Blinov [2] pointed out that this description is not suited to fit the experimental data in the energy regions $E_n$ < 0.5 MeV and $E_n$ > 6 MeV. The differences determined in various experiments are much greater than the uncertainties estimated for these experiments.

On the other hand the Cf spectrum is recommended as a reference standard for calibration purposes [3] and requested with high priority [4]. This situtiion is unsatisfying, in particular, because most of the measurements were not performed with a normalization.

All the improved experiments recently presented [5-9] were carried out using neutron time-of-flight spectroscopy and cover in total the energy range from 1 keV up to 30 MeV. It is proved in several papers [7,8] that the prescription to analyze and normalize the experimental tof spectra had to be substantially improved and that the properties of the fission detector and the geometrical setup influence the neutron spectrum measured. A variety of further corrections has been investigated experimentally and/or estimated theoretically.

In addition, a review of the theoretical approaches and extensive numerical calculations compared with experimental data are available [10].

This paper compiles the essentials of the experimental method (section 2) and the theoretical approaches (section 3). The results are discussed in section 4.

## 2. Experimental Method

### 2.1 Time-of-Flight Technique

The Cf source is deposited inside a fission fragment detector which is followed by fast electronics. Fission rates $A \sim 10^5\ s^{-1}$ are processed and a ns-timing as well as a fission detection efficiency $\varepsilon_f \simeq 1$ are achieved. Depending on the energy range to be investigated flight paths between 6.25 cm (keV region [5,6]) and 1 200 cm (MeV region [8]) are used. Due to the neutron detection efficiency $\varepsilon_d$ ($E_n$) and the solid angle $\Omega_d$ of the neutron tof detector with respect to the neutron source the neutron detection

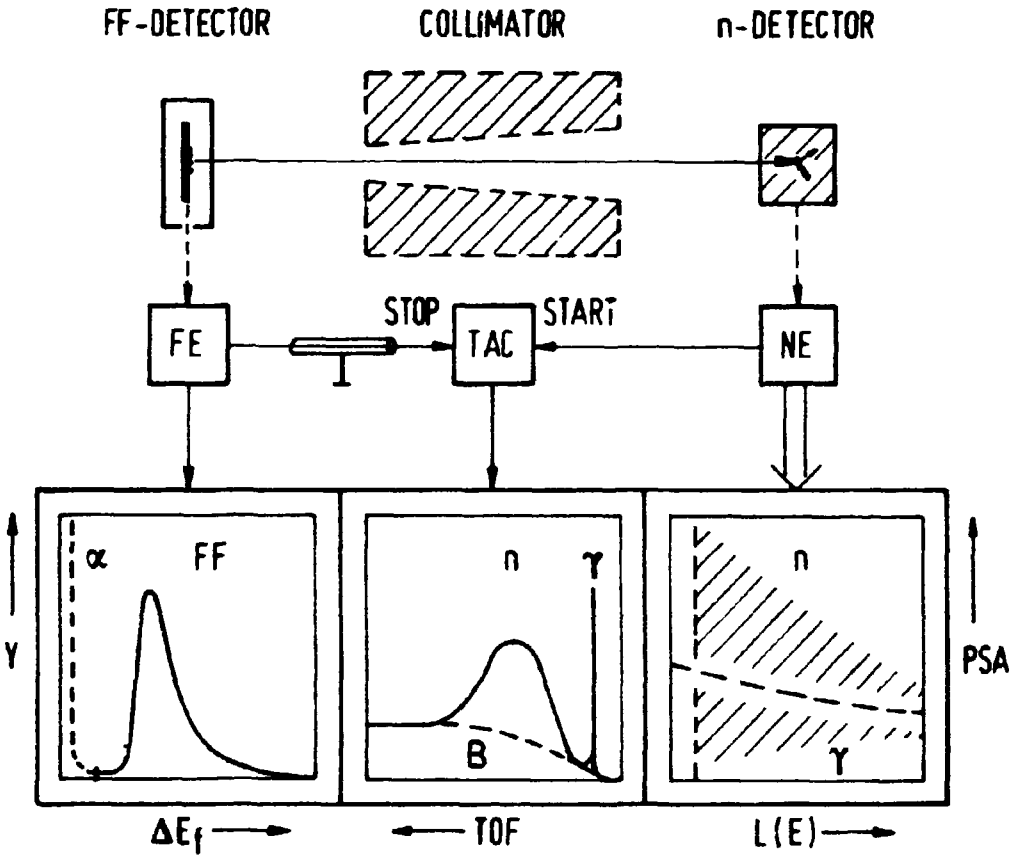


Fig.: Typical setup for tof measurements with a $^{252}Cf$ fission source
a) fission fragment (FF) detector, i.e. an ionisation chamber, followed by fast electronics (FE),
b) a neutron tof detector with standard nuclear electronics (NE), i.e. NE 213 liquid scintillator with n-γ-discrimination properties PSA depending on the light response L(E),
c) tof analysis TAC in an inverse time scale.

rate is significantly smaller than the fission rate. In order to avoid additional dead time losses, an inverse time scale is introduced. The fission signal is appropriately delayed by about the range $T_R$ of the time analyzer and serves as the stop for the associated neutron signal (see fig.).

In addition to the tof-spectra the energy loss $\Delta E_f$ of the fission fragments as well as the response spectra of the neutron detector may be simultaneously analyzed in a multiparameter mode [8,9] in order to determine the efficiencies, to introduce restrictive conditions such as an n-γ-discrimination, or to study correlations between different parameters.

For this arrangement the neutron energy spectrum N(E) to be extracted from the tof measurement will be described by

$$(1)\ N(E) = A \cdot \bar{\nu} \cdot n(E) \cdot \frac{\Omega d}{4\pi} \cdot \varepsilon_d(E) \cdot C(E,\vec{\Omega})$$

where n(E) denotes the density distribution function to be determined and $\bar{\nu}$ the neutron multiplicity for a spontaneous fission. Finally the function $C(E,\vec{\Omega})$ takes into account all corrections due to structural materials and directional correlations.

## 2.2 Properties of the Fission Fragment Detector

Fast ionization chambers [6,8,9] or gas scintillation detectors [5,7] are used to detect at least one of the fission fragments ($2\pi$ geometry). Even for thin, pure $^{252}Cf$ sources electro-deposited on highly polished backings a small fraction of fission is lost if both fragments are absorbed due to the roughness of the backing [7,8]. The nonisotropic loss causes the coincident neutron rate to be dependent on the angular position of the neutron detector with respect to the areal source. This interpretation could be quantified by means of Monte Carlo simulations (see figs. 1,2 of ref. 8). The measured neutron energy distribution also changes remarkably with the angular position (see fig. 8 of ref. 7), but the energy dependent correction function can be determined experimentally by analyzing the correlation between the energy loss $\Delta E_f$, which approximately defines the direction of the fission fragment, and the associated tof-spectrum [8,11]. In the case of a high fraction of nonisotropic detection losses a remarkably hardened neutron spectrum will be measured if the detector is positioned perpendicular to the areal source on the backing.

The neutron source strength ($A \cdot \bar{\nu} \cdot \varepsilon_f^{-1}$) may be alternatively determined by an absolute neutron counting using a water or manganese bath. In any case, the angle- and energy dependent correction as well as the disturbance due to structural materials have to be considered.

## 2.3 Analysis of the TOF Spectra

The tof spectrum I(t) measured in the above-mentioned inverse time scale consists of:

a) a random background $I_R(t)$ caused by the neutrons for which an associated fission fragment was not detected (fraction $(1 - \varepsilon_f)$). This background is statistically distributed and can be fitted to the contributions above the prompt photon peak,
b) the pulse overlap or uncorrelated stop background originating from all neutron tof measurements, which are statistically stopped before the associated fission event occurs, and
c) the remaining neutron tof measurements which were correctly terminated (see fig. 3 of ref. 8).

As will be derived in detail in ref. 11, the corrections chiefly depend on the deadtime behaviour of the fission detector channel. Assuming a non-extended

deadtime $\tau$ in the fission channel the following approximation can be used to calculate the corrected tof spectrum $I_c(t)$ [8]:

$$(2)\quad I_c(t) \sim REN(t) \cdot \left\{ I'(t) - A \cdot \Delta t \cdot \sum_{t' \geq t}^{T_R} I'(t') \right\}$$

$$(2a)\quad I'(t) = I(t) - I_R(t)$$

$$(2b)\quad REN(t) = \begin{cases} (1 + A \cdot \tau) & 0 \leq t < \tau \\ (1 + A \cdot \tau) \cdot \exp(A \cdot (t - \tau)) & \tau \leq t \leq T_R \end{cases}$$

It should be noted that beside the time calibration constant [time interval per channel] $\Delta t$ of the time analyzer the channel corresponding to a vanishing time difference has to be known in order to calculate the time dependent renormalization REN(t). This correction has been correctly applied by Böttger et al. [8] and by Pönitz and Tamura [7] in the ideal limit $\tau = 0$. For $\tau \geq T_R$, the net spectrum has to be corrected for the deadtime losses by a time independent factor.

The time-dependent renormalization which increases the high energy part of the spectrum (in the region $t \geq \tau$) may compensate the energy-dependent correction discussed in section 2.2. Thus, the shape analysis can deliver the correct result if both corrections are neglected, but the absolute normalization fails.

## 2.4 Detection Efficiency $\varepsilon_d(E)$

The efficiency of some of the tof detectors used in recent experiments can be attributed to the well known cross sections of the dominant reactions, i.e. $^6Li(n,t)$ [5], $^{235}U(n,f)$ [6] and n-p scattering in the case of a "black" detector [7]. The influence of the structural materials (capsules, collimator) and of the surrounding air (inscattering, attenuation) has to be carefully calculated [7] or be determined experimentally [5,6]. If thin liquid scintillators ($\varepsilon_d \sim 0.2 \ldots 0.3$) are used to increase the time resolution and the n-$\gamma$ discrimination properties, Monte Carlo calculations should be accompanied by experimental calibrations, in particular in the energy range $E_n > 8$ MeV where the various reactions on carbon compete with the n-p scattering [8].

## 2.5 Correction Functions $C(E,\vec{\Omega})$

Further corrections not yet discussed in sections 2.2 to 2.4 are combined in $C(E,\vec{\Omega})$, i.e. the inscattering from and additional neutron production in the structural material of the fission detector. These corrections estimated by theoretical approaches [8] and MC simulations [7] or determined experimentally [5,6] generally increase with decreasing energy.

If the neutron tof is determined with respect to the prompt fission photons errors due to low energy delayed photons should be avoided by increasing the

threshold. The final uncertainties must be estimated to be included in the covariance matrix. The energy scale can be checked by means of transmission experiments [7].

## 3. Theoretical Approaches

Basically two analytical density distributions n(E) are used to fit the experimental data as measured in the LAB system. Both, the Maxwellian distribution [12] and the Watt distribution [13] are rough approaches to describe the spectrum of neutrons originating from the fission process and are based on the evaporation theory [14].

Assuming an energy independent cross section for the inverse process, the neutron energy distribution in the CM system of the fission fragment is given by

$$(3)\quad \phi(\eta) = T^{-2} \cdot \eta \cdot \exp(-\eta/T)$$

with Weisskopf's energy parameter T. Taking into account an isotropic emission in the CM system of two fully accelerated fission fragments of equal mass the transformation into the LAB system leads to the tabulated Gaussian integrals (Feather's spectrum [12]).

Terrell [12] modified the approximation by considering two different fragment masses and up to seven temperatures simulating a triangular temperature distribution. It turned out that the superposition of the different Feather's spectra could be approximated by a Maxwellian distribution in the LAB-system (see fig. 8 of ref. 12):

$$(4)\quad n(E) = 2 \cdot \pi^{-1/2} \cdot E_0^{-3/2} \cdot E^{1/2} \cdot \exp(-E/E_0)$$

The energy parameter $E_0$ corresponds to the mean energy $\langle E\rangle = 3 \cdot E_0/2$ and is fitted by comparison with experimental data.

On the other hand Madland and Nix [10] showed that the evaporation spectrum (equ. 3), correctly folded with the triangular temperature distribution, may also be described by a Maxwellian distribution in the CM frame of the fission fragments. Transformation into the LAB system, assuming isotropic emission and equal fragments, delivers the Watt spectrum [13]:

$$(5)\quad n(E) = \left[\exp(-E_f/T) \cdot \pi^{-1/2} \cdot E_f^{-1/2} \cdot T^{-1/2}\right] \cdot \exp(-E/T) \cdot \sinh\left[2 \cdot E^{1/2} \cdot E_f^{1/2}/T\right]$$

with the mean kinetic energy per nucleon $\langle E_f\rangle \sim 0.78$ MeV of the fully accelerated fragments being related to the mean energy and the energy parameter T by $\langle E\rangle = \langle E_f\rangle + 3T/2$.

Madland and Nix [10] gave up most of the restrictive assumptions and introduced in their extensive numerical calculations

a) an energy dependent inverse capture process, where the cross section was calculated by means of various optical potentials, and
b) a realistic mass distribution including light ($\langle E_f^L \rangle \sim 1.06$ MeV) and heavy ($\langle E_f^H \rangle \sim 0.50$ MeV) fragments.

The comparison of the various approaches (see fig. 7 of ref. 10) shows that the description is very similar in the energy region $E_n < 5$ MeV while in the upper part, the Maxwellian distribution overestimates and the Watt spectrum underestimates the numerically 'exact' solution.

## 4. Discussion of Recent Results

Experimental details of recent measurements [5-9] have been compared in the table as far as they were available from the short publications. These experiments cover in total the energy range from 1 keV up to 30 MeV. Most of the results are preliminary ones, at least with respect to the uncertainties to be estimated realistically. However, the main trends can be discussed.

For the low energy range ($E_n \leq 0.5$ MeV) Blinov et al. [5,6] were unable to confirm the deviations from a Maxwellian distribution established by the NBS evaluation. The experimental data taken with a $^6$LiI(Eu) crystal [5] or a $^{235}$U fission chamber [6] were carefully corrected and are in excellent agreement with a Maxwellian distribution with $E_o = 1.42$ MeV (fig. 4 of ref. 6). The medium energy range (2 MeV $\leq E \leq$ 15 MeV) seems to be well described by the NBS segment fit [8,9] while the energy range $E_n > 15$ MeV is strongly underestimated [9]. Excellent new data were also presented by the Argonne group [7]. The experimental spectrum agreed with the Maxwellian shape to within ±5 % for the energy range 0.5 MeV $\leq E \leq$ 7 MeV. Nevertheless the authors favour the Watt approximation which underestimates the measurements above 5 MeV (see fig. 10 of ref. 7).

The most exciting perspective comes from the comparison of the experimental data with recent numerical calculations. Madland and Nix [10] demonstrate that besides the spectral shapes, the energy dependence of the neutron multiplicity $\bar{\nu}(E_n)$ is reasonably well described for the neutron induced fission of $^{235,238}$U and $^{239,240}$Pu. In the case of the spontaneous fission of $^{252}$Cf the calculated multiplicity $\bar{\nu}_{calc} = 3.80$ is in excellent agreement with the recent experimental value $\bar{\nu}_{exp} = 3.77$ [15] while the mean energies $\langle E \rangle_{calc} = 2.217 \ldots 2.279$ MeV calculated on the basis of different mass formulas [10] differ significantly from the experimental values $\langle E \rangle_{exp} = 2.13 \ldots 2.16$ MeV [7]. Due to this fact it is not surprising that the calculated distribution cannot describe the measured spectrum (see fig. 10 of ref. 7). Pönitz pointed out that the ratios between the measured as well as the calculated spectrum and a Maxwellian distribution corresponding to the same mean energy show very similar trends (fig. 11 of ref. 7). Thus it can be expected that by fitting free parameters, in particular with regard to the level density parameter, the mass distributions and the energy excess, sufficient agreement can be achieved for both the neutron multiplicity $\bar{\nu}$ and the energy density distribution n(E).

Table : Parameters of recent tof measurements

| | | Blinov et al. ref. 5 (1982) | Blinov et al. ref.6 (1982) | Pönitz,Tamura ref. 7 (1982) I | Pönitz,Tamura ref. 7 (1982) II | Böttger et al. ref. 8 (1982) | Märten et al. ref. 9 (1982) |
|---|---|---|---|---|---|---|---|
| FF-detector | type | gas sc. | ion ch. | gas scint. | | ion ch. | ion ch. |
| | backing/(cm) | | Ni/0.015 | Pt/0.0254 | | Au/0.01 | Ta/0.0125 |
| | radius (cm) | | 0.4 | 0.953 | | 0.5 | 0.5 |
| | $\Phi$ ($10^5$ f/s) | | 2...5.1 | 1.43 | | 1.0 | 3.4 |
| | $\varepsilon_f$ | ~0.99 | ~0.99 | ~0.71 | | 0.954 | |
| | $\varepsilon_{cf}/\Phi_o$ (deg) | /0 | /0 | (0.93/0) | | 0.975/≤20 | /0 |
| n-TOF detector | type | $^6$LiI(Eu) | $^{235}$U | equiv.NE 213 | | 4xNE 213 | NE 213 |
| | height (cm) | 0.5 | 1.2 | 17.76 | 37.0 | 5.08 | 12.5 |
| | diameter (cm) | 1.7 | 10.0 | 7.62 | 10.0 | 25.4 | 12.5 |
| | $E_n^{min}$(keV)- $E_n^{max}$(keV) | 1- 2000 | 10- 7000 | 200- 4000 | 600- 10000 | 2000- 14000 | 10000- 30000 |
| | $\varepsilon_d(E_n^{min})$- $\varepsilon_d(E_n^{max})$ | ~ $\sigma_{n,\alpha}$ | ~ $\sigma_{n,f}$ | 0.98- 0.83 | 0.96- 0.77 | 0.25- 0.15 | 0.30- 0.15 |
| | $\Delta\varepsilon/\varepsilon$ (%) | | (≤ 4) | ≤ 2 | ≤ 2 | ≤ 5 | |
| TOF-spectroscopy | flight path (cm) | 6.25-50 | 25-100 | 258 | 347 | 1200 | 450 |
| | TAC-range (ns) | 150 | 200 | ~1000 | | ≤1000 | 200 |
| | channel width (ns) | (~ 1) | ( ~1) | (~ 1) | | < 1 | 2.37 |
| | FWHM $\Delta t_\gamma$ (ns) | 1.5 | 1.5 | | (≤ 4) | 1.5 | 1.8 |
| | deadtime $\tau$ (ns) | (200) | ~200 | | (~ 50) | 530 | |
| | $\Delta t_o$ (ns) | (≤0.2) | ≤ 0.2 | | | ≤ 0.2 | ≤0.2 |
| Corrections | tof-backgr./renorm. | | | calc. ($\tau$=0) | | calc. | |
| | noniso. fiss. loss | | | | | exp. | |
| | struct. mat. (det.) | exp./calc. | | ≤ 0.2 % estim. | | ≤ 0.2 % est. | |
| | inscatt. (air, coll.) | exp./calc. | | ≤ 0.2 % estim. | | ≤ 0.5 % est. | |

## 5. Conclusion

Important progress was made in the last years to improve the knowledge of the neutron energy spectrum from the spontaneous fission of $^{252}$Cf. Recent measurements were performed using the tof method, carefully analyzed and corrected for various disturbing effects. The correct renormalization - the problem was at first recognized by A. Chalupka [16] in 1979 - was applied by some authors [7,8]. In addition, the influence of the non-isotropic detection losses of fission fragments on the measured neutron spectrum was investigated and corrected for [7,8].

The theoretical concept should be supported by additional experiments. In particular, the assumptions have to be proved that the neutrons are isotropically emitted in the CM frame of fully accelerated fission fragments. In addition, the fraction of scission neutrons estimated to contribute with about 25 % to the prompt fission neutrons [17] has carefully to be determined by means of correlation experiments.

A new evaluation on the basis of the data recently available is necessary. Earlier tof measurements [17,18,19] should only be taken into account if a unique reanalysis can be performed. Furtheron, recent numerical calculations and additional experimental data using different methods should be considered; e.g. integral measurements taking advantage of the foil activation technique cover the energy range of interest [20] and relate the Cf spectrum to various reaction cross sections. It is to be expected that an improved density distribution will replace the NBS segment fit as well as the approximations.

The application of the 'standard' spectrum for calibration purposes may, however, be as difficult as the determination itself due to the various corrections listed above.

Acknowledgement: Valuable discussions with Drs. Böttger and Chalupka during the joint experiments and with Drs. Blinov, Mannhart and Pönitz are gratefully acknowledged.

References

1. J.A. Grundl, C.M. Eisenhauer; NBS-425 (1975) 250-253
2. M.V. Blinov; INDC (NDS)114/GT (1980) 79-106
3. Nucler Standards File; INDC-36/LN (1980) 338-345
4. WRENDA 81/82; INDC (SEC)-78/URSF 122-123
5. M.V. Blinov, V.A. Vitenko, V.N. Dishin, V.I. Yurevich; NIM 198 (1982) 455-460
6. M.V. Blinov, G.S. Boykov, V.A. Vitenko; Proceedings of the Int. Conf. on "Nuclear Data for Science and Technology" in Antwerp, to be published 1983 (preprint)
7. W.P. Pönitz, T. Tamura; ibid. (preprint)
8. R. Böttger, H. Klein, A. Chalupka, B. Strohmaier; ibid. (preprint)
9. H. Märten, D. Seeliger, B. Stobinski; ibid. (preprint) and INDC (DDR)-17/L (1982)
10. D.G. Madland, J.R. Nix; NSE 81 (1982) 213-271
11. R. Böttger, H. Klein, A. Chalupka, B. Strohmaier; to be submitted to NSE
12. J. Terrell; Phys. Rev. 113 (1959) 527-541
13. B.E. Watt; Phys. Rev. 87 (1952) 1037-1041
14. J.M. Blatt, V.F. Weisskopf; "Theoretical Nuclear Physics" p. 365-374, John Wiley Inc. New York 1952
15. R.R. Spencer; NBS-594 (1980) 728-732
16. A. Chalupka; NIM 165 (1979) 103-108
17. L. Green, J.A. Mitchell, N.M. Steen; NSE 50 (1973) 257-272

18. H.H. Knitter, A. Paulsen, H. Liskien, M.M. Islam;
Atomkernenergie 22 (1973) 84-86
19. J.W. Boldemann, D. Culley, J.J. Cawley;
Trans. Am. Nucl. Soc. 32 (1979) 733-735
20. W. Mannhart; published as ref. 6-9 (preprint)

# THE HIGH-ENERGY END OF THE NEUTRON SPECTRUM FROM SPONTANEOUS FISSION OF $^{252}Cf$

H. Märten, D. Seeliger, and B. Stobinski
Technische Universität Dresden, Sektion Physik, Dresden, DDR

## 1. Introduction

As an addition to the refs. 1 and 2, this paper summarises some experiences of fission neutron spectrum measurements up to very high emission energies emphasizing experimental principles and necessary corrections of the data. Applying an effective particle suppression method to reduce the background and measuring the time of flight (TOF) of the neutrons and the corresponding light output (LO) in the scintillator two-dimensionally we were able to detect the high-energy end of the $^{252}Cf(sf)$ neutron spectrum from 11 up to 30 MeV.

## 2. Experimental arrangement

The following synopsis includes the main data characterising the experimental set-up and the long-time measurement [1,2]:

| | | |
|---|---|---|
| Cf source | : | 34000 fissions per s, Tantalum backing (0.125 mm thick, 5 mm source diameter) |
| Fragment detection (STOP signal) | : | fast ionization chamber [3] (1.5 at methane, 3 mm electrode distance, $\Delta E$ mode ) - current preamplifier - fast amplifier (about 100 ns dead time) - zero-cross-over timing - cable delay |
| Neutron detection | : | scintillator NE 213 (5`` x 5``) - fast photomultiplier XP 2041 - constant-fraction trigger (2.8 MeV-threshold regarding proton recoil energy) |
| Range of the time-to-amplitude converter | : | 200 ns |
| TOF-bin width | : | 2.372 ns |
| Background suppression | : | electronic charge comparison method [4] ($n/\gamma\mu$-discrimination) |
| Flight path | : | 4.50 m |
| Collimator | : | polyethylene, graphite liner, Pb, Fe |
| Whole running time | : | 1218.5 h subdivided in single runs; intermediate checks of thresholds, $n/\gamma\mu$-discrimination, and response functions |
| LO calibration | : | analysis of the response functions for given TOF channels in comparison with Monte Carlo calculations (NEUCEF code - ref. 5) |

## 3. Background suppression and spectrum analysis

Using the electronic charge comparison method the experiment-specific $\gamma$-background as well as the annoying pulses caused by cosmic myons with energies around 1 GeV are suppressed intensively [1,2]. The application of large scintillators involves an influantial cosmic background at relatively high LO. Another possibility to avoid such pulses is the employment of a scintillator shield in connection with an anticoincidence arrangement.

Measuring neutron TOF and LO two-dimensionally one is able to select the

optimum LO threshold for a given TOF channel to minimize the statistical error. This analysis procedure which represents an indirect background suppression is realized by the comparison of the remaining random background LO spectrum with the measured response functions for fixed TOF channels. The optimum LO thresholds for the neutron spectrum ranges around 5, 10, and 15 MeV were found to be 2.5, 5.5, and 8 MeV respectively (regarding proton recoil energy).

The detector efficiency data were calculated using the NEUCEF code [5] and considering an realistic resolution parameter. Their experimental test [1] resulted in an estimation of errors: 8 % for the energy range from 10 to 15 MeV, 12 % for the range from 15 to 20 MeV and about 15 % above.

## 4. Data correction

As discussed by Böttger et al. [6], a TOF-channel-depending background part has to be attributed to uncorrelated stop signals. It was confirmed by a supplementary investigation that the corresponding correction and renormalization is neglegible in the present case due to the energy range limitation and the moderate fission rate.

The measurable neutron spectrum of the Cf source depends on the angle between the neutron detector direction and the electrode plane because of the anisotropic fragment detection [6]. Therefore, the neutron detector was located perpendicular to the electrode plane [1]. In this case, necessary corrections concern the low-energy part of the spectrum only. The measured energy distribution is actually undisturbed at energies above about 5 MeV (This assertion concerns the employed fission chamber.). Counting the processed stop signals (behind the delay device) the energy spectrum could be normalized absolutely.

In the present case, the correction for air scattering was weakly energy-dependent (3.1 ÷ 3.6 %).

The correction for time resolution which depends on neutron energy because of the scintillator dimensions amounted to 2.8 % at 10 MeV and 15.2 % at 19 MeV. The influence of the TOF-bin width correction was smaller (0.2 and 1.9 % respectively). Both corrections which have been carried out by iterative methods were lower than 1 % at energies above 21 MeV due to the presence of a hard emission component predominant at energies higher than 20 MeV (Fig. 1)

Further details of the experiment are described in ref. 1.

## 5. Results and discussion

Within the experimental errors, the NBS evaluation [7] was confirmed for the energy range from 11 to 20 MeV (in a qualified sense for energies above 16 MeV). The measured energy spectrum can suitable be described by a pure Maxwellian distribution with a temperature parameter kT = 1.248 MeV in the region from 11 up to 19 MeV. The integral over N(E) from 21.5 to 26.7 MeV amounts to $(6.0 \pm 3.4) \cdot 10^{-6}$. This neutron yield is much more higher than expected.

Fig. 1 shows the measured high-energy part of the $^{252}Cf(sf)$ neutron spectrum in comparison with the result of a complex cascade evaporation calculation [8]. The experimental data indicate the presence of a hard emission component which cannot be explained assuming the main emission mechanism, i. e. neutron evaporation from fully accelerated fragments. Hence, one should consider non-equilibrium emission of fission neutrons due to strong single-particle excitations during the fission process [2,8].

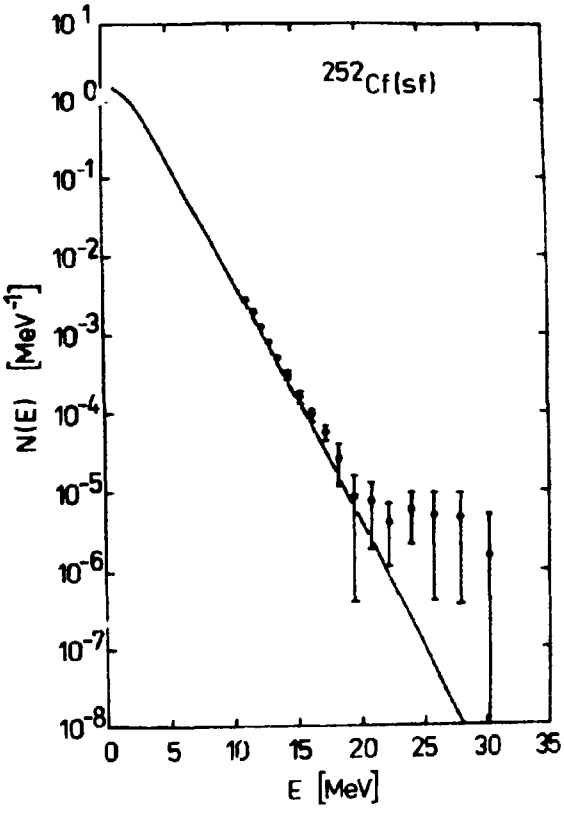


Fig. 1
The measured high-energy part of the neutron spectrum from spontaneous fission of 252-Cf in comparison with the result of a complex cascade evaporation calculation (ref. 8).

## References


1. H. Märten et al., INDC(GDR)-17/L (1982)
2. H. Märten et al., Contribution to the Int. Conf. on Nuclear Data for Science and Technology, Antwerp, 6-10 Sept. 1982
3. M. Adel-Pawzy et al., Kernenergie 24 (1981) 107
4. H.-G. Ortlepp, Proc. X$^{th}$ Int. Symp. on Nuclear Electronics, Dresden, 1980
5. N. R. Stanton, COO-1545-92 (1971),
   D. Hermsdorf, ZfK-315 (1977) 192
6. R. Böttger et al., Contribution to the Int. Conf. on Nuclear Data for Science and Technology, Antwerp, 6-10 Sept. 1982,
   H. Klein, this conference
7. J. Grundl, C. Eisenhauer, Natl. Bur. Stds. Publ., NBS-493, 1977
8. H. Märten et al., submitted to J. of Phys. G

# CALCULATION OF DOUBLE-DIFFERENTIAL EMISSION CROSS SECTIONS OF NEUTRONS FROM SPONTANEOUS FISSION OF $^{252}$Cf ON THE BASE OF THE CASCADE EVAPORATION MODEL

H. Märten, D. Neumann, and D. Seeliger
Technische Universität Dresden, Sektion Physik, Dresden, DDR

Assuming the main emission mechanism of fission neutrons, i. e. the evaporation from fully accelerated fragments, a complex cascade evaporation model [1,2] (CEM) is applied to describe neutron energy spectra in the center-of-mass system (cms) as a function of both the fragment mass number A and the total kinetic energy TKE of the fragments. The mass number ratio $A_L/A_H$ of complementary fragments and TKE appoint the scission configuration (asymmetry and elongation respectively). The initial distributions of excitation energy $P_0(E^x)$ are deduced from experimental data on neutron multiplicity and $\gamma$-ray emission [3] as a function of both A and TKE [2]. The used method for level density description takes into account the dependence of shell effects on excitation energy semi-empirically [4]. Considering the occurance probability

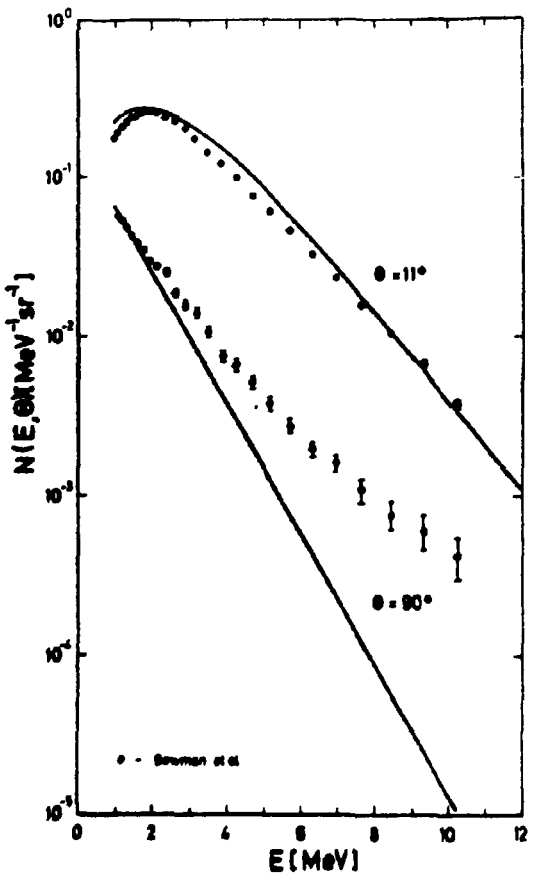


Fig. 1 The calculated energy spectra in 11° and 90° direction in comparison with the experimental data of Bowman et al. (ref. 5)

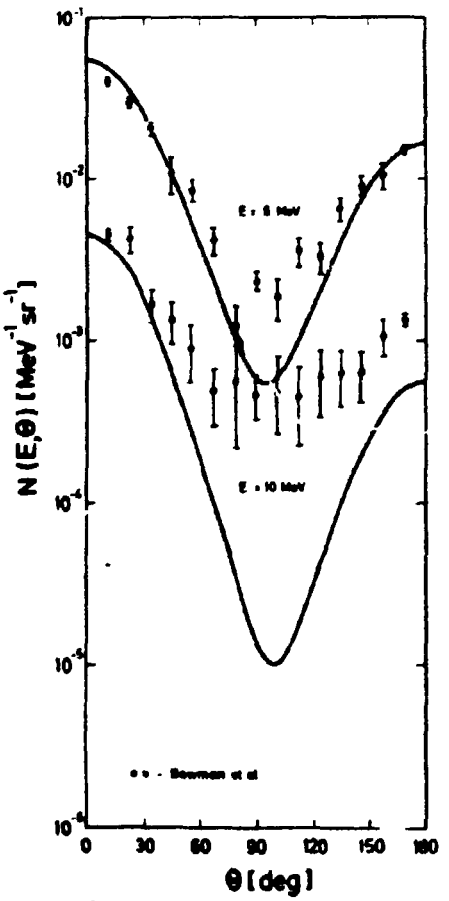


Fig. 2 Calculated angular distributions at two selected emission energies in comparison with measured data (ref. 5)

$P(A_L/A_H, TKE)$ the double-differential emission cross section may be deduced in dependence on both $A_L/A_H$ and TKE, in dependence on $A_L/A_H$ or TKE only as well as for the whole fission reaction. The neglection of the TKE dependence modifies the calculated energy spectra and angular distributions in the laboratory system (ls) at high emission energies considerably [2].

The CEM was used to calculate the integral ls energy spectrum N(E) of the neutrons from spontaneous fission of $^{252}Cf$ [2]. We were able to obtain a rather good agreement with experimental data up to 20 MeV. The comparison of the calculated spectrum with our recent experimental results on the high-energy end of the energy distribution [1] indicates the presence of a hard spectrum component which should be attributed to non-equilibrium emission of fission neutrons due to strong single-particle excitations in fission [1,2].

The Figures 1 and 2 represent a comparison of the calculated integral (regarding the dependence on both TKE and $A_L/A_H$) distribution $N(E,\Theta)$ ($\Theta$ - ls angle of the neutrons with reference to the light fragment direction) with the experimental results of Bowman et al. [5] Obviously, the central component [5] of fission neutrons (scission neutrons) becomes more predominant at higher emission energies. However, the recent results of Riehs [6] do not confirm the data of Bowman et al. The reason of this contradiction is not clarified. Nevertheless, one should expect that there is an connection betbeen the central component found at emission energies in the MeV range and the hard emission component predominant at extremely high emission energies.

A more precise interpretation of the presented results seems to be only possible in connection with measurements of double-differential emission cross sections as a function of both $A_L/A_H$ and TKE and further theoretical analysis of single-particle excitations in fission. Hitherto, the partial spectra of the different eventual kinds of scission neutrons are not founded theoretically (see ref. 2 and the refs. therein).

According to the experimental results of Samyatnin et al. [7] scission neutrons are predominantly emitted in the case of compact scission configurations which include a magic or double-magic fragment ($A_H \approx 132$ especially). Fig. 3 represents calculated angular distributions which were calculated for $A_L/A_H$ = 120/132 and different TKE values (maximum, average, minimum). Their shapes depend on the partition of the total excitation energy mainly. The ratio of the final excitation energies of complementary fragments is appointed by shell effects on the scission configuration modified by intrinsic temperature [2]. Fig. 3 shows that a measurement carried out for the stated parameters should be sensitive to the angular distribution of scission neutrons at angles higher than about 40°.

It is emphasized that no arbitrary normalisations or free parameters are introduced in the calculations. As confirmed by some comparisons with experimental data, the described method is feasible to explain the main characteristics of fission neutron emission. It represents an essential precondition for the study of scission neutrons.

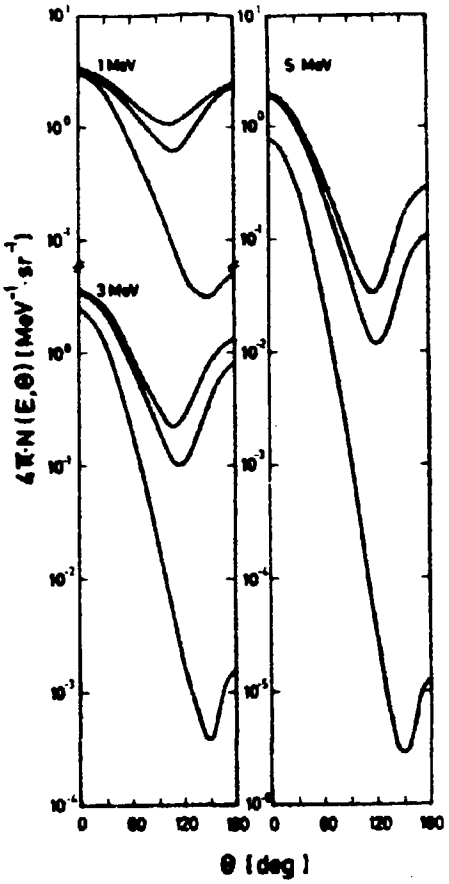


Fig. 3

Angular distributions of fission neutrons calculated for the fragment mass number ratio 120/132 and different values of TKE.
The upper (middle, lower) curve corresponds to the minimum (average, maximum) TKE in each case.
The stated parameter represents the le emission energy.

## References


1. H. Märten et al., Contribution to the Int. Conf. on Nuclear Data for Science and Technology, Antwerp, 6-10 Sept. 1982;
   H. Märten et al., this conference
2. H. Märten et al., submitted to J. of Phys. G
3. H. Nifenecker et al., Proc. 3rd IAEA Symp. on the Physics and Chemistry of Fission, Rochester, 1973, vol. ii, 117 (Vienna, IAEA)
4. A. V. Ignatyuk et al., Nejtronnaya Fizika (Proc. IVth All Union Conf., Kiev, 1977) 1 (1977) 60
5. H. R. Bowman et al., Phys. Rev. 126 (1962) 2120;
   H. R. Bowman et al., Phys. Rev. 129 (1963) 2133
6. P. Riehs, Acta Physica Austriaca 53 (1981) 271
7. Ju. S. Samyatnin et al., Yad. Fiz. 29 (1979) 595

# СПЕКТР ЗАДЕРЖАННЫХ НЕЙТРОНОВ СПОНТАННОГО ДЕЛЕНИЯ $^{252}Cf$

В.Н. Нефедов

Научно-исследовательский институт атомных реакторов им. В.И. Ленина, Димитровград, СССР

В работе приведены результаты измерений, подтвердивших существование дискретной структуры спектров мгновенных нейтронов деления. Выполнены прямые измерения спектра задержанных нейтронов, испускаемых при спонтанном делении $^{252}Cf$.

В многомерных измерениях спектров мгновенных нейтронов деления $^{235}U$ тепловыми нейтронами в зависимости от кинетической энергии осколков деления [I] нами была обнаружена дискретная структура спектров нейтронов испускаемых осколками с массами A = I32 и A = 85, имеющих один или несколько нейтронов сверх замкнутых оболочек в 50 и 82 нейтрона. Для объяснения этого явления было выдвинуто предположение о существовании небольшой доли нейтронов, названных задержанными, имеющих дискретный спектр и испускаемых спустя $10^{-9}$-$10^{-7}$с после момента деления ядра. Тонкая структура была также обнаружена в работе [2]. Однако в ряде других работ существование задержанных нейтронов не подтверждено [3,4,5].

Настоящая работа была поставлена для решения вопроса о существовании задержанных нейтронов. Постановка экспериментов основывалась на предполагаемых свойствах задержанных нейтронов (задержка испускания и дискретный спектр). Поэтому при измерении спектра нейтронов методом времени пролета с использованием в качестве "старта" импульсов от осколков деления, отдельные линии от задержанных нейтронов растянутся во времени в результате задержки их испускания после момента деления и дискретная структура будет слабо заметна. Могут наблюдаться лишь линии, образованные задержанными нейтронами с временем испускания, значительно меньшим, чем время пролета регистрируемых нейтронов ($< 10^{-8}$сек).

При использовании в качестве "старта" импульсов от $\gamma$-квантов, сопровождающих моменты деления и вылета задержанных нейтронов, дискретная структура от задержанных нейтронов должна хорошо наблюдаться, так как исчезает размытие во времени момента вылета задержанных нейтронов. Однако, в этом случае необходимо обеспечить малую эффективность регистрации актов деления (< I04I5 %) с тем, чтобы исключить подавление регистрации $\gamma$-квантов, сопровождающих испускание задержанных нейтронов, предварительной регистрацией мгновенных $\gamma$-квантов деления. С учетом этого замечания были выполнены измерения спектра нейтронов спонтанного деления $^{252}Cf$ методом времени пролета.

Блок-схема эксперимента приведена на рис.I.

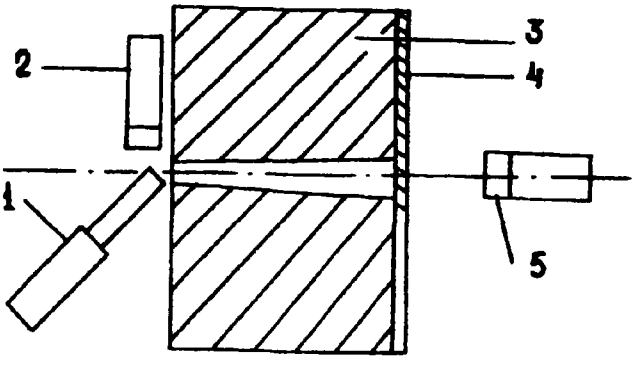


Рис.I. Схема эксперимента
I. Детектор осколков деления. 2. Детектор $\gamma$-квантов. 3. Защита из полиэтилена с бором. 4. Свинец толщиной 10 мм. 5. Детектор нейтронов.

Для исключения регистрации рассеянных на деталях установки нейтронов использовалась полиэтиленовая защита с добавкой бора толщиной 0,2 м. Детектор осколков деления представлял собой слой $^{252}Cf$, помещенный между двумя пленками из сцинтиллирующей пластмассы толщиной 1мг/см$^2$. Слой укреплен в торце тонкостенной (0,05 мм) трубки из латуни длиной 0,2 м, установленной открытым концом на фотокатоде ФЭУ-30. Использовался слой $^{252}Cf$ активностью $5.10^4$ с$^{-1}$. Регистрация $\gamma$-квантов деления осуществлялась жидкостным сцинтиллятором на основе фторбензола $C_6F_6$ с размерами 50х50 в сочетании с ФЭУ-30. В качестве нейтронного детектора использовался кристалл стильбена 0,04х0,02 м. Измерения выполнялись в следующем порядке. В начале каждой серии измерений измерялся спектр при использовании в качестве "стартового" детектора осколков деления. Затем, в тех же условиях, измерялся спектр нейтронов с детектором $\gamma$-квантов в качестве "стартового", работающего в совпадении с детектором осколков деления. Использование метода совпадений необходимо для исключения возможных эффектов от регистрации обычных запаздывающих нейтронов. Были выполнены измерения на пролетных расстояниях $L$ = 0,5 и I м. На рисунке 2 приведены результаты измерений.

Из рисунка видно, что на кривых, полученных в измерениях при старте от $\gamma$-квантов, отчетливо наблюдается дискретная структура, сдвигающаяся пропорционально пролетному расстоянию. В то же время кривая, полученная в измерениях с использованием в качестве "стартовых" импульсов от осколков деления, практически гладкая. Полученный результат позволяет сделать заключение о реальности дискретной структуры, и подтверждает предположение о том, что она образована задержанными нейтронами, испускаемыми позже момента деления ядра. С целью прямой проверки существования задержанных нейтронов были проведены измерения спектра задержанных нейтронов из осколков деления, пролетевших расстояние в 0,05 м. Измерения выполнялись методом времени пролета на пролетном расстоянии 0,25 м. Геометрия опыта показана на рис.3. Детектор осколков деления представлял собой цилиндрическую вакуумную

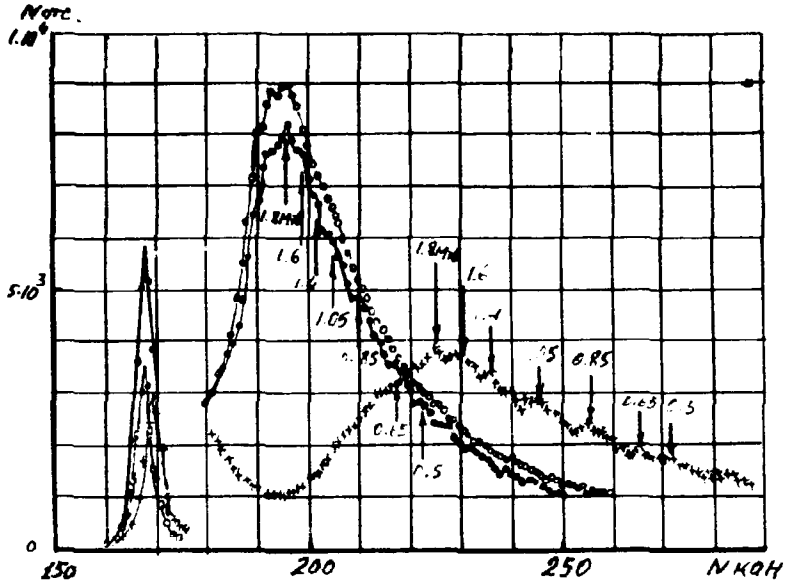


Рис.2. Экспериментальные кривые
∘ – старт от осколков деления, $L$ = 0,5 м; • – старт от – квантов, $L$ = 0,5 м; + – старт от $\gamma$-квантов, $L$ = 1 м.

камеру диаметром $1.10^{-1}$м, изготовленную из стали толщиной $1.10^{-3}$м. Односторонний слой калифорния интенсивностью $3.10^{5}$ $c^{-1}$ нанесен на алюминиевую подложку толщиной $1.10^{-4}$м. Для предотвращения распыления калифорния слой закрыт алюминиевой фольгой толщиной $1,5^{мг}/см^{2}$.

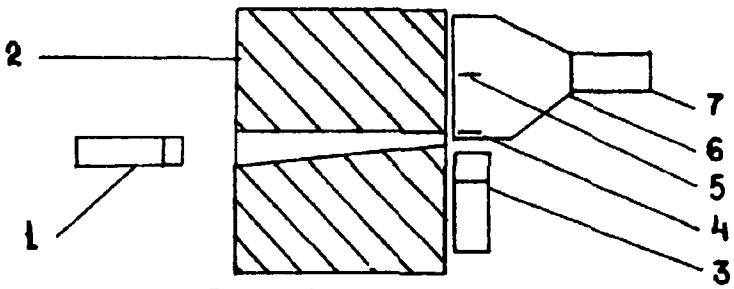


Рис.3. Геометрия опыта
1. Детектор нейтронов. 2.Защита. 3.Детектор $\gamma$-лучей. 4.Слой $ZnS(Ag)$. 5.Слой калифорния. 6.Вакуумная камера. 7. Фотоумножитель ФЭУ-30.

Слой установлен в центре камеры и обращен к детектирующему слою $ZnS(Ag)$, нанесенному на боковую грань камеры. Световые вспышки, возникающие в слое $ZnS(Ag)$ регистрируются фотоумножителем ФЭУ-30, установленном на противоположном торце вакуумной камеры. Размер слоев $Cf$ и $ZnS(Ag)$ 0,02x0,04 м. Вакуумная камера могла поворачиваться на 180° так, что в первом случае слой $ZnS(Ag)$ был виден нейтронным детектором, а при повороте закрывался защитой. Стартовый импульс брался от детектора $\gamma$-лучей, расположенного около слоя $ZnS(Ag)$. В качестве детектора $\gamma$-квантов исполь-

зовался детектор, описанный в первой части работы. Для уменьшения фона детектор $\gamma$ -лучей включался на совпадения с детектором осколков деления. Счет совпадений составлял 12-14 $c^{-1}$ при фоне ложных совпадений около 1 $c^{-1}$. В ходе измерений поочередно проводились измерения при расположении слоя $Zn\,S(Ag)$ вблизи от детектора $\gamma$ -лучей в 1-ом случае, и при повороте вакуумной камеры на 180°, во втором. В первом случае регистрировался измеряемый эффект вместе с фоном от нейтронов, рассеянных на стенке камеры. Во втором случае - фон от рассеяния. Была также выполнена экспериментальная проверка эффекта от запаздывающих нейтронов, который оказался пренебрежимо малым. В результате измерений на протяжении 4 месяцев непрерывной работы были получены спектры, приведенные на рис.4.

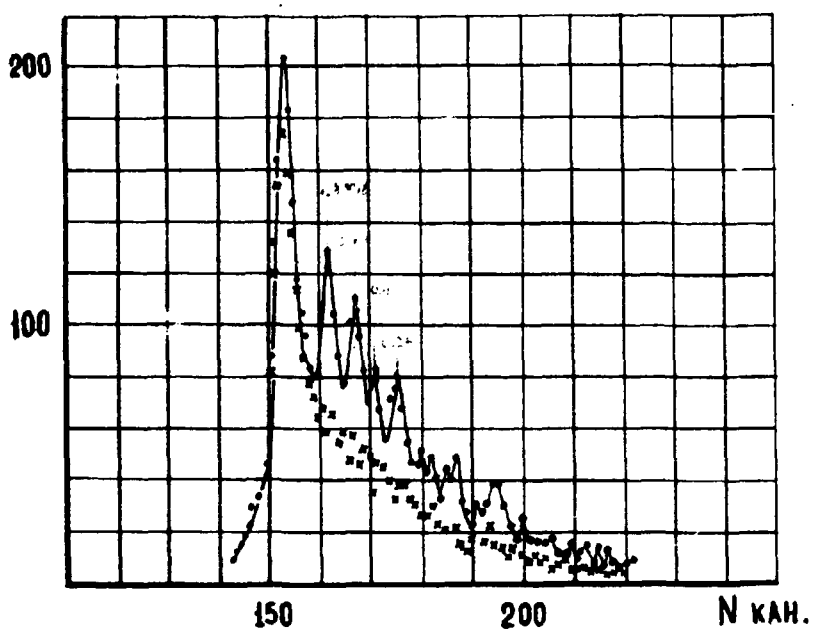


Рис.4. Экспериментальный спектр задержанных нейтронов
• -спектр для 1-го положения вакуумной камеры; x-спектр фона.

Несмотря на ограниченную статистику, надежно наблюдаются отдельные линии, практически совпадающие с отдельными линиями дискретной структуры спектра мгновенных нейтронов деления, полученной в первой части работы. Полученные результаты подтверждают существование задержанных нейтронов, испускаемых отдельными осколками после момента деления ядра и имеющими дискретную структуру [1].

Литература

1. Нефедов В.Н. Препринт ИЯИАР Р-52 (1969)
2. Аверченков В.Л., Нефедов В.Л., Жилков В.В. Ядерная физика, 1971, т.14, вып.6, с.1134-1143
3. Батенков О.Л., Блинов Л.З., Зитенко В.А., Гуз В.Т. Сборник нейтронная физика, М.Атомиздат, 1977, ч.3, с.201-204.
4. Блинов Л.З., Зитенко В.А., Крисюк И.Т. Препринт Р1-30-л., 1974
5. Дьяченко П.П., Ликсайкин В.Т., Лаптин А. Ядерная физика, 1974, т.19, вып.6, с.1212-1215.

# MASS DISTRIBUTIONS OF FISSION FRAGMENTS EMITTED BY HIGHLY EXCITED NUCLEI

L.N. Andronenko, A.A. Kotov, M.M. Nesterov, *W. Neubert,
N.A. Tarasov and L.A. Vaishnene

Leningrad Nuclear Physics Institute, Gatchina, U.S.S.R.
*Zentralinstitut für Kernforschung, Rossendorf, G.D.R.

Provided that shell effects disappear with increasing nuclear excitation energy it is possible to calculate the cross sections for the nuclear fission process, induced by high-energy protons /1/, in the framework of the cascade-evaporation model and the BOHR-WHEELER approach. In ref. /1/ it has been shown that the statistical model of FONG /2/ without structural effects reproduces satisfactorily the mass distributions of fission fragments, which are emitted by highly excited heavy nuclei ($A > 200$ $E^* > 50$ MeV). A treatment of the fission process in medium-weight and light nuclei in the framework of the same model is a further task. The region of Ag take a special interest, because the liquid-drop model predicts a drastical change of the fragment mass distribution /3/.
The fission process in medium-weight and light nuclei can be experimentally investigated in nuclear reactions which lead to highly excited nuclei. High-energy protons allow to investigate the fission channel of such nuclei with a relative small imparted angular momentum. Compared to it the fragment mass distribution of heavy-ion induced fission may be influenced by angular momentum effects and the initial mass asymmetry of the target-ion system.
Our experiment was performed by using the external proton beam of 1 GeV provided by the LNPI synchrocyclotron. The energies of both coincident fragments and the velocity of one of them were measured by means of a double-arm spectrometer /4/.
The binary fission process can be unambiguously separated from other inelastic channels by this method. Fig. 1 shows the mass distributions obtained for Bi, Au, W and Ag targets irradiated by 1 GeV protons. The histogramms demonstrate the increase of the asymmetry with decreasing mass number of the target nuclei. The symmetric form, which is typical for nuclei like Bi, Au and W, vanishes in the case of Ag.

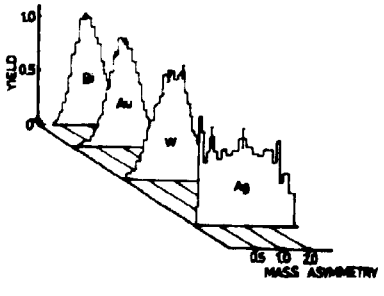


Fig. 1

In fig. 2 we compare the measured mass distributions, obtained from Bi and Ag targets, with the theoretical ones. These calculations, which were performed with the cascade-evaporation model and the statistical method of FONG /2/, show the fragment mass distributions after the evaporation of light particles. Experiment and theory are in a good agreement. It should be mentioned that both experimental and calculated mass distributions represent the result of averaging over different nucleonic composition and excitation energies of the fissioning nuclei.

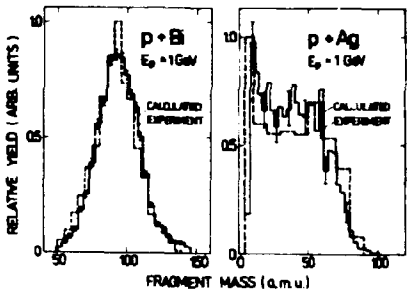


Fig. 2

Fig. 3 shows the calculated distributions of the excitation energy for Bi and Ag nuclei leading to fission. Both distributions extend over several hundred MeV. The average excitation energy increases with decreasing mass number of the fissioning nuclei and corresponds to the experimentally observed growth in the imparted longitudinal momentum for mediumweight target nuclei /5/.

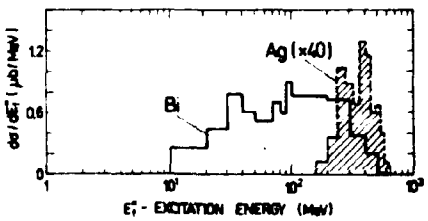


Fig. 3

Fig. 4 represents the influence of the excitation energy on the fragment mass distribution immediately after scission of a nucleus with $A_f$ = 100 and $Z_f$ = 45. These calculations predict a pronounced mass asymmetry which depends strongly on the excitation energy

We conclude, that the observed mass distribution of fission fragments is caused by relative high excitation energies involved in the fission process of Ag. More details of the fission process have to be investigated experimentally in order to check these theoretical predictions.

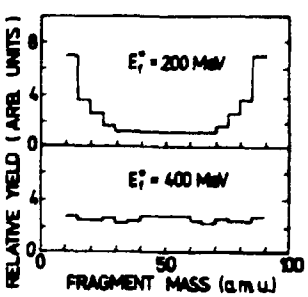


Fig. 4

**References:**

/1/ M.M. Nesterov, V.F. Petrov and N.A. Tarasov, Yad. Fiz. 35 (1982) 1131.

/2/ P. Fong, Phys. Rev. C17 (1978) 1731.

/3/ U.L. Businaro and S. Gallone, Nuovo Cimento 1 (1955) 629 and 1277. J.R. Nix, Nucl. Phys. A130 (1969) 241.

/4/ A A. Kotov, W. Neubert, L.N. Andronenko, B.L. Gorshkov, G.G. Kovshevny, L.A. Vaishnene and M.I. Yazikov, Nucl. Instr. Methods 178 (1980) 55.

/5/ A.A. Kotov, G.G. Semenchuk, L.N. Andronenko, M.N. Andronenko, B.L. Gorshkov, G.G. Kovshevny, V.R. Reznik and G.E. Solyakin, Yad. Fiz. 19 (1974) 756.

# ABSOLUTE FISSION CROSS SECTION MEASUREMENTS ON 233U, 235U, 238U, 237NP, 239PU and 242PU AT NEUTRON ENERGIES OF 2.6 MEV, 8.4 MEV AND 14.7 MEV

R. Arlt, M. Josch, G. Musiol, H.-G. Ortlepp, G. Pausch, R. Teichner, W. Wagner
Technische Universität Dresden, Sektion Physik, Dresden, DDR
I.D. Alkhazov, L.V. Drapchinsky, O.I. Kostochkin, S.S. Kovalenko, V.I. Shpakov
Khlopin - Radiuminstitute, Leningrad, USSR

## 1. Introduction

The requests of accuracy for fission cross section (f.c.s.) data in the energy region from 1 to 2o MeV are few percent [1]. Espacialy for the standard f.c.s. of 235U an accuracy of 1% is required. Also the f.c.s. of 237Np is proposed as a standard cross section in the MeV region.
One way to obtain this high accuracy is the normalization of f.c.s.-shape measurements employing absolute f.c.s. values at certain spot-points of neutron energy. The time correlated associated particle method (TCAPM) is well established now to get such absolute values with high precision in the region of 14 MeV neutron energy [2-5].

## 2. Measurements

Absolute f.c.s. measurements have been carried out using the TCAPM in the frame of the joint measurement program of the TU Dresden (GDR) and the Khlopin - Radiuminstitute Leningrad (USSR). The experiments are independent but correlate in some degree and a correlation analysis has been carried out.
Starting with the measurements at some 14.7 MeV the use of the TSAPM for f.c.s. measurements has been extended to neutron energies of 2.6 MeV and 8.4 MeV [6,7]. Typical values of the corrections and uncertainities are given in Tab. 1.

Tab. 1 Typical values of corrections and uncertainities for the result of f.c.s. measurements using the TCAPM

| | correction | uncertainities |
|---|---|---|
| areal density of the target | | |
| weighing | -- | 1.0% |
| inhomogenity | -- | o.9% |
| effective target thickness in the cone | - o.2% | o.1% |
| number of fission events | | |
| statistics | -- | o.7...1.5% |
| random coincidences | - 5.o% | o.5% |
| efficiency of the fission chamber: | | |
| extrapolation to zero pulse height | + 2.o% | o.6 % |
| absorption of fragments in the layer | + 2.o% | o.6% |
| number of associated particles | | |
| statistics | -- | $1o^{-5}$ |
| background at $E_n$ = 14.7 MeV | + o.3% | o.1% |
| $E_n$ = 8.4 MeV | + 3.o% | o.4% |
| $E_n$ = 2.6 MeV | + 2.5% | o.5% |
| neutron scattering | o.2...1.o% | o.4% |

## 3. Results

In table 2 the results of the f.c.s. measurements carried out at the TU Dresden are given. Some of them were done several times. Independent measurements have been carried out at the RI Leningrad in the 14 MeV neutron energy region.

Tab. 2 Results of the f.c.s. measurements using the TCAPM at the TU Dresden

| | $\bar{E}_n$ / MeV | $\sigma_f$ / $10^{-24}$ cm$^2$ | | $\Delta\sigma_f / \sigma_f$ | Ref. |
|---|---|---|---|---|---|
| 233U | 14.7 | 2.244 | ±0.041 | 1.8 % | |
| 235U | 2.56 | 1.215 | ±0.020 | 1.5 % | 7 |
| | 8.4 | 1.801 | ±0.043 | 2.4 % | 6 |
| | 14.7 | 2.085 | ±0.023 | 1.1 % | 5 |
| 238U | 14.7 | 1.166 | ±0.021 | 1.8 % | 5 |
| 237Np | 8.4 | 2.151 | ±0.045 | 2.1 % | 8 |
| | 14.7 | 2.226 | ±0.024 | 1.1 % | 5 |
| 239Pu | 14.7 | 2.394 | ±0.024 | 1.0 % | 5 |
| 242Pu | 14.7 | 2.143 | ±0.046 | 2.1 % | |

For the standard f.c.s. of 235U a set of 3 absolute values has been obtained which can be used for normalization of shape measurements. The result of the renormalization of the shape measurement of Czirr and Sidhu [9] using the absolute values of this work is presented in fig. 1. This normalization has been carried out in two different ways:

i) minimizing the sum of squares of the differences between shape and absolute values (full line)

ii) taking into account a linear dependence of the normalization factor from the energy (dotted line).

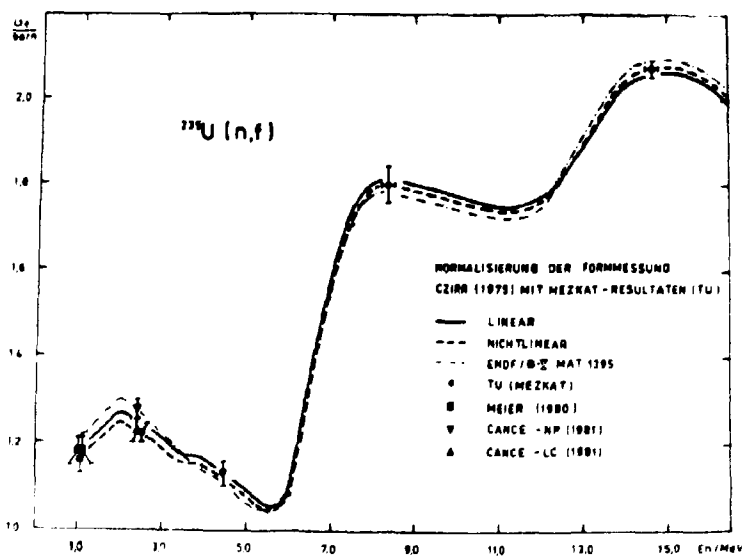


Fig. 1 Normalization of the shape measurement of Czirr and Sidhu in comparison with other experimental f.c.s. values

The f.c.s. of 237Np (proposed as a standard cross section in the MeV region) has been measured at the neutron energies of 14.7 MeV and 8.4 MeV. The first value at 14.7 MeV has already been taken into account in a new evaluation of the f.c.s. for 237Np carried out by Derrien [10]. Also the other value, recently obtained in this work at 8.4 MeV is in good agreement with this evaluation (see fig. 2).

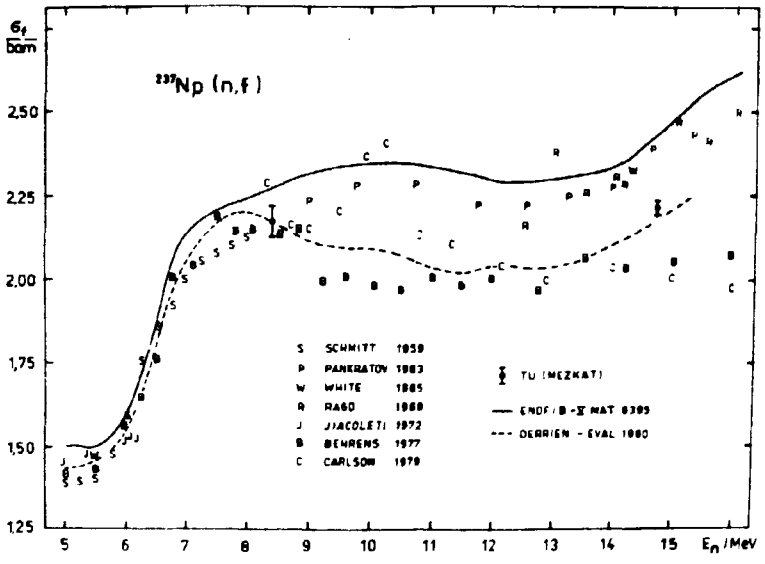


Fig. 2 The f.c.s. values of this work for 237Np compared to other experimental values and the evaluation by Derrien and the file ENDF/B-V

## References


1. D.W. Muir (Ed.), WRENDA 1979/80, INDC(SEC)-73, IAEA Vienna, 1979
2. I.D. Alkhazov et al., in: Proc. of the II-nd Conf. on Neutron Physics, Kiev 1973, part 3, page 13
3. M. Cance, G. Grenier, Nucl. Sci. Engng. 68 (1978) 197
4. O.A. Wasson et al., Nucl. Sci. Engng. 80 (1982) 282
5. R. Arlt et al., Kernenergie 24 (1981) 48
6. R. Arlt et al., in: Proc. of the X-th Internat. Symp. on Selected Topics of the Interact. of Fast Neutrons and Heavy Ions with Atomic Nuclei, Gaussig 1980, ZfK - 459 (1981) 35
7. R. Arlt et al., Kernenergie 25 (1982) 199
8. R. Arlt et al., in: Proc. of the XI-th Internat. Symp. on the Interact. of Fast Neutrons with Nuclei, Rathen 1981, ZfK -476 (1982) 63
9. J.B. Czirr, G.S. Sidhu, Nucl. Sci. Engng. 57 (1975) 18 and 58 (1975) 371
10. H. Derrien et al., INDC(FR)-42/L (1980)

# STATISTICAL ANALYSIS OF THE EXPERIMENTAL DATA OF FISSION CROSS SECTION MEASUREMENTS ON $^{233,235,238}U$, $^{237}Np$, $^{239,242}Pu$ AT NEUTRON ENERGIES OF 2.56, 8.4, 14.5 MEV

V.N. Dushin, A.V. Fomichev, S.S. Kovalenko, K.A. Petrzhak and V.I. Shpakov
V.G. Khlopin Radium Institute Leningrad, USSR

R. Arlt, M. Josch, G. Musiol, H.-G. Ortlepp and W. Wagner
Technical University of Dresden, Section of Physics, GDR

## 1. Introduction

The instrumentation utilized in the joint fission cross section measurement programme of the V.G. Khlopin Radium Institute Leningrad (RIL) and the Technical University of Dresden (TUD) has been improved continuously during the period of several years needed for the design and the construction of the equipment and for the comletion of the time consuming measurements. Quite a few independent runs were usually carried out in the course of a fission cross section measurement. These runs were seperately corrected for systematical uncertainties and combined afterwards in order to obtain the final experimental value which appeared in the publication. Several independent experiments have been carried out in some cases. In this way experimental results, not completely statistical independent, were obtained and published.

A comprehensive analysis of the results and uncertainties of these experiments has been carried out by means of a correlation analysis considering the single runs of each experiment. Final fission cross section values including all measurements performed in Leningrad and Dresden have been obtained.

## 2. Correlation analysis

Covariance matrices $\mathrm{cov}(\sigma_f^i, \sigma_f^j)$ of the results have been calculated from the covariance of the partial uncertainties of the cross sections using the expression: $\mathrm{cov}(\sigma_f^i, \sigma_f^j) = S_i^T \, \mathrm{cov}(x_l^i, x_k^j) \, S_j$

with

$\sigma_f^i, \sigma_f^j$ - results of different fission cross section measurements

$\mathrm{cov}(x_l^i, x_k^j)$ - covariance matrix of the partial uncertainties of the measurements

$S_i, S_j$ - coefficients of sensitivity

$x_l^i, x_k^j$ - values which are used for the calculation of the fission cross section and it's corrections if the time correlated associated particle method is employed.

The final results of the analysis will be published in a forthcoming paper containing the details of the analysis, the covariance matrices the mean values of the cross sections and their uncertainties.

# ON THE IMPROVEMENT OF THE ACCURACY OF ABSOLUTE FISSION CROSS SECTION MEASUREMENTS USING PARALLEL PLATE FISSION CHAMBERS

R. Arlt
Technische Universität Dresden, Sektion Physik, Dresden, DDR

## 1. Introduction

Following the concept of employing absolute determined reference fission cross section values for the normalization of shape measurements which can be carried out at a low level of systematical uncertainties a further improvement of the data basis for the fission cross sections considered as standards can be gained.
It has to be mentioned, however, that there still exist unresolved measurement problems in order to meet the requirement of the 1 per cent accuracy for a fission cross section considered as a standard e.g. the $^{235}U$ cross section.
The aim of this paper is it to review the most striking of them from the point of view of an experimentalist and to make suggestions how to overcome these difficulties. Thereby emphasis is put on such issues which on our opinion may hide unaccounted contributions to the systematical uncertainties of an absolute fission cross section measurement.

## 2. Systematical uncertainties in absolute fission cross section measurements

These uncertainties can be subdivided into two groups the first of which is of general character (i, ii), whereas the second group (iii-v) shows a more specific character depending on the measurement method used (e.g. associated particle counting or the use of a black neutron detector):

i) counting of the fission events (inefficiency of the fission chamber)
ii) characterization of the fission foils (weight or areal density, nonuniformity, chemical and isotopic composition, surface roughness, backing)
iii) neutron fluence determination
iv) distortions of the neutron field (scattering and absorbtion of neutrons)
v) electronics (dead time, stability, pile up, random coincidences)

In the following the systematical uncertainties connected with the registration of fission products (FP) using a parallel plate fission chamber (FC) shall be considered, because this device is one of the most frequently applied in fission cross section measurements on low alpha active samples as it is the case for $^{235}U$.

## 3. Systematical uncertainties connected with the registration of fission products in a parallel plate fission chamber

The inefficiency of the FC-a value amounting to about few per cent-has to be well known in an absolute measurement in contrast to a relative measurement, where the energy dependence of the inefficiency introduces second order effects only [1].

Usually two sources of uncertainties are taken into account-the number of events below the electronic threshold ("threshold losses") and the losses due to absorbtion of fission products within the fission foil ("absorbtion losses") An analysis of recent absolute fission cross section measurements of different groups has been carried out.
The following recommendations are made aiming at an increase of the accucacy of determination of the "threshold losses":

- a standardization of the p r i n c i p l e of the FC signal processing used in in absolute fission cross section measurements has to be introduced in order to allow a clear comparison of the results of different experiments and to guarantee a true energy proportional shape of the FP spectrum especially at it's low energy region
- a theoretical and experimental justification of the "linear extrapolation approach" to zero pulse height has to be carried out
- the question has to be answered, wether the neglection of the ionization defect $\Delta$ [2] in the above mentioned extrapolation procedure does not cause a systematical uncertainty (see Fig. 1).

Fig. 1 Crude estimation of a possible systematical uncertainty of the "extrapolation to zero height" procedure caused by the neglection of the ionization defect. The value $\Delta \sim 6$ MeV [2] has been taken from ref. for a Ar+3% $CO_2$ mixture. Typical values have been assumed for the electronic threshold and the "threshold losses". The underestimation of the fission cross section would amount to 1% in this case.

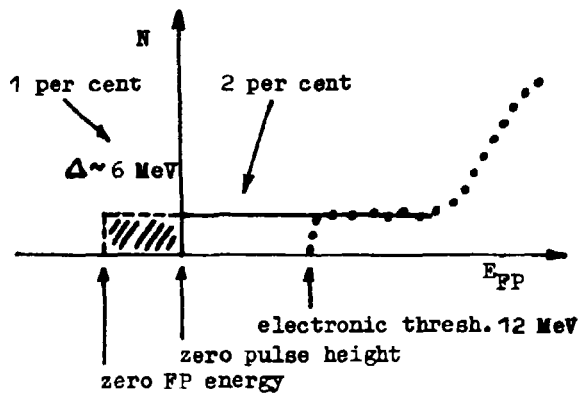


The following obstacles exists in reaching a precise determination of the "absorbtion losses":

- some of the parameters which have to be put into the commonly used formulas for the calculation of these losses are not known with sufficient accuracy
- the influence of the surface roughness of the backing of the deposit on the FP losses is difficult to predict
- scattering processes of the FP contribute to the "absorbtion correction" but are often neglected.

Methodical experiments are under way to determine experimentally the inefficiency of the FC used in our fission cross section measurements and in order to test procedures used for the theoretical estimation of the FC ineffiency [3].

References

1. G. W. Carlson et al., Preprint UCRL-51727, Livermore, 1974
2. H. W. Schmitt and R.B. Leachman, Physical Review 102 (1956) 183
3. see for example C. Herbach, Forschungspeleg TU Dresden, 1981; C. Herbach, Diplomarbeit TU Dresden, Sektion Physik, 1982; R. Arlt et al. ZfK-459, p.48, Rossendorf, 1981

# ELECTRONIC EQUIPMENT FOR FISSION CROSS SECTION MEASUREMENTS AT THE TECHNICAL UNIVERSITY OF DRESDEN

H.-G. Ortlepp
Technische Universität Dresden, Sektion Physik, Dresden, DDR

## 1. Introduction

A computer coupled CAMAC measurement system was developed to carry out absolute determination of fission cross sections using the time correlated associated particle method (TCAPM). Technical details of the 14.7 MeV neutron energy experiments are described in [1]. For the later measurements at other incident neutron energies the same data acquistion system has been used. The present paper is dealing with some electronic features of the recently developed associated particle counting systems of the 2.6 MeV and 8.4 MeV experiments using semiconductor detectors instead of scintillation counters and with the fission chamber pulse processing.

## 2. Fast pulse hight spectrometry with semiconductor detectors

A new pulse shaping system was developed consisting of a delay line shaper which rectangular output signals of the length T are integrated and checked for pile up in a gated integrator [2]. The pulse processing time and the double pulse resolution time have been reduced (table 1), allowing the delayed timing signal to be gated with the energy window information.

Table 1: Comparison of the fast spectroscopy system with the spectroscopy amplifier using semigaussian shaping at the same serial noise response and at minimal processing time (noise level about twice higher)

| | spectroscopy amplifier $\tau_d = \tau_i = 0.25\ \mu s$ | delay line shap + gated integr. $T = 0.5\ \mu s$ | delay line shaper + gated integr. at minimal T |
|---|---|---|---|
| time to peak | 0.7 µs | 0.5 µs | 0.07 µs |
| double pulse resolution for accepted events | 2.5 µs | 1.5 µs | 0.6 µs |
| same for unaccepted events | 2.5 µs | 0.6 µs | 0.1 µs |
| resolution time of the pile up detection | | 30 ns | 10 ns |

The resulting associated particle signal is fed to the fast coincidence avoiding slow coincidences. The random coincidence correction becomes simple, leading to a low uncertainty in the precise fission cross section measurements. Spectrum distortions due to undetected pile up can be neglected up to some times $10^5$ pulses per second. A special feature of this time variant system is the possible selection of the events before the processing in the gated integrator which is fired from valid events only. In the $\Delta E - E$ telescope of the 8.4 MeV experiment [3] the main counting rate is coused by scattered beam deutrons. Such events are not accepted because the gated integrators in

both channels are started by the fast $\Delta E - E$ coincidence output signals and deutron pulses do not exceed the $\Delta E$ timing threshold.

## 3. The fission chamber channel

The parallel plate fission chamber with an electron collection time of 30 ns is connected with a fast current preamplifier ($t_r$ = 3 ns). It's 30 ns long output pulses are fed into a timing filter amplifier. No differentiation is applied. An integration time constant of 5 ... 10 ns gives optimal energy and time information, both derived from the amplified current signals. The energy information is obtained from the peak value of these short signals using a fast strecher [1], the time information by a constant fraction trigger. The use of the peak current as a measure of the energy loss of the fission fragment excludes the induction effect as the energy information becomes independent on the fragment flight direction without applying of a Frisch - grid.
A rough theoretical estimation of the preamplifier input noise contribution to the energy and time resolution of this electronical scheme predicts values in agreement with the experimetally obtained 2.4 MeV and 1 ns FWHM, respectively. Both values could be improved by a factor of about three applying the best present known electronical components and different shaping in separate energy and timing amplifiers.

## References

1. R. Arlt et al, Nucl. Instr. and Meth., 169 (1980) 381.

2. K. Andert, ZfK - 299, Rossendorf, DDR, 1975.

3. R. Arlt et al, Proc. Xth Intern. Symp. on Selected Topics of the Interaction of Fast Neutrons and Heavy Ions with Atomic Nuclei, Gaussig 1980, ZfK - 459 (1981) 35.

# OPTIMIZATION OF PARALLEL PLATE FISSION CHAMBERS FOR PRECISE FISSION CROSS SECTION MEASUREMENTS

R. Arlt, C. Herbach, H.-G. Ortlepp
Technische Universität Dresden, Sektion Physik, Dresden, DDR

The conditions of an absolute measurement of fast neutron fission cross section using the time correlated associated particle method demand a special choice of the fission chamber (FC) parameters to meet the following requirements [1]:

i) the FC has to possess nanosecond time resolution to get a fast coincidence with the associated particle (AP) detector
ii) the inefficiency of the FC has to be known with a high accuracy
iii) multiplate FC-s have to be used in order to cope with the low counting rate of fission events
iv) a small distance between the plates is necessary for several reasons:
   - to minimize the area of the fission foils located outside the neutron cone and thereby to gain a reduction of the random coincidences between fission products (FP) and AP-s guaranteeing at the same time that all deposites are fully placed in the neutron cone
   - to obtaine short current pulses in order to reduce $\alpha$-pile up if high $\alpha$-active targets are measured
v) the FC has to guarantee a correct spectrometry of the low energetic FP in order to permit a precise estimation of the FP losses due to the electronic threshold
vi) neutron scattering corrections have to be minimized leading to a chamber design with thin walls and therefore the pressure of the filling gas is limited

One of the main points of the optimisation of the FC working parameters especially for the measurement with high $\alpha$-active targets is the achievement of a good separation between the $\alpha$-pulses and the low energy edge of the FP distribution.

The shape of the FC spectrum is strongly influenced by the FC geometry. Because of the smaller range of FP in the chamber gas compared to the $\alpha$-particles, FC-s working as a $\Delta E$-detector are often used in fission cross section measurements. In a parallel FC without collimator $\alpha$-pulses with high amplitudes are caused by pile up of pulses from $\alpha$-particles wich have lost a great part of the energy when they pass the chamber gas nearly parallel to the surface of the target. FP form the smallest pulses when they have been emited perpendiculare to the deposit (energy losses in the layer are negleceted). The region between these FP pulses and the pulses from $\alpha$-pile up in the pulse height distribution we call plateau (fig.1). It is filled by pulses from FP, which have lost the most of their energy before emerging from the target.

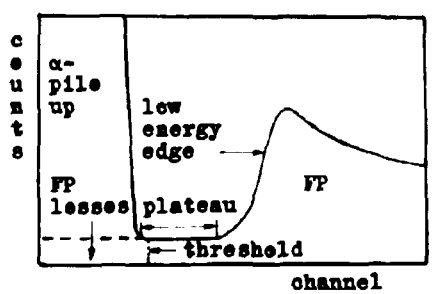


fig.1: schematic pulse hight distribution of a $\Delta E$-fission chamber

For our FC configuration the pulse hight distribution of α-pile up has been calculated in dependence on the target activity, the distance between the plates and the energy resolution of the spectrometer [2]. All possible trajectories in the chamber volume and the energy losses in the layer have been considered. For the calculation of α-pile up formation corresponding the Poisson-statistics [3] rectangular current pulses have been assumed.
As the other interesting part of the FC spectrum the energy level of the low energy edge from the FP's has been calculated. From a measured FP spectrum of 239-Pu employing the electronics discribed in [1] the end of the plateau (13.7 MeV) and the portion of FP pulses below this limit (3.4 %) for special FC parameters (filling gas: metham, pressure 108 kPa, distance of plates: 3 mm) have been estimated. These values completed with the calculated lowest possible level of electronic threshold to discriminate the α-pile up determine the absolute value and the accuracy of the correction due to FP losses below the threshold. A summary of the data obtained for several effective α-activities is given in the table 1:

| α-activity (2π-geom.) ($MB_q$) | gated fission rate ($10^{-3}s^{-1}$) | electronic threshold (MeV) | correction (%) | uncertainty of cross section (%) |
|---|---|---|---|---|
| 1.1 | 1.6 | 8.5 | 2.1 | 0.28 |
| 3 | 4.2 | 9.0 | 2.2 | 0.31 |
| 5 | 7 | 9.4 | 2.3 | 0.34 |
| 10 | 14 | 10.0 | 2.5 | 0.39 |

Table 1: Correction due to the α-discrimination for different α-activities from 239-Pu (pulse width = 30 ns, FWHM = 2.4 MeV, fission events=4500)

An extrapolation of the FP spectrum for other plate distances has been performed. The widest plateau region between α-pile up and the low energy edge of the FP has been observed for this FC configuration for a distance of the plates of about 8 mm (nearly the range of the heavy FP ). Compared with smaller distances of the plates there is a greater influence of the α-pile up, but the shift of the FP pulses to higher energies in the FC spectrum is dominant. In summary the correction becomes greater a little bit, but its certainty is better.
The use of this estimated optimum of the distances contradicts the demand of a compact FC construction. The results of the calculations indicate, that it will be possible to discriminate an α-activity of 5 $MB_q$ employing a FC with a distance of plates of 3 mm with a sufficient accuracy. Therefore for the projected cross section measurements on 239-Pu at $E_n$=8.4 MeV a five plate FC with this configuration will be used.
Further effort is made to proof experimentaly the calculations.

## Reference

1. Wagner, W. ,Dissertation TU Dresden, Sektion Physik 1982
2. Herbach, C. ,Diplomarbeit TU Dresden, Sektion Physik 1982
3. Rossi, B.B., Staub, H.H. ,Ionization Chambers and Counters, New York, Toronto, London 1949

# ОБМЕН ЭНЕРГИЕЙ МЕЖДУ ВНУТРЕННИМИ И КОЛЛЕКТИВНЫМИ СТЕПЕНЯМИ СВОБОДЫ ПРИ ДЕЛЕНИИ ЯДЕР $^{232}Th$ НЕЙТРОНАМИ.

Б.Д.Кузьминов, В.В.Малиновский, В.Ф.Митрофанов, В.М.Пиксайкин, Н.Н.Семенова, А.И.Сергачев.

Физико-энергетический институт, Обнинск, СССР

Аннотация

В работе представлены результаты измерения среднего числа мгновенных нейтронов $\bar{\nu}_p$ при делении ядер тория-232 нейтронами в диапазоне энергий I,3 - 6,3 МэВ. Полученные результаты анализируются совместно с опубликованными ранее данными по кинетической энергии осколков деления $\bar{E}_K$. Отмечается наличие двух механизмов перераспределения энергии, влияющих на энергетические зависимости $\bar{\nu}_p$ и $\bar{E}_K$.

Совместный анализ влияния энергии возбуждения делящегося ядра на среднее число мгновенных нейтронов - $\bar{\nu}_p$ и среднюю кинетическую энергию осколков деления - $\bar{E}_K$ представляет одну из возможностей исследования процесса обмена энергией между внутренними и коллективными степенями свободы при делении ядер. Кинетическая энергия осколков складывается в основном из кулоновской энергии отталкивания осколков в момент разрыва и предразрывной трансляционной энергии движения ядра к точке разрыва. Среднее число мгновенных нейтронов характеризует энергию возбуждения осколков, которая формируется из энергии возбуждения делящейся системы и энергии деформации формирующихся осколков в момент разрыва. Таким образом $\bar{E}_K$ является мерой энергий коллективных движений, а $\bar{\nu}_p$ - энергия внутренних движений.

В ранее выполненной работе [I], посвященной изучению деления ядер $^{232}Th$ нейтронами, наблюдались значительные изменения $\bar{E}_K$ при росте энергии возбуждения делящегося ядра. В настоящей работе выполнены тщательные исследования энергетической зависимости $\bar{\nu}_p$ при делении ядер $^{232}Th$ нейтронами в том же интервале энергий возбуждения. Результаты обеих работ представлены на рисунке. Для подтверждения достоверности наблюдавшихся в наших работах эффектов на том же рисунке приведены перенормированные результаты работ [2, 3].

Средняя кинетическая энергия осколков быстро увеличивается с ростом энергии нейтронов от I,2 МэВ до 2,5 МэВ. При дальнейшем увеличении энергии нейтронов, вызывающих деления ядер $^{232}Th$, скорость $\bar{E}_K$ замедляется. Замечательной особенностью кривой зависимости $\bar{E}_K$ от $E_n$ является наличие провала вблизи энергии $E_n$ = 2,I5 МэВ и превышение скоростью роста $\bar{E}_K$ единицы ( $dE_K / dE_n > I$) при $E_n < I,8$ МэВ. Последний факт означает, что кинетическая энергия осколков забирает на себя всю энергию возбуждения, вносимую нейтронами, и дополнительную добавку от энергии деления. Если принять, что в области энергий нейтронов $E_n < 2,5$ МэВ средняя энергия деления $\bar{E}_f$ остается постоянной, то при величинах $dE_K / dE_n > I$ следует ожидать уменьшения $\bar{\nu}_p$ с ростом $E_n$.

Результаты настоящей работы и работы [3] (см.рисунок) действительно свидетельствуют об уменьшении $\bar{\nu}_p$ при росте $E_n$ от I,2 до I,7 МэВ.

Принимая $\bar{E}_f$ = const, мы провели расчеты значений $\bar{\nu}_p$ с учетом изменений кинетической энергии осколков:

$$\bar{\nu}_p(E_n) = \bar{\nu}_p(E_n^o) + \alpha\left[(E_n - E_n^o) - (E_K - E_K^o)\right]$$

где выбрано $E_n^o$ = I,9 МэВ и принято $\alpha = -0,I$ МэВ$^{-I}$.

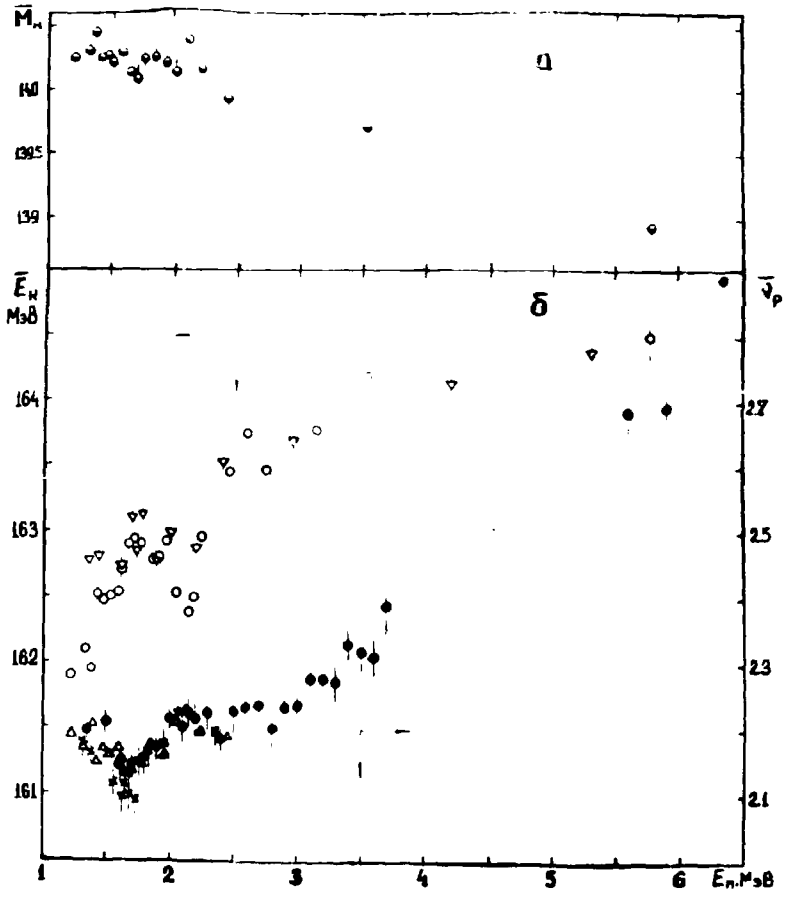


а) Энергетическая зависимость средней массы тяжелого осколка при делении ядер $^{232}Th$ нейтронами.

б) Зависимость средней кинетической энергии осколков (О - [1], ▽ - [2]) и среднего числа мгновенных нейтронов (● - настоящая работа, x - [3], Δ - результаты расчета) от энергии нейтронов, вызывающих деления ядер $^{232}Th$.

Обоснование такому значению $\alpha$ дано в работе [4]. Результаты расчета приведены на рисунке. Они вполне удовлетворительно совпадают с измеренными значениями $\bar{\nu}_p$. Таким образом в пределах ошибок эксперимента можно констатировать наличие однозначного соответствия изменений $\bar{E}_K$ и $\bar{\nu}_p$ в области энергий нейтронов $E_n < 2,5$ МэВ.

Предложено несколько модельных подходов для объяснения механизма перераспределе-

ния энергии между коллективными и внутренними степенями свободы при делении ядер [I]. Основываясь на рассмотренных в данной работе результатах можно сузить круг допустимых концепций. Отпадают разные варианты модельных представлений, согласно которым за меру обмениваемой энергии принята энергия переходных состояний. Перераспределение энергии происходит на более поздних стадиях, чем седловая точка. Другое заключение состоит в том, что в областях энергий нейтронов справа и слева от $E_n \approx 2{,}5$ МэВ механизмы перераспределения энергии различны.

Отметим, что для значений массы тяжелого осколка $132 < M_H < 155$, охватывающем подавляющую долю способов деления, с уменьшением $M_H$ происходит приблизительно линейное увеличение $\overline{E}_K$ ( $dE_K / dM_H = -1{,}1$ МэВ). В верхней части рисунка показана зависимость среднего массового числа тяжелого осколка $M_H$ от энергии нейтронов $E_n$ .

При изменении $E_n$ от 2,5 МэВ до 5,8 МэВ происходит уменьшение $M_H$ на I аем, что должно соответствовать увеличению $\overline{E}_K$ примерно на I МэВ. Т.е. в этой области энергий нейтронов практически весь рост $\overline{E}_K$ обязан изменению распределения осколков по массам. Поскольку эти изменения влекут за собой также изменеия и средней энергии деления $\overline{E}_f$ , то количественное сопоставление энергетических зависимостей $\overline{\nu}_p$ и $\overline{E}_K$ становится более сложным и не входит в рамки настоящей работы.

Итак, по мере изменения энергии возбуждения происходит перераспределение полной энергии между коллективными и внутренними степенями свободы, причем механизм перераспределения не является единым в изученном интервале энергий нейтронов, вызывающих деления ядер $^{232}Th$ .

Литература


I. Н.П.Дьяченко, Б.Д.Кузьминов, В.Ф.Митрофанов, А.И.Сергачев. "Ядерные константы" вып.I(40), стр.53, I98I г.

2. J.Trochon, H.Abou Yehia, F.Brisard, Y.Pranal, Nucl. Phys., 1979,A318, 63.

3. J.Trochon, H.Abou Yehia, J.Boldeman, J.Frehaut, G.Simon, "Dynamical effects in the neutron induced fission of $^{232}Th$", 10 th European Conference on Physics and Chemistry of Complex Nuclear Reactions, Lillehammer 1981.

4. Б.Д.Кузьминов, А.И.Сергачев. "Исследование факторов, влияющих на энергетическую зависимость среднего числа мгновенных нейтронов деления". Препринт ФЭИ-579, Обнинск, I974 г.

# THE ANGULAR ANISOTROPY OF FISSION FRAGMENTS WITH DIFFERENT YIELDS

B.M.Goehberg,L.D .Kozlov,S.K. Lisin,L.N.Morozov,N.A.Morozov,V. A .Pchelin,L.V.Chistyakov,V.A.Shigin,V.M .Shubko
I.V.Kurchatov Atomic Energy Institute,Moscow,USSR

The fragment angular anisotropy is a consequence of fission through a limited number of quantum states.The limitation of number of states involved in fission is possible at the stage of low nuclear excitation.Therefore these states are commonly associated with the states of the second barrier or second well,the energy being tied mainly by nuclear vibration.

The fragment mass distribution is usually proposed to be formed at the later stage of fission near the scission point.Therefore the fragments with different masses and different yields pass through the same set of states at the second barrier and hence have the same angular anisotropy.(Here and below in similar cases the term "fragment" is used to denote the fragment pair with a given fragment.)The another picture arises if the fragments are formed before the second barrier.In this case the different fragments can have the different barriers.This results in their different yields and different sets of barrier states and hence in different angular anisotropies of the fragments with different yields.

Experimentally this point is not clear enough.In present work we measured the angular anisotropy of the fragments with highly different yields. The new method was used with high efficiency and high mass resolution.It was achieved by using a lot of collimators with small cells for angular separation of fragments and a radiochemical method for their mass separation.The monoenergetic neutrons used in measurements were produced at an electrostatic accelerator.

The experimental assembly consisted of a large number of uranium or thorium foils alternating with polystyrene foils.The foils were separated one from another by collimators.The neutron irradiations were performed alternatively for two positions:with collimator axis directed along the neutron flux (the yield at $0^{\circ}$ ) and across it(the yield at $90^{\circ}$).The neutron flux was monitored by a counter. After irradiation the number of fragments for several masses in polystyrene foils was determined radiochemically.The ratio between fragments yields for both positions gave the experimental anisotropy A.Note the angular and energy resolution of the set was low for the sake of efficiency to overhead the fragment detector background.

The measurements were done for $^{236}U$, $^{238}U$ and $^{232}Th$ near the fission barriers at the neutron energy related to the region of relatively high anisotropy in each case.Unlike the published experiments present measurements were performed for fragments with very different yields(up to 700 times difference with symmetrical fission included).From 11 to 16 irradiations were performed for each nucleus.The statistical calculation of its permits to evaluate the experimental errors.

The results are shown in figure. The anisotropy A is shown versus the fragment yield Y related to the fragment yield $Y^p$ for the most probable mass ratio of fragments. The anisotropies of different fragments in the region of the most probable mode of fission were found the same for each nucleus and are denoted by the points $A^p$ in figure.

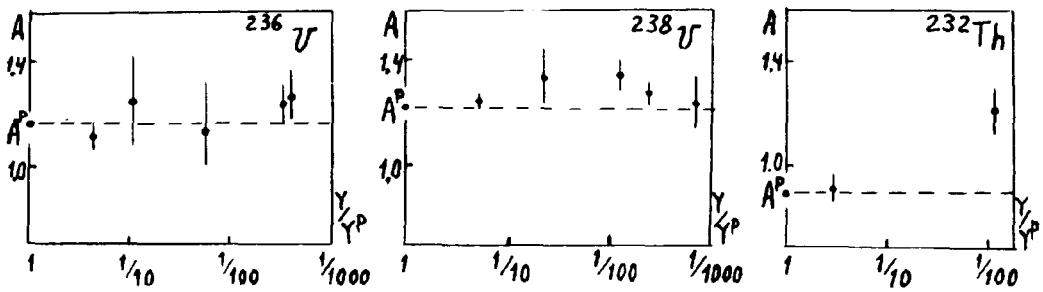


Figure. The angular anisotropy of fragments A as a function of their yields Y.

One can see, that for $^{236}U$ there are no deviations in anisotropy for fragment with different yields within the limit of errors. For $^{238}U$ there is a little systematic deviation in the anisotropy for some fragments as compared with $A^p$, reaching twofold error value at maximum. For $^{232}Th$ the deviation is relyable enough and exceeds the error value by three times $A/A^p = 1.33 \pm 0.10$. The change is of qualitative character and is accompanied by alteration of the predominent yield at $90^\circ$ ($A < 1$) by that one at $0^\circ$ ($A > 1$).

These results can be accounted for as follows. It is known that among the anisotropies for various excitation energies and various nuclei the anisotropy $A > 1$ occures more frequently. For $^{236}U$ and $^{238}U$ the anisotropy of fragments with the most probable yields $A^p$ is more than one and does not differ strongly from frequently meeted values. Therefore the deviation of anisotropy A for different fragments from $A^p$ will be expected to be small as a rule. On the other hand the low angular and energy resolution of our installation reduces the observed deviations and as a result the deviations can turn out to be within experimental errors. For $^{232}Th$ the anisotropy $A^p < 1$ and the deviations can be large enough to be observed.

Hence present results show the different fragments can have different angular anisotropy and, therefore, different second barriers. In this case the fragments are formed near the second barrier that is at more early stage of fission than it is usually proposed. For final solving of this problem it is nessecery to perform the measurements with another nuclei and especially in the region where the anisotropy $A^p$ is lower than one.

# ИССЛЕДОВАНИЕ ВЛИЯНИЯ НЕПОЛНОЙ РЕГИСТРАЦИИ АКТОВ ДЕЛЕНИЯ НА ИЗМЕРЕННУЮ ВЕЛИЧИНУ $\bar{\nu}_p$

В.В.Малиновский, В.Г.Воробьева, Б.Д.Кузьминов, В.М.Пиксайкин, Н.Н.Семенова
Физико-энергетический институт, Обнинск, СССР

Аннотация

Подробно изучена зависимость измеренного значения $\bar{\nu}_p$ как от толщины делящихся слоев, так и от амплитудной дискриминации импульсов камеры деления. С учетом проведенных исследований обсуждается расхождение полученных разными авторами данных по $\bar{\nu}_p$ при делении нептуния-237 нейтронами.

К настоящему времени опубликованы три работы [1-3] с результатами измерений среднего числа мгновенных нейтронов $\bar{\nu}_p$ при делении $^{237}Np$ моноэнергетическими нейтронами. Различие приведенных данных превышает указанные авторами погрешности, что свидетельствует о наличии систематических ошибок в измерениях. Значения $\bar{\nu}_p$ для $^{238}U$ [4] и [5,6], полученные теми же группами авторов в условиях, аналогичных работам [2] и [3] соответственно, согласуются в пределах погрешностей измерений. Наши работы [2] и [4] с методической точки зрения отличаются лишь величиной поправки в $\bar{\nu}_p$ ( 4,7% [2] и 0,2% [4] ), зависящей от эффективности регистрации осколков деления. В связи с этим нами подробно исследовано влияние неполной регистрации актов деления на измерения $\bar{\nu}_p$.

Число, энергетический спектр и угловое распределение нейтронов деления зависят от массы, кинетической энергии и энергии возбуждения осколков. Поэтому выборочная дискриминация актов деления может привести к искажению измеренной величины среднего числа мгновенных нейтронов деления $\bar{\nu}_p$. В подавляющем большинстве измерений $\bar{\nu}_p$ события деления регистрируются ионизационной камерой. При этом вероятность регистрации акта деления зависит от толщины делящегося слоя, в котором теряется часть осколков, и от уровня амплитудной дискриминации импульсов камеры.

Влияние толщины используемого слоя делящегося вещества на результаты измерения $\bar{\nu}_p$ изучалось в работах [7,8]. Однако, полученные результаты не обладают должным согласием по величине. Мы исследовали зависимость измеренной величины $\bar{\nu}_p$ как от толщины слоя делящегося вещества, так и от уровня дискриминации импульсов камеры деления.

Детектор нейтронов состоял из 16 счетчиков, наполненных $^3He$ и расположенных в полиэтиленовом замедлителе. Характеристики детектора, электронная схема регистрации нейтронов и метод обработки экспериментальных результатов описаны в [2]. События деления регистрировались плоско-параллельной ионизационной камерой, наполненной аргоном с 10%-ной добавкой углекислого газа до давления 1,4 атм. Зазор между электродами составлял 3 мм, диаметр делящегося слоя 30 мм. Импульсы с камеры деления поступали на зарядочувствительный предусилитель и далее на спектрометрический усилитель с постоянной времени формирования 0,5 мкс. Для исследования использовались слои из гомогенной смеси окиси-закиси естественного урана и калифорния-252 толщиной от 0,1 до 1,95 мг/см$^2$. Роль "бесконечно тонкого" выполнял слой $^{252}Cf$ , изготовленный методом самопереноса в электрическом поле.

Полное количество актов деления в слоях определялось по $\alpha$-активности и по интенсивности нейтронного излучения для каждого слоя. Нейтроны в последнем случае

регистрировались детектором без совпадений с осколками деления. Это позволило установить соответствие между уровнем дискриминации импульсов камеры деления и эффективностью регистрации актов деления для каждого слоя с точностью не хуже 2%.

Для этих слоев измерялась величина $\bar{\nu}_p$ при нескольких значениях уровня амплитудной дискриминации импульсов камеры деления. Метод измерений идентичен описанному в [2]. За "истинное" значение $\bar{\nu}_p^o$, соответствующее 100% эффективности регистрации делений, принималась величина, полученная в измерениях с "бесконечно тонким" слоем $^{252}Cf$ .

Полученные результаты позволили разделить изменение значения $\bar{\nu}_p/\bar{\nu}_p^o$ за счет потери актов деления при полном торможении осколков в слое и за счет амплитудной дискриминации импульсов камеры деления. Значения $\bar{\nu}_p/\bar{\nu}_p^o$, соответствующие нулевому уровню дискриминации, получались линейной аппроксимацией ближайших к $\varepsilon$ = 100% точек.

На рис.I приведена полученная зависимость $\delta = (1 - \bar{\nu}_p/\bar{\nu}_p^o)$ от толщины слоя. Указаны статистические ошибки измерений. Описание методом наименьших квадратов:

$$\delta = ((0{,}113 \pm 0{,}524) + (3{,}154 \pm 0{,}459)\Delta)\cdot 10^{-3},$$

где $\Delta$ - толщина слоя делящегося вещества в мг/см$^2$.

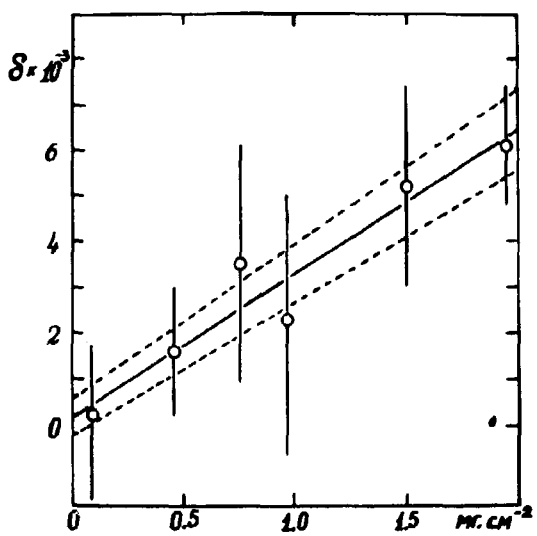


Рис.I. Зависимость $\delta = (1 - \bar{\nu}_p/\bar{\nu}_p^o)$ от толщины слоя делящегося вещества.

На основе результатов для $^{252}Cf$ , гомогенизированного в слое $^{238}U_3O_8$ , и данных по кинетическим энергиям, массам и пробегам осколков [9,10] была рассчитана величина $\delta$ для случаев деления $^{235}U$ и $^{239}Pu$ тепловыми нейтронами. Результат приведен в таблице, где указаны статистическая погрешность и оценка точности пересчета от калифорния к урану и плутонию. Для сравнения приведены аналогичные результаты из работы [8]. Значения $\delta$ , полученные нами, превышают величины из работы [8], хотя различия не превышают погрешностей. Одна из причин этих различий - в использовании нейтронных детекторов, обладающих разной энергетической и угловой зависимостью эффективности. К сожалению, описание эксперимента в [8] недостаточно подробно. Измерения для разных толщин поглотителя осколков выполнены, по-видимому, при фиксированном уровне амплитудной дискриминации в канале регистрации осколков. Однако в этом случае по мере роста толщины слоя эффективность регистрации осколков уменьшается, что может оказаться причиной завышения поправки, полученной в [8] для больших толщин поглотителя.

Таблица

Уменьшение измеренной величины $\bar{\nu}_p$ за счет толщины слоя делящегося вещества

| Состав слоя делящегося вещества | Данная работа | | | Величина в % для толщины слоя I мг/см$^2$ [8] *) |
|---|---|---|---|---|
| | Величина в % для толщины слоя I мг/см$^2$ | Статистическая погрешность | Погрешность аппроксимации | |
| Гомогенная примесь $^{252}Cf$ в слое $U_3O_8$ | 0,315 | 0,046 | | |
| $^{235}U$ | 0,195 | 0,028 | 0,010 | 0,169 |
| $^{235}U_3O_8$ | 0,350 | 0,051 | 0,010 | 0,282 |
| $^{239}Pu$ | 0,186 | 0,027 | 0,012 | 0,165 |
| $^{239}PuO_2$ | 0,314 | 0,046 | 0,020 | 0,251 |

*) Точность результатов работы [8] оценивается авторами в 20 %.

Зависимость измеренного значения $\bar{\nu}_p$ от уровня дискриминации импульсов камеры деления существенно меняется при смене полярности напряжения на камере, состоящей из двух пластин. На рис.2 светлыми кружками указаны результаты измерений в случае, когда положительное напряжение приложено к чистому электроду, а темными - к электроду со слоем делящегося вещества толщиной 0,97 мг/см$^2$. Причиной различия является то, что при смене напряжения заметно изменяется связь амплитуды импульса с энергией и направлением вылета осколка деления в камере. На рис.2 $\varepsilon$ = 100% соответствует уровню нулевой дискриминации. Через экспериментальные точки проведены методом наименьших квадратов кривые второго порядка. На рис.2 указаны результаты измерения такой же зависимости авторами [II] для $^{242}Pu$ (толщина слоя около 0,9 мг/см$^2$) и $^{252}Cf$. Рассматриваемая зависимость определяется, конечно, конкретными условиями работы камеры деления и используемого детектора нейтронов, поэтому данные из [II] имеют для нас скорее характер примера. (Используемый в [II] детектор нейтронов, впрочем, по своим характеристикам близок к нашему - набор $BF_3$ счетчиков в водородосодержащем замедлителе). Авторы [II] использовали для введения поправок показанную на рисунке линейную аппроксимацию.

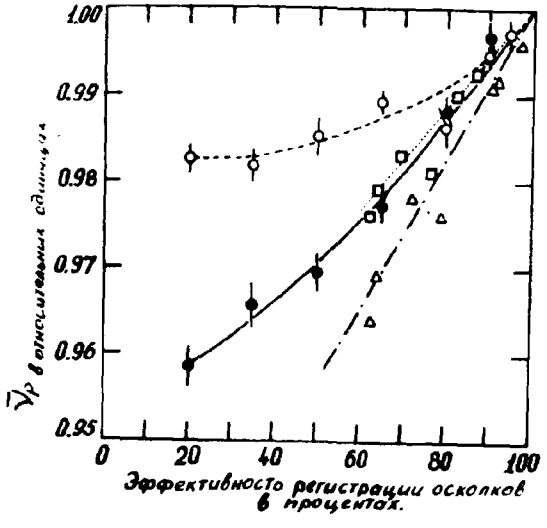


Рис. 2. Зависимость измеренной величины $\bar{\nu}_p$ от эффективности регистрации осколков камерой деления. ○ и ● - результаты нашей работы. □ и Δ - результаты из [II] соответственно для $^{242}Pu$ и $^{252}Cf$.

В наших измерениях $\bar{\nu}_p$ для $^{237}Np$ [2] использовались два варианта камер деления. В одном камера состояла из 6 секций с десятью двусторонними слоями делящегося вещества и суммарным количеством нептуния около 130 мг в каждой секции. В этих камерах даже с использованием импульсов тока удалось получить эффективность регистрации событий деления около 55%. В другом случае каждая из 6 секций камеры содержала один слой нептуния (7 мг). Эффективность регистрации осколков достигала при этом 80%. Экстраполяция к 100% эффективности осуществлялась по трем значениям $\bar{\nu}_p$, одно из которых было получено для первого варианта камеры деления (эффективность - 55%) и два - для второго ( эффективность - 60 и 80%).

Учет новых результатов (рис.2) привел к изменению поправки на дискриминацию с 4,7% [2] до 3,7%. Поправку на толщину слоя делящегося вещества следует изменить с 0,1% [2] до 0,3%. Таким образом результаты измерений $\bar{\nu}_p$ из работы [2] следует уменьшить на 0,8%.

Уточнение поправки на дискриминацию позволило обработать результаты измерений с малым количеством нептуния с эффективностью регистрации 80% при энергии нейтронов 1,66 и 2,79 МэВ.

В целях поиска оптимальной конструкции камеры деления (сочетание максимальной эффективности регистрации актов деления с максимальной загрузкой делящегося вещества) были выполнены измерения с использованием спиральной ионизационной камеры деления. Слой нептуния толщиной 1 мг/см$^2$ (общее количество 55 мг) наносился на алюминиевую фольгу шириной 5мм. Зазор между электродами 0,5 мм, внешний диаметр спирали 25 мм. Камера заполнялась смесью аргона и углекислого газа до давления 3 атм.

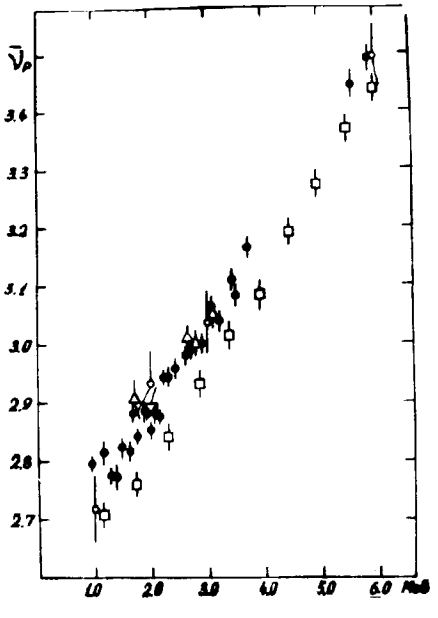


Рис.3. Результаты измерения $\bar{\nu}_p$ для $^{237}Np$ . ● - исправленные значения из работы [2], Δ - измерения с малым количеством $^{237}Np$ , ∇ - со спиральной камерой, ○ - [1], □ - [3] (ошибки - статистические)

Измерения проводились для двух значений (45% и 70%) эффективности регистрации осколков деления при энергии нейтронов 2,0 МэВ. Исправленные из работы [2] и обсуждавшиеся здесь новые результаты сравниваются на рис.3 со значениями, полученными в [1,3]. Систематическое расхождение между нашими результатами и работой [3] сохраняется, при том, что энергетический ход зависимости $\bar{\nu}_p$ практически одинаков. В работе [12] приводятся возможные объяснения расхождения данных [1-3], которые сводятся вкратце к следующему. Данные [1] завышены из-за некорректного учета фона, а данные [2] - из-за возможного завышения поправки на дискриминацию.

Действительно, в работе [1] измерения фона проводятся не в совпадении с событиями деления, что может приводить к недооценке фона, как справедливо указывается в [6]. Однако во-первых, при измерениях $\bar{\nu}_p$ в диапазоне энергии нейтронов от 1 до 14 МэВ отношение фона к эффекту существенно изменяется (уменьшается при высоких энергиях). Поэтому систематическая ошибка в определении фона едва ли даст практически параллельный сдвиг данных. Во-вторых, возможный результат "недоучета" фона зависит от конкретных

условий эксперимента. Пересчет данных по $\bar{\nu}_p$ для $^{235}U$, $^{238}U$ и $^{239}Pu$ [5] на исправленный фон с учетом результатов [6] привел к увеличению значений $\bar{\nu}_p$ до энергии нейтронов примерно 9-9,5 МэВ, оставив данные при более высоких энергиях практически неизменными. К тому же измерения $\bar{\nu}_p$ для $^{238}U$ в работе [I] при энергии нейтронов I4,7 МэВ согласуются с данными [5].

Замечания по поводу учета дискриминации в [2], по-видимому, достаточно подробно разобраны в настоящей работе. В свою очередь следует сказать, что использовавшаяся авторами [3,5] зависимость счета нейтронов деления от эффективности регистрации [I3] снята с полупроводниковым детектором и едва ли соответствует условиям измерений $\bar{\nu}_p$ с камерами деления с малым зазором, где зависимость амплитуды импульсов от энергии осколков имеет совсем другой характер. Это может привести в конечном счете к недооценке указанного эффекта авторами [3]. Однако недостаточно полное представление экспериментальных подробностей как работы [I] так и [3] затрудняет окончательное утверждение.

Литература


I. L.R.Veeser, Phys. Rev., 1978, C17,p. 385-387
2. В.Г.Воробьева, Б.Д.Кузьминов, В.В.Малиновский, Н.Н.Семенова, В.И.Володин, Вопросы атомной науки и техники, сер. Ядерные константы, 1980, вып.3(38), с. 44
3. J.Frehaut, R.Bois, A.Bertin, Note CEA-N-2196, 1981
4. В.Г.Воробьева, Б.Д.Кузьминов, В.В.Малиновский, В.М.Пикасайкин, Н.Н.Семенова, Вопросы атомной науки и техники, сер. Ядерные константы, 1981, вып.I(40), с. 62
5. M.Soleilhac, J.Frehaut, J.Gaurian, Jorn. Nucl. Energy, 1969, v.23, p. 257
6. Ж.Фрео, Доклад на 2-ой Всесоюзной конференции по нейтронной физике, Киев 1973 "Нейтронная физика", Обнинск, 1974, ч. 3, с. I65
7. H.Conde and M.Holmberg, Arkiv for fysik, 1965, 29, 33
8. J.W.Boldeman and J.Frehaut, Nuclear Science and Engineering, 1980, v.76, 49
9. L.C.Northcliff and R.F.Shilling, Nuclear Data Tables, 1970, A7, 233
10. J.P.Unik, J.E.Gindler et al. in Proc. of the 3d IAEA Symp. Phys. and Chem. of Fission, Rochester, New York, IAEA, 1973, v. 2, 19
11. G.Edwards, D.J.S.Findlay and E.W.Lees, Annals of Nuclear Energy, 1982, v.9, p. 127
12. J.Frehaut, "Some comments on $\bar{\nu}_p$ for $^{237}Np$",Contribution on 5th research coordination meeting for the coordinated research project on the intercomparison of evaluations of actinide neutron nuclear data, Antwerp, Belgium, September, 1982, N° P2N-683/82
13. E.Baron, J.Frehaut, F.Ouvry, M.Soleilhac, in Nuclear Data for Reactors, Conf. Proceedings, Paris 1966, IAEA, Vienna 1967, v.2, p. 57

# EVALUATION OF NEUTRON NUCLEAR REACTION DATA FOR FISSIONABLE NUCLEI USING NUCLEAR THEORY

M. Uhl
Institut für Radiumforschung und Kernphysik, Universität Wien, Austria

Abstract

Nuclear model calculations of neutron cross section data are reviewed with emphasis on elastic and inelastic scattering, fission and prompt fission neutron spectra. The role of the model parameters is discussed.

## 1. Introduction

The design and operation of fast breeder reactors requires the knowledge of many cross sections for neutron induced reactions for energies up to 15 MeV. In spite of the extensive experimental efforts during the past years the needed data base is far from being complete. Many important cross sections as e.g. those for elastic and inelastic scattering are known only at certain energies and others only in restricted energy regions. The cross sections needed for the assessment of the build-up and the burn-out of actinide nuclei involve instable nuclei and hence no experimental data exist at all. In all those cases nuclear model calculations can be used to bridge gaps and to extrapolate available data to higher energies or neighbouring nuclei and thus prove to be a valuable tool in nuclear data evaluation.

In this short survey only average cross section will be considered. The main nuclear reaction models for average cross sections are the generalized optical model for elastic and direct inelastic scattering, the compound nucleus model suitably extended to account for fission and at higher incident energies models for preequilibrium decay. The emphasis will be on the former two as their application to actinide nuclei raises special problems related to large permanent deformations and to the fission process.

A characteristic feature of calculations involving these models is that they rely on additional information in terms of model parameters which for the time being cannot be derived from pure nuclear theory with sufficient accuracy; examples are optical potential parameters, level density parameters and fission barrier characteristics. Therefore model calculations cannot replace experiment as these model parameters have to be adjusted carefully to reproduce experimental data. The predictive power of model calculations critically depends on the quality of the experimental data base for the choice of the parameters.

After a short recapitulation of the relations between the models for average cross sections, recent developments in their application to elastic and inelastic scattering, to fission and other reactions and finally to the calculation of prompt fission neutron spectra will be presented.

## 2. Average cross sections and nuclear reaction models

Due to the many degrees of freedom involved in a nuclear reaction the energy dependence of cross sections is very complicated and best described in terms of statistics. For applications in the region of overlapping resonances one is mainly concerned with averages of cross sections $\sigma(E)$ with respect to energy E

$$\langle\sigma\rangle = \frac{1}{\Delta E}\int dE\ \sigma(E)\ .$$

In nuclear reaction theory cross sections are expressed in terms of the scattering matrix $S_{ab}$. Except for trivial factors the integrated cross section from channel a to channel b is given by

$$\sigma_{ab}(E) = |\delta_{ab}-S_{ab}(E)|^2 \qquad (2.1.)$$

For particles and photons the channel symbols a,b,... have the usual meaning as defined by Lane and Thomas [1]; fission channels will be discussed further in section 4. Time reversal invariance and flux conservation require $S_{ab}$ to be symmetric and unitary. In the statistical theory of reactions the S-matrix is decomposed into its average $\langle S_{ab}\rangle$ and a fluctuating part $S^{fl}_{ab}$:

$$S_{ab}(E) = \langle S_{ab}\rangle + S^{fl}_{ab}(E) \qquad (2.2.)$$

The average $\langle S_{ab}\rangle$ is related to direct reactions (DI) and can be calculated by models involving relatively few degrees of freedom: the single channel (or spherical) optical model in case that $\langle S_{ab}\rangle$ is diagonal or the multi-channel optical model otherwise. The fluctuating part $S^{fl}_{ab}(E)$ reflects the excitation of many degrees of freedom and thus describes - at least at moderate energies - compound nucleus (CN) reactions. The resulting average cross sections

$$\langle\sigma_{ab}\rangle = |\delta_{ab} - \langle S_{ab}\rangle|^2 + \langle|S^{fl}_{ab}|^2\rangle = \sigma^{DI}_{ab} + \langle\sigma^{fl}_{ab}\rangle \qquad (2.3.)$$

consist of two contributions: the DI-cross section and the average of the fluctuating cross section $\langle\sigma^{fl}_{ab}\rangle = \langle|S^{fl}_{ab}|^2\rangle$ which at moderate energies represents the CN-contribution.

The statistical theory of nuclear reactions which is reviewed in refs. [2-5] aims at expressing the average of the fluctuating cross section in terms of the average scattering matrix, i.e. at relating the CN-cross sections to the optical model (Hauser-Feshbach problem). The crucial quantity in doing so is Satchler's [6] penetration matrix

$$P_{ab} = \delta_{ab} - \sum_c \langle S_{ac}\rangle\langle S_{bc}\rangle^* \qquad (2.4.)$$

which represents the unitary deficit of $\langle S\rangle$ and thus a generalization of the (single channel) optical model transmission coefficients $T_c$. In fact, for diagonal $\langle S\rangle$ we have $P_{ab} = \delta_{ab}T_a = \delta_{ab}(1 - |\langle S_{aa}\rangle|^2)$.

In presence of direct reactions (i.e. $\langle S\rangle$ is not diagnonal) the calculation of $\langle\sigma^{fl}_{ab}\rangle$ proceeds in two steps. At first the Hermitean matrix $P_{ab}$ is diagonalized by means of the unitary Engelbrecht-Weidenmüller transformation U[7]

$$(UPU^+)_{ab} = \delta_{ab}T'_a\ . \qquad (2.5.)$$

The matrix U and its transpose $U^T$ can then be used to construct a transformed S-matrix S'

$$S'_{ab} = (USU^T)_{ab} \qquad (2.6.)$$

with diagonal average. Further it can be shown that $S'^{fl}_{ab}$ has the same statistical properties as the S-matrix in absence of direct reactions [8,9]. Therefore in the second step the average of the fluctuating cross section is expressed in terms of U and S'

$$\langle\sigma^{fl}_{ab}\rangle = \sum_{efgh} U^*_{ea}U^*_{fb}U_{ga}U_{hb}\ \langle S'^{fl}_{ef}\ S'^{fl*}_{gh}\rangle \qquad (2.7.)$$

and the averages of the bilinear terms in $S'^{fl}$ are calculated as functions of

the eigenvalues $T_c'$ of the penetration matrix by technics developed for the case without direct reactions; see refs. [8,9] for the justification of the procedure and more details.

Several formulae have been proposed which, in absence of direct reactions ($\langle S_{ab}\rangle = \delta_{ab} \langle S_{aa}\rangle$), express $\langle\sigma_{ab}^{fl}\rangle$ in terms of the optical model transmission coefficients $T_c = 1 - |\langle S_{cc}\rangle|^2$. As an example the results of Moldauer's "M-cancellation priciple" [10,11] are presented:

$$\langle\sigma_{ab}^{fl}\rangle = W_{ab} \frac{T_a T_b}{\Sigma T_c}$$

$$W_{ab} = (1 + \frac{2}{\nu_a} \delta_{ab}) \int_0^\infty dt \prod_c (1 + \frac{2t}{\nu_c} \frac{T_c}{\Sigma T_{c'}})^{-(\frac{1}{2}\nu_c + \delta_{ac} + \delta_{bc})} \qquad (2.8.)$$

$$\nu_c = 1.78 + (T_c^{1.212} - 0.78) \exp [-0.228\ \Sigma T_c]$$

For isolated resonances ($T_c \ll 1$) eq. (2.8.) reduces to the Hauser-Feshbach formula [13] corrected by the factor $W_{ab}$ for fluctuations of the partial widths [14]. In the limit of many strongly absorbing channels eq. (2.8.) gives essentially the Hauser-Feshbach formula with a compound elastic enhancement by a factor of two:

$$\langle\sigma_{ab}^{fl}\rangle = (1 + \delta_{ab}) \frac{T_a T_b}{\Sigma T_c} = (1 + \delta_{ab})\sigma_{ab}^{HF} \qquad (2.9.)$$

Another method, the HRTW approach, was formulated in papers by Hofmann, Tepel, Richert and Weidenmüller [8,14] and recently improved by Hofmann et al. [15]. Numerical studies showed that both approaches essentially agree.

These generalizations of the Hauser-Feshbach formula are based on statistical properties of a S-matrix characterizing an equilibrated compound nucleus and hence $\langle\sigma_{ab}^{fl}\rangle = \langle\sigma_{ab}^{CN}\rangle$. They do, however, not account for preequilibrium decay and the range of application is restricted to energies below a few MeV. Recently several fundamental approaches were proposed which describe preequilibrium decay in the frame of fundamental reaction theory [16-20]. For applications, however, preequilibrium emission is mostly calculated by various phenomenological models as reviewed by Blann [21] and Seeliger [22]. So, for higher incident energies, $\langle\sigma_{ab}^{fl}\rangle$ is decomposed into a CN-contribution $\langle\sigma_{ab}^{CN}\rangle$ and a preequilibrium contribution $\langle\sigma_{ab}^{pre}\rangle$ :

$$\langle\sigma_{ab}^{fl}\rangle = \langle\sigma_{ab}^{CN}\rangle + \langle\sigma_{ab}^{pre}\rangle \qquad (2.10.)$$

## 3. Elastic and inelastic scattering to low lying collective levels

These processes are described in the frame of the optical and the compound nucleus model. The analysis of the experimental data helps to find an appropriate neutron optical potential which is essential for the calculation of all cross sections of interest.

At first the direct reaction contributions are considered. Actinide nuclei are permanently deformed and hence pose particular problems. While for spherical nuclei elastic and inelastic scattering can to a good approximation readily be calculated in the frame of the spherical optical model and the DWBA-method, respectively, the strong coupling between the low lying rotational states of deformed nuclei requires coupled channels calculations [23] which are notorious for their excessive computer time requirements. Due to the small spacings even between the lowest levels of actinide nuclei neutron data which separate elastic and inelastic scattering exist only for incident energies up to about 4 MeV.

Most investigations employ a phenomenological, axially symmetric deformed optical

potential of the following type

$$U(\vec{r}) = -V_R f(r,a_R,R_R) + 4ia_D W_D \frac{d}{dr} f(r,a_D,R_D) + 2.V_S \vec{l}.\vec{\sigma} \frac{1}{r}\frac{d}{dr} f(r,a_S,a_D) \quad (3.1a.)$$

$$f(r,a,R) = \{1 + \exp[(r-R)/a]\}^{-1} \quad (3.1b.)$$

$$R = R(\theta') = r_o A^{1/3}(1 + \sum_\lambda \beta_\lambda Y_{\lambda o}(\theta')) \quad (3.1.c.)$$

where the standard notation is used. The angle $\theta'$ refers to the body fixed system and usually only even order deformations $\beta_\lambda$ are considered. For moderate incident energies ($E \lesssim 20$ MeV) only a surface absorptive term is required. The deformation of the spin orbit term is often neglected. As usual for local phenomenological potentials the depths $V_R$ and $W_D$ of the real and the imaginary components depend on the incident energy. Insertion of the deformed potential (3.1.) into the Schrödinger equation of the scattering problem leads for each eigenvalue of the total angular momentum and parity to a system of coupled differential equations for the radial wave functions in the different channels. Numerical solution of this system under appropriate boundary conditions gives the average S-matrix elements $\langle S_{ab}\rangle$ from which the DI-cross sections and the penetration matrix elements $P_{ab}$ are obtained.

The numerous parameters of the deformed optical potential are determined by comparison with suitable experimental data. Due to the ambiguities of such a procedure it is important to find "reasonable" parameters that change smoothly between neighbouring nuclei and are supported by microscopic theories of optical potentials [24]. Only such a coherent set of parameters can be used for extrapolations to nuclei with no experimental data. A very efficient method to find such a set is the "SPRT-method" developed by Delaroche et al. [25]. This method relies on average resonance data (s- and p-wave strength functions and scattering radii), total cross sections as well as on elastic and inelastic scattering. It was successfully applied in many optical model studies of the Bruyère-le-Châtel group which were reviewed by Lachkar [26], Haouat [27] and recently with particular emphasis of the application of the coupled channel method to actinide nuclei by Lagrange [28].

Examples of the strengths and geometrical parameters of optical potentials as defined in eq. (3.1.) are presented in table 1.

Table 1: Examples of optical potential parameters for actinide nuclei potential depths V and incident energy E in MeV, geometrical parameters $a, r_o$ in fm

| Nucleus Author | $V_R$ | $a_R$ | $r_{oR}$ | $W_D$ | $a_D$ | $r_{oD}$ | $V_S$ | $a_S$ | $r_{oS}$ |
|---|---|---|---|---|---|---|---|---|---|
| $^{232}$Th Fasoli et al.[29] Garg et al.[30] | 48.412-.963E+ + .036E$^2$ 1.5<E<20 | .65 | 1.25 | 3.0+.25E- -6.75E$^{-3}$ | .47 | 1.25 | 6.5 | .65 | 1.25 |
| $^{232}$Th Guenther [31] | 46.824-0.261E | .758 | 1.217 | 4.031+.215E | .485 | 1.212 | 8.0 | .758 | 1.217 |
| $^{238}$U Lagrange [32] | 47.5-0.3E | .62 | 1.24 | 2.7+0.4E E<10 6.7 E≥10 | .58 | 1.26 | 7.5 | .62 | 1.24 |
| $^{238}$U Konshin [33] | 45.87-0.3E | .626 | 1.256 | 2.95+0.4E | .555+ +.0045E | 1.26 | 7.5 | .62 | 1.2335 |
| $^{239}$Pu Konshin [33] | 46.10-0.3E | .626 | 1.256 | 3.0+0.4E | .555+ +.0045E | 1.26 | 7.5 | .62 | 1.2335 |

A global optical potential for the actinide nuclei was developed by Madland and Young [34]. It is based on a simultaneous fit to experimental data for $^{232}Th$, $^{233,235,238}U$ and $^{239}Pu$.

In addition to the depths and radii of the potential coupled channels calculations require the deformation parameters $\beta_\lambda$. Usually only $\beta_2$ and $\beta_4$ are considered as the determination of $\beta_6$ and $\beta_8$ is subject to large uncertainties. Provided that adequate experimental data are available accurate deformations can be determined from neutron-nucleus interaction. The multipole moments $Q_\lambda$ of the potential which correspond to these deformations

$$Q_\lambda = Z[\int d\vec{r}\ \mathrm{Re}U(\vec{r})\, r^\lambda Y_{\lambda o}]/[\int d\vec{r}\,\mathrm{Re}U(\vec{r})]$$

agree rather well with multipole moments of the mass distribution derived from Hartree-Fock-Bogoliubov calculations. This is illustrated for the quadrupole moments in fig. 1 which is taken from Lagrange's review [28]

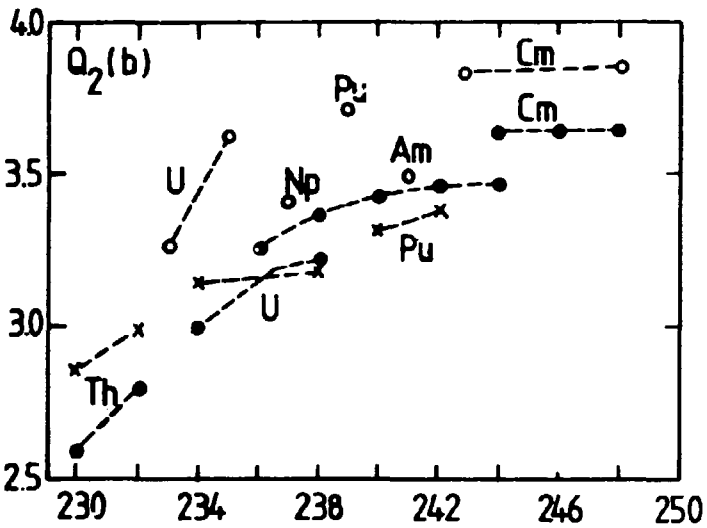


Fig. 1 taken from ref. [26], Quadrupole moments calculated by means of the Hartree-Fock-Bogoliubov method (full circles) and derived from deformed optical potentials for neutrons (crosses for even A and open circles for odd A).

Thus theoretical deformations can be used for extrapolation; in that case one should account for the empirical odd even effect exhibited by the experimental deformations.

The time requirements of coupled channels calculations drastically increase with the number of coupled states. As long as one is interested in the potential parameters and accurate total and elastic cross sections and in generalized transmission coefficients it is sufficient to use as coupling basis the three lowest members of the ground state rotational band [28].

The quality of phenomenological optical potentials critically depends on the experimental data they rely on. By inclusion of proton data the data base for neutron potentials can be extended decisively. Proton measurements are often easier to perform due to the overall better energy resolution of charged particle detection systems and the need for smaller samples. Compared to neutrons proton data extend to much higher energies.

A simultaneous treatment of neutron and proton scattering is provided for by the Lane potential formalism [35]. In Lane's charge independent formulation of the optical model the nuclear part of the nucleon-nucleus potential U consists of an isoscalar and an isovector portion $U_o$ and $U_1$ respectively

$$U = U_o + \frac{4}{A}(\vec{t}.\vec{T})U_1. \qquad (3.2.)$$

Here $\vec{t}$ and $\vec{T}$ are isospin operators for projectile and target. When averaged over the eigenstates of $\vec{T}_t = \vec{t} + \vec{T}$ eq. (3.2.) leads to $U_o \pm [(N-Z)/A]U_1$ where the upper sign holds for neutrons and the lower for protons; this dependence on the nuclear symmetry parameter is considered by many global potentials for nucleous. The isovector term in eq. (3.2.) gives rise to the quasi-elastic charge exchange reaction $(p,\tilde{n})$ which excites the analogue of the target ground state at an energy $\Delta_c$ (the Coulomb displacement) above the parent state. The coherent treatment of proton elastic and quasi-elastic scattering requires the solution of Lane's coupled equations. A nucleon optical potential is called Lane-model consistent if it simultaneously reproduces the respective neutron and proton data as well as $(p,\tilde{n})$ quasi-elastic scattering. This demand puts severe restriction on the parameters of an phenomenological potential.

The Lane-formalism can also be used to derive neutron optical potentials from proton scattering data. A simultaneous reproduction of (p,p)-, (p,p')- and $(p,\tilde{n})$ data at proton energy $E_p$ fixes the isoscalar and isovector component and thus, also the neutron potential at energy $E_p-\Delta_c$. Such investigations in the actinide region are being performed at the Lawrence Livermore Laboratory and were recently surveyed by Hansen [36]. Fig. 2 displays for $^{232}$Th and $^{238}$U the neutron elastic scattering cross section at 7 MeV inferred from a Lane-model analysis of (p,p) and $(p,\tilde{n})$ data at 27 MeV ($\Delta_c \sim 20$ MeV). The experimental data are reproduced as well as with the global neutron potential by Madland and Young [34] which is optimized for this mass and energy region. Thus, the applicability of the Lane-formalism is confirmed even for very heavy nuclei. Hansen [35] points out that in order to achieve such an agreement very extensive coupled channels calculations are required. The coupling base for the analysis of (p,p), (p,p') and $(p,\tilde{n})$ includes the three lowest rotational levels on the ground state and on its analogue; the coupling between the two bands is caused by the isovector potential. In fact, if the Lane coupled equations are solved by the DWBA method a much poorer reproduction of the neutron data results.

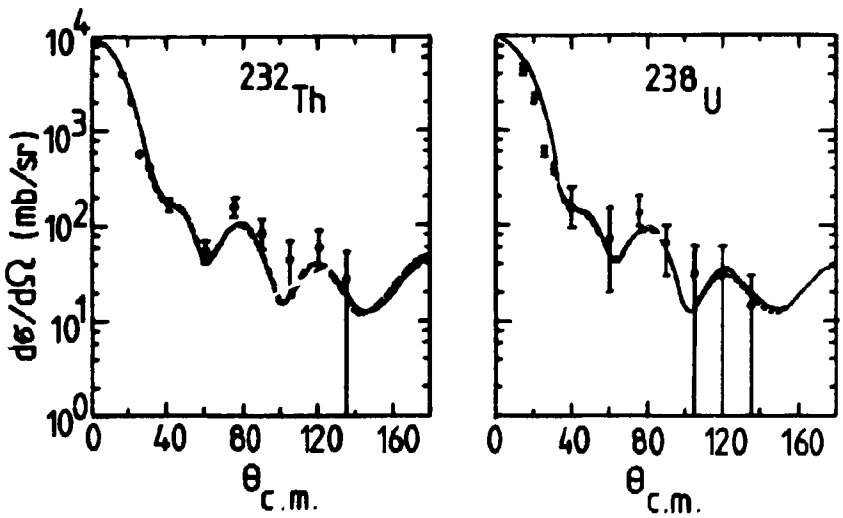


Fig. 2 (taken from ref. [36])
Neutron elastic scattering cross sections at 7 MeV. The full curve represents calculation with a deformed potential infered from (p,p), (p,p') and $(p,\tilde{n})$ data while the dashed curve is obtained with the global deformed neutron potential of Madland and Young [34]. The experimental data are from R.Batchelor and J.H.Towle, Nucl.Phys.65(1965)236.

A major problem with the application of the coupled channels method is its eccessive computer time requirement. In particular for odd A nuclei the numbers of coupled equations is in general much larger than for even nuclei. An essential reduction of the computing time for odd A nuclei can be achieved by a method proposed by Lagrange [28] and by Lagrange et al. [37]. This procedure is a generalization of the strong coupling model of Blair [38]. Instead of considering the ground state band of an odd A nucleus with spins I = K, K+1, K+2, ... where K is the projection of I on the symmetry axis, the calculations are performed for the K = 0 band with I = 0,2, ... $\lambda_{max}$ of an fictitious even nucleus. The cross section for a final state with angular momentum $I_f$ is approximately given by

$$\frac{\partial\sigma}{\partial\Omega}(I_f) = \sum_{\lambda = 0,2,\ldots\lambda_{max}} \langle I_o\lambda KO|I_f K\rangle^2 \frac{\partial\sigma}{\partial\Omega}(\lambda) \qquad (3.3.)$$

where $\frac{\partial\sigma}{\partial\Omega}(\lambda)$ is the cross section for the state with spin $\lambda$ of the fictitious nucleus. $I_o$ and K in the Clebsh-Gordon coefficient $\langle I_o\lambda KO|I_f K\rangle$ refer to the ground state of the real nucleus. Test calculations at 4 MeV neutron energy for $^{239}$Pu (K = 1/2) and $^{241}$Pu (K = 5/2) are shown in table 2. For K = 1/2 bands the approximation is excellent. For K > 1/2 the results are less precise as far as the inelastic cross sections are concerned but the agreement improves with increasing energy [28].

Table 2: (taken from ref. [39])
Comparison of $^{239}$Pu(K = 1/2) and $^{241}$Pu(K = 5/2) cross sections (in barn) using the "real" and the "fictitious" levels in coupled channels calculations

| | $^{239}$Pu | | $^{241}$Pu | |
|---|---|---|---|---|
| | real | fictitious | real | fictitious |
| $\sigma_{tot}$ | 7.797 | 7.796 | 7.821 | 7.831 |
| $\sigma_{abs}$ | 3.124 | 3.124 | 3.171 | 3.120 |
| $\sigma_{el}$ | 4.249 | 4.247 | 4.343 | 4.398 |
| $\sigma_1$ | 0.1233 | 0.1232 | 0.1533 | 0.1660 |
| $\sigma_2$ | 0.1845 | 0.1847 | 0.0864 | 0.0751 |
| $\sigma_3$ | 0.0522 | 0.0517 | 0.0418 | 0.0674 |
| $\sigma_4$ | 0.0646 | 0.0646 | 0.0268 | 0.0117 |

$\sigma_i$ refers to the inelastic cross sections of the first four excited states.

Raynal [40] developed a powerful procedure to solve the coupled equations by sequential iteration. This ECIS-method (équations couplées en iteration sequentielle) is incorporated into Raynal's ECIS code which recently became internationally available through the N.E.A. Nuclear Data Bank Program Library. Besides including several optious not available in many coupled channels codes (e.g. deformed spin orbit potential, axially asymmetric deformations, folding model) the program is very fast. So for $^{238}$U, 2.5 MeV incident energy and a ($0^+$, $2^+$, $4^+$, $6^+$) coupling base the running time on our CDC-CYBER 170/72 computer was ba a factor of about 7 shorter than that with Tamura's [23] widely used JUPITOR code; the memory requirement for ECIS (∿ 50 k words) is somewhat larger than that for JUPITOR (∿ 32 k words).

Besides direct reactions also compound nucleus processes contribute to the excitation of low lying collective levels. One may distinguish two ways to calculate the CN-cross sections.

The standard formalism neglects the correlations in $S_{ab}^{fl}$ caused by direct reaction components. The diagonal elements of the penetration matrix eq. (2.4.) are used as generalized transmission coefficients $T_a' = P_{aa} = 1 - \Sigma|\langle S_{ab}\rangle|^2$ in the generalized Hauser-Feshbach formulae (eq. (2.8.) or in those of the HRTW-approach). These transmission coefficients account for the flux going into DI channels. The impact of the Engelbrecht-Weidenmüller transformation is neglected. Arguments for such a procedure can be found in a paper by Moldauer [9] who showed by means of computer experiments that the effect of DI-processes on CN cross section is large only in case that two channels are strongly coupled by the direct mechanism and relatively small if the coupling comprises more channels. It is believed that the latter applies to actinide nuclei.

Recently an extensive investigation of elastic and inelastic neutron scattering on $^{232}$Th, $^{233,235,238}$U and $^{239,242}$Pu for energies between 0.6 and 3.4 MeV was reported by Haouat et al. [41]. The data comprise the excitation of the first 3 to 6 levels of the ground state rotational band. The CN-contributions proved to be important for incident energies below 1.5 MeV and were calculated by means of the standard-formalism. Very good agreement between theory and experiment was achieved; two examples are displayed in fig. 3.

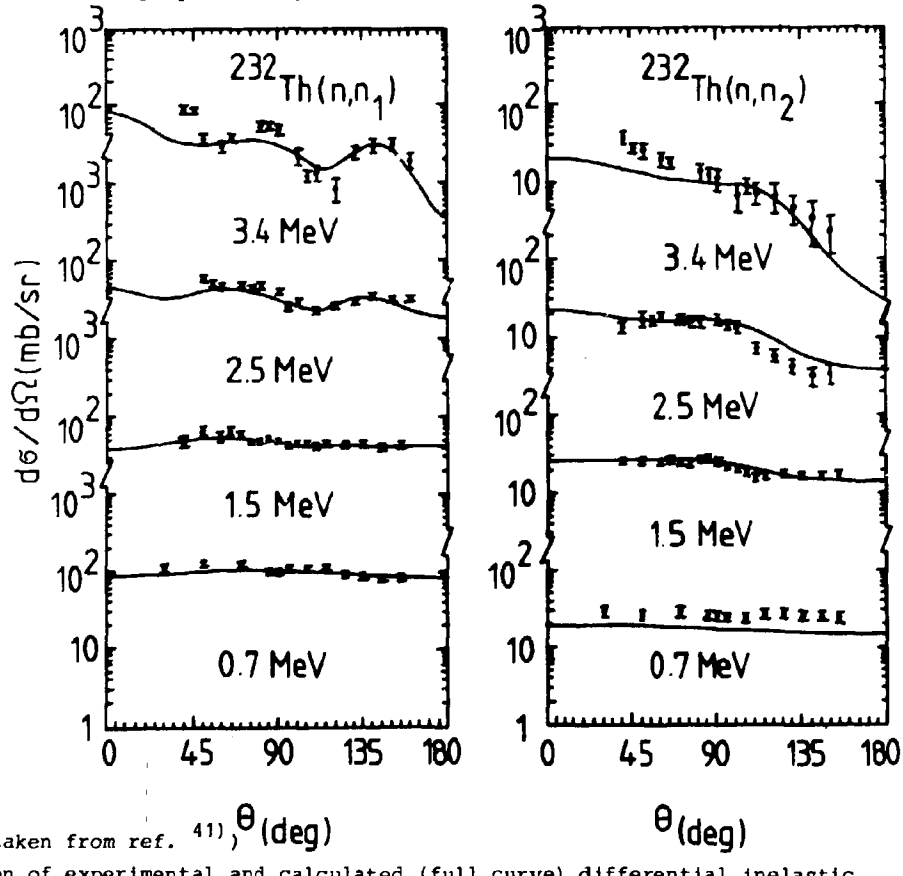


Fig. 3 (taken from ref. [41]).

Comparison of experimental and calculated (full curve) differential inelastic neutron scattering cross sections to the first two excited states of $^{232}$Th.

Recently an ambitious program concerning the interpretation of DI- and CN-reactions has been started at the University of Lowell by Chan, Sheldon and collaborators [42-44]. These authors aim at an "unified formalism" which is based on the application of the Engelbrecht-Weidenmüller transformation as described in section 2. Angle integrated cross sections for inelastic neutron scattering on $^{232}Th$, $^{238}U$ and $^{240,242}Pu$ were compared to experimental data for incident energies up to 2.5 MeV. The considered levels are members of rotational bands built upon the ground state and on the lowest quadrupole and octupole vibrational states. Deformed optical model parameters were taken from Lagrange et al. [89]. The calculations were performed with the program NANCY which by means of extended routines of Tamuras JUPITOR code [23] generates the average S-matrix $\langle S_{ab} \rangle$ and the corresponding DI-cross sections, constructs the matrix $U_{ab}$ of the Engelbrecht-Weidenmüller transformation and finally applies the most recent version of the HRTW-approach [15] to obtain the ensuing CN-cross sections. These calculations require a tremendous amount of CPU-time though the direct coupling was restricted to 3 or 4 states at one time.

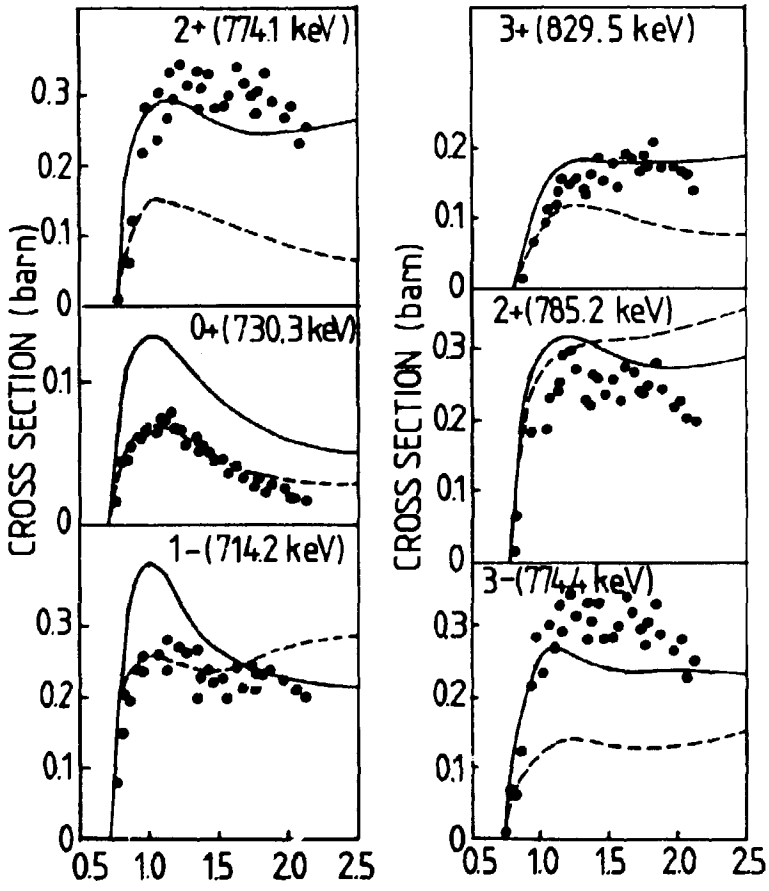


Fig. 4 (taken from ref. [43])

Comparison of theoretical and experimental excitation functions for $^{232}Th(n,n')$ to 6 excited states. Full curves represent calculations employing the "unified formalism" and dashed curves are the results of the "standard formalism". The data points have typical errors of 10%.

Typical results are shown in fig. 4 taken from ref. [43]. The full curve represents the results of the unified formalism and the dashed curve those of the "standard formalism". Among the cases studied in ref. [43] there are many in which the unified formalism gave better fits to the data than the standard one and vice versa. There are also several excitation functions which could not be fitted by any of the two approaches. The authors conclude: "regarded overall, the unified theory has a better record in fitting the experimental data than the standard theoretical approach ...". Nevertheless, the numerous cases where the unified approach yields poor fits are disturbing. Several further improvments of the code NANCY are planned; they refer to the extension of the coupling base and to the treatment of fission.

## 4. Cross sections for fission and other reactions

It is generally assumed that in the energy range of interest for reactor physics fission can be described in the frame of the CN-model. Therefore fission cross sections depend on the competing neutron and gamma decay and conversely all other cross sections are strongly influenced by fission competition.
The inclusion of fission into the Hauser-Feshbach theory requires the definition of transmission coefficients for fission channels. Though fission can formally be accounted for in exact reaction theories (see recent reviews of Bjørnholm and Lynn [45] and of Weigmann [46] which contain the references to the original papers) for actual calculations simple static concepts are used.
Following A. Bohr [47] fission channels are related to intrinsic states of the nucleus as it passes over a barrier of the deformation energy surface. Each such transition state, characterized by excitation energy $E_i$, spin $J_i$ parity $\Pi_i$ and eventually the projection $K_i$ of $J_i$ on the symmetry axis, defines a barrier of height $E_i$. For a single-humped fission barrier the transmission coefficient $T_{f_i}(E)$ for channel i and excitation energy E is given by the penetrability for the vibrational motion (i.e. the fission motion) through the associated barrier:

$$T_{f_i}(E) = \{1 + \exp[-\frac{2\pi}{\hbar\omega}(E-E_{f_i})]\}^{-1} = \{1 + \exp[-\frac{2\pi}{\hbar\omega}(E-U_i-E_f]\}^{-1} \quad . \qquad (4.1.)$$

Here the Hill-Wheeler formula [48] for the penetrability through a parabolic barrier with curvature $\hbar\omega$ is used; in the second step the excitation energy $U_i$ is referred to the barrier height $E_f$ i.e. the excitation energy of the lowest transition state. Usually at higher excitation energies $U > U_c$ the transition states are represented by a continuous level density $\rho(U,J,\Pi)$. For the total fission transmission coefficient $T_f^{J\Pi}(E)$ for compound nucleus states of excitation energy E, spin J and parity $\Pi$ one obtaines

$$T_f^{J\Pi}(E) = \sum_i{}' \{1 + \exp[-\frac{2\pi}{\hbar\omega}(E-E_f-U_i]\}^{-1} + \int_{U_c}^{\infty} dU\rho(U,J,\Pi) \{1 + \exp[-\frac{2\pi}{\hbar\omega}(E-E_f-U)]\}^{-1} \quad . \qquad (4.2.)$$

The sum in eq. (4.2.) is restricted to the transition states with appropriate angular momentum and parity.
By analogy with the situation at equilibrium deformation one assumes for the discrete portion of the transition state spectrum rotational bands built upon collective levels in case of even or upon single particle states in case of odd-A or odd nuclei [49]. The complexity of the rotational bands depends on the symmetry of the saddle point shape [50]. This fact is also very important for the level density

$\rho(U,J,\Pi)$ [51]. Only indirect experimental information on the transition states is available in form of the fission cross sections themselves and of the angular distributions of fission products which critically depend on the angular momentum quantum numbers $J_i$ and $K_i$ [52].

The fission transmission coefficients defined in equs. (4.1.) and (4.2.) can now be used in the generalized Hauser-Feshbach theory described in section 2 and all cross sections can be calculated without complications. Though it is well established that for actinide nuclei the fission barrier is at least double-humped, the results obtained for a single barrier are useful if the heights of the two barriers are different and the excitation energy is beyond the lower barrier. In fact, many successful calculations on this basis were reported e.g. by Jary et al. [53], by Arthur et al. [54] and by Konshin [33]; in particular the last paper contains very valuable systematic investigations on the influence of different formulations of the Hauser-Feshbach theory and different models for level densities and gamma-ray transmission coefficients.

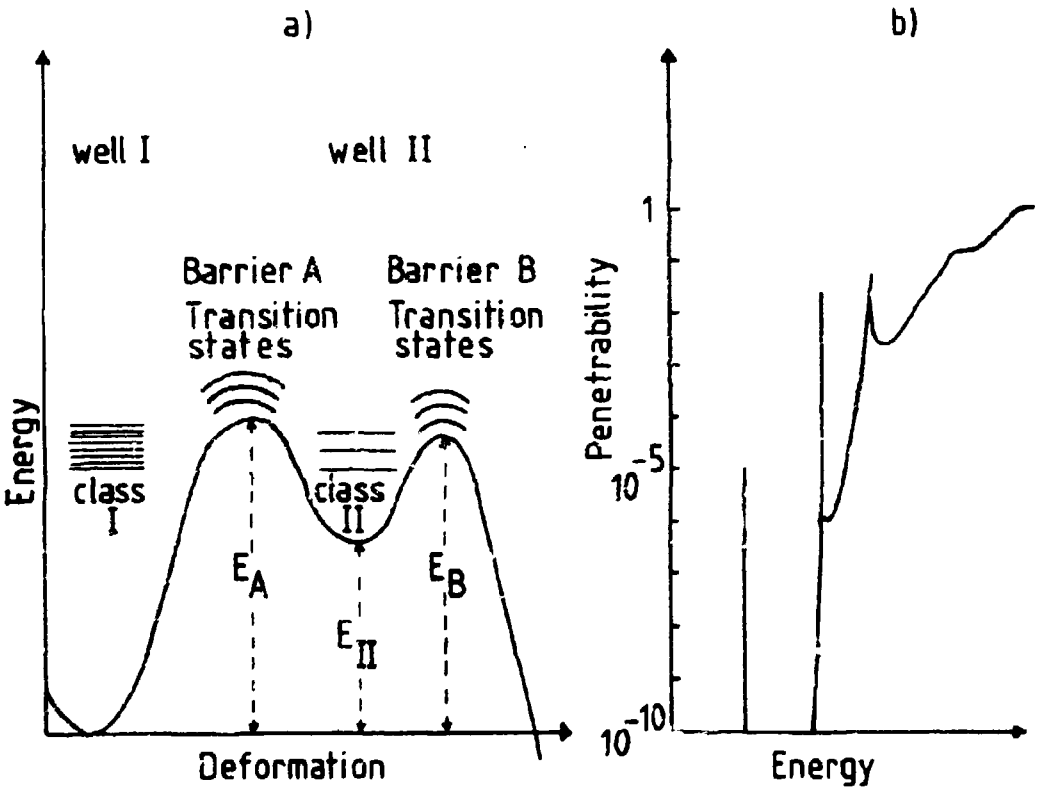


Fig. 5

a) Some of the concepts relevant for a double-humped fission barrier

b) Pentrability through a double-humped barrier (schematic)

However, many features of fission cross sections can be treated properly only under the assumption of a double-humped fission barrier. Fig. 5a illustrates some of the pertinent concepts and fig. 5b displays, in a qualitative way, the penetrability through such a barrier as a function of energy. In contrast to the smoothly rising behaviour characteristic for a single barrier (see eq. (4.1.)) sharp resonances

("vibrational resonances") appear at energies corresponding to quasi-bound states in the second well.

The double-humped barrier is responsible for various intermediate structure phenomena which are relevant for the calculations of average cross sections. They are briefly described in the following; for more details see the reviews of Weigmann [46], Bjørnholm et al. [45] and Michaudon [55,56].

For an excitation energy below the top of the inner barrier A one has to distinguish between class-I states and class-II states, according to the well which contains the major amplitude of the vibrational component of their wave function.

Class-I states: For excitation energies encountered in neutron induced reactions the class-I vibrational motion is fully damped into the complicated class-I compound states. Class-I compound states have "normal" neutron width and compared to class-II states negligible fission width.

Class-II states have a reduced effective excitation energy due to the difference in deformation energy between the two wells. Therefore their density at the same excitation energy is much less than that of class-I states. Various extents of the coupling between the vibrational motion and the intrinsic degrees of freedom are possible (see fig. 6): no damping, partial and full damping of the vibrational motion into the complicated class-II compound states which is determined by the depth of the second well and the even-odd character of Z and N. Class-II states have compared to class-I states negligible neutron width and large fission width.

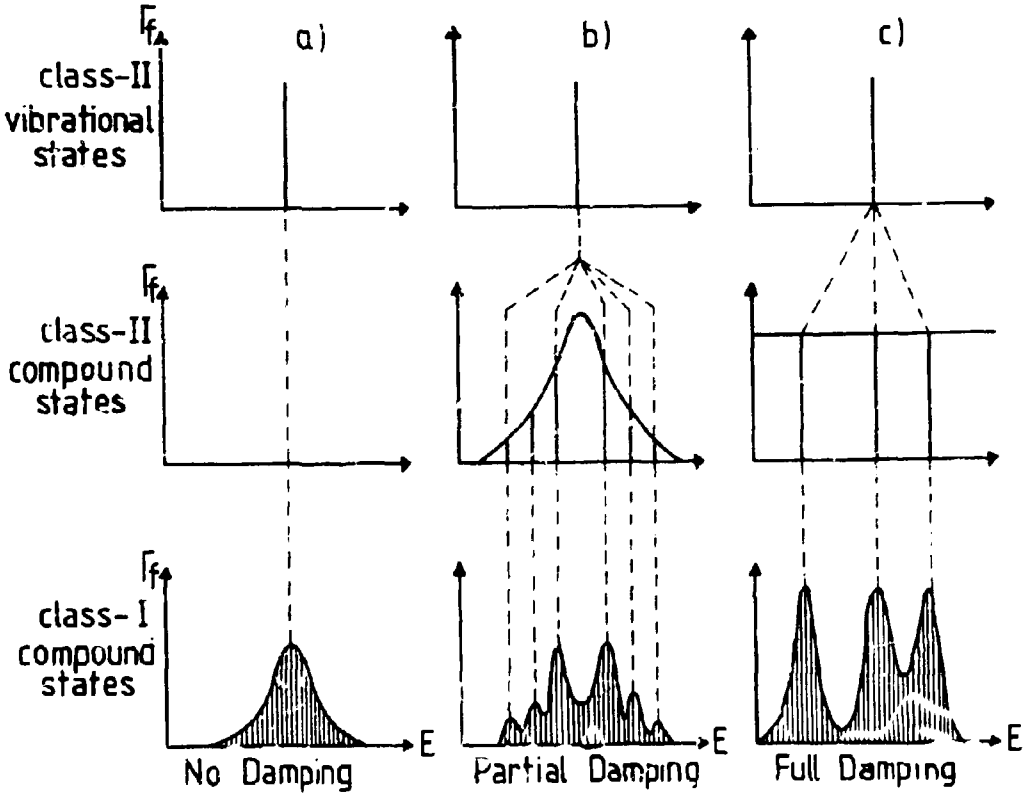


Fig. 6 (adapted from ref. [56])

Schematic illustration of the hierarchy of states relevant for intermediate structure for three different types of damping of the class-II vibrational motion into class-II compound states.

Residual interactions couple class-I and class-II states. The wave functions describing the fine-structure resonances are composed of class-I and class-II components. Due to their large fission width class-II states play the role of doorways for the fission channel. Class-I compound states with energies near that of a class-II state give rise to fine-structure resonances with enhanced fission width. The acutal intermediate structure effects depend on the coupling conditions. Most important with regard to average neutron cross sections is the "moderately weak coupling" situation which can be treated in picket fence approximation [45,46]. Near a class-II state the fission widths $\Gamma_{\lambda f}$ of the fine-structure resonances at energy E are on the average (with statistical fluctuation of Porter-Thomas type) distributed along a Lorentzian form

$$\Gamma_\lambda = \frac{D_I}{2\pi} \frac{\Gamma_{\lambda II}(f)\ \Gamma_{\lambda II}(c)}{(E_{\lambda II}-E_\lambda)^2 + \frac{1}{4}\Gamma_{\lambda II}^2}\ ,\ \Gamma_{\lambda II} = \Gamma_{\lambda II}(c) + \Gamma_{\lambda II}(f)\ . \qquad (4.3.)$$

Here $\Gamma_{\lambda II}(c)$ and $\Gamma_{\lambda II}(f)$ are, respectively, the coupling and the fission width of the class-II state at energy $E_{\lambda II}$ and $D_I$ is the average class-I state spacing. In case of complete damping (fig. 6c) of the class-II vibrational component into class-II compound states the average coupling and fission width are given by

$$\overline{\Gamma_{\lambda II}(c)} = \frac{D_{II}}{2\pi} T_A \text{ and } \overline{\Gamma_{\lambda II}(f)} = \frac{D_{II}}{2\pi} T_B\ , \qquad (4.4.)$$

where $T_A$ and $T_B$, respectively, are the total transmission coefficients for barrier A and B and $D_{II}$ is the average spacing. $T_A$ and $T_B$ are given in terms of the Hill-Wheeler penetrabilities and the transition states in the same way as the quantity $T_f$ in eq. (4.2.). This coupling situation is realized in the sub-barrier fission of some nuclei as e.g. $^{240}$Pu ref. [57] or $^{237}$Np ref. [58] where clusters of resonances with large fission width are separated by resonances with negligible fission width.

In the other extreme, i.e. no damping (fig. 6a), the pure vibrational state leads to an undamped vibrational resonance. In the vicinity of such a resonance eq. (4.3.) can be used. The coupling and fission width, however, are given by

$$\Gamma_{\lambda II}(c) = \Gamma_A = \frac{\hbar\omega_{II}}{2\pi} T_A \text{ and } \Gamma_{\lambda II}(f) = \Gamma_B = \frac{\hbar\omega_{II}}{2\pi} T_B \qquad (4.5.)$$

where $T_A$ and $T_B$ have the same meaning as in eq. (4.4.) and $\hbar\omega_{II}$ is the spacing of pure vibrational states which exceeds $D_{II}$ in eq. (4.4.) by about three orders of magnitudes.

Finally, for partial damping (fig. 6b), the coupling and the fission width $\Gamma_{\lambda II}(c)$ and $\Gamma_{\lambda II}(f)$ near a damped vibrational resonance at energy $E_v$ follow on the average (with statistical fluctuations of Porter-Thomas type) a Lorentzian form

$$\Gamma_{\lambda II}(c) = \frac{D_{II}}{2\pi} \frac{\Gamma_A\ \Gamma_D}{(E_{\lambda II}-E_v)^2 + \frac{1}{4}\Gamma_v^2}\ ,\ \Gamma_{\lambda II}(f) = \frac{D_{II}}{2\pi} \frac{\Gamma_B\ \Gamma_D}{(E_{\lambda II}-E_v)^2 + \frac{1}{4}\Gamma_v^2}\ ,$$
$$\Gamma_v = \Gamma_A + \Gamma_B + \Gamma_D. \qquad (4.6.)$$

In this equation $\Gamma_D$ is the damping width (mostly obtained from phenomenology) and the quantities $\Gamma_A$ and $\Gamma_B$ are defined in eq. (4.5.). Vibrational resonances are observed in direct reaction induced fission experiments [59] and in neutron induced fission [60]. For their analysis also the rotational bands built upon vibrational state (not shown in fig. 6) have to be considered.

In connection with the analysis of direct reaction induced fission experiments Back et al. [61] proposed a flexible model for the fission transmission coeffi-

cients which accounts to some extent for the intermediate structure effects described before. This model, or at least some of its special cases, is incorporated in many of the widely used nuclear reaction codes as e.g. COMNUC (LASL-version)[62], EVAPF [49], HAUSER [63], NRLY [64] and STAPRE [65]. In order to account for damping of the vibrational motion in the second well an absorptive imaginary part is added to the real deformation potential in the region of the second well. Solving the transmission problem for a complex barrier results in a transmitted and an absorbed flux, both of them exhibiting vibrational resonances. Accordingly one has two contributions to the total fission transmission coefficient. The direct contribution $T_f^D$ is given by the transmitted flux. The indirect contribution $T_f^I$ results from fission decay of the excited class-II compound states (with branching ratio $T_B/(T_A + T_B)$ and is therefore related to the total absorbed flux $\mathcal{A}$ and affected by intermediate structure due to class-II compound states (see figs. 6b and 6c). In an energy intervall around $E_o$ which contains many class-II states but, on the other hand, is small enough that all other energy dependent quantities ($\mathcal{A}$, $T_f^D$, $T_A$, $T_B$) are constant therein, the proposed expression for the total fission transmission coefficient $T_f(E)$ reads

$$T_f(E) = T_f^D + T_f^I(E), \quad T_f^I(E) = \mathcal{A}\frac{T_B}{T_A+T_B} f(D_{II},\bar{\Gamma}_{\lambda II}, E-E_o)$$
$$f(D_{II},\bar{\Gamma}_{\lambda II},E-E_o) = \frac{\sinh\left(\frac{\pi}{D_{II}}\bar{\Gamma}_{\lambda II}\right)}{\cosh\left(\frac{\pi}{D_{II}}\bar{\Gamma}_{\lambda II}\right) - \cos\left(\frac{2\pi}{D_{II}}(E-E_o)\right)}, \quad \bar{\Gamma}_{\lambda II} = \frac{D_{II}}{2\pi}(T_A+T_B). \tag{4.7.}$$

The normalized weight function $f(D_{II},\bar{\Gamma}_{\lambda II},E-E_o)$ describes the intermediate structure fluctuations around the average $\bar{T}_f = T_f^D + \mathcal{A}\, T_B/(T_A+T_B)$. The result in the second line of eq. (4.7.) was derived by Lynn et al. [66] in picket fence approximation by summing the Lorentzian forms for the fine-structure fission widths resulting from an infinite set of equidistant class-II compound states with equal width $\bar{\Gamma}_{\lambda II}$.

Eq. (4.7.) for the total fission transmission coefficient simplifies in the full damping limit (fig. 6c). The direct flux vanishes and the absorbed flux is given by $T_A$. At higher energies, when full damping is realized and the intermediate structure is smeared out, $T_f$ is given by the well-known simple expression

$$T_f = \frac{T_A\, T_B}{T_A+T_B} \tag{4.7.'}$$

If eq. (4.7.) is used in the formulae of the generalized Hauser-Feshbach theory the resulting fission cross section $\langle\sigma_{nf}(E-E_o)\rangle$ is averaged with respect to fine-structure but exhibits the energy dependence caused by the intermediate structure The average with respect to intermediate structure is obtained by integrating $\langle\sigma_{cf}\rangle$ over a period $D_{II}$ of the weight function $f(D_{II},\bar{\Gamma}_{\lambda II},E-E_o)$:

$$\overline{\sigma_{cf}}(E_o) = \frac{1}{D_{II}} \int_{E_o-D_{II}/2}^{E_o+D_{II}/2} dE \, \langle\sigma_{cf}(E-E_o)\rangle \tag{4.8.}$$

The effect of this procedure is to reduce the cross section compared to the result obtained by employing the average fission transmission coefficient $\bar{T}_f$. This is because the overall fission strength is concentrated in a small number of resonances whereas the bulk of the resonances has a very small fission width; the contribution of the resonances with very large fission width, however, is limited by their neutron width.

The use of the picket fence approximation for the class-II compound states dis-

regards the fluctuations of their widths and spacings. Weigmann [67]) showed by means of a Monte-Carlo simulation that the effect of these fluctuations is considerable for sub-barrier fission. His calculations assume the full damping limit and consider two sequences of compound states: class-II with fission- and coupling width sampled from Porter-Thomas distributions with mean-values $\bar{\Gamma}_{II(f)}=(D_{II}/2\pi)T_B$ and $\Gamma_{II(c)} = (D_{II}/2\pi)T_A$, respectively, and class-I with neutron width sampled from a Porter-Thomas distribution with average value $\langle\Gamma_n\rangle = (D_I/2\pi)T_n$ and a constant capture width $\Gamma_c = (D_I/2\pi)T_c$. Depending on the actual value of $\Gamma_{II(c)}$ compared to $D_I$ the coupling is treated either in perturbation - or in moderately weak coupling approximation. The ratio $W_{nf} = \overline{\sigma_{nf(sim.)}}/\sigma_{nf}^{HF}$ of the average fission cross section $\overline{\sigma_{nf(sim)}}$ resulting from this simulation to the simple Hauser-Feshbach cross section $\sigma_{nf}^{HF}$ given by eq. (2.9.) is shown in fig. 7 as function of the average fission probability $\overline{P_f}$ evaluated in picket fence approximation [66])

$$\overline{P_f} = (1/D_{II})\int_{E_o-D_{II}/2}^{E_o+D_{II}/2} dE \frac{T_f(E)}{T_f(E)+T_n+T_c} = \{1 + (\frac{T'}{\bar{T}_f})^2 + 2(\frac{T'}{\bar{T}_f})\coth \tfrac{1}{2}(T_A+T_B)\}^{-1/2} \tag{4.9.}$$

$$\bar{T}_f = T_A\, T_B/(T_A+T_B),\ T' = T_n + T_c\ .$$

It turns aut that for sub-barrier fission various combinations of $(T_A,T_B)$ corresponding to the same $\overline{P_f}$ yield similar results for $\overline{\sigma_{nf(sim.)}}$. The dashed curve in fig. 7 represents the width-fluctuation factor eq. (2.8.) for Porter-Thomas distributions for all fine-structure widths (all $\nu_c = 1$) and an effective fission transmission coefficient $T_{f,eff} = \overline{P_f}\ T'/(1-\overline{P_f})$ which approximately accounts for intermediate structure in picket fence approximation (see eq. (4.9.)).

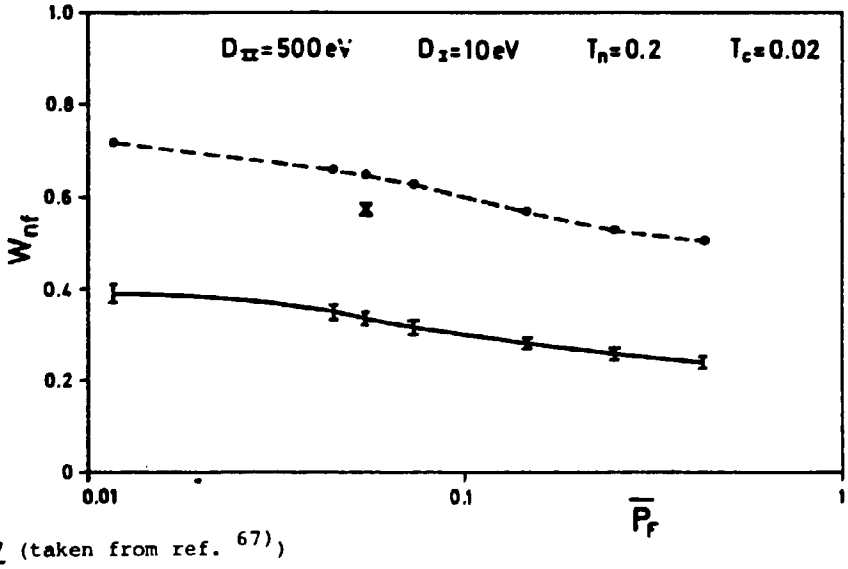


Fig. 7 (taken from ref. [67])

Reduction of the fission cross section due to statistical fluctuation of the class-I and class-II compound state parameters (see text). The symbols Δ and ∇ at $\overline{P_f}$ = 0.054 show, respectively, the isolated effect of class-I and class-II fluctuations.

Fig. 7 shows that the fluctuations of the class-II state parameters cannot be neglected. These results represent an upper limit for fluctuation effects as Porter-Thomas type fluctuations are expected to hold in case that only one barrier channel determines $T_A$ and $T_B$ i.e. for extreme sub-barrier fission. As soon as more

channels contribute the fluctuations are reduced.
Unfortunately such Monte-Carlo simulations are time consuming and not very convenient for routine calculations. To my knowledge, analytical results that account for fluctuations in fine- and intermediate structure are available only in some limiting cases which are discussed by Bjørnholm et al. [45] and by Lynn [49]. Some of these formulae are used in Lynn's code AVXS [49]. This is a sophisticated program specially designed for low energy fission that includes many features not available in the codes mentioned before as e.g. the population of fission isomers by gamma decay in the second well.
Actual calculations require as fission model parameters information on the barrier characteristics and on the spectrum of transition states. Usually fission barriers are represented by smoothly joined parabolic sections. The most important barrier parameters are the heights ($E_A$,$E_B$) and the curvatures ($\hbar\omega_A$, $\hbar\omega_B$) of the inner and the outer barrier, respectively. If partial damping is relevant one additionally needs the depth and curvatures ($E_{II}$, $\hbar\omega_{II}$) of the second well and the strength of the absorptive potential. The results of theoretical calculations of the deformation potential based on the Strutinsky method [68] are at present not accurate enough for cross section calculations. Hence barrier parameters have to be taken from analysis of experimental fission data. At sub-barrier energies fission cross sections are sensitive mainly to the barrier heights and curvatures and on the first few transition states; with increasing energy of the fissioning nucleus they also depend on the density of transition states. In general deduced barrier parameters are affected by the assumptions on the level density of transition states and, conversly, extracted level densities critically depend on the underlying barrier parameters. Theoretical calculations indicate that the fissioning nucleus is axially asymmetric at the inner barrier [69] and axially symmetric but reflexion asymmetric at the outer barrier [70]. Due to the aforementioned implications of symmetry on the rotational bands one has to assume different transition state spectra at the two barriers.
In the past years two comprehensive sets of barrier parameters were reported. The first one was presented by Britt [71] and is mainly based on the fission probability measurements performed at Los Alamos. Level densities at the first well and at the two barriers were obtained under consideration of "rotational enhancement". A microscopic calculation which accounts for the single particle spectrum at the respective deformations and for pairing provides the density of intrinsic states (band heads) to which the contribution of the rotational bands are added in adiabatic approximation. The construction of the rotational bands accounts for the symmetry properties of the nuclear shape as proposed by Bjørnholm et al. [51]. As a result of the different symmetries the level densities at the first and the second barrier exceed, at moderate energies, that of the axially and reflection symmetric first well by factors of about 7 and 2. Britt points out that these symmetry dependent enhancements were essential for reproducing the energy dependence of the fission probability between threshold and 10 MeV. A still open question is the energy range these enhancements can be used in. With increasing energy shell effects and therefore different symmetries should disappear. Also the adiabatic approximation used for the derivation of the enhancement factors breaks down at higher energy; the latter problem was investigated for preactinides by Ignatyuk et al. [72].
The second set of barrier parameters was developed by Lynn [73] and is based on

accurately known (n,f)-cross sections up to about 3 MeV and on fission probability measurements. This complete set comprises in particular also transition state densities in terms of constant termperature formulas for excitation energies up to 5 MeV; the level density parameters empirically account for the deformation dependent rotational enhancement. The estimated errors of the barrier heights are ± 0.2 MeV for most nuclei and upt to ± 0.5 MeV in some unfavourable cases. For the most recent version of Lynn's parameter set see refs. [45,49].

Fig. 8 displays for some actinides a comparison of barrier heights deduced by different authors. In addition to those of Britt and Lynn it shows results obtained by Weigmann [46] from the analysis of sub-barrier intermediate structure and by Arthur [74] from fits to (n,2n) cross sections. The differences in the barrier height are rather large, considering the fact that even a 0.2 MeV difference in the barrier height changes the penetrability by a factor of about 5 at energies 0.5 MeV below the top of the barrier and has still a marked effect on cross sections at energies far above the barrier (see fig. 11). One reason for this unsatisfactory situation may be that the three types of experiments involve different spin populations in the fissioning nucleus.

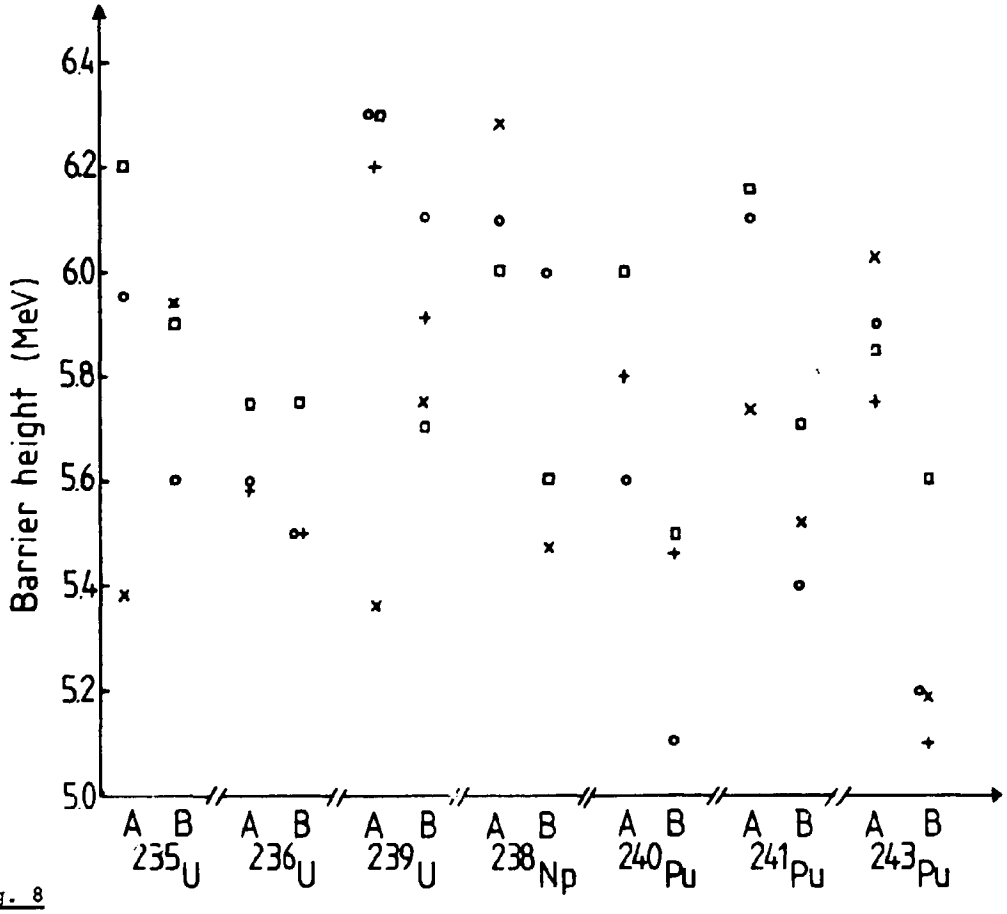


Fig. 8

Comparison of the heights of the inner and outer barrier deduced by different methods.

○ fission probabilities and (n,f)-cross sections, ref.[45] □ fission probabilites, ref.[71]

× sub-barrier intermediate structure, ref.[46] + (n,f)-cross sections

It is evident that due to the large number of parameters entering in the determination of the barrier heights the result is not unique. Due to the aforementioned interdependency of barrier heights and transition state densities both quantities should be taken from the same parameter set. In this sense Lynn's results are more convenient, as most nuclear reaction codes cannot handle the calculation of microscopic level densities as required for the Los Alamos set.
Fission cross sections employing Lynn's set were reported by Fort et al. [75] and Derrien et al. [76]. In order to avoid the calculation of microscopic level densities Arthur [74] employed for the calculation of the transition state densities at both barriers the Gilbert-Cameron model [77] with the same parameters as in the first well and applied semiempirical enhancement factors.
Model parameters are required also for neutron-and photon emission, the other two important decay modes in the actinide region. Neutron transmission coefficients are related to the optical model described in section 3. For the dominant E1-radiation it is recommended [33,49] to use the Brink Axel model that relates the gamma-ray transmission coefficients $T_{\gamma E1}$ to the parameters of the giant dipole resonance. Similar considerations as for the transition states apply to the density of levels at normal deformations which are populated by neutron and gamma decay. Most routine calculations employ the phenomenological Gilbert-Cameron model [77] the parameters of which can be determined from low lying levels and from resonance spacings. Recently V.A. Maslov et al. [78] applied the semi-empirical level density model of Ignatyuk et al. [79] to extract level density parameters for actinides; this model accounts for shell effects, pairing and collective enhancements and thus provides a better basis for extrapolations as the Gilbert-Cameron model.
Preequilibrium emission affects the cross section for first chance fission by depletion and those for higher chance fission by the resulting hard component in the neutron spectrum. A successful reproduction of fission-, (n,2n)- and (n,3n)-cross sections under consideration of preequilibrium decay and incident energies between 5 and 20 MeV was reported by Bychkov et al. [80]. In this paper a simple parametrisation of the fission probability is used instead of barrier paramters and transition state densities.

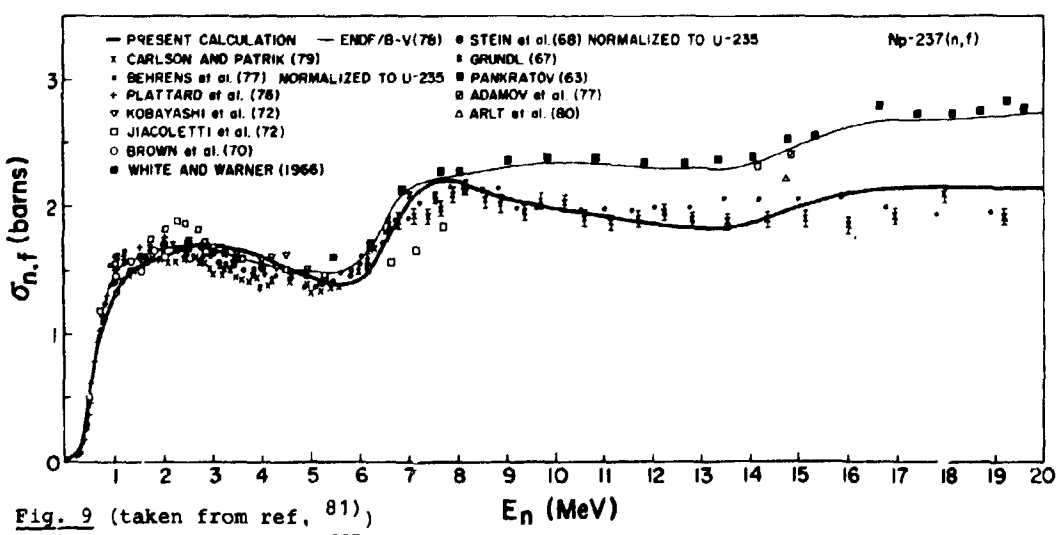


Fig. 9 (taken from ref. [81])
Comparison of the calculated $^{237}Np(n,f)$ cross section with experimental data.

As an example for the problems encountered in the calculation of cross sections for fission and other reactions some results for neutrons on $^{237}$Np are displayed in figs. 9 and 10. The calculations were performed by Bak et al. [81] by means of the code STAPRE [65] and employed for fission the parameters of Lynn as starting values; the Fermi-gas formula was used for the level densities of transition states if the excitation energy exceeds the upper limit of the constant temperature formulas proposed by Lynn. The parameters were then adjusted so as to reproduce experimental fission cross sections from threshold up to 20 MeV. For energies above 6 MeV, when second and higher chance fission comes into play, the more recent data of Behrens et al. [82] and of Carlson et al. [83] were prefered (see fig. 9). The calculations also reproduce the experimental capture cross sections available up to about 3 MeV.

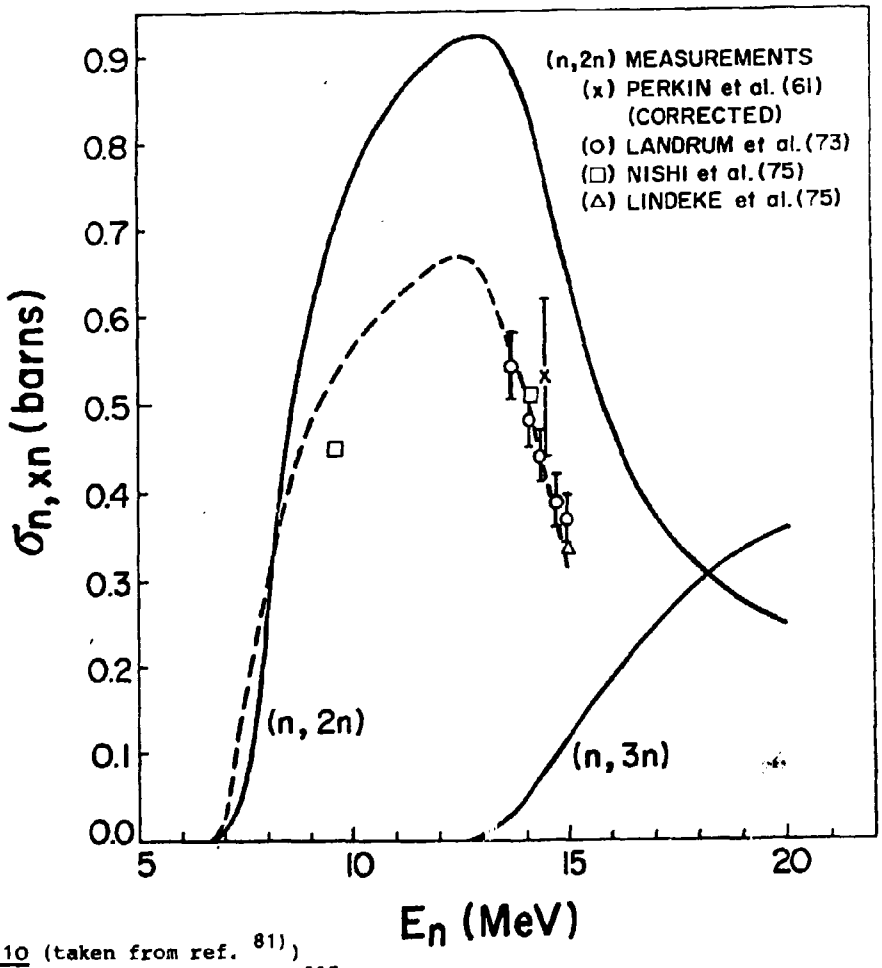


Fig. 10 (taken from ref. [81])
Comparison of the calculated $^{237}$Np(n,2n) cross section (full curve) with experimental data. The dashed curve represents the evaluation of Caner et al., rept. IA-1346 (1977).

The calculated (n,2n) cross section, however, considerably exceeds the experimental data. This discrepancy may be related to uncertainties in the competition between neutron and fission decay for $^{237}$Np. Reduction of the barrier heights $E_A$ and $E_B$ for $^{237}$Np by 0.2 and 0.4 MeV, respectively, increases the fission cross section and reduces the (n,2n) cross section as shown in fig. 11. With the re-

duced barrier heights the experimental (n,2n) cross sections are better reproduced but now the calcualted fission cross sections exceed the data of Behrens et al.[82] and Carlson et al. [83]. Fig. shows that differences in the barrier heights between 0.2 and 0.4 MeV are not unusual.

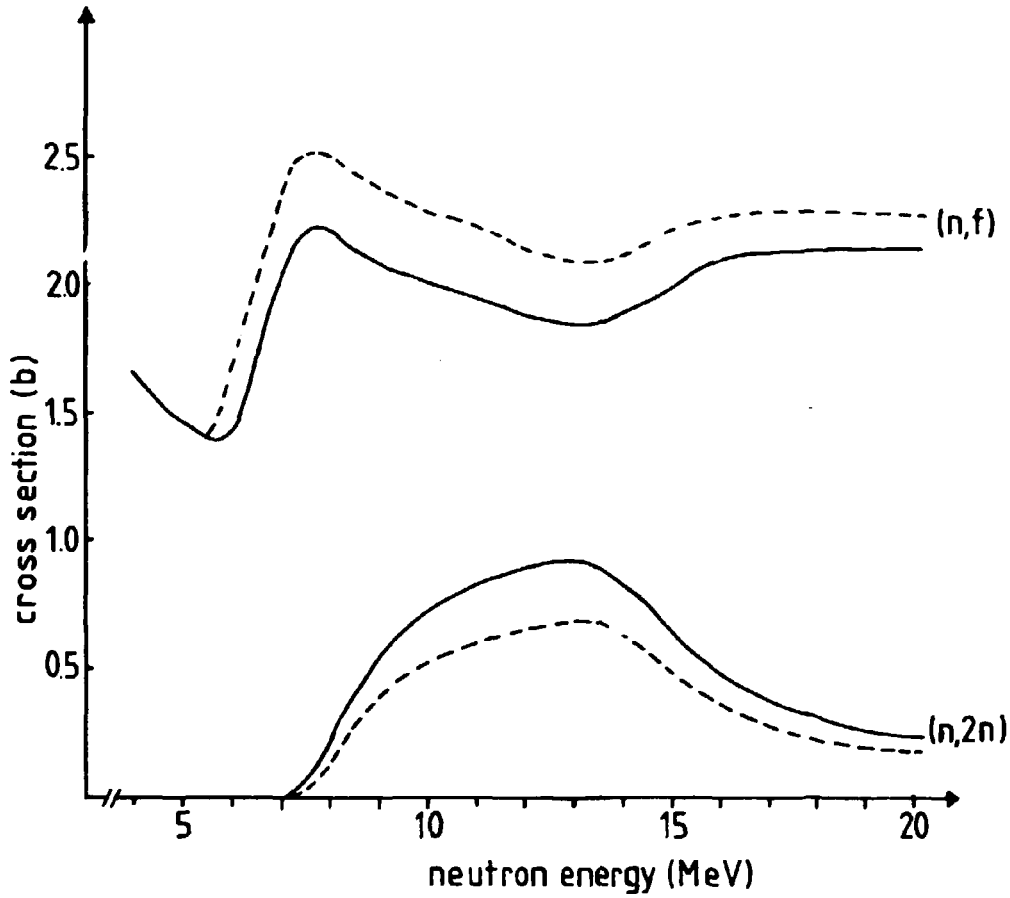


Fig. 11
The full curves were calculated with the parameters described in ref. [81]. For the dashed curve the barrier heights ($E_A$,$E_B$) of $^{237}$Np were changed from (5.99, 5.82) to (5.79, 5.42) MeV while all other parameters are unchanged.

It is difficult to make a general statement on the predictive power of model calculations. The accuracy depends on the experimental data available to adjust the model parameters and must, in each individual case, be estimated by sensitivity studies.

## 5. Prompt fission neutron spectra

In the past years Madland and Nix [84,85] developed a simple model to calculate the prompt neutron fission spectrum as function of the fissioning nucleus and its excitation energy. The calculation of the spectrum involves two steps.
At first the centre of mass neutron spectrum $\varphi(\varepsilon,T)$ emitted from a fragment of given excitation energy is calculated by Weisskopf's simple evaporation formula[86]

$$\varphi(\varepsilon,T) = k(T)\ \sigma_c(\varepsilon)\ \exp(-\varepsilon/T) \qquad (5.1.)$$

where $\varepsilon$ is the CM-neutron energy; $\sigma_c(\varepsilon)$ represents the inverse cross section, T

the nuclear temperature of the fission fragment residual nucleus and k(T) a normalization constant. The temperature T depends on the excitation energy of the fragment. Based on the work of Terrel [87] the excitation energy distribution of the fragments is transformed into a distribution P(T) of fission fragment residual temperature of triangular shape:

$$P(T) = \begin{cases} 2T/Tm^2 & , \quad T \leq Tm \\ 0 & \quad T > Tm \, . \end{cases} \tag{5.2.}$$

The maximum temperature Tm is related to the inital average total excitation energy of the fragments $\langle E^* \rangle$ by the Fermi-gas relation

$$Tm = (\langle E^* \rangle / a)^{1/2} \tag{5.3.}$$

where a is the level density parameter which is approximately calculated in terms of the mass number A of the fissioning nucleus

$$a = A/11 \ (\mathrm{MeV}). \tag{5.4.}$$

The initial average total excitation energy $\langle E^* \rangle$ of the fission fragments is given by

$$\langle E^* \rangle = \langle E_r \rangle + B_n + E_n - \langle E_f^{tot} \rangle \tag{5.5.}$$

Here, $\langle E_r \rangle$ is the average total energy release, $E_n$ and $B_n$ are kinetic and separation energy of the neutron inducing fission and $\langle E_f^{tot} \rangle$ is the average total kinetic energy of the fission fragments, which can be taken from experiment. The average total energy release is calculated by averaging the individual mass differences over the fission fragment charge and mass distributions; experimental or systematic masses are used in this procedure.
The centre of mass neutron spectrum for each fragment is obtained by integrating the spectrum for a given temperature over the triangular temperature distribution given by eq. (5.2.)

$$\phi(\varepsilon) = \int_0^\infty dt \ P(T) \varphi(\varepsilon, T). \tag{5.6.}$$

The same distribution P(T) is assumed for all fragments.
In the second step the CM-spectrum given by eq. (5.6.) is transformed to the laboratory system under the assumption that the neutrons are emitted isotropically

$$N(E,E_f) = \frac{1}{4\sqrt{E_f}} \int_{(\sqrt{E} - \sqrt{E_f})^2}^{(\sqrt{E} + \sqrt{E_f})^2} d\varepsilon \ \phi(\varepsilon) \frac{1}{E} \, . \tag{5.7.}$$

Here, E is the laboratory system neutron energy and $E_f$ is the fragments kinetic energy per nucleon. The mass and the kinetic energy distributions of the fragments are replaced by their averages: the light fragment with mass $A_L$ and the heavy fragment with mass $A_H$; the respective kinetic energies per nucleon are $E_f^L$ and $E_f^H$. The total neutron spectrum in the laboratory system N(E) is calculated as average of the spectra $N(E,E_f^L)$ and $N(E,E_f^H)$ of the light and the heavy fragment:

$$\left.\begin{aligned} N(E) &= \tfrac{1}{2}[N(E,E_f^L) + N(E,E_f^H)], \\ E_f^L &= \frac{A_H}{A_L} \frac{\langle E_f^{tot} \rangle}{A} \, , \quad E_f^H = \frac{A_L}{A_H} \frac{\langle E_f^{tot} \rangle}{A} \end{aligned}\right\} \tag{5.8.}$$

The calculations of Madland and Nix rather well reproduce experimental prompt neutron spectra for energies of the emitted neutron up to about 15 MeV. An example is shown in fig. 12.

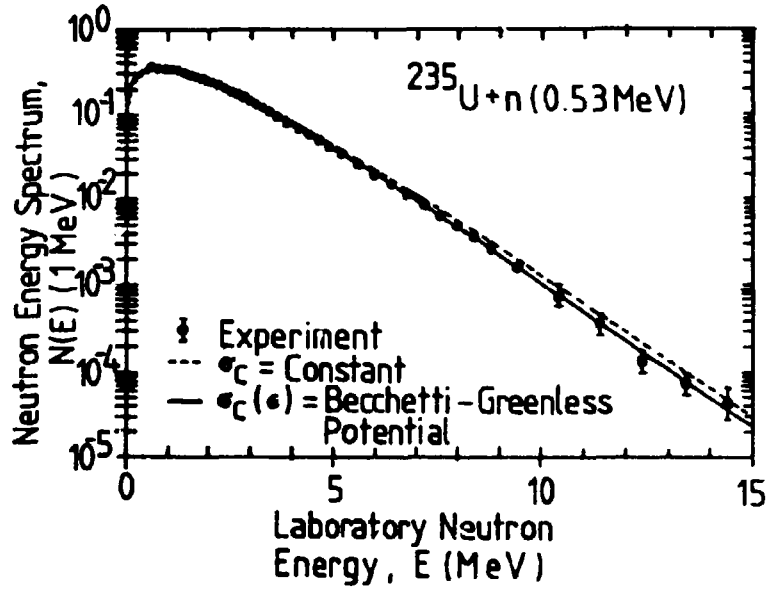


Fig. 12 (taken from ref. [84])

Prompt fission neutron spectrum in the laboratory system for the fission of $^{235}U$ induced by 0.53 MeV neutrons. For the dashed curve the inverse cross section $\sigma_c(\varepsilon)$ in eq. (5.1.) is energy independent while for the full curve $\sigma_c(\varepsilon)$ is deduced from the optical model using the potential of Becchetti and Greenless (Phys. Rev. 182 (1969) 1190). The experimental data are those of Johannson et al. (Nucl.Sci.Eng. 62 (1977) 695).

Calculations of this type, however, do not explain the high intensity of neutrons with energy beyond 20 MeV which was observed in prompt fission neutron spectra by the Dresden group [88].

The results for the prompt fission neutron spectrum can be used also for the calculation of the average neutron multiplicities; the additional information required is the average total gamma-ray energy and the average neutron separation energy. Experimental average multiplicities are reproduced within a few percent. The just described procedure can be extended to account for neutrons from (n,n'f) and (n,2nf) processes [84].

Due to its success in reproducing experimental data and its simplicity the model proposed by Madland and Nix is extremely valuable for nuclear reactor related applications.

## References


1. A.M. Lane and R.G. Thomas, Revs.Mod.Phys. 30 (1958) 257
2. P.A. Moldauer, Proc.Trieste Course on Nuclear Theory for Applications (1978), IAEA-SMR-43, p.165
3. C. Mahaux and H. Weidenmüller, Ann.Rev.Nucl.Part.Sc. 29 (1979) 1
4. T.A. Brody et al., Revs.Mod.Phys. 53 (1981) 385
5. H.A. Weidenmüller, Proc.Conf.Nuclear Data for Science and Technology, Antwerp 1982, to be issued
6. G.R. Satchler, Phys.Lett. 7 (1963) 55
7. C.A. Engelbrecht and H.A. Weidenmüller, Phys.Rev. C8 (1973) 859
8. H.M. Hofmann et al., Ann.Phys. N.Y. 90 (1975) 403

9. P.A. Moldauer, Phys.Rev. C12 (1975) 744
10. P.A. Moldauer, Phys.Rev. C11 (1975) 426
11. P.A. Moldauer, Nucl.Phys. A344 (1980) 185
12. W. Hauser and H. Feshbach, Phys.Rev. 87 (1952) 366
13. A.M. Lane and J.E. Lynn, Proc.Phys.Soc. London LXX8-A (1975) 557
14. J.W. Tepel et al., Phys.Lett. B49 (1974) 1
15. H.M. Hofmann et al., Z.Phys. A297 (1980) 153
16. D. Agassi et al., Phys.Lett. C22 (1975) 145
17. V.E. Bunakov, Proc.Trieste Course on Nuclear Theory for Applications (1978), IAEA-SMR-43, p.255
18. H. Feshbach et al., Ann.Phys. (N.Y.) 125 (1980) 425
19. W.A. Friedmann et al., Phys.Reports (Rev. Section of Phys.Lett.) 77 (1981) 47
20. T. Tamura et al., preprint (1982)
21. M. Blann, Ann.Rev.Nucl.Sci. 25 (1975) 123
22. D. Seeliger, Proc.Trieste Course on Nuclear Theory for Applications (1978), IAEA-SMR-43, p.283
23. T. Tamura, Rept. ORNL-4152 (1967) and Revs.Mod.Phys. 37 (1965) 679
24. J.P. Jeukenne et al., Phys.Rev. C15 (1977) 10 and C16 (1977) 80
25. J.P. Delaroche et al., IAEA-190 (1976) Vol. I, p.251
26. J. Lachkar, Proc. of the Int. Conf. on Neutron Physics and Nuclear Data for Reactors and other Applied Purposes, Harwell 1978, p. 136
27. G. Houat, Proc. of the Second Int. Symp. on Neutron Induced Reactions, Smolenice 1979, VEDA, Bratislava 1980, p.333
28. Ch. Lagrange, Proc. Specialists Meeting on Fast Neutron Scattering on Actinide Nuclei, Paris 1981, (NEANDC-158U) p.96
29. U. Fasoli et al., Nucl.Phys. A151 (1970) 369
30. S.B. Garg et al., Proc. of the Int. Conf. on Nuclear Cross Sections for Technology, Knoxville 1979, p.711
31. P.T. Guenther et al., Nucl.Sci.Eng. 65 (1978) 174
32. Ch. Lagrange, Act.Phys.Slov. 26 (1976) 32
33. V.A. Konshin, Proc.Trieste Course on Nucl. Theory for Applications (1980), IAEA-SMR-68/I, p.139
34. D.G. Madland and P.G. Young, Proc. of the Int. Conf. on Neutron Physics and Nuclear Data for Reactors and other Applied Purposes, Harwell 1978, p.349
35. A.M. Lane, Phys.Rev.Lett. 8 (1962) 171 and Nucl.Phys. 35 (1962) 676
36. L.F. Hansen, Proc. Specialists Meeting on Fast Neutron Scattering on Actinide Nuclei, Paris 1981, (NEANDC-158U), p.116
37. Ch. Lagrange et al., to be published in Nucl.Sci.Eng. 1982
38. J.S. Blair, Phys.Rev. 115 (1959) 928
39. P.G. Young, Proc. Conf. Nuclear Data for Science and Technology Antwerp 1982, to be issued
40. J. Raynal, "Computing as a Language of Physics", IAEA-SMR-9/8 (1972)
41. G. Haouat et al., Nucl.Sci.Eng. 81 (1982) 491
42. D.W.S. Chan et al., Phys.Rev. C26 (1982) 841
43. D.W.S. Chan and E. Sheldon, Phys.Rev. C26 (1982) 861
44. E. Sheldon, Proc. Conf. Nuclear Data for Science and Technology, Antwerp 1982, to be issued
45. S. Bjørnholm and J.E. Lynn, Revs.Mod.Phys. 52 (1980) 725

46. H. Weigmann, Proc.Trieste Course on Nucl.Theory for Applications (1980), IAEA-SMR-68/1, p.91
47. A. Bohr, Proc.Int.Conf. Peaceful Uses Atom.Energy, Geneva 1955, United Nations, New York, Vol. 2, p.220
48. D.L. Hill and J.A. Wheeler, Phys.Rev. 89 (1953) 1102
49. J.E. Lynn in Nuclear Fission and Neutron-Induced Fission Cross-Sections, A. Michaudon Editor, Pergamon Press, Oxford (1981) p.157
50. A. Bohr and B.R. Mottelson, Nuclear Structure, Benjamin, New York (1975) Vol.2
51. S. Bjørnholm et al., Proc.Physics and Chemistry of Fission 1973, IAEA, Vienna, Vol. 1, p. 367
52. R. Vandenbosch and J.R. Huizenga, Nuclear Fission, Academic Press, New York and London (1973)
53. J. Jary, Proc. of the LANDC Topical Discussion on "Critique of Nuclear Models and their Validity in the Evaluation of Nuclear Data", Tokyo 1974, Rept. NEANDC(J)38?-INDC(JAP)25L, p.76
54. L.R. Veeser and E.D. Arthur, Proc. of the Int. Conf. on Neutron Physics and Nuclear Data for Reactors and other Applied Purposes, Harwell 1978, p.1054
55. A. Michaudon Advances in Nuclear Physics 6 (1973), Plenum Press, p.1
56. A. Michaudon in Nuclear Fission and Neutron Induced Fission Cross-Sections, A. Michaudon Editor, Pergamon Press, Oxford (1981) p.5
57. E. Migneco and J. Theobald, Nucl.Phys. A112 (1968) 603
58. A. Michaudon, Neutron Cross Sections and Technology, NBS Special Publication 299 (1968) Vol. I, p.427
59. H.J. Specht et al., Proc. Physics and Chemistry of Fission 1969, IAEA, Vienna, p.3?3
60. G.D. James et al., Nucl.Phys. A189 (1972) 225
61. B. Back et al., Phys Rev. C9 (1974) 1924
62. C.L. Dunford, Rept.AI-AEC-12931 (1970) and E.D. Arthur, Rept. LA-9262-PR (1982) p.9
63. F.M. Mann, Rept. HEDL-TME 78-83 (1978)
64. J. Jary, Rept. NEANDC(E)227"L", INDC(FR)54/L (1982) p.28
65. B. Strohmaier and M. Uhl, Proc.Trieste Course on Nuclear Theory for Applications (1978), IAEA-SMR-43, p.313
66. E.J. Lynn and B.B. Back, J.Phys. A7 (1974) 395
67. H. Weigmann, Proc.Int.Conf. on Nuclear Data Evaluation Methods and Procedures, Brookhaven (1980) Vol. II, p.777
68. V.M. Strutinsky, Ark.Fys. 36 (1967) 629 and Nucl.Phys. A95 (1967) 420
69. S.E. Larsson and G. Leander, Proc.Physics and Chemistry of Fission 1973, IAEA, Vienna, Vol. I, p.177
70. P. Möller and S.G. Nilsson, ibid, p. 103
71. H.C. Britt, Proc.Physics and Chemistry of Fission 1979, IAEA, Vienna, Vol.I, p.3
72. A.V. Ignatyuk et al., Sov.J.N.Phys. 29 (1979) 626
73. J.E. Lynn, rept. AERE-R7468 (1974)
74. E.D. Arthur, Proc. Specialists Meeting on Fast Neutron Scattering on Actinide Nuclei, Paris 1981, (NEANDC-158U) p.145
75. E. Fort et al., Proc. of the Int.Conf. on Nuclear Cross Sections for Technology, Knoxville 1979, p.862
76. H. Derrien and E.Fort et al., ibid, p.872

77. A. Gilbert and A.G.W. Cameron, Can.J.Phys. 43 (1965) 1446
78. V.A. Maslov et al., Proc. IAEA Consultants Meeting on Uranium and Plutonium Resonance Parameters, Vienna 1981, INDC(NDS)-129/GJ p.329
79. A.V. Ignatyuk et al., Sov.J.N.Phys. 29 (1979) 450
80. V.M. Bychkov and V.I. Plyaskin, Sov.J.N.Phys. 34 (1981) 380
81. H.I. Bak et al., J. of the Korean Nucl.Soc. 13 (1981) 207
82. J.W. Behrens et al., Rept. UCID-17370 (1977)
83. A.D. Carlson and B.H. Patrik, Proc.of the Int.Conf. on Nuclear Cross Sections for Technology, Knoxville 1979, p.971
84. D.G. Madland and J.R. Nix, Nucl.Sci.Eng. 81 (1982) 213
85. D.G. Madland and J.R. Nix, Proc.Conf. Nuclear Data for Science and Technology, Antwerp 1982, to be issued
86. V.F. Weisskopf, Phys.Rev. 52 (1937) 295
87. J. Terrel, Phys.Rev. 113 (1959) 527
88. H. Maerten and D. Seeliger, Proc. Int. Symp. on Special Topics of the Interaction of Fast Neutrons and Heavy Ions with Atomic Nuclei, Gaußig 1980, p.98
89. Ch. Lagrange and J. Jary, Rept. NEANDC E)196"L"

# NUCLEAR DATA EVALUATION FOR FISSILE NUCLEI
## - Am and Cm Isotopes -

B. Goel and F.H. Fröhner

Kernforschungszentrum Karlsruhe, Institut für Neutronenphysik und Reaktortechnik,
P.O.Box 3640, D-7500 Karlsruhe, Federal Republic of Germany

Recently at KfK the neutron nuclear data were evaluated for the isotopes of Am and $^{242}$Cm for the use in thermal and fast reactor calculations. These nuclei are produced in reactors in quantities sufficient to influence the core neutronics and they contribute substantially to the radiation hazard of the spent reactor fuel. Their fission and capture cross sections are needed with an accuracy of 10 - 30 % for the core design and for the production of hazardous isotopes and with 20-50 % accuracy for more general studies of transplutonium nucleus production in the context of fuel recycling or nuclear incineration. The energy range for which these data are required stretches from 1 meV to 10 MeV. Most stringent accuracy requirements are for the thermal cross section and for the keV neutron energy range. At the 1975 IAEA conference on the actinide isotopes it was stated[1] that theoretical calculations can predict the cross sections to an accuracy of 25 - 30% . In the light of this encouraging statement it is disturbing to see that different nuclear data libraries show large discrepancies even for the total cross section (Fig. 1). The uncertainty in the total cross section should be of the order of a few per cent, its calculation being straight forward, and its dependence on mass is small. Thus a new evaluation based on well established theoretical tools and the available experimental data was required. The available experimental information on these isotopes is marked by wide ranges of missing data. In regions where experimental data are available they are often duped with strong discrepancies, as is the case for fission or the thermal capture cross section for $^{241}$Am. In addition to the prediction of unknown data theoretical methods can help discarding the wrong experimental data.

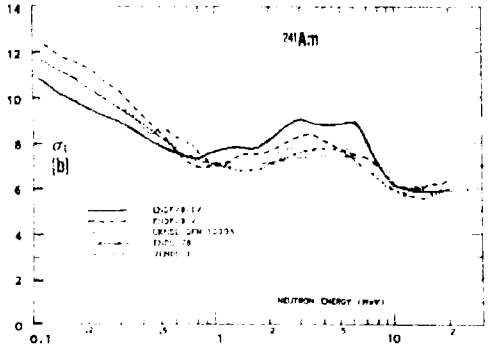


Fig.1: $^{241}$Am total cross section in different nuclear data libraries (status 1979)

## Theoretical Tools

At thermal energies and in the resolved resonance region the multi level Breit-Wigner resonance representation is used. Unknown level spins and fission channel interference precludes a more rigorous resonance description. The unknown distant levels are described in level statistical approximation and one bound level is determined per nucleus so as to ensure the correct thermal cross sections (see Ref.2) For each nucleus a complete set of point cross sections is generated coherently (i. e. for all reaction types from the same parameters) for zero temperature with the multi level program STRUMA.

Above the resonance region a spherical optical model with the Hauser-Feshbach partitioning in different channels including width fluctuation corrections is used. It is a recognised fact that global optical model potential parameters describe the cross sections only approximately. For a precise calculation of cross sections the potential parameters are to be determined locally for the mass region of interest. This is particularly important for the actinide region as here we have to deal with strongly deformed nuclei. It has been shown[3,4,5] that for deformed nuclei also the spherical optical model can lead to equally good fits to the experimental total cross section as the coupled channel calculations provided the parameters are adjusted to the mass region of investigation. Since at the onset of this evaluation no total cross section measurement for the Am or Cm isotopes was available, the optical model parameters were determined[5] for the neighbouring nucleus $^{238}U$. Total, elastic and inelastic cross sections were carefully analysed to fix the parameters of the real Woods-Saxon and imaginary Woods-Saxon derivative potential (for detail see Ref. 5). The result of this search is:

$$V = 47.01\ \text{MeV} - 0.267\ E - 0.00118\ \text{MeV}^{-1}\ E^2$$
$$R_r = 1.21\ \text{fm}\ A^{1/3}\ , \qquad a_r = 0.66\ \text{fm}\ ,$$

$$W = 9.0\ \text{MeV} - 0.53\ E$$
$$R_i = 1.30\ \text{fm}\ A^{1/3}\ , \qquad a_i = 0.48\ \text{fm}\ .$$

Capture transmission coefficients were calculated with giant dipole resonance profiles according to the prescription given in Ref. 6. To calculate fission transmission coefficients a double-hump fission barrier, approximated by two inverted parabolas, is used. The penetrability of each barrier is calculated by the Hill-Wheeler formula[7]. In cases considered here, the height of the two barriers is sufficiently different (Table I) to allow the use of the complete damping model, i.e. the reciproce of the total fission probability can be obtained by the addition of the reciproce of the two fission probabilities.

Table I - Recommended Fission Barrier Parameters

| Target Nucleus | First Barrier $E_b$ | First Barrier $\hbar\omega$ | Second Barrier $E_b$ | Second Barrier $\hbar\omega$ |
|---|---|---|---|---|
| $^{241}Am$ | 6.4 | 0.65 | 4.8 | 0.48 |
| $^{242m}Am$ | 5.9 | 0.75 | 4.8 | 0.55 |
| $^{243}Am$ | 6.2 | 0.58 | 4.8 | 0.55 |
| $^{244}Cm$ | 5.9 | 0.6 | 5.0 | 0.52 |

The level density is calculated using the usual Gilbert and Cameron formula[8]. The energy dependence of the level density parameter a is calculated by using the prescription of Ignatyuk et al.[9]. Width fluctuation corrections were calculated in the approximation of Tepel et al.[10]. The computer code used in this region is a modified version of the code HAUSER*4 (see Refs. 5,11 and 12). Toward the resolved resonance region, where more experimental data are available, these calculations are replaced by more specific ones with the newly developped program FITACS. This code adjusts level statistical parameters for l=1,2,3,4 by a simultaneous fit to all angle integrated average cross section data (total, capture, fission, scattering) available for a given nucleus up to 100-200 keV, ensuring

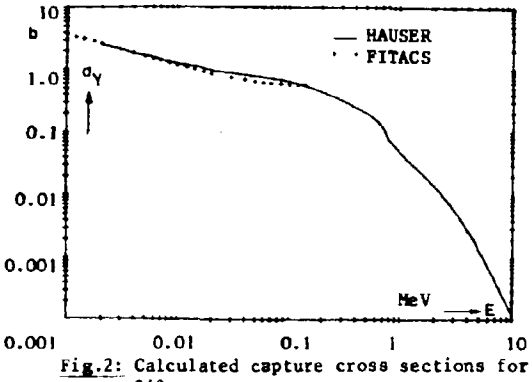


Fig.2: Calculated capture cross sections for $^{242m}$Am+n.

compatibility with strength functions, level densities, average radiation and fission widths derived from resolved resonance parameters (see Ref. 13). Inelastic scattering is fully taken into account. Width fluctuation corrections are calculated according to Moldauer[14]. The necessary s-wave strength functions and level spacings, corrected for missing levels, are obtained from resolved resonances as maximum likelihood estimates with the code STARA[15].

In the region of overlap of the two methods i.e., from a few keV to about 200 keV good agreement is observed between the results of the two methods (Fig. 2).

In the followings we describe the evaluation in different energy regions.

## Thermal Cross Sections

For the thermal capture cross section information is available mostly as the spectrum averaged cross section measured in a thermal reactor using the cadmium cutoff technique (see Ref. 16). The interpretation of these measurements is complicated due to the presence of two strong resonances near or below the Cd-cutoff energy (Fig. 3). The information on the cutoff energy is not always well documented.

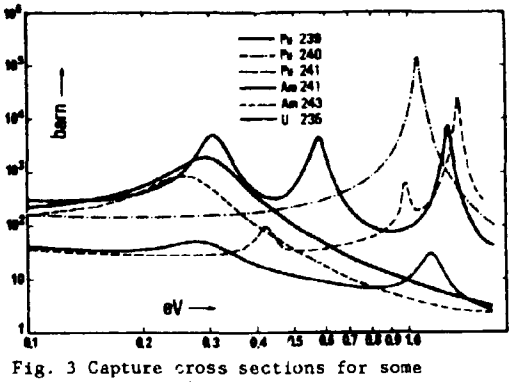


Fig. 3 Capture cross sections for some fissionable nuclei.

Fig. 4 shows the change in the thermal cross section of $^{241}$Am due to the change in the Cd-cutoff energy. The thermal cross section is evaluated via a careful analysis of the effective thermal cross section and differential data[17-19] putting the constraint set by the accurate total cross section measurements by Adamchuk et al.[20] and by Kalebin et al.[21].

The effect of low energy resonances on the thermal cross section is less dominant for the other isotopes studied here[22] The recommended

TABLE II

**Recommendet thermal cross sections:**

| Target Nucleus | $\sigma_t$ (b) | $\sigma_\gamma$ (b) | $\sigma_f$ (b) | $\sigma_n$ (b) |
|---|---|---|---|---|
| $^{241}$Am | 625±16 | 610±19 | 3.15±0.16 | 12±3 |
| $^{242}$Am | 8250±900 | 1400±860 | 6840±180 | 10±5 |
| $^{243}$Am | 85±5 | 79.3±2.0 | 0 | 5.7±4.5 |
| $^{244}$Cm | 23±3 | 14.4±1.1 | 1.03±0.18 | 7.57±3.20 |

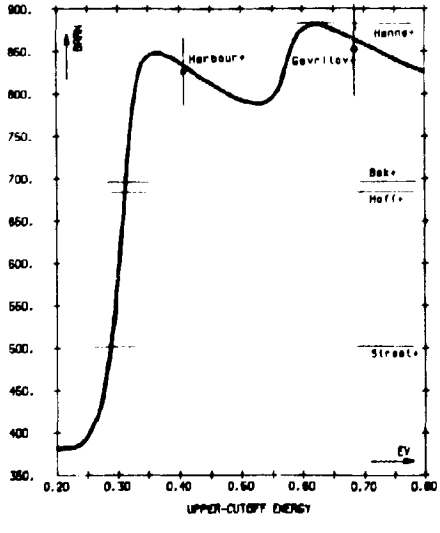


Fig. 4 Effect of Cd-cutoff energy on the thermal cross section of $^{241}$Am. ----->>>

thermal cross sections are listed in Table II. The details of the evaluation procedure and the underlieing data base is give in Refs. 13 and 16.

Resolved Resonance Region

The resonance parameters of $^{241}$Am were taken as weighted averages over all available data. These data were renormalised or discarded whereever deemed necessary. For $^{241}$Am good agreement between the absorption measurement of Weston and Todd[17] and the transmission measurement of Derrien and Lucas[18] is reported. However, the thermal cross section used by Weston and Todd to normalise their data is about 4.5% lower than our recommended value. Therefore, we have renormalised their data to our recommended thermal cross sections which meant essentially an increase of neutron widths by about 4 % . First it was feared that this would destroy the good agreement between the two measurements. Although for many of the weak levels this happens to some extent, the agreement for the strong levels is mostly improved. A mean value of $\Gamma_\gamma$ = 45 ± 2 meV is determined from the low lieing resonances with the most accurate widths, and this average is used to recalculate the fission widths of Gayther and Thomas[23] who had used a radiation width of 40 meV. Again agreement with Ref. 18 is improved. Missing fission widths were generated by Monte Carlo sampling from the $\chi^2$-distribution.

For $^{242m}$Am parameters are only available for the first six resonances[24]. Since no radiation widths had been measured we adopt Moore's level statistical estimate, 49 meV (Ref. 25). For $^{242}$Am the "barn book" values[26] (based essentially on the results of Simpson et al.[27]) are used except for a redetermination of the bound level. Evaluation of $^{244}$Cm resonance parameters[28-32] required reassessment of the radiation widths. The weighted average of the first two resonances gives a value of $\Gamma_\gamma$ = 36.2 ± 1.1 meV. All parameter sets are then reevaluated with this value in such a way that transmission dip areas remained unchanged while the change of capture and fission peak areas is minimal. Unphysical fluctuations of $\Gamma_\gamma$ as reported by Simpson et al.[32] are thus removed.

Unresolved Resonance and Fast Neutron Region

To obtain level statistical parameters for $^{241}$Am a FITACS fit to all available capture data[17,31,33] and to the parameters from the resolved resonances is made. Fission barrier parameters are adjusted so as to be compatible with the average fission width in the resolved resonance region and to fit the best fission data[34-37] in the fission threshold region up to 200 keV. At higher energies the results from HAUSER*4 calculations are adopted, with neutron transmission coefficients from the optical model described earlier. Both codes give similar results in the overlap region so that matching is unproblematic. Fig. 5 shows the calculated fission cross section together with the most recent data. In Fig. 5 the results of HAUSER*4 calculations in

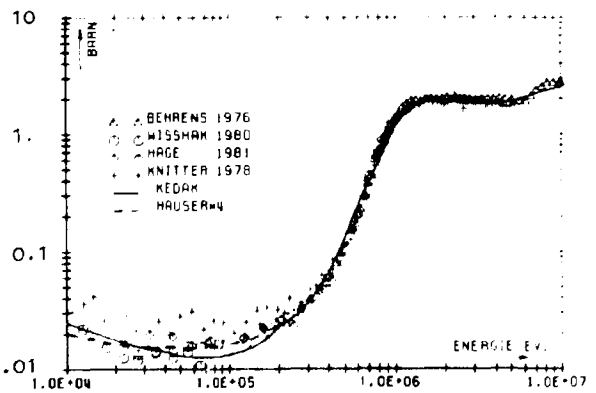


Fig. 5 fission cross section for $^{241}$Am

the lower energy region are also shown. The agreement between the results of the two calculational methods is good and well below the experimental spread.

This evaluation supports the results of Shpak[34] and more recent data[35-37] and agrees well with the evaluation of Fort et al.[38] but is totally incompatible with older bomb shot results[39] in the low energy region. When the transmission results of Philipps and Howe[40] became available they agreed well with the HAUSER*4 results. It is pointed out that these data were not available at the time evaluation procedure and the parameters were fixed. Thus the good agreement shown in Fig. 6 strengthens the confidence in the optical potential used.

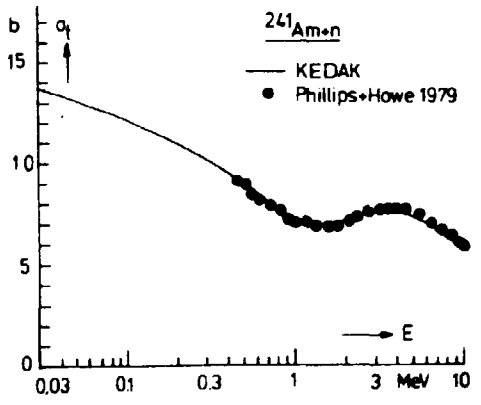


Fig. 6 calculated and experimental total cross section for $^{241}$Am

Due to the lack of experimental data for $^{243}$Am in the region of unresolved resonances results of HAUSER*4 calculations are adopted above 1 keV. The fission barrier parameters were chosen so as to reproduce Behrens' fission data[42]. Fig. 7 shows the capture cross sections thus obtained together with the ENDF/B-V evaluation and new data of Wisshak and Käppeler[45]. These experimental data became available after the evaluation was completed and reflect on the predictive value of the evaluation procedure.

The s-wave strength function for $^{244}$Cm is a compromise between a statistical analysis of resolved resonances and the value obtained from the optical model for actinides. The radiation width is that from the resolved resonances. Fission parameters were adjusted to fit the data of Moore and Keyworth[30]. The FITACS calculation was adopted up to 140 keV, HAUSER*4 results above. Agreement between both in the overlap region is good.

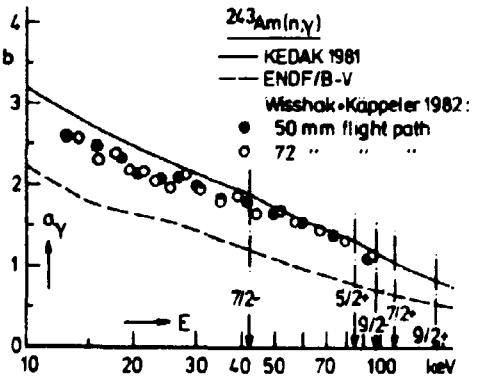


Fig. 7 Capture cross section for $^{243}$Am

## Discussion of Results and Conclusions

The evaluation proceedure and data for the KEDAK-4 library have been confirmed by the differential measurements which became available either during the evaluation or after the evaluation was completed. The KEDAK evaluation for these actinides is based to a large extent on consequent utilisation of nuclear theory. All cross sections are coherently calculated from suitably parameterised reaction formalisms. The various tests and experience with newly published data seem to indicate that with our optical potential for actinides total cross sections can be predicted with about 2-5 % uncertainty and capture cross sections below a few hundred keV with perhaps 5-20 %, at least in cases where good resonance data define the radiation width and the level density reasonably well. In cases where the data base is poor, as for $^{242}$Am, the latter margin may be somewhat larger, but still the giant dipole resonance model seems to yield very reasonable radiation strengths.

The validity of the evaluated data for thermal reactors has been verified and discussed in detail in Ref. 22. The measured resonance integrals are consistent with those calculated with the KEDAK-4 data except for $^{242}$mAm. For this isotope the experimental information both differential and integral is yet scarce. The isotope production and burn-up code KORIGEN[44] which operates with KEDAK-4 data predicts the isotope production in thermal reactor fuel with good accuracy[22,44]

For fast reactors also we have checked the evaluated data on experiment made in fast assemblies[45]. These data again became available to us after the evaluation had been completed. The agreement between the calcultion and experiment is good to excellent.

References


1. Proc. of the IAEA advisory Group Meeting on the Transactinium Isotope Nuclear Data, Karlsruhe, 3 - 7 Nov 1975, IAEA-186 Vol. I p. 20
2. F.H. Fröhner, Conf. Nucl. Data Eval. Meth. and Proced. 1980, BNL-NCS-51363 (1981)
3. D. G. Madland and P. G. Young, LA-UR-78-2510 (1978)
4. W.P. Poenitz, J.F. Whalen and A.B. Smith, Nucl. Sci. Eng. 78 (1981) 333
5. U. Fischer, KfK 2907, Karlsruhe (1980)
6. J.A. Holmes, S.E. Woosley, W.A. Fowler and B.A. Zimmermann, At. and Nucl. Data Tables 18 (1976) 306
7. D.L. Hill and J.A. Wheeler, Phys. Rev. 89 (1953) 1102
8. A. Gilbert and A.G.W. Cameron, Can. J. Phy. 43(1965) 1446
9. A.V. Ignatyuk, G.N. Smirenkin and A.S. Tishin, Sov. J. Nucl. Phys. 21 (1975) 255
10. J.W. Tepel, H.M. Hoffman and H.A. Weidenmüller, Phys. Letters 49B(1974)1
11. F.M. Mann, HEDL-TME 76-80, Hanford (1976)
12. F. Fröhner, B. Goel, H. Jahn, U. Fischer, Intrnational Conf. on Nuclear data for Science and Technology, Antwerp, Sept. 6-10,1982 and KfK 3415, Karlsruhe (in print)
13. F.H. Fröhner, B. Goel and U. Fischer, Meeting on Fast-Neutron Capture Cross Sections, ANL 1982 (in print)
14. P. Moldauer, Nucl. Phys. A344(1980)185
15. F.H. Fröhner, Proc. Meeting on Neutron Cross Sections of Fission Product Nuclei, Bologna 1979, RIT/FIS-LDN(80)1, p. 145
16. B. Goel, Proc. Meeting on Neutron Cross for Higher Pu and Am isotopes, Brookhaven, Nov. 20-22,1978, BNL-50991 (1978) p.177
17. L.W. Weston and J.H. Todd, Nucl. Sci. Eng. 61(1976)356
18. H. Derrien and B. Lucas, Nucl. Cross Sections and technology, Washington D.C., NBS SP 425(1975)637
19. K. Wisshak, J. Wickenhauser, F. Käppeler, G. Reffo and F. Fabbri, Nucl. Sci. Eng. 81(1982)396
20. Y.B. Adamchuk et al., Conf. on Peaceful Uses Atomic Energy, Geneva (1955),Vol.4, p.216
21. S.M. Kalebin, V.S. Artamonov, R.N. Ivanov, G.V. Pukolaine, T.S. Belanova, A.G. Kolesov, V.A. Safonov, Sov. At. Energy 40(1976)373
22. B. Goel and U. Fischer, Intrnational Conf. on Nuclear data for Science and Technology, Antwerp, Sept. 6-10,1982 and KfK 3449, Karlsruhe (1982)
23. *D.B. Gayther and B.W. Thomas*, Proc. Kiev Conf. on Neutron Physics, vol. 3, p. 3, Moscow (1977)
24. C.D. Bowman, G.F. Auchampaugh, S.C. Fultz and R.W. Hobbs, Phys. Rev. 166(1968)1219

25. M.S. Moore, Conf. on Neutron Phys. and Nucl. Data, Harwell (1978), p. 313
26. S. Mughabghab and D.I. Garber, BNL 325, 3rd ed., Brookhaven (1973)
27. O.D. Simpson, F.B. Simpson, J.A. Harvey, G.G. Slaughter, R.W. Benjamin and C.E. Ahlfeld, Nucl. Sci. Eng. 55(1974)
28. J.R. Berreth, F.B. Simpson and B.C. Rusche, Nucl. Sci. Eng. 49(1972)145
29. R.E.Cote, R.F. Barnes and H. Diamond, Phys. Rev. 134B(1964)1281
30. M.S. Moore and G.A. Keyworth, Phys. Rev. C3(1971)1656
31. S.M. Kalebin, Proc. of the IAEA advisory Group Meeting on the Transactinium Isotope Nuclear Data, Karlsruhe, 3 - 7 Nov 1975, IAEA-186 Vol. II p. 121
32. O.D. Simpson, F.B. Simpson and T.E. Young, ANCR-1088, Idaho Falls (1972)
33. V.F. Gerasimov, Sov. J. Nucl. Phys. 4(1975)706
34. D.L. Shpak, Y.B. Ortopenko and G.N. Smirenkin, Sov. Phys. JETP 10(1969)175
35. K. Wisshak and F. Käppeler, Nucl. Sci. Eng. 6(1980)148
36. H.H. Knitter and C. Budtz-Jorgensen, Atomkernenergie-Kerntechnik 33(1979)205
37. W. Hage, K. Wisshak and F. Käppeler, Nucl. Sci. Eng. 78(1981)248
38. E. Fort, M. Darrouzet, H. Derrien, P. Hammer and L. Martin-Deidier, Nucl. Cross Sections for Technology 1979, NBS SP 594, Knoxville(1980)636
39. P.A. Seeger, A. Hemmendinger and B.C. Diven, Nucl. Phys. A96(1967)605
40. T.W. Phillips and R.E. Howe, Nucl. Sci. Eng. 69(1979)375
41. J.C. Browne, R.E. Howe, R.J. Dougan, R.J. Dupsyk and J.H. Landrum, Conf. on Neutron Physics and Nucl. Data, Harwell (1978), p. 887
42. J.W. Behrens, UCID-17504, Livermore (1977)
43. K. Wisshak and F. Käppeler, Intrnational Conf. on Nuclear data for Science and Technology, Antwerp, Sep. 6-10,1982
44. U. Fischer and H.-W. Wiese, KfK 3140 (in print)
45. R.A.P. Wiltshire, A.D. Knipe, D.W. Sweet, J.M. Stevensen, K.M. Glover and B. Whittaker, Intrnational Conf. on Nuclear data for Science and Technology, Antwerp, Sept. 6-10, 1982 and private communication.

# INDL - The IAEA Evaluated Nuclear Data Library

H.D. Lemmel and D.E. Cullen
IAEA Nuclear Data Section
A-1400 Vienna, Austria
P.O. Box 100

When we speak of evaluated nuclear data we mean

- best available nuclear data resulting from a critical analysis of all available experimental data and from best available nuclear theory,

- presented in a form suitable for the data user, specifically for computer calculations in reactor physics, shielding, dosimetry, radioisotope production, etc.

Ideally, there should be a single nuclear data library with internationally recommended best values for all practical purposes. For various reasons, this ideal goal cannot be reached, and although we are still far away from it we are working in the direction towards this goal.

Historically, different evaluated nuclear data libraries have been created independently from each other for national projects of reactor design, whereby contents and format of these libraries were determined. Specifically, these were

- ENDF/B, the national nuclear data library of the USA, operated at the Brookhaven National Laboratory under the guidance of a Cross-Section Evaluation Working Group (CSEWG);

- ENDL at the Lawrence Livermore National Laboratory, USA;

- UKNDL at Winfrith and Harwell, UK, partly in cooperation with Australia and Italy;

- KEDAK at the Kernforschungszentrum Karlsruhe, FRG, partly in cooperation with Israel;

- JENDL at JAERI, Japan;

- SOKRATOR in the USSR, in cooperation with the GDR and other socialist countries;

- and, more recently, ChENDL at the Nuclear Data Center in Peking, People's Republic of China.

In addition, there exists a large variety of nuclear data libraries for various specialized applications.

Most of the national data libraries had different formats which could not easily be converted into each other. Consequently, there was a lot of duplication of efforts despite of the fact that none of the supporting countries had sufficient manpower to keep its data library up-to-date. The situation started to improve only a few years ago by two developments forming the basis for an improved international cooperation.

1. The so-called "7 Standards File" of the US ENDF/B library gained international recognition. This file contains neutron reaction data for the nuclides 1-H-1, 2-He-3, 3-Li-6, 5-B-10, 6-C-12, 79-Au-197, 92-U-235. The cross sections of these nuclides are frequently used as reference standards for other data, and it was an essential progress when evaluators in different countries used the same standard reference values for their evaluations. The standard data are recurrently reviewed by subcommittees of the International Nuclear Data Committee INDC and of NEANDC, the Nuclear Data Committee of the OECD Nuclear Energy Agency (NEA). In addition to the ENDF/B-formatted computer file, the "1982 INDC/NEANDC Nuclear Standards File" is being published by the IAEA in the form of a handbook.

2. The Japanese and subsequently also the West and East Europeans decided to adopt the American ENDF/B format, which can now be regarded as the international format for evaluated neutron nuclear data. (For experimental nuclear data the international exchange format EXFOR exists already since 1969.) At the OECD Nuclear Energy Agency the West European and Japanese evaluation efforts are now coordinated and a Joint Evaluated File, JEF, is being created.

The IAEA Evaluated Nuclear Data Library INDL was started in 1980 in ENDF/B format. At present, INDL contains approximately 200 evaluations for 150 nuclides contributed from 13 institutes in 11 countries. However, so far only about 30 of the evaluations are 'complete evalutions' covering all reactions in the full energy range from 0 up to 15 or 20 MeV.

INDL meets several purposes:

1. It collects evaluations that are not part of one of the large recognized libraries. These evalutions would be ignored, if they were not made available through INDL.

2. Considerable effort was devoted to convert evaluations from special formats into the international ENDF/B format. This relates to the libraries SOKRATOR, BOSPOR and a collection of evaluations compiled earlier in EXFOR format.

3. In the field of actinides neutron cross-sections the IAEA organized an international coordinated research programme with the result of a comprehensive actinides data library that can be used for fuel burnup calculations. This ENDF/B formatted file will also include actinide decay data based on recommended values resulting from another international coordinated research programme.

All the evaluations mentioned so far do not have the status of internationally recommended data. The library represents merely a collection of existing evaluations. In the case of actinides, however, we have started a project of testing and validation of the neutron cross-section data in order to obtain an improved and well tested data file.

4. The first part of INDL which is likely to be recognized as an internationally recommended file is the International Reactor Dosimetry File 'IRDF'. This consists of recommended data for 38 neutron reactions used for reactor neutron dosimetry by multiple foil activation. The first version has been issued in January 1982. An improved version will be issued in 1983 on the basis of feedback received from data users.

To obtain a single data file to be recommended for international use, is not a trivial problem. The work of an evaluator involves some elements of personal judgment about the reliability of nuclear models and experimental data. It may therefore be quite desirable to have two competing evaluations for the same nuclide, where the differences may give some feeling for the data uncertainty. In the specific fields of nuclear data standards, reactor neutron dosimetry and other applications, a single international file is essential in order to be able to compare results from different institutes.

As the evaluation efforts of the OECD countries are now coordinated in the projects of the libraries ENDF/B and JEF, the IAEA Nuclear Data Section is concentrating on collecting in INDL evaluations from all non-OECD countries. However, within the present priority items of dosimetry data and actinides, contributions from OECD countries are included as well. Many data included in INDL are, at the same time, part of national libraries such as JENDL or SOKRATOR. This should not be regarded as a duplication of effort: Data included in national libraries are distributed through the IAEA without any change to the data; INDL, on the other hand, is our working file in which we aim at improving the data by checking and by updating with new experimental data, in close contact with the author of the original evaluation. In this case a clear documentation is indispensable for the original evaluation and for the subsequent improvements performed. Data users are therefore advised to identify the evaluations used not only by library name and accession-number (called "MAT" number in ENDF/B) but in particular also by the revision number, which shows up at the beginning of each data file.

ENDF/B as an international format has advantages but also some disadvantages. The advantages are obvious: The common format allows easy international exchange of evaluations, so that more data and more uptodate data will become available. The common format also allows the development of a rich fund of computer processing codes, which can be adapted to a variety of different computers.

The main disadvantage is that a common format necessarily represents a compromise which will not fully satisfy everybody's requirements. For several evaluations that we entered in INDL, we observed that the evaluator had produced data types or reaction parameters that are not defined in the ENDF/B-5 format. In this case we must enter in the file the best approximation and must store additional information elsewhere, and here we have two options: Either we can store additional information in a special section of the file, so that it is not lost but does not disturb the ENDF/B processing codes. Or we can store the author's original evaluation in the more flexible EXFOR format, in parallel to the best suitable approximation in ENDF/B format.

There are other important evaluations, for example reaction data of neutrons above 20 MeV on carbon, for which the ENDF/B format is not suitable. Such evaluations we continue to store in EXFOR format only, the so-called "EXFOR-V" subseries.

First steps have been undertaken to coordinate the international discussion on the further development of the ENDF/B format and the related computer codes. Proposals are collected and submitted to the US group responsible for the definitions to be adopted for ENDF/B-6. It is obvious, however, that the considerable number of existing computer codes requires a long-term stability of the ENDF/B format.

The ENDF/B computer codes available cover a wide spectrum of data checking, various format conversions, group data calculations, etc. A modern evaluation of the neutron reaction data for a given nucleus can be quite complex and voluminous and correspondingly, the ENDF/B formats and conventions are complex. Checking of the evaluated data requires a set of computer codes which are available at the IAEA Nuclear Data Section. No evaluator can be expected to have all of these codes in operation, and we recommend a close cooperation between evaluator and data center which will assist the evaluator in the computerized checking of his evaluations.

The checking codes which we apply to INDL data, have two important purposes,

1. to validate the accuracy of the data as presented in the ENDF/B format and insure that all ENDF/B conventions are conformed to,

2. to validate the physical accuracy of the data by comparison to models and experimental data.

The codes presently available are used in the following sequence:

(1) CHECKER - ENDF/B format checking code. This code should be applied first and all detected errors should be eliminated before proceeding to use any of the other codes listed below.

(2) FIZCON - ENDF/B physics checking code. This code includes a wide variety of checks to insure that the evaluated data is physically acceptable. For example, it is checked that the resonance parameters or Legendre coefficients given do not imply negative values of the corresponding cross-sections. The consistency between reaction threshold and Q-values is checked, etc.

(3) LINEAR
(4) RECENT
(5) SIGMA1 - Reconstruct energy dependent, Doppler broadened cross sections from the sum of resonance and background cross section contributions. LINEAR converts all cross sections to linearly interpolable form, RECENT adds the resonance contribution and SIGMA1 may be used to Doppler broaden cross sections. The resulting cross sections may be compared to experimentally measured energy dependent cross sections.

(6) GROUPIE - Calculate multigroup cross sections for any arbitrary user-specified energy group structure. The result may be compared to experimentally measured broad energy group data.

(7) EVALPLOT - Plot cross sections, angular distributions and energy distributions. Visually checking of data is an extremely helpful means of checking on the consistency of data.

(8) COMPARE2 - Compare two evaluations by examining the ratio of physically comparable reactions and indicating where they differ. This program is a very convenient means of comparing different versions of the same evaluation (e.g. ENDF/B-IV vs. V) or evaluations from different evaluated libraries (e.g. KEDAK vs. ENDF/B).

All of these codes are used at the Nuclear Data Section of the International Atomic Energy Agency in order to validate the accuracy of evaluated data, before it is distributed for use.

These codes are also available to data evaluators or users from the NEA Data Bank. As a minimum evaluators should use program CHECKER in order to insure that their evaluation as coded in the ENDF/B format confirms to ENDF/B formats and conventions. Failure to do so can result in an evaluation being improperly interpreted by users. In addition to CHECKER, the physics checking code FIZCON is also highly recommended to evaluators. This code is now quite sophisticated and is continually being improved to perform a multiple of physics validity tests.

The two codes CHECKER and FIZCON are small and very inexpensive to run on a computer; as such they are ideal to use by evaluators. In contrast, the other codes (particularly LINEAR, RECENT and SIGMA1) can be quite expensive to run and as such are better suited to use at a centralized data center, which provides evaluated checking services for users.

The codes LINEAR, RECENT, SIGMA1 and GROUPIE are also used by data users in order to process ENDF/B cross sections into a form that can be used in transport or diffusion calculations. LINEAR, RECENT and SIGMA1 can be used to prepare energy dependent cross sections for use in Monte Carlo calculations and GROUPIE can be used to prepare self-shielded multigroup constants. COMPARE2 is a convenient code to use in order to determine how a new generation of a multigroup library differs from the preceeding library; this allows the data user to estimate which of this calculations may be effected by a change in data library.

In the past it became evident that some of the ENDF/B data processing codes were not sufficiently accurate and produced errors that exceeded the uncertainty of the data. Consequently, the IAEA Nuclear Data Section maintains a project on the verification of nuclear cross-section processing codes. (The NEA Data Bank maintains a more comprehensive project for other computer codes.) Users of data processing codes are, therefore, advised to keep contact with the data centers in order to verify whether their codes are uptodate.

In the near future, the work related to the IAEA evaluated nuclear data library will include:

- to continue the verification of data processing codes;
- to further improve services to data evaluators with respect to provision of experimental data and checking of evaluations;
- to support additional data evaluators in non-OECD countries;
- to continue the validation of data in the fields of actinides and reactor neutron dosimetry;
- to contribute to the next version of INDC/NEANDC standards data file (specifically the U-235 fast fission cross-section and the Cf-252 spontaneous fission neutron spectrum);
- to try to coordinate evaluations for the structural materials.

References:

The nuclear data libraries held at the IAEA Nuclear Data Section are documented in the IAEA-NDS-... documentation series. Related to INDL are the following documents:


| | |
|---|---|
| IAEA-NDS-7 Rev. 1 (1982): | Index of Nuclear Data Libraries available from the IAEA Nuclear Data Section. (H.D. Lemmel). Rev. 2 (1983) is in preparation. |
| IAEA-NDS-31 Rev. 2 (1982): | INDL/V - IAEA Nuclear Data Library for various neutron reaction calculations in ENDF/B-5 format; contents and documentation. (V. Pronyaev, D.E. Cullen, H.D. Lemmel, P.K. McLaughlin, O. Schwerer). Rev. 3 (1983) is in preparation. |
| IAEA-NDS-12 Rev. 6 (1982): | INDL/A - IAEA Nuclear Data Library for evaluated neutron reaction data of actinides; contents and documentation. (H.D. Lemmel). Rev. 7 (1983) is in preparation. |
| IAEA-NDS-48 (1982): | IRDF-82, the International Reactor Dosimetry File; energy-dependent form. (D.E. Cullen, N. Kocherov, P.K. McLaughlin). Rev. 1 (1983) is in preparation. |
| IAEA-NDS-41 (1982): | IRDF-82, the International Reactor Dosimetry File. multigroup form. (D.E. Cullen, N. Kocherov, P.K. McLaughlin). Rev. 1 (1983) is in preparation. |
| IAEA-NDS-10 Rev. 1 (1981): | ENDF/B Format, brief summary. (M.A. Khalil). |
| IAEA-NDS-10/102 (1979): microfiche | Data Formats and Procedures for the ENDF/B-5 format. (Editor R. Kinsey). |
| IAEA-NDS-39 (1981): | Summary of ENDF/B Pre-Processing Codes. (D.E. Cullen). |
| IAEA-NDS-29 (1980): | ENDF/B Processing Programs. (N. DayDay). |
| INDC(NDS)-134 (1982): | Verification of nuclear cross-section processing codes. (D.E. Cullen, W.L. Zijp, R.E. MacFarlane). |
| IAEA-NDS-34 Rev. 1 (1982): | EXFOR-U, IAEA Evaluated Nuclear Data File for various evaluations in EXFOR format. (K. Okamoto, O. Schwerer, H.D. Lemmel). |
| IAEA Technical Report ... | (to be published in 1983): The 1982 INDC/NEANDC Nuclear Standards File. (Editors H. Condé, A. Lorenz, A.B. Smith). |
| INDC(NDS)-127 (1981): | Proposed recommended list of heavy element radionuclide decay data. (Editor A. Lorenz) The 1982 edition is in preparation. |

# ОЦЕНКА СЕЧЕНИЙ РАДИАЦИОННОГО ЗАХВАТА БЫСТРЫХ НЕЙТРОНОВ НЕЧЁТНЫМИ ИЗОТОПАМИ НЕОДИМА, САМАРИЯ и ЕВРОПИЯ.

Т.С.Беланова, А.И.Блохин, А.В.Игнатюк, В.Н.Кононов, Г.Н.Мантуров, Б.Д.Юрлов

Физико-энергетический институт, Обнинск, СССР

Аннотация.

На основе анализа экспериментальных данных по сечениям радиационного захвата и систематики нейтронных и радиационных силовых функций получены рекомендуемые кривые сечений для изотопов $^{143,145}Nd$, $^{147,149,151}Sm$ и $^{151,153,155}Eu$ в области энергий нейтронов до I МэВ.

Нечётные изотопы неодима, самария, европия относятся к числу наиболее важных продуктов деления, определяющих отравление активной зоны реактора. Для всех этих изотопов существует значительный разброс в оценках сечений захвата нейтронов, и устранение этого разброса оценок является весьма актуальным. Экспериментальная информация о сечениях радиационного захвата представлена на рис.I. Большинство измерений выполнены методом, основанным на регистрации мгновенных $\gamma$-лучей захвата с применением техники времени пролёта или времени замедления для определения энергии нейтронов. В имеющихся экспериментальных данных наблюдаются некоторые общие закономерности. В интервале энергий от I5 кэВ до 80 кэВ данные как правило согласуются в пределах экспериментальных погрешностей. Ниже I5 кэВ сечения, измеренные на электростатических ускорителях обычно идут выше других данных. Выше I00 кэВ наблюдается превышение над остальными данных, полученных на линейных ускорителях электронов. Что касается результатов, полученных на спектрометре по времени замедления нейтронов в свинце, то они практически всегда лежат ниже данных других работ. Причины такого своеобразного поведения данных, повидимому, связаны с особенностями используемых экспериментальных методик. Более детальное обсуждение возможных погрешностей соответствующих методик и данных содержится в работе /I/, и эти погрешности принимались во внимание при проведении рекомендуемых кривых сечений захвата. Мы использовали общепринятую процедуру оценки сечений /2-4/, основанную на соотношениях статистической теории ядерных реакций. Однако, в отличие от работ /2-4/, требуемые значения нейтронных $S_\ell$ и радиационных $S_\ell^\gamma$ силовых функций для различных парциальных волн определялись из совместного анализа параметров изолированных резонансов и средних нейтронных сечений в диапазоне энергий до I МэВ. При расчётах сечений учитывались вклады парциальных волн с орбитальным моментом до 3 включительно, и оптимальные рекомендуемые кривые сечений находились методом максимального подобия. Энергетическая зависимость радиационных ширин вычислялась в предположении лоренцовой зависимости функций дипольных переходов и плотности уровней модели ферми-газа с учётом коллективных эффектов /5/. В широком диапазоне энергий нейтронов чувствительность сечения радиационного захвата к различным параметрам расчётной модели разная. В частности, при энергиях до 50 кэВ $\sigma_c(E_n)$ определяется в основном значениями $S_0$ и $S_0^\gamma$. При более высоких энергиях начинают играть заметную роль $p$- и $d$-волны, и их вклад при $E_n \sim$ I МэВ становится определяющим. Кроме того, уже ощутимым становится влияние принятой энергетической зависимости радиационных ширин, параметров плотности уровней и схемы уровней ядра-мишени. Полученные нами оптимальные значения средних резонансных параметров представлены в таблице I. Соот-

Таблица I. Оптимальны параметры статистического описания сечений захвата.

| Изотоп / Параметр | I43 | I45 | I47 | I49 | I5I | I5I | I53 | I55 |
|---|---|---|---|---|---|---|---|---|
| $10^4 \cdot S_0$ | 3.43 | 3.43 | 4.6 | 5.I | 3.65 | 3.70 | 2.50 | 2.35 |
| $10^4 \cdot S_1$ | 0.30 | 0.3I | 0.I5 | 0.30 | 0.25 | 0.I0 | 0.24 | 0.65 |
| $10^4 \cdot S_2$ | I.30 | 4.65 | I.30 | I.50 | 4.0 | 2.5 | 4.4 | 3.5 |
| $10^4 \cdot S_\gamma$ | 33.4 | 65.5 | 420 | 900 | I200 | 3200 | 2I00 | 2200 |
| $R'$ ,фм | 5.6 | 5.0 | 7.5 | 7.5 | 8.0 | 7.68 | 8.I6 | 8.2 |
| $a$ ,МэВ$^{-I}$ | I3.I | I6.6 | I8.79 | 20.I | 20.2 | 20.26 | 20.44 | I8.0 |
| $\sigma_c$(30 кэВ) мбарн | 285 | 482 | I650 | 2602 | 2594 | 4092 | 3I05 | 3I46 |
| $\sigma_t$(30 кэВ) мбарн | I0250 | 9620 | I4280 | I4960 | I28II | I337I | I2539 | I2503 |

ветствующие этим параметрам рекомендуемые кривые сечений радиационного захвата нейтронов ронов приведены на рис.I. Для сравнения на рисунке нанесена также оценка JENDL-I, сопоставление которой с более ранними оценками других авторов /3-4/ можно найти в работе /2/. Анализ имеющихся данных, теоретических расчётов и других оценок позволяет сделать следующие выводы: а)Экспериментальной информации по сечениям захвата исследованных продуктов деления по-прежнему недостаточно. Необходимы новые измерения сечений как в области энергий нейтронов до 50 кэВ, так и при энергиях I МэВ, где надежные экспериментальные данные практически отсутствуют. б)Различные оценки сечений захвата продуктов деления ещё не удовлетворяют требуемой точности. Практически для всех рассматриваемых ядер оценки не совпадают между собой, образуя полосу значений шириной в 20÷30%. Это различие существенно увеличивает в области энергии нейтронов ~ I МэВ. в)Для корректировки оценок сечений захвата продуктов деления в последнее время привлекаются интегральные эксперименты. Для неодима и самария соответствующие изменения средних сечений захвата в одногрупповом представлении после учёта интегральных измерений показаны в таблице 2. Можно видеть, что для RCN-2A /6/ хорошо согласуется с нашей оценкой. Аналогичное согласие имеется между нашими результатами и от-

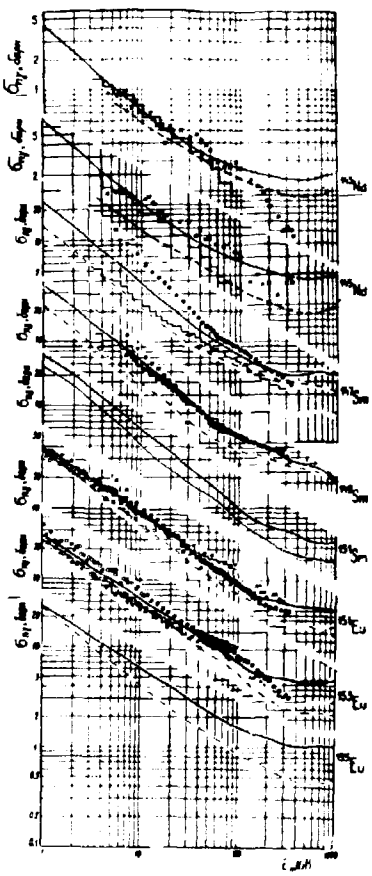

Рис.I. Совокупность экспериментальных данных и рекомендуемые средние сечения (сплошные кривые) радиационного захвата нейтронов нечётными изотопами неодима, самария и европия. Пунктиром показана оценка JENDL-I (2).

корректированными сечениями ENDF/B-V /7/ для $^{145}Nd$, $^{147,149}Sm$. Однако для этих элементов обращает на себя внимание значительное расхождение изменений одногрупповых сечений, требуемых в разных интегральных экспериментах, в частности на STEK и на EBR-2 /6,7/. То есть, имеющихся интегральных данных, по-видимому, ещё также недостаточно для однозначной корректировки результатов оценок микроскопических сечений захвата.

Таблица 2. Сравнение сечений $\overline{\sigma}_c$, усреднённых по спектру быстрого реактора SNR-300.

| Оценка / Изотоп | RCN-2 /3/ | RCN-2A /6/ | ENDF-IV /4/ | ENDF-V /7/ | Настоящая работа |
|---|---|---|---|---|---|
| $^{143}Nd$ | 247 | 228 | 241 | 292 | 234 |
| $^{145}Nd$ | 347 | 361 | 230 | 352 | 384 |
| $^{147}Sm$ | 1003 | 911 | 670 | 1042 | 1094 |
| $^{149}Sm$ | 1662 | 1659 | 1496 | 2050 | 1828 |
| $^{151}Eu$ | 1526 | 1303 | 1510 | - | 1659 |

Литература.


1. Е.Д.Орлов, Т.С.Беланова, А.И.Блохин, А.В.Игнатюк, В.Н.Кононов, Г.Н.Мантуров. Вопросы атомной науки и техники. Сер. "Ядерные константы", 1982, вып.4.
2. Y.Kikuchi et al. JAERI-1268 (1981).
3. H.Gruppelaar. ECN-13C (1975), ECN-33 (1977), ECN-65 (1979).
4. T.R.England, R.E.Schenter. LA-6116-MS (1975).
5. А.И.Блохин, А.В.Игнатюк, В.П.Платонов, В.А.Толстиков. Вопросы атомной науки и техники. Сер. "Ядерные константы", 1976, вып.21, с.3.
6. H. Gruppelaar. Proc. of Meeting on Neutron Cross-Sections of Fission Product Nuclei. Bologna, 1979, p. 299
7. R.E. Schenter, T.R. England. Ibid., p. 253

# РОЛЬ НЕСТАТИСТИЧЕСКИХ ЭФФЕКТОВ В ОЦЕНКЕ СЕЧЕНИЙ РАДИАЦИОННОГО ЗАХВАТА НЕЙТРОНОВ ИЗОТОПАМИ ЦИРКОНИЯ И МОЛИБДЕНА

**О.Т.Грудзевич, А.В.Игнатюк, В.И.Пляскин**

**Физико-энергетический институт, Обнинск, СССР**

**Аннотация**

**Анализируется влияние модельных представлений о механизме захвата на описание энергетической зависимости средних сечений радиационного захвата быстрых нейтронов.**

Изучению нестатистических эффектов в радиационном захвате нейтронов в последнее десятилетие уделялось достаточно много внимания. Для ряда ядер были получены убедительные доказательства существования прямого механизма валентного захвата резонансных нейтронов / I /, а для значительно большей совокупности ядер обнаружены эффекты, свидетельствующие о проявлении нестатистических механизмов более сложной природы / 1, 2 /. В данной работе мы хотим обсудить влияние [illegible] эффектов на результаты [illegible] сечений захвата нейтронов.

Независимо от предположений о [illegible] на большых [illegible] ширин резонансов соотношения для усредненного [illegible] можно представить в виде

$$\sigma_{n,\gamma}(E_n) = \pi \lambda_n^2 \sum_{\ell j} g_J T_{\ell j}^{J\pi} \frac{T_{\gamma stat}^{J\pi} F_{\gamma}^{J\pi} + T_{\gamma non}^{J\pi} F_{non}^{J\pi}}{T_{rstat}^{J\pi} + T_{rnon}^{J\pi} + \sum_{\ell' j'} T_{\ell' j'}^{J\pi}} \qquad (1)$$

Статистическая и нестатистическая компоненты радиационных силовых функций ( $T_{\gamma}^{J\pi} = 2\pi \Gamma_{\gamma}^{J\pi} / D^{J\pi}$ , где $D^{J\pi}$ - среднее расстояние между резонансами) могут иметь совершенно разные энергетические зависимости, и также сильно отличаться своими флуктуационными свойствами. В частности для валентного захвата нестатистическая компонента радиационных ширин оказывается скоррелированной со входными нейтронными ширинами, и флуктуационная поправка $F_{non}^{J\pi}$ определяется соотношениями, аналогичными каналу упругого рассеяния нейтронов.

Рассмотрим описание средних сечений радиационного захвата быстрых нейтронов четно-четными изотопами стронция и циркония, в которых валентный механизм захвата проявляется наиболее сильно / 3 /. В табл.I представлены экспериментальные значения средних резонансных параметров для этих ядер / 4 /, и на рис.I - соответствующие расчеты сечений захвата. Чтобы получить согласие с наблюдаемыми сечениями в расчетах несколько варьировалась величина среднего расстояния между резонансам и найденные значения $D_{cap}^{S}$ приведены в последнем столбце табл.I. На рис.I показаны также результаты расчетов, выполненных в предположении о чисто статистическом механизме захвата $p$ -нейтронов. Даже для изотопа $^{88}Sr$ , в котором нестатистические эффекты наиболее сильны, диаметрально противоположные предположения о механизме захвата $p$ -нейтронов сравнительно слабо отражаются на энергети-

ческой зависимости полного сечения захвата, а различия в абсолютной величине сечений легко устраняются вариациями $D_{cap}$.

Таблица I. Средние параметры нейтронных резонансов для изотопов с большими значениями ширин валентного захвата

| Ядро-мишень | $\Gamma_\gamma^S$, мэВ | $\Gamma_\gamma^P$, мэВ | $\Gamma_{\gamma val}^{P}$ *), мэВ | $D_{res}^S$, кэВ | $D_{cap}^S$, кэВ |
|---|---|---|---|---|---|
| $^{88}Sr$ | 220 ± 50 | 390 ± 90 | 340 | ~ 40 | I60 |
| $^{90}Zr$ | I30 ± 20 | 250 ± 50 | I20 | 8,6 ± I,6 | 20 |
| $^{92}Zr$ | I35 ± 20 | 220 ± 50 | 75 | 3,I ± I,0 | 3,6 |
| $^{94}Zr$ | 85 ± 20 | I50 ± 30 | 75 | 3,8 ± I,0 | 5,5 |

*) Валентная ширина оценена на основе наблюдаемых коэффициентов корреляций нейтронных и радиационных ширин резонансов / 3 /

Таким образом в области энергий до I00 кэВ описание средних сечений захвата определяется главным образом выбором радиационных силовых функций $S$ - и $P$-нейтронов, и вопрос разбиения их на статистическую и нестатистическую компоненты не играет существенной роли. Однако решение этого вопроса становится важным при переходе к более высоким волнам, для которых мы не имеем прямой экспериментальной информации о радиационных ширинах. Обычно в расчетах радиационные ширины четных волн принимаются равными $\Gamma_\gamma^S$, а нечетных - $\Gamma_\gamma^P$. Для ядер со значительными нестатистическими эффектами результаты расчетов полных сечений захвата будут достаточно сильно зависеть от применения данного предположения к полным ширинам или только к их статистическим компонентам. Для выбора между этими альтернативными предположениями большой интерес представляли бы достаточно прецезионные измерения сечений захвата нейтронов данными изотопами в области энергий до I МэВ. Кроме рассмотренных выше ядер валентный механизм захвата нейтронов отчетливо проявляется также в изотопах молибдена / 5, 6 /. В этом случае, однако, его вклад в интегральную ширину $\Gamma_\gamma^P$ оказывается заметно меньшим, чем в изотопах циркония, и соответственно более слабой будет зависимость результатов расчета сечений от моделирования радиационных ширин четных и нечетных волн. Для изотопов $^{95,97,98,100}Mo$, которые входят в список наиболее важных продуктов деления, отравляющих топливо быстрого реактора, имеющиеся экспериментальные данные по сечениям захвата представлены на рис.2 вместе с результатами теоретического описания сечений. Использованные в расчетах резонансные параметры приведены в табл.2.

Таблица 2. Параметры нейтронных резонансов изотопов молибдена

| Ядро-мишень | Оценка JENDL-1 | | Настоящая оценка | | | Анализ резонансов | |
|---|---|---|---|---|---|---|---|
| | $\Gamma_\gamma$, мэВ | $D^S$, эВ | $\Gamma_\gamma^S$, мэВ | $\Gamma_\gamma^P$, мэВ | $\Gamma_{\gamma val}^P$, мэВ | $D^S$, эВ | $D^S$, эВ |
| $^{95}Mo$ | I80 | 69,2 | I60 | I80 | 20 | 65 | 80 ± 25 /4/ |
| $^{97}Mo$ | I70 | 72,3 | I30 | I50 | 20 | 56 | 42 ± I5 /4/ |
| $^{98}Mo$ | 93 | не приведены | 86 | I25 | I5 | II50 | 950 ± I50 /4/ |
| $^{100}Mo$ | 75 | - " - | 70 | 90 | 0 | 640 | 700 ± 50 /8/ |

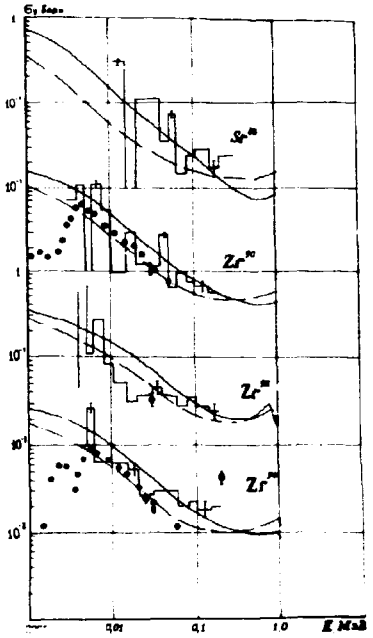


Рис.I. Описание сечений радиационного захвата нейтронов в предположении чисто статистического механизма (пунктир) и с учетом валентного механизма (сплошные кривые)

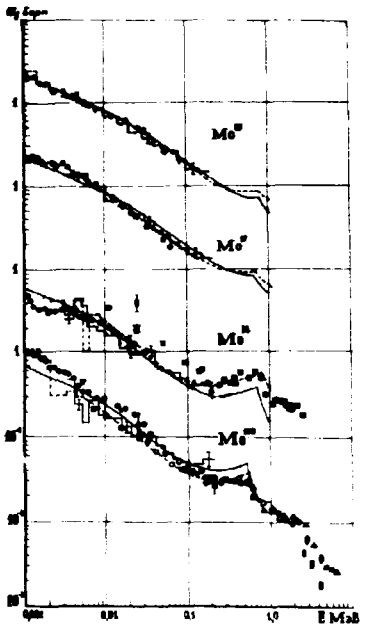


Рис.2. Сечения радиационного захвата нейтронов изотопами молибдена. Сплошные кривые - данная работа, пунктир - оценка JENDL-1 / 7 /

Несмотря на определенные расхождения параметров наших расчетов и работы / 7 /, качество описания экспериментальных данных оказывается примерно одинаковым. Сопоставление этих экспериментальных данных с оценками других авторов содержится в работе / 7 /, и сравнительно слабое расхождение различных оценок позволяет сделать вывод, что для изотопов молибдена требуемая практическими задачами точность оценки средних сечений захвата быстрых нейтронов $\sim$ I5% в области энергий до 200 кэВ, по-видимому, достигнута.

При более высоких энергиях на результаты расчетов сечений захвата наряду с приведенными радиационными силовыми функциями $d$ - и $f$-волн существенное влияние начинает оказывать выбор энергетической зависимости плотности уровней и сечения фотопоглощения. Как экспериментальные данные / 6, 8 /, так и последовательные микроскопические модели / 9 / демонстрируют целый ряд значительных отклонений низкоэнергетического участка сечений фотопоглощения от широко используемой в расчетах радиационных ширин лоренцовой параметризации хвоста гигантского резонанса. Дальнейшее накопление экспериментальных данных по сечениям захвата нейтронов в области энергий до 3 ÷ 4 МэВ представляет несомненный интерес для уточнения микроскопических расчетов ширин.

Литература

1. S.F.Mughabghab. 3 School on Neutron Physics (Alushta, 1978). Dubna, JINR, D3-11787, p.328.

2. Ф.Бечварж. Труды Международной школы по структуре ядра (Алушта, 1980). Дубна, ОИЯИ, ДУ-80-385, с.31.
3. J.V.Boldeman et al. Nucl.Phys., A269, 31, 1976; A269, 397, 1976.
4. A.R.Musgrove et al. Neutron Physics and Nuclear Data (Harwell, 1978). OECD, 1978, p.449.
5. A.R.Musgrove et al. Nucl.Phys., A270, 108, 1976.
6. K.Rimawi, R.Chrien. Phys.Rev., C15, 1271, 1977.
7. S.Igarasi et al. Japan Evaluated Nuclear Data Library. JAERI-1268 (1981).
8. H.Weigmann, S.Raman. Phys.Rev., C20, 115, 1979.
9. А.В.Игнатюк. Proc. Intern. Conf. on Neutron In duced Reactions. Smolenice, 1982.

# EVALUATION OF NEUTRON NUCLEAR DATA FOR SILICON

D. Hermsdorf, E. Paffrath, H. Philipp and L. Neumann
TU Dresden, Sektion Physik, Dresden, DDR

## 1. Introduction

An independent evaluation of neutron nuclear data for Silicon appeared desirable after 1975 by the reasons that available files offer contradictory data and / or insufficient data to satisfy most recent requests. This situation has been reviewed by the authors formerly [1]. Producing a re-evaluated data file care was paid to neutron-induced charged-particle and $\gamma$-quanta production cross sections. Some preliminary results have been published already [2,3]. In this contribution, we report on special methods applied to obtain the final set of evaluated data for Silicon.

## 2. Neutron Cross Sections in the Resolved and Unresolved Resonance Region

In the resolved resonances energy range Cierjack's data [4] have been proved to be the most reliable and best resolved ones. Starting from parameters taken from literature the resonance structure has been fitted by successive variation of Single-Level-Breit-Wigner (SLBW) parameters. Within the limitations of the SLBW formalism a satisfactory approximation was achieved in the range from $10^{-5}$ eV to $1.5 \cdot 10^{6}$ eV by an adjusted set of parameters [5].

The evaluation of data in the unresolved resonances region proceeds from experimental data smoothed by a Gaussian-shaped profil function to reduce statistical errors.

## 3. Neutron Scattering and Production Cross Sections

To evaluate neutron elastic and inelastic scattering cross sections optical model as well as equilibrium and preequilibrium models applied conventionally have been used [1] whereas angular distributions for inelastic scattering to low-lying levels were treated by Streil [6] in terms of CCBA. Special care was taken to calculate neutron emission spectra resulting from multi-step particle emission.

## 4. Charged-Particle Production Cross Sections

In most pertinant studies of data requests the importance of charged-particle cross sections are emphasized for Silicon. According to this, a systematical interpretation of experimental data have been carried out yielding clear evidence for direct reaction contribution to (n,p), (n,d) and (n,$\alpha$) reactions [2,7]. These modes have been investigated in terms of charge and mass-exchange reaction models of knock-out and pick-up types in DWBA.

Total charged-particle production cross sections have been calculated in terms of the extented H-F-model including contribution from multi-step-reactions also. So, the He-generation cross section at 14.8 MeV predicted to be 200 mb compares fa-

vourable with a value of 218±11 mb measured recently by Kneff et al. [8].

## 5. Gamma-Ray Production Cross Sections

Because of a stringend lack of data any evaluation of $\gamma$-ray emission cross sections must rely upon more ore lees justified theoretical calculations. Generally, a reasonable prediction can be achieved by the statistical model formulation for particle transitions taking into account $\gamma$-ray caecades in terms of Axel-Brink approximation for the strongest multipol orders of electro-magnetic transitions. This concept yields good results for $\gamma$-rays with transition energies below 10 MeV roughly [3].

At higher energies transition enhancements due to direct modes became important. Formulations in frame of a pre-equilibrium model have been proved to produce data in better agreement with experimental ones [9].

## 6. Data Compilation and Checking Procedures

All data have been compiled and formatted according to ENDF/B-V. At present some tests are underway to check the numerical figures against consistency and integral measurements. A full description of the data stored in the file is in press [10].

## References


1. D. Hermsdorf and L. Neumann
   "Proc. IX$^{th}$ Int. Symp. on Int. of Fast Neutron with Nuclei", Gaussig, 1979, ZfK-410 (1980) 147
2. D. Hermsdorf
   "Proc. X$^{th}$ Int. Symp. on Int. of Fast Neutrons with Neutrons", Gaussig, 1980, ZfK-459 (1981) 158
3. D. Hermsdorf and E. Paffrath
   ibid. p. 169
4. S. Cierjacks et al.
   Report KfK-1000, 1968
5. D. Hermsdorf and H. Philipp
   Annual Report 1981, in press
6. T. Streil et al.
   "Proc. X$^{th}$ Int. Symp. on Int. of Fast Neutrons with Nuclei", Gaussig, 1980, ZfK-459 (1981) 164
7. D. Hermsdorf
   Report INDC(GDR)-18/L, in press,
   "Proc. 3$^{rd}$ Conf. on Neutron-Induced Reactions", Smolenice, 1982, in press
8. D.W. Kneff and H. Farrar IV
   Report DOE/ER-0046/8, Vol. 1, 1982
9. B. Basarragtscha, D. Hermsdorf and E. Paffrath
   " , Phys. G: Nucl. Phys." 8 (1982) 275
10. D. Hermsdorf
    Report INDC(GDR)-20/L, in press

# COMPILATION AND EVALUATION OF /n,t/ CROSS SECTIONS

Z.T.Bödy
Institute of Experimental Physics, Kossuth University, Debrecen, Hungary

K.Mihály
Training Reactor, Technical University, Budapest, Hungary

A compilation and evaluation programme has been started to survey the available data. Some previous results are the following:

1/ The vast majority of the experiments is related to the lightest elements /Li,Be,B/. E.g. about the third of the measurements concerns the $^{6}$Li/n,t/ process if one takes into account data at all energies.

2/ For other elements the experimental data are very scarce.

3/ Neglecting cross sections integrated for a broad energy range /the fission average cross sections of Heinrich[1/] and those measured by Qaim using deuteron break-up neutrons[2/]/, the following statements appear to be true for the atomic number range $10 \leq Z \leq 92$ :

a/ Measurements were performed only for thirty elements or at least for one isotope of them. /In four cases for two isotopes of the same element./

b/ For more than the half of the elements there are no experimental data at all. There are wider atomic number ranges /Z=33-37, 53-56, 62-67 and 69-78/ where no experimental data is available.

c/ In the $14.2 \leq E_n \leq 14.9$ MeV energy range 54 cross-section measurements were performed. In addition to this in 7 cases upper limits were given and in 8 cases partial cross sections were determined /lower limits/.

d/ Excitation functions /measurements at least for two energies/ were determined only in 8 cases.

4/ Cross-section measurements by different authors frequently yield very different results. The maximum discrepacy can reach three order of magnitude /$^{32}$S, $^{40}$Ca/. These cases might be exceptional, however, a one order of magnitude deviation is not unfrequent. In many cases — if activation method is used — high cross-section /n,2n/ or other reactions leading to the same product nucleus can increase the value of the measured /n,t/ cross section. E.g. in the case of $^{32}$S the $^{31}$P contamination and in the case of $^{40}$Ca the $^{39}$K contamination must be less than about 0.01 % in order not to disturbe the results appreciably.[3/]
A further probleme arises if one uses the annihilation radiation; here the separation of the /n,t/-product radioactive nuclei from the disturbing other ones can only be achived by the difference between the half-lives. E.g. in the case of $^{40}$Ca the activity of /7.7 min./ $^{38}$K must be separated from that of /9.98 min./ $^{13}$N resulting from /n,2n/ reaction on the nitrogen in the air.[4/]

In accordance with a previous investigation[5/] it can be stated that /n,t/ cross sections on odd target nuclei are greater by about an order of magnitude than those on even target nuclei. /See Fig.2./ For the $Z > 20$ atomic number region it can be established that all experimental data are inside in the following intervals:

$$76 \exp/-9.2 \frac{N-Z}{A}/ \leq \sigma/n,t/ \leq 2oo \exp/-8.3 \frac{N-Z}{A}/ \quad /\mu b/ \text{ for even,}$$

$$4500 \exp/-23.5 \frac{N-Z}{A}/ \leq \sigma/n,t/ \leq 5400 \exp/-13.9 \frac{N-Z}{A}/ \quad /\mu b/ \text{ for odd}$$

target nuclei.

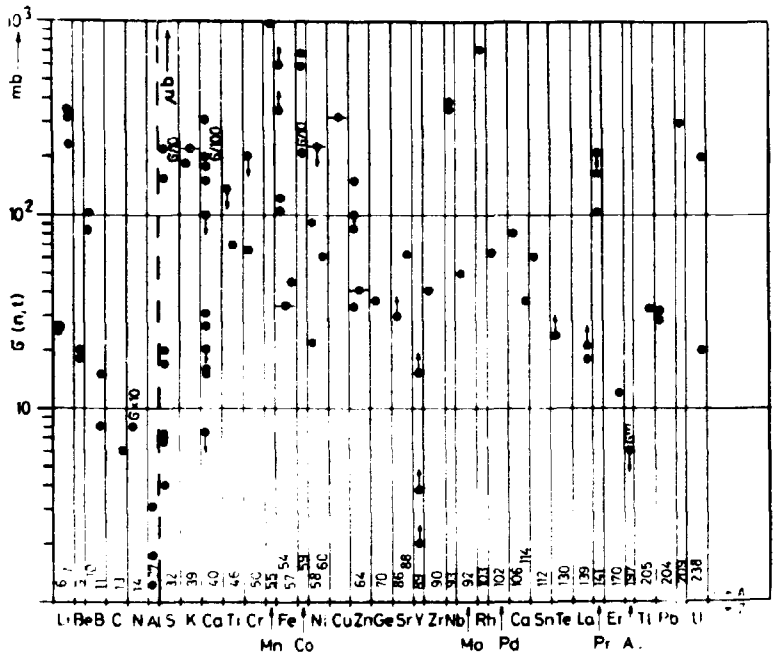


Fig.1. Cross sections for /n,t/ reactions at 14 MeV.

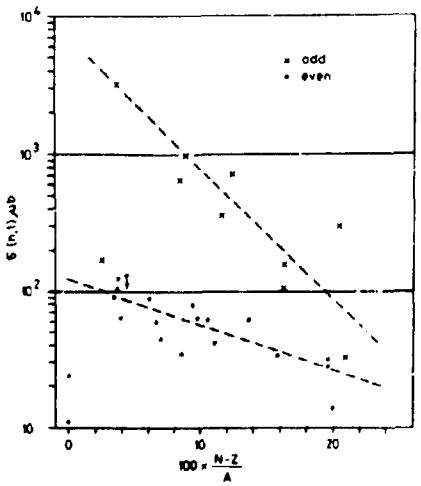


Fig.2. Dependence of $\sigma_{n,t}$ on $\frac{N-Z}{A}$.

The quality of the empirical formula of Qaim[6]

$$\sigma/n,t/=4.52/A^{1/3}+1/^2\exp/-1o\frac{N-Z}{A}/$$

and that of Woo[7]

$$\sigma/n,t/=7.684/A^{1/3}+1/^2\exp/-13\frac{N-Z}{A}/$$

was analysed. /Both formulae give cross sections in microbarns./ It was found that these formulae are good only for even nuclei where their qualities are about the same. However, for the range $2o < Z \leq 44$ the formula of Qaim is better, while for $Z > 44$ Woo's formula is preferable. For odd nuclei the calculated values should be multiplied by about ten in order to have a resonable estimate /except $^{2o5}Tl$/.

The measured data of excitation functions were described by functions of the form $\exp/ax^2 + bx + c/$ with fitted parameters a, b and c. /See Table 1./ Here $x = /\frac{A}{A+1} E_n + Q/^{-\frac{1}{2}}$, where $E_n$ : bombarding neutron energy /in lab. system/, A : mass number and Q : reaction energy /in c.m. system/.

Table 1. Empirical and semi-empirical excitation function parameters.

| target nuclei | Q /MeV/ | parameters a /MeV/ | b /MeV/ | c | energy range /MeV/ | comment |
|---|---|---|---|---|---|---|
| $^{27}Al$ | -10.92 | -5.00 | 2.21 | 8.29 | 13.5 - 19.5 | pure empirical |
| $^{32}S$ | -12.72 | -30.57 | 24.39 | 2.28 | 14.5 - 20.0 | pure empirical |
| $^{40}Ca$ | -12.92 | -7.47 | 4.25 | 4.71 | 14.5 - 20.0 | pure emp. $\sigma^g$ only |
| $^{55}Mn$ | -9.32 | -58.25 | 37.67 | 1.74 | 13.5 - 15.5 | semi-empirical |
| $^{59}Co$ | -8.92 | -27.95 | 10.43 | 6.90 | 14.5 - 19.0 | semi-empirical |
| $^{58}Ni$ | -11.12 | -34.81 | 9.31 | 9.32 | 13.5 - 15.5 | semi-empirical |
| $^{93}Nb$ | -6.22 | 214.09 | -151.77 | 32.85 | 14.5 - 19.0 | pure empirical |

The parameters of Table 1. with the prescribed function give the cross sections in microbarns. The "pure empirical" excitation functions are recommended in the given intervals except $^{93}Nb$. The "semi-empirical" excitation functions are the Hauser-Feshbach calculations of Sudár[8] fitted to the experimental points.

In order to develop a semi-empirical interpolation formula the logarithmic derivatives of the excitation functions at a fixed excess energy above the threshold /5 MeV/ were plotted against the atomic number Z and a /nearly/ linear dependence was established:

$$\left(\frac{d \ln \sigma}{dE}\right)_{E=5\ \mathrm{MeV}} = \alpha + \beta Z, \text{ where } \alpha = -0.667\ \mathrm{MeV}^{-1} \text{ and } \beta = 0.056\ \mathrm{MeV}^{-1}.$$

The reason for choosing just 5 MeV excess energy is that around this energy value we have common interval where all /used/ excitation functions have measured values. The above linear form has a theoretical basis: if we want to describe the energy dependence by the product of the Gamow penetration factor — $\exp/- B/E/^{-\frac{1}{2}}Z/$ — and a slowly varying function /f/ of E, then we have

$$\left(\frac{d \ln \sigma}{dE}\right)_{E=5\ \mathrm{MeV}} = \left(\frac{f'}{f} + \frac{1}{2}\frac{BZ}{E^{3/2}}\right)_{E=5\ \mathrm{MeV}} = \alpha' + \beta' Z, \text{ with } \beta' = 0.076\ \mathrm{MeV}^{-1}.$$

The constant $\alpha'$ cannot be determined without knowing f. It can be seen that although $\beta \neq \beta'$, the two values are near each other.

By using this result for the $13 \leq Z \leq 28$ region, one can estimate a cross-section value $/\sigma/$ at $E = E_0 + \Delta E$ from the value of the cross section $/\sigma_0/$ at $E_0$. Let us denote by y the quantity $/\alpha + \beta Z/\Delta E$, then we have

$$\sigma = \sigma_0 /1 + y/ \quad \text{for } y > 0, \qquad /1/$$

$$\sigma = \sigma_0 /1 + |y|/^{-1} \quad \text{for } y < 0. \qquad /2/$$

A pure empirical observation that instead of eq./2/ we can use

$$\sigma = \sigma_0 /1 + |y|/\exp/2y/ \quad /\text{for } y < 0/ \qquad /3/$$

and reach a far better result if $|y|$ is nearer the unity than zero./For small arguments the two formulae yield about the same result./ Otherwise, eq./1/ has a precision better than 7 % for $\Delta E = 0.5$ MeV and better than 15 % for $\Delta E = 1.0$ MeV. Similarly, eq./2/ gives values within 20 % for $\Delta E = -0.5$ MeV and within 85 % for $\Delta E = -1.0$ MeV. These later two pe:-

centages should be compared to 11 % and 2o % obtained from eq. /3/ for the same energy differences.

The authors wish to acknowledge the financial support of the International Atomic Energy Agency, Vienna, under contract No. 3114/RB.

References

1. F.Heinrich, F.Tanner, Helvetia Phys. Acta 36 /1963/ 298
2. S.M.Qaim, R.Wölfe, Nucl. Phys. A295 /1978/ 15o
3. Thesis of S.Sudár, 1979, Debrecen /in Hungarian/
4. S.M.Qaim, G.Stöcklin, J. Inorg. Nucl. Chem. 35 /1973/ 19
5. S.Sudár, J.Csikai, Nucl. Phys. A319 /1979/ 157
6. S.M.Qaim, G.Stöcklin, Nucl. Phys. A257 /1976/ 233
7. T.W.Woo, G.N.Salaita, Proc. Int. Conf. on Nucl. Cross Sections for Techn., Knoxville, TN, USA, Oct. 22-26, GC12 /1979/ 853
8. Priv. comm. of S.Sudár and ref. 5.

# COLLECTIVE EXCITATION IN NEUTRON SCATTERING ON 28-SI FOR ENERGIES 6.8 TO 14.8 MEV

T. Streil, D. Schmidt and D. Seeliger
Technische Universität Dresden, Sektion Physik, Dresden, DDR

## 1. Introduction

The direct excitation is known to give an essential contribution to the reaction mechanism in neutron scattering on lowlying collective states in the target nucleus.

The aim of the present work is the theoretical analysis of the experimental data, obtained under the same conditions with a consistent set of parameters in a wide energy and including higher excited states to get more information about reaction mechanism and also the nuclear structure.

## 2. Experimental procedure

The differential cross sections were measured with the tandem facility in the CINR Rossendorf. The measurements were carried out with a computer-coupled multiangle TOF-detector system consisting of eight detectors [1,2].
The background from elastically scattered non-monoenergetic neutrons of deuterium gas target [3] have been into account for the calculation of the cross sections of higher inelastic neutron groups using a special computer code.
The 14.8 MeV data were measured at a 150 keV DT-generator [4].

## 3. Analysis of the experimental data and conclusions

The aim of the theoretical interpretation is to show, that the superposition of compound and direct reaction contributions including multistep processes describes sufficiently well the experimental data in the full energy range called above. As shown in refs. [1,5,6] the HF-contribution as well as the CC-part have been calculated using the same energy-dependent imaginary term $W_s(E) = 0.6 \cdot E$.
The nucleus 28-Si has an interest intermediate position between nuclei with typical rotational structure (as 24-Mg) and ones with vibrational mode in the collective excitation (as 32-S) [7]. The analysis has been performed for oblate and prolate gro nd state deformation, respectively (see fig. 1), and shows that the ground and first $2^+$ state angular distributions can be described quite well in both the cases. If the higher-excited states are included, the analysis points out a

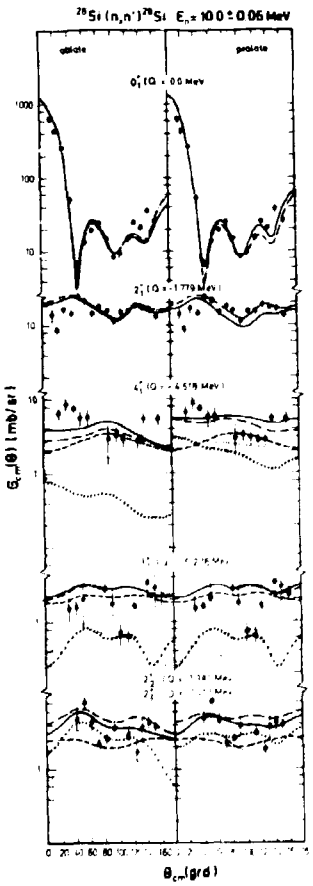


Fig. 1
Angular distr. to $0^+, 2^+, 4^+, 3^+, 2_2^+, 2_3^+$ level (- -HF, ...CC; xxxCC'; —HF+CC; -·-HF+CC').

slightly preference of the prolate g.s. deformation. For this calculations the coupling scheme due to fig. 2 has been used. As shown in ref. [6] the $2_1^+$ and $4_1^+$ states are excited dominantly from the g.s. (see coupling Cs'1). The $2_2^+$, $2_3^+$ doublet was interpreted in the following way: the $2_3^+$ state is assumed to be the member of a rotational band formed in a second minimum of the axially deformed potential. Than the $2_2^+$ vibrational state is coupled th this rotational band (see Cs2). As seen in fig. 1 the calculations for this doublet are sensitive with respect to deformation mode, whereby the assumption of a prolate g.s. deformation and the oblate deformed second minimum of the potential energy using Cs2 gives a good description. The dependence of the reaction mechanism from the bombarding energy can be conclude from the excitation functions related to the excited states resolved. Fig. 3 shows for the $3_1^+$ level a direct contribution which is already at $E_0$=12 MeV in the same order as the HF-part and doesn't change essentially with energy. The compound part decreases strongly because of the rapidly increasing number of open channels, thus the direct mechanism will be dominant relatively. The direct excitation shows threshold behaviour. It increases after opening of the inelastic channel, but than a decreasing occurs by coupling to the higher-lying states.

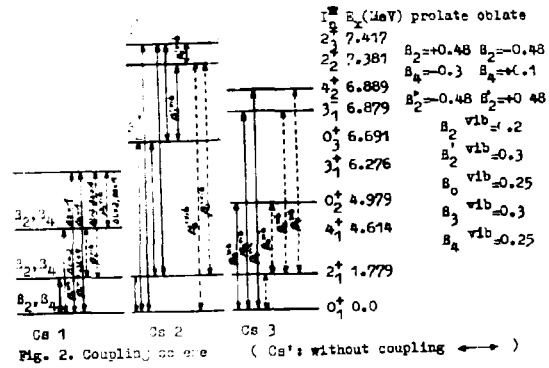


Fig. 2. Coupling scheme

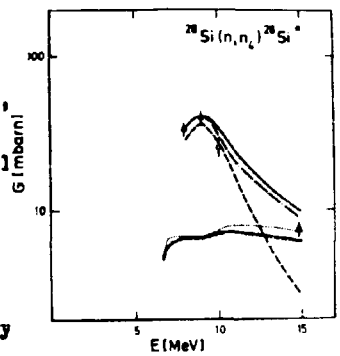


Fig. 3
Excitation function to the $3_1^+$ level (for notation see fig. 1, $\phi$, $\Delta$ angle integrated experimental cross sections).

## References


1. T. Streil, thesis, Technical University Dresden (1981)
2. P. Eckstein et al., Nucl. Instr. Meth. 169 (1980) 533
3. S. Mittag, W. Pils, D. Schmidt, D. Seeliger, T. Streil, Kernenergie 22 (1979) 237
4. J. Höhn, H. Pose, D. Seeliger, R. Reif, Nucl. Phys. A134 (1969) 289
5. D. Schmidt, D. Seeliger, T. Streil, Proc. of V. Conf. on Neutron Physics, Kiev, September 1980, Vol. 1, p. 229
6. D. Schmidt, D. Seeliger, T. Streil, report ZfK-459, Rossendorf (1981) 164
7. R. Reif, report ZfK-185, Rossendorf (1969) 119

# НЕУПРУГОЕ РАССЕЯНИЕ НЕЙТРОНОВ В ОБЛАСТИ ЭНЕРГИЙ 5 - 8 МэВ НА ИТТРИИ

С.П. Симаков, Г.Н. Ловчикова, В.П. Лунев, О.А. Сальников, С.Э. Сухих
Физико-энергетический институт, Обнинск, СССР

Аннотация

Методом времени пролета измерены дважды дифференциальные сечения неупругого рассеяния нейтронов с энергиями 4,86; 6,08; 7,02 и 7,94 МэВ на иттрии. Приведены основные параметры спектрометра, кратко освещены методики постановки эксперимента и обработки первичной информации. Проведено сравнение полученных результатов с данными других авторов. Теоретический анализ показал, что реакция неупругого рассеяния нейтронов протекает посредством двух механизмов - статистического и прямого. Расчеты сечений выполнены по модели Хаузера-Фешбаха и в рамках борновского приближения искаженных волн.

## I. Эксперимент

Дважды дифференциальные сечения неупругого рассеяния нейтронов на $^{89}Y$ измерены с начальными энергиями $E_0$ = 4,86 ± 0,06; 6,08 ± 0,07; 7,02 ± 0,08 и 7,94 ± 0,09 МэВ под шестью углами рассеяния $\theta'$ = 31°, 46°, 61°, 91°, 121° и 151° (при $E_0$ = 7,02 МэВ дополнительно еще под углами $\theta'$ = 76°, 106° и 136°).

Эксперимент выполнен методом времени пролета. Источником нейтронов служила газовая тритиевая мишень [1], бомбардируемая импульсным пучком протонов из ускорителя ЭГП-10М. Длительность протонных сгустков на мишени ~1 нс при частоте следования 5 МГц и среднем токе 1,5 мкА. При давлении трития в мишени 2 атм в центре рассеивателя, расположенного на расстоянии 16 см от мишени, создавался поток нейтронов ~$6 \cdot 10^5$ н/см$^2$·с. Исследуемый образец (рассеиватель) был выточен из металлического иттрия в форме полого цилиндра с размерами: внешний диаметр 4,5 см, внутренний - 3,0 см, высота 4,4 см. Образец содержал 1,94 моля ядер $^{89}Y$. Рассеянные нейтроны регистрировались на пролетной базе 200 см сцинтилляционным детектором, окруженным массивной защитой. Полное временное разрешение спектрометра составляло 3 ÷ 4 нс. Эффективность нейтронного детектора определялась по спектру нейтронов спонтанного деления $^{252}Cf$ (предполагалось, что его форма описывается распределением Максвелла с температурой T = 1,42 МэВ [2]). Абсолютные значения сечения реакции $^{89}Y(n,n')$ получены из их привязки к сечению $n$- p рассеяния [3]. Мониторирование отдельных измерений осуществлялось по спектру сцинтилляционного детектора, регистрирующего выход нейтронов из тритиевой мишени под углом 49° на пролетной базе 410 см. Разделение упруго- и неупругорассеянных нейтронов проводилось во временных спектрах. Форма пика упругорассеянных нейтронов определялась на основе измерений спектра прямого потока нейтронов из мишени под углом 0°.

В дифференциальные сечения рассеяния вводились поправки на ослабление и многократные взаимодействия нейтронов в образце. Необходимые для этих расчетов сечения взаимодействия нейтронов с иттрием при энергиях меньших 5 МэВ взяты из комплилляции [4]. Из дифференциальных сечений неупругого рассеяния получены полные сечения $\sigma_{nn'}$, для чего экспериментальные спектры экстраполировались в область ниже пороговой энергии эксперимента 0,6 МэВ в соответствии с распределением Максвелла. Параметр этого распределения T определялся в интервале

энергий рассеянных нейтронов $E' = 0,6 - 2,0$ МэВ. Значения T и $\sigma_{nn'}$ приведены в табл. I. Численная информация о дважды дифференциальных сечениях неупругого рассеяния и дифференциальных сечениях упругого рассеяния нейтронов ( ~1300 точек) направлена в Центр по ядерным данным (г. Обнинск). Методика измерений и обработки данных более подробно излагалась в предыдущих работах [5].

Таблица I. Параметр T и полные сечения неупругого рассеяния нейтронов для $^{89}Y$.

| | | | | |
|---|---|---|---|---|
| $E_0$, МэВ | 4,86 ± 0,06 | 6,08 ± 0,07 | 7,02 ± 0,08 | 7,94 ± 0,09 |
| T , МэВ | 0,72 ± 0,04 | 0,56 ± 0,03 | 0,70 ± 0,04 | 0,68 ± 0,04 |
| $\sigma_{nn'}$, б | I,73 ± 0,I4 | I,89 ± 0,I5 | I,97 ± 0,I6 | I,80 ± 0,I4 |

Сечения рассеяния нейтронв на иттрии в рассматриваемой области энергий ранее измерялись авторами работ [6 - 8]. В работе [6] при $E_0 = 6,04$ МэВ получено $\sigma_{nn'} = (2,3 \pm 0,3)$ б и $T = (0,56 \pm 0,06)$ МэВ, а в работе [7] при $E_0 = 9,I$ МэВ - $\sigma_{nn'} = (I,88 \pm 0,2I)$ б и $T = (0,69 \pm 0,05)$ МэВ. Как видно, эти данные совпадают с результатами настоящего эксперимента в пределах погрешностей измерений. В работе [8] измерены сечения возбуждения отдельных уровней (групп уровней) $^{89}Y$ при неупругом рассеянии нейтронов с энергиями от 4,I9 до 8,56 МэВ. С целью сравнения эти сечения были распределены по энергии возбуждения остаточного ядра в соответствии с функцией энергетического разрешения нашего спектрометра. Полученный спектр показан на рис. I вместе с данными настоящей работы. Принимая во внимание разницу начальных энергий, можно отметить хорошее согласие интегральных спектров, полученных в двух экспериментах.

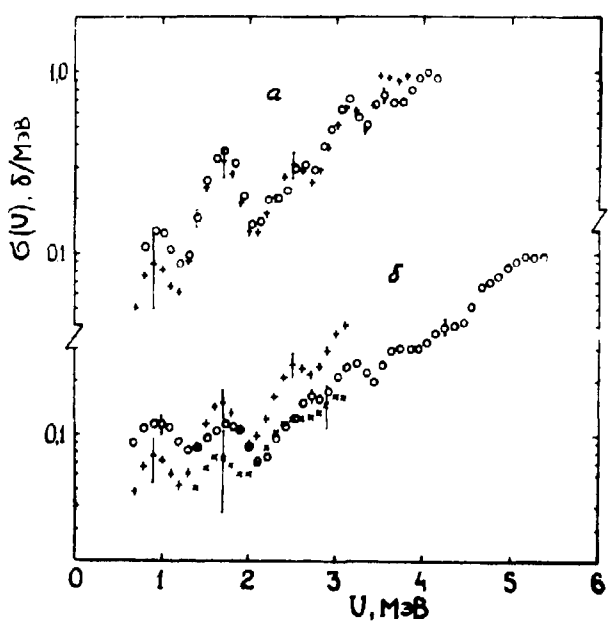


Рис. I. Сечения возбуждения состояний в ядре $^{89}Y$ при неупругом рассеянии нейтронов. Данные работ:
а) + - [8], $E_0 = 5,00$ МэВ,
o - настоящей, $E_0 = 4,86$ МэВ,
б) + и x - [8], $E_0 = 5,50$ и 6,44 МэВ,
o - настоящей, $E_0 = 6,08$ МэВ

## 2. Теоретический анализ

Анализ сечений неупругого рассеяния нейтронов на иттрии проведен в предположении, что взаимодействие быстрых нейтронов с ядрами происходит посредством двух механизмов: статистического и прямого. Справедливость такого подхода ранее демонстрировалась на других элементах [9].

Сечения неупругого рассеяния в рамках статистического механизма рассчитывались по медели Хаузера-Фешбаха (ХФ), алгоритм которой реализован в программе СМТ-80 [10]. В расчетах использованы параметры оптического потенциала Лагранжа [11], подобранные по совокупности экспериментальных данных о взаимодействии нейтронов с $^{89}Y$ в диапазоне энергий от 0,01 до 20 МэВ. До энергий возбуждения 3,8 МэВ в рамках статистической модели рассматривались переходы на дискретные состояния ядра $^{89}Y$ [12]. Выше неизвестная схема уровней моделировалась функцией плотности состояний, предсказываемой моделью ферми-газа [13], так как при таких энергиях возбуждения парные корреляции сверхпроводящего типа в ядре $^{89}Y$ отсутствуют, а влияние оболочечных эффектов не существенно. Параметр энергетической зависимости плотности состояний $a$, эффективное смещение энергии возбуждения $\Delta$ и момент инерции ядра $\eta$ (выраженный в единицах момента инерции эквивалентного твердого шара) определялись из условия наилучшего описания энергетических и угловых распределений неупругорассеянных нейтронов (для анализа были взяты низкоэнергетические части спектров $E' < 2,0 \div 2,5$ МэВ, где вклад прямого механизма не значителен). Для ядра $^{89}Y$ значения параметров плотности уровней получились следующими: $a = 8,9$ МэВ$^{-1}$, $\Delta = 1,8 \pm 0,2$ МэВ, $\eta = 0,45 \pm 0,30$.

Расчет сечений неупругого рассеяния нейтронов в рамках прямого механизма проводился в первом порядке борновского приближения искаженных волн (БПИВ), Формфакторы прямых переходов рассматривались в макроскопическом подходе - обобщенной модели ядра. Возбужденные состояния вибрационной природы характеризовались мультипольностью и четностью $\lambda^{\pi}$ и параметрами динамической деформации $\beta_{\lambda}$. В расчетах по методу БПИВ использован такой же нейтронный потенциал, что и в расчетах по модели ХФ. Значения $\lambda^{\pi}$ и $\beta$ взяты из аналогичного (макроскопического) анализа сечений реакции $^{89}Y(p, p')$ при энергиях протонов 24,5 МэВ [14] и 20,5 МэВ [15]. Следует отметить, что исследования природы первых возбужденных состояний в ядре $^{89}Y$ в микроскопическом подходе [14-16] показывает, что эти состояния имеют одночастичный характер или промежуточный между одночастичным и коллективным. В таких случаях расчеты в рамках обобщенной модели следует рассматривать как параметризацию вклада прямого механизма рассеяния.

В табл. 2 приведены результаты расчетов сечений неупругого рассеяния нейтронов на иттрии по модели ХФ и методу БПИВ с указанными выше параметрами.

Для удобства сравнения с экспериментальными данными, расчетные сечения возбуждения дискретных уровней были распределены по энергии в соответствии с функцией энергетического разрешения спектрометра. Полученные интегральные спектры и угловые распределения неупругорассеянных нейтронов показаны на рис. 2 и 3. Как видно на рисунках и из данных табл. 2, статистический механизм является доминирующим в реакции неупругого рассеяния нейтронов с энергиями 5 - 8 МэВ на иттрии. Однако, с ростом начальной энергии в высокоэнергетической части спектра становится заметным вклад прямых процессов: энергетическая зависимость спектров

становится более слабой, а угловые распределения приобретают направленность вперед.

Таблица 2. Расчетные сечения неупругого рассеяния нейтронов на $^{89}Y$. Сечения даны в мб, энергии - МэВ, $\alpha$ - в%.

| $E_0$ | $\sigma$ БПИВ | | | $\sigma$ ХФ | $\sigma_{nn'} = \sigma$ ХФ + $\sigma$ БПИВ | $\alpha = \frac{\sigma \text{ БПИВ}}{\sigma_{nn'}}$ |
|---|---|---|---|---|---|---|
| | $0,9 < U_\lambda < 2,9$ $\beta_\lambda$ из (14) | $3,1 < U_\lambda < 4,6$ $\beta_\lambda$ из (15) | $0,9 < U_\lambda < 4,6$ | | | |
| 4,86 | 55 | 24 | 79 | 1884 | 1963 | 4,0 |
| 6,08 | 57 | 31 | 88 | 1836 | 1924 | 4,6 |
| 7,02 | 57 | 34 | 91 | 1843 | 1934 | 4,7 |
| 7,94 | 56 | 33 | 89 | 1848 | 1937 | 4,6 |

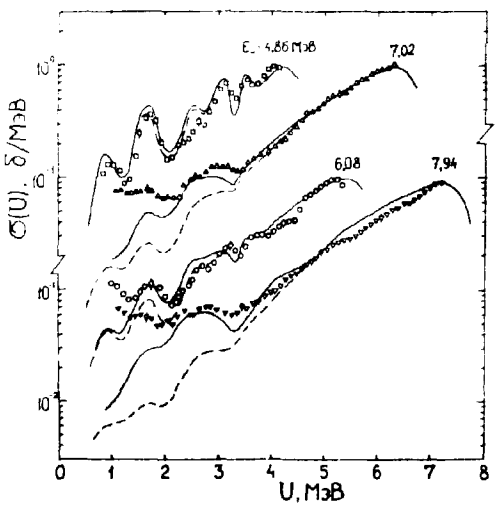


Рис. 2. Сечения возбуждения состояний в $^{89}Y$ при неупругом рассеянии нейтронов.

□,Δ,○,▽ - экспериментальные данные, расчетные кривые: - - - - по модели ХФ, ——— - сумма ХФ и БПИВ.

Рис. 3. Угловые распределения нейтронов неупругорассеянных на $^{89}Y$ (сечения проинтегрированны в указанных интервалах энергий возбуждения $U$) при $E_0$ = 4,86 (а); 6,08 (б); 7,02 (в) и 7,94 МэВ (г).

○ - экспериментальные данные, рассчетные кривые:

- - - - - по модели ХФ,

—·—·— - по методу БПИВ,

——— - сумма ХФ и БПИВ.

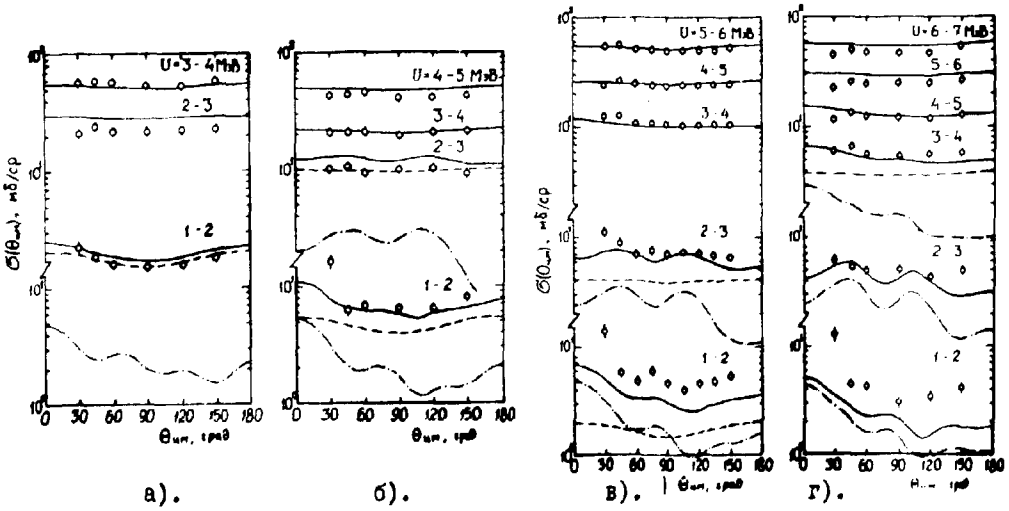

При расчетах сечений прямых переходов следует иметь в виду различие параметров $\beta_\lambda$ при рассеянии протонов и нейтронов. Эти отличия объясняются вкладом изовекторной компоненты ядерных сил [17] и для состояний коллективной природы получили убедительное подтверждение в соответствующих экспериментах [18]. В частности, для ядер с заполненной нейтронной оболочкой $N = 50$ ($^{88}Sr$, $^{90}Zr$) отношение параметров квадрупольной деформации, извлеченных из рассеяния нейтронов и протонов, составляет $\beta_2^{(n)} / \beta_2^{(p)} = 1{,}2$. Для состояний одночастичной природы такие отличия могут быть еще значительней [19]. Нижайшие состояния в $^{89}Y$ ($U_\lambda < 2$ МэВ) могут быть рассмотрены как одночастичные переходы в протонной оболочке [16], поэтому учет изовекторной зависимости ядерных сил улучшил бы согласие результатов расчета и эксперимента в высокоэнергетической части спектров.

Литература


1. С.П. Симаков, Н.И. Фетисов и др.
   Вопросы атомной науки и техники , Сер. Ядерные константы, 1981, вып. 2(41), с. 8.
2. J.A. Grundl and C.M. Eisenhauer, IAEA-208, 1978, v. 1, p. 53,
3. A. Horsley, Nuclear Data, 1966, v. A 2, p. 243,
4. D.I. Garber and R.R. Kinsey, BNL-325 (3rd Edition), 1976, v. 2,
5. С.П. Симаков, Г.Н. Ловчикова и др., Нейтронная физика, М., ЦНИИАИ, 1980, ч. 1, с. 320,
   Вопросы атомной науки и техники, Сер. Ядерные константы, 1980, вып. 4(39), с. 7, там же, 1981, вып. 5(44), с. 23, Атомная энергия, 1981, т. 51, с. 244,
6. R.M. Wilenzick, K.K. Seth et.al. Nucl. Phys., 1965, v. 62, p. 511,
7. Н.С. Бирюков, Б.В. Журавлев и др., Нейтронная физика, М., ЦНИИАИ, 1976, ч. 4, с. 113, там же, с. 118,
8. F.G. Perey and W.E. Kinney, Report ORNL - 4552, 1970,
9. Г.Н. Ловчикова, А.В. Игнатюк и др., Ядерная физика, 1982, т. 36, с. 6,
   А.В. Игнатюк, Physics and Applications, Bratislava, 1980, v. 6, p. 245,
10. Н.Н. Титаренко, Препринт ФЭИ-1260, Обнинск, 1982,
11. Ch. Lagrange, Нейтронная физика, М., ЦНИИАИ, 1976, ч. 3, с. 65,
12. C.M. Lederer, V. Shirley, Tables of Isotopes, N.Y. Wiley Press, 1978,
    J.P. Towle, Nucl. Phys., 1969, v. A 131, p. 561,
13. H.A. Bethe, Phys. Rev., 1936, v. 50, p. 332,
14. W. Benenson et.al., Phys. Rev., 1968, v. 176, p. 1268,
15. L. Hulstman, H.P. Blok et.al., Nucl. Phys., 1975, v. A 251, p. 269,
16. B. Weißbach, ZfK-410, Dresden, 1980, p. 88,
17. V.R. Brown et.al., Phys. Rev., 1975, v. C 12, p. 1298,
    V.A. Madsen et.al., Ibid., p. 1205,
    А.И. Блохин и др., Нейтронная физика, М., ЦНИИАИ, 1980, ч. 1, с. 89,
18. G. Hacwat, Physics and Applikations, Bratislva, 1980, v. 6, p. 333,
19. M.B. Johnson et.al.. Phys. Rev., 1966, v. 142, p. 748.

# BLOCKING EFFECT AT FINITE TEMPERATURE FOR SPHERICAL NUCLEI

W. Augustyniak
Laboratorio Dati Nucleari del ENEA, via Mazzini 2, 40138 Bologna, Italy and
Institute of Nuclear Research, Hoza 69, 00681 Warsaw, Poland

## 1. Introduction

Experimental data on level densities have been analysed traditionally by statistical method. Frequently used, simple analitical formulae with adjustable parameters were derived from schematic assumptions like equally spaced and non-degenerated single particle states [1-3]. Great progress was made in calculation owing to the BCS procedure with equidistant single particle state [4-5] or realistic set [6-7].

In the closed analitical formulae it has been found possible to reproduce the experimental level densities of neighbouring doubly even, odd-A and doubly odd nuclei by a proper shift of excitation energy. Also Behkami and Huizenga - using the BCS theory for doubly even nuclei - have successfully shifted in the energy scale the theoretical results on doubly even nuclei in order to reproduce the date for A-odd neighbour was found to be equivalent to that required to produce one quasiparticle. Another procedure used by Behkami and Huizenga consisted in proper reduction of the pairing energy gap, so that condensation energy of odd-A nuclei was reduced in proportion to the doubly even nuclei to give the even-odd ground state energy shift.

A different solution was found by Abboud et al. [9]. Level densities of odd-A and doubly odd nuclei were determined by averaging the level densities of double even neighbours properly shifted in the energy scale. The energy shift is a sum of two components. The first one takes account of the energy difference between the ground states. The second component accounts for the fact that in vicinity of the closed shell, the addition of an odd nucleon affects the properties of highly excited nuclei.

Maiho et al.[10] used the blocking method in order to reproduce the level densities for deformed nuclei with odd-A. They determined the level density at an excitation close to neutron binding energy treating the pairing gap as an adjustable parameter.

In this paper the blocking method for spherical nuclei with $A \approx 60$ was investigated. The calculations have been made without adjustable parameters for two sets of single particle states: Seeger (data from Hillman and Grover [12]) and Seeger-Howard [13]. Three mentioned above methode: Behkami-Huizenga, Abboud et al. and blocking method were compared.

## 2. Calculation procedure

The state and level density of doubly even nuclei for realistic set of single particle levels may be described by grand partition function method for the system containing the pairing interactions. This method was discussed in detail in many papers [4-9].

The density of states for odd Z(N) and even N(Z) nuclei $\omega$ was determined from the density of states of doubly even nuclei $\tilde{\omega}_{\epsilon_k}$ - calculated with the blocked two single particle states with energy $\epsilon_k$ . It was defined in the following

way:

$$\omega(Z+1,N,U) = \sum_k 2\,\tilde{\omega}_{\varepsilon_k}(Z,N,U), \tag{1}$$

where N, Z are even.
The ground state energy was calculated according to:

$$E_g(Z+1,N) = \mathrm{Min}[\tilde{E}_g^{\varepsilon_k}(Z,N)+\varepsilon_k] - \tilde{E}_g^{\varepsilon_{k_0}} + \varepsilon_{k_0} \tag{1a}$$

The excitation energy then becomes

$$U = \tilde{E}^{\varepsilon_k} + \varepsilon_k - \tilde{E}_g^{\varepsilon_{k_0}} + \varepsilon_{k_0} \quad . \tag{1b}$$

All values labeled by tilda in this paper were calculated with blocked single particle states - the states with the same quantum numbers except for the sign of the spin projection. As can be seen from formulae (1), (1a) and (1b) the density of states for odd-A nuclei was defined by set of thermodynamical systems with different degrees of freedom created by blocked states. Formula (1) may be extended to doubly odd nuclei by changing the single sum to a double sum:

$$\omega(Z+1,N+1) = \sum_{k,L} 4\,\tilde{\omega}_{\varepsilon_k,\varepsilon_L}(Z,N), \tag{2}$$

where $\varepsilon_K$ and $\varepsilon_L$ mean energies of blocked states in neutron and proton systems. It is easy to expect, keeping in mind the exponential behaviour of the function $\omega(U)$, that only few terms of that sum will be significant. However, a degeneracy of single particle states results in additional simplification. For that reason formulae (1) may be rewritten:

$$\omega(Z+1,N,U) = \sum_L (2j_L+1)\,\tilde{\omega}_{\varepsilon_L}(Z,N,U), \tag{3}$$

where: $L(n,L,j_L)$ is the index of subshell; $\varepsilon_L$ and $j_L$ are energy and spin of subshell. Looking into formulae (3) it is easy to deduce that the function of the level density and spin distribution will be determined by the set of spin cut-off parameters:

$$\rho(U) = \sum_L \frac{2j_L+1}{\sqrt{2\pi}\,\sigma_L^2}\,\tilde{\omega}_L = \sum_L (2j_L+1)\,\tilde{\rho}_L(U), \tag{4}$$

$$\rho(U,I) = \sum_L \frac{(2j_L+1)(2I+1)}{2(2\pi)^{1/2}\sigma^3}\,\omega(U)\exp\left[-\frac{(I+1/2)^2}{2\sigma_L^2}\right] . \tag{5}$$

## 3. Results and discussion

In this section a comparison of the level densities calculated in microscopic theory with experimental ones [14,15,16] for $^{55}Mn$, $^{59}Co$ and $^{63}Cu$ nuclei is presented. The calculations were carried out with two sets of single particle states: the one of Seeger's and the other of Seeger-Howard's. The pairing interaction constants $G_p=5.12\,A^{-0.741}$ and $G_p=4.04\,A^{-0.734}$ [17], determined for Nilsson's set from the mass differences in a wide range of A, have been used. Additional analysis of mass differences for $A\simeq 60$, performed with Seeger's set and Vapstra data [20] gives the values for these constants being in reasonable agreement with those chosen in calculations. Also, the comparison of experimental levels densities with theoretical ones for $^{56}Fe$, $^{60}Ni$ approves used parameters. It should also be noted that for Seeger's set the superconducting parameters obtained in this paper are consistent with adjustable ones of ref.[8].

For $^{56}Fe$ there are equal: $\Delta^{n}$=1.11 MeV, $\Delta^{p}$=1.58 this paper and $\Delta^{n}$=1.1 MeV, $\Delta^{p}$=1.4 MeV ref. (8).

In order to present the validity of blocking method for odd-A it is necessary to check the used parameters. The comparison of experimental level density with the theory for $^{56}Fe$ has been shown in fig. 1. As can be seen the microscopic theory works better with Seeger and Seeger-Howard then with Nilsson set. The similar description has been obtained also for on other even-even nuclei from this region. Apart from the good description of experimental data provided by the theory with Seeger and Seeger-Howard set, the level densities predicted by theory lie higher than experimental ones at low excitation energy but lower than experimental ones at low excitation energy. In the end of the discussion of parameters it should be emphasized that the theory is very sensitive to the G values. An 10% change of the G value could change the results of the calculations by more than a factor 2.

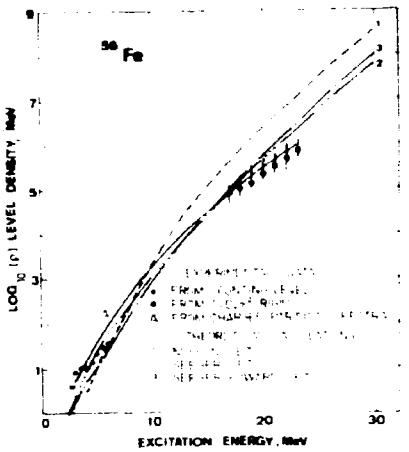


Fig. 1 Comparison of experimental level density of $^{56}Fe$ with the microscopic theory including the nuclear pairing interaction. The calculations were performed with single particle states of Nilsson [11], Seeger [12] and Seeger-Howard [13].

In the figs. 2a, 2b and 2c, the comparison of the experimental data for $^{55}Mn$, $^{59}Co$ and $^{63}Cu$ with three calculation methods: Behkami-Huizenga, Abboud et al. and the blocking method have been shown. The Behkami-Huizenga calculations have been done with Seeger-Perisho set [19], Abboud et al. with Seeger-Howard set. It can be seen that the data predicted by the blocking method are higher than the others.

Behkami-Huizenga conclude that the methods consisting in the energy shift and reducing superconducting parameter are equivalent. They found that the level density for $^{55}Mn$ may be described by 2.0 MeV energy shift or by 50%

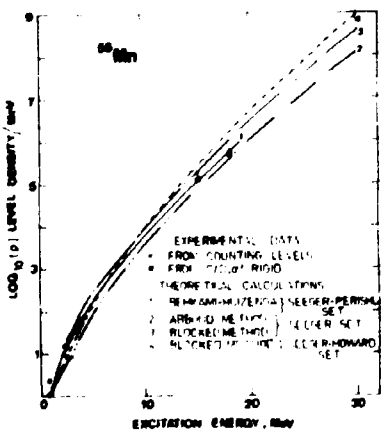


Fig. 2a

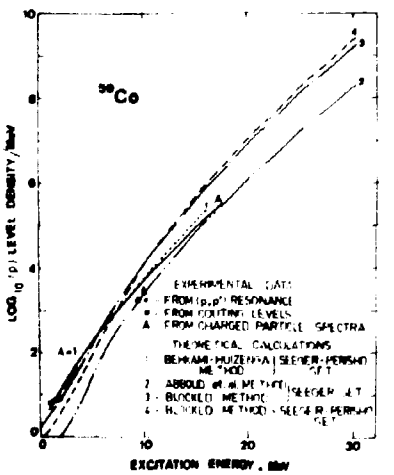


Fig. 2b

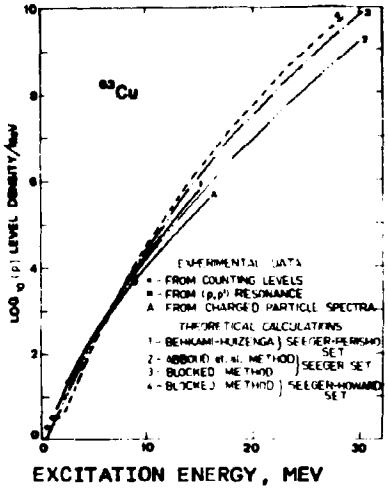


Fig. 2

Comparison of the experimental level density with microscopic theory including the nuclear pairing interaction. The calculation for the blocking method were performed with Seeger's and Seeger-Howard's sets, for Abboud method with Seeger's one.

Fig. 2c

reduced $\Delta^p$ for $^{56}Fe$. For the pair of $^{59}Co$ and $^{60}Ni$ this numbers are equal: 1.2 MeV and 58%. However it is easy to find certain correspondence between the method of Behkami-Huizenga and Abboud et al. If the averaging is omitted and "shell shift" neglected the Abboud et al. and Behkami-Huizenga methods will be equivalent. The shell shift is small for nuclei far from the closed shell but important [9] for the nuclei near the closed shell and produces the fictive ground state. However, there may be found some points of similarity and contrast between the Behkami-Huizenga method and first term of the blocking method. In the case when the calculation will be done with the same set of single particle levels and G values the observed difference in the slope comes only from the blocked state.

From the analysis of particular terms of the blocking method it need be noted that for $^{55}Mn$ only one term is important, just opposite to $^{53}Co$ and $^{63}Cu$ where only at low excitation energy the total level density is mainly determined by one term.

The blocked levels generated a different structure of accesible single particle states. At low excitation energy it would change also the superconducting parameters. Therefore at low excitation energy the irregular behaviour at particular terms are observed. At high excitation energy, where superconducting effects vanish, only the influence of changes in the sets particle states are expected. The curves are much more regular but parallel only if $|\epsilon_K - \epsilon_L| \ll \dot{u}$. The exact numerical values of all contributions for excitation energies: 5, 1o, 15, 2o, 25 and 3o MeV have been shown in table 4. This information completes of table 2, where characteristics of configurations at T = 0 are given. The data at T = 0 are reduced to those predicted by Wahlborn [18]: the excitation energy is lower than $|\epsilon_x - \epsilon_{K_0}|$

TABLE 1 Dependence of total level density on particular terms generated by blocked states for $^{55}Mn$ calculated with Seeger-Howard set.

| Excitation energy(MeV) | Total level density | Per cent of level density calculated for the following sub-shell with blocked states | | | | | |
|---|---|---|---|---|---|---|---|
| | | $1f_{7/2}$ | $2s_{1/2}$ | $1f_{5/2}$ | $2p_{3/2}$ | $1g_{9/2}$ | $1d_{3/2}$ |
| 5.0 | $1.5437 \cdot 10^{2}$ | 94.12 | 1.22 | 1.72 | 0.75 | 0.00 | 2.17 |
| 10.0 | $8.9774 \cdot 10^{3}$ | 83.09 | 2.66 | 5.60 | 2.47 | 1.21 | 4.95 |
| 15.0 | $2.8766 \cdot 10^{5}$ | 67.37 | 4.05 | 11.77 | 5.78 | 3.36 | 7.66 |
| 20.0 | $5.6135 \cdot 10^{6}$ | 60.44 | 4.83 | 13.04 | 6.81 | 5.63 | 9.23 |
| 25.0 | $8.1844 \cdot 10^{7}$ | 54.90 | 5.40 | 14.20 | 7.68 | 7.40 | 10.39 |
| 30.0 | $9.4495 \cdot 10^{8}$ | 50.71 | 5.84 | 14.91 | 8.28 | 8.95 | 11.29 |

TABLE 2 Properties of states at T = 0 for $^{55}Mn$ generated by bocked states for $^{55}Mn$ calculated with Seeger-Howard set.

| Protons subshell with blocked states | Excitation energy(MeV) | Excitation energy with G=0 (MeV) | Correlation functions | |
|---|---|---|---|---|
| | | | $\Delta p$ (MeV) | $\Delta n$ (MeV) |
| $1\ f_{7/2}$ | 0.0 | 0.0 | 1.53 | 1.19 |
| $2\ s_{1/2}$ | 2.36 | 3.21 | 1.78 | 1.19 |
| $1\ f_{5/2}$ | 3.00 | 4.48 | 1.77 | 1.19 |
| $2\ p_{3/2}$ | 3.44 | 4.94 | 1.78 | 1.19 |
| $1\ g_{9/2}$ | 5.26 | 6.84 | 1.81 | 1.19 |
| $1\ d_{3/2}$ | 2.45 | 3.30 | 1.79 | 1.19 |

The consequence of the fact that blocking method describes the odd-A nucleus by means of the set of thermodynamical systems with the different degrees of freedom is not Gaussian spin distributions, even when the Gaussian spin distribution is valid for even-even. In agreement with the formulae (5) the function describing the spin distribution is parametrized by a set of the spin cut-off factors. The spin distribution for $^{55}Mn$ at 30 MeV excitation energy has been shown in the fig. 3. It can be seen that the lower values of spins are populated with higher probability than in the case of random populations.

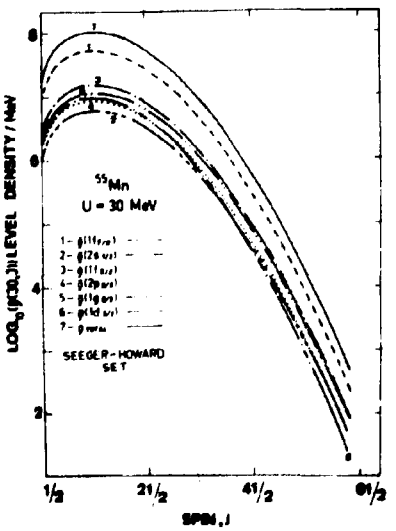


Fig. 3

The spin distributions for $^{55}Mn$ generated by different blocked states at 30 MeV excitation energy

To sum it up, it should be emphasized that the blocking method predicts dependences of the level density on excitation energy different than other methods. This difference increases with excitation energy. The blocking method predicts also the different than Gaussian spin distribution. In fact, the blocking method gives values greater than experiment, but most of analysed data have been model dependent. Some uncertainties come from the pairing constants used.

The author is mostly indebted to dr G. Reffo, dr A. Ventura and dr G. Maino who aided him in his research. This work was supported financially by a 3 months grant from ENEA.

References

1. A. Gilbert, A.G.W. Cameron, Can. J. Phys. 43 (1965) 1446
2. T.D. Newton, Can. J. Phys. 34 (1956) 808
3. H. Baba, Nucl. Phys. A159 (1970) 625
4. H. Sano, S. Yamasaki, Progr. Theor. Phys. 29 (1963) 277
5. T. Kammuri, Progr. Theor. Phys. 31 (1964) 595
6. J.R. Huizenga, L.G. Moretto, Ann. Rev. Nucl. Sci. 22 (1972) 427
7. P. Decowski, W. Grochulski, A. Marcinkowski, K. Siwek, Z. Wilhelmi, Nucl. Phys. A110 (1968) 129
8. A.N. Behami, J.R. Huizenga, Nucl. Phys. A217 (1973) 78
9. A. Abboud, P. Decowski, W. Grochulski, A. Marcinkowski, J. Piotrowski, K. Siwek, Z. Wilhelmi, Nucl. Phys. A139 (1969) 42
10. G. Maino, E. Menapace, A. Ventura, Nuovo Cim. 57A (1980) 427
11. J.R. Huizenga, H.K. Vonach, A.A. Katsanos, A.J. Gorski, C.J. Stephan, Phys. Rev. 182 (1969) 1149
15. A.A. Katsanos, R.W. Shaw Jr., R. Vandenbosch, D. Chamberlain, Phys. Rev. C1 (1970) 594
16. C.C. Lu, L.C. Vaz, R.J. Huizenga, Nucl. Phys. A190 (1972) 229
17. P. Decowski, W. Grochulski, A. Marcinkowski, Nucl. Phys. A194 (1972) 384
18. S. Wahlborn, Nucl. Phys. 37 (1962) 554
19. P.A. Seeger, R.C. Perisho, Los Alamos Scientific Laboratory report LA - 3751 (1957)
20. A.H. Vapstra, N.B. Gove, Nuclear Data Tables 9 (1971) 267